University of Southampton

THE DYNAMIC RESPONSE OF A WEDGE SEPARATED HYPERSONIC FLOW AND ITS EFFECTS ON HEAT TRANSFER

by

Andrew John Darwin Smith, B.Sc. (Hons.)

Thesis submitted for the Degree of
Doctor of Philosophy

Faculty of Engineering and Applied Science
Department of Aeronautics and Astronautics

June 1993

UNIVERSITY OF SOUTHAMPTON

ABSTRACT

FACULTY OF ENGINEERING AND APPLIED SCIENCE
DEPARTMENT OF AERONAUTICS AND ASTRONAUTICS

Doctor of Philosophy

THE DYNAMIC RESPONSE OF A WEDGE SEPARATED HYPERSONIC FLOW AND ITS EFFECTS ON HEAT TRANSFER

by Andrew John Darwin Smith, B.Sc. (Hons.)

The dynamic response of a wedge separated hypersonic flow has been investigated experimentally, with emphasis on its heat transfer effects. Tests were performed in a Mach 6.85 freestream flow, at a unit Reynolds number of 2.45×10^6/m. The unsteady separated flowfield was generated by rapidly deflecting a trailing edge flap control surface through an angle of 35 degrees in approximately 20 ms, with velocities approaching 3000 degs./s. The principal measurements made were of the model centre line chord heat transfer distributions. These were complemented with flow visualisation of the separated flow structures, and liquid crystal surface thermographs.

The unsteady response of the separated flow was interpreted by comparing measurements at instantaneous dynamic flap angles throughout the deflection range with those obtained at corresponding fixed flap angles. It was determined through the application of established criteria that the steady separated flows in these experiments were transitional, although their length scales were more typical of the fully laminar regime. In the dynamic flap tests there were no indications from the heat transfer measurements of a significant unsteady effect on the location, or process, of transition.

The unsteady separated flow was observed to maintain the typical features of steady wedge type separations during its evolution. However, the heat transfer measurements, and flow visualisation, were consistent in identifying the development of a lag in its growth at moderate to high flap angles with respect to the quasi-steady separation lengths. Simple analytic models of the unsteady separated flow response, based on distinct fundamental flow adjustment mechanisms, indicated that at high flap angles these lags in growth were significantly larger than could be attributed only to pressure communication times across the interaction lengths. This was apparent for tests made both with, and without, side plates fitted to the model. It was concluded that the lags in growth at high flap angles were substantially due to mass entrainment requirements for a growing separated flow. Locally about the unsteady separation point the free-interaction process appeared maintained.

There were no significant unsteady separated flow effects on the heat transfer distributions ahead of the flap in these tests. In the reattachment region there was an increase in the peak heating measured for the dynamic flap condition at its highest deflection angle compared to the level for the steady separated flow induced at an identical fixed flap angle. There also occurred an additional local rise in heat transfer towards the flap trailing edge for the unsteady separated flow.

Contents.

	Page
List of Figures.	v
List of Tables.	viii
Acknowledgements.	ix
Author's Declaration.	x
List of Symbols.	xi
1. General introduction.	1
PART I - LITERATURE REVIEW AND PERSPECTIVE OF THE PRESENT INVESTIGATION.	4
2. General characteristics of steady separated hypersonic flows.	5
2.1 Geometries of separation.	5
2.2 Transition.	8
2.3 Free-interaction	12
2.4 Surface measurements in compression corner interactions downstream of sharp edged flat plates.	15
2.4.1 Pressure distributions.	15
2.4.2 Heat transfer distributions.	18
2.5 Effects on the scale of separation.	21
2.5.1 Flap angle.	21
2.5.2 Freestream Mach number.	22
2.5.3 Freestream Reynolds number.	23
2.6 Three-dimensional influences in nominally two-dimensional experiments.	25
2.7 Relationship of experiments to a real hypersonic vehicle.	26
2.8 The development of theoretical models of shock wave - boundary layer interaction.	27
3. Review of unsteady separated flows.	29
3.1 Definition of unsteady separation.	29
3.2 Mechanisms of unsteady separation adjustment.	30
3.3 Response of separated flows to changing wall geometries.	33
3.4 Numerical solutions.	36
3.5 Discussion.	38
PART II - EXPERIMENTAL SET-UP AND MEASUREMENT TECHNIQUES.	39
4. Introduction to the experimental work.	40

5. The isentropic light piston compression tube (ILPT) hypersonic wind tunnel. 41

5.1 Low freestream Reynolds number operation of the ILPT facility. 42

6. Dynamic / Fixed trailing edge flap model. 44

6.1 Design of side plates. 45

7. Heat transfer instrumentation. 47

7.1 Introduction. 47

7.2 Heat transfer gauges. 48

7.3 The thin film resistance heat transfer gauge. 50

7.3.1 Thermal model. 50

7.3.2 Measurement of surface temperature with thin film gauges. 51

7.3.3 Evaluation of the surface heat flux from a temperature signal. 52

7.3.4 Correction for temperature effects on the substrate thermal properties. 55

7.3.5 Construction methods for analogue lines. 56

7.3.6 Analogue time response. 59

7.3.7 Thin film gauge manufacture. 60

7.4 Heat transfer instrumentation arrangements. 62

7.4.1 Conventional gauge signal - analogue arrangement. 62

7.4.2 Low noise instrumentation. 63

7.4.3 Evaluation of the surface temperature rise when using the low noise arrangement. 64

7.5 Calibrations of the heat transfer instrumentation. 65

7.6 Sources of error. 68

8. Liquid crystal thermography. 70

8.1 Introduction. 70

8.2 Liquid crystals as a surface thermometer. 71

8.3 Development of a liquid crystal technique for measuring heat transfer in short duration hypersonic test facilities. 72

8.4 Application of liquid crystal thermography to the present trailing edge flap model. 73

8.5 Model construction for surface thermography. 74

8.6 Liquid crystal formulations. 75

9. Schlieren flow visualisation. 76

PART III - STEADY SEPARATED FLOW EXPERIMENTS. 77

10. Introduction to the steady separated flow experiments. 78

11. Determination of the stagnation temperature. 80

12. Model position. 84
13. Steady separated flow results and discussion. 88
13.1 Separated flow lengths. 88
13.2 Plateau pressures. 91
13.3 Three-dimensional effects. 93
13.4 Heat transfer distributions. 95
13.4.1 Effects of side plates. 97
13.4.2 Peak heat transfer. 97
13.5 Transition. 99
13.6 Influence of hinge line bleed. 100
13.7 Effect of finite flap chord length. 101
13.8 Summary. 101

PART IV - DYNAMIC FLAP SEPARATED FLOW EXPERIMENTS. 103
14. Introduction to the dynamic flap experiments. 104
15. Unsteady measurement considerations. 105
15.1 Schlieren flow visualisation. 105
15.2 Heat transfer measurements. 105
15.2.1 Thin film gauge response time. 105
15.2.2 Data sampling and filtering. 108
16. Dynamic separation results. 112
16.1 Schlieren flow visualisation. 112
16.2 Heat transfer distributions. 114
16.3 Summary. 119

PART V - SIMPLE ANALYTIC MODELS OF THE DYNAMIC FLAP SEPARATED FLOW RESPONSE. 122
17. Separation growth. 123
17.1 Separation adjustment with respect to pressure waves. 123
17.2 Mass transfer adjustment of the wedge separated flow. 125
17.2.1 Steady wedge separation solution. 125
17.2.2 Dynamic response. 134
17.3 Discussion. 149
18. Dynamic effects on heat transfer. 150
18.1 Separated flow region. 150
18.2 Peak reattachment heat transfer. 153

PART VI - GENERAL DISCUSSION AND CONCLUSIONS. 156

19. General discussion. 157

20. Recommendations. 162

21. Conclusions. 163

APPENDICES. 164

1. Tables. 165

2. Correction to measured heat transfer rates for the temperature effects on the pyrex substrate thermal properties. 168

3. Frequency limits of an RC analogue line operation. 171

4. Heat transfer measurement errors. 173

5. Effects of weak viscous interaction on flat plate heat transfer. 179

6. Estimate of the freestream stagnation temperature from the measured run duration. 180

7. Signal power spectrums. 182

8. Numerical filtering algorithm. 183

9. Phase lag correction for the low pass analogue filtered signals. 186

10. Published papers. 188

References. 204

Figures.

List of Figures.

1 Examples of strong viscous interaction regions occurring on hypersonic vehicles.

2 Basic types of two-dimensional shock wave - boundary layer interaction.

3 Schematic of the compression corner separated flow.

4 Typical form of surface pressure, and heat transfer, distributions in compression corner separated hypersonic flows.

5 Mass transfer mechanism to an unsteady base separated flow (Ihrig & Korst 1963).

6 Wake transient energy system proposed by Battin (1963).

7 Wilkinson's (1966) model of mass transfer adjustment in an unsteady separated flow.

8 The University of Southampton ILPT hypersonic wind tunnel.

9 The ILPT open jet test section.

10 The fixed / dynamic flap test model.

11 The test model dimensions.

12 Example of a thin film resistance gauge insert.

13 Conventional RC analogue arrangement with the thin film resistance gauge temperature signal.

14 Firing cycle for the manufacture of painted thin film resistance gauges.

15 Comparison of an RC analogue, and numerical, conversion of temperature to heat transfer.

16 Correction factor for the measured heat transfer to account for the temperature effects on the substrate ρck.

17 Low noise circuit arrangement for the measurement of heat transfer with thin film resistance gauges.

18 Calibration circuit for the gauge substrate thermal product.

19 Numerical evaluation of an RC analogue input impedance v's frequency.

20 Temperature distribution through the three substrate model of liquid crystal, paint, and semi-infinite metal base.

21 Surface temperature rise for different types of semi-infinite model substrate construction.

22 Layout of the conventional single pass schlieren system.

23 Liquid crystal surface thermographs. Effects of the model position, flap angle, and side plates. $M_\infty = 6.85$, $Re_\infty = 2.45 \times 10^6$/m.

24 Schlieren flow visualisation. Effect of the model position. Flap angle = 35 degrees. $M_\infty = 6.85$, $Re_\infty = 2.45 \times 10^6$/m.

25 Schlieren flow visualisation. Effect of freestream Reynolds number. Flap angle = 35 degrees. $M_\infty = 6.85$.

26 Fixed flap separation lengths (measured from the schlieren photographs). Effect of the model position. $M_\infty = 6.85$, $Re_\infty = 2.45 \times 10^6$/m.

27 Nozzle wave heights above the flow centre line (at the flap trailing edge location). $M_\infty = 6.85$, $Re_\infty = 2.45 \times 10^6$m.

28 Fixed flap separation lengths with the model moved forward (measured from the schlieren photographs). Effect of the freestream Reynolds number. M_∞ = 6.85.

29 Correlation of the separation lengths.

30 Correlation of laminar plateau pressures using Chapman's (1958) free-interaction parameters.

31 Comparison of the absolute stagnation pressure, and heat transfer signal from the first plate thin film resistance gauge (ahead of the separation interaction). M_∞ = 6.85, Re_∞ = 2.45x10^6/m.

32 Flat plate heat transfer distribution. M_∞ = 6.85, Re_∞ = 2.45x10^6/m.

33 Heat transfer distributions at fixed flap angles, with, and without side plates. M_∞ = 6.85, Re_∞ = 2.45x10^6/m.

34 Effects of transition on the separated flow heat transfer distribution, and the signal noise content. Flap angle = 25 degrees. M_∞ = 6.85, Re_∞ = 2.45x10^6/m.

35 Comparison of schlieren flow visualisation, thin film gauge measurements, and liquid crystal thermography. M_∞ = 6.85, Re_∞ = 2.45x10^6/m.

36 Comparison of the peak reattachment heat transfer values with laminar interference heating correlations.

37 Bushnell & Weinstein (1968) correlation of peak reattachment heating for laminar, and turbulent, wedge separated flows.

38a A correlation of the hinge line bleed data of Ball & Korkegi (1968).

38b Application of the correlation in Fig.38a to the present data. M_∞ = 6.85, Re_∞ = 2.45x10^6/m.

39 Correlation of finite flap length effects on the scale of wedge separated flows (Ball 1969).

40 Profile measurement of a surface deposited thin film resistance gauge.

41 Comparison of the quasi-steady, and measured dynamic, heat transfer signals at the flap gauge no.9. M_∞ = 6.85, Re_∞ = 2.45x10^6/m.

42 Power spectrums of the constructed quasi-steady, and dynamic heat transfer signal, in Fig.41.

43 Numerical filter frequency response.

44 Dynamic flap motion.

45 Dynamic flap velocity as a function of the angle of deflection.

46 Schlieren flow visualisation of the dynamic, and equivalent fixed flap, induced separated flows. M_∞ = 6.85, Re_∞ = 2.45x10^6/m.

47 Unsteady, and steady, separation lengths measured from the schlieren flow visualisation. M_∞ = 6.85, Re_∞ = 2.45x10^6/m.

48 Shear layer deflection angles measured from the schlieren photographs. M_∞ = 6.85, Re_∞ = 2.45x10^6/m.

49 Examples of the unsteady heat transfer signals (no side plates), compared with the flap deflection. M_∞ = 6.85, Re_∞ = 2.45x10^6/m.

50 Comparison of the dynamic, and fixed flap heat transfer distributions. No side plates. M_∞ = 6.85, Re_∞ = 2.45x10^6/m.

51 Comparison of the dynamic, and fixed flap heat transfer distributions.

Side plates attached. M_∞ = 6.85, Re_∞ = 2.45x10^6/m.

52 Heat transfer distributions on the flap, reduced using a turbulent recovery factor. No side plates. M_∞ = 6.85, Re_∞ = 2.45x10^6/m.

53 Heat transfer distributions on the flap, reduced using a turbulent recovery factor. + side plates. M_∞ = 6.85, Re_∞ = 2.45x10^6/m.

54 Effect of the flap wall temperature on the separated flow. Flap angle = 35 degrees, no side plates. M_∞ = 6.85, Re_∞ = 2.45x10^6/m.

55 Characteristic length for pressure wave communication in the unsteady separation.

56 Method of determining the unsteady separation growth with respect to pressure wave adjustment.

57 Comparison of the predicted lags in unsteady separation growth, based on pressure wave adjustment, and the experimental measurements (corrected for model position effects).

58 Cooke's (1963) simplified flowfield for the modelling of a supersonic wedge separation.

59 Steady wedge separation lengths predicted with Cooke's (1963) analytic model.

60 Mass transfer mechanism in the growth of an unsteady wedge separated flow.

61 Modelled unsteady separation growth based on mass exchange, assuming an isentropic reattachment process, with N = 0.5.

62 Comparison of the predicted lags in unsteady separation growth (isentropic reattachment, N = 0.5) with the experimental measurements.

63 Modelled unsteady separation growth based on mass exchange, with the measured, and modelled, steady separation lengths matched.

64 Comparison of the predicted lags in unsteady separation growth with the experimental measurements. Measured, and modelled, steady separation lengths matched.

65 Mass balance in a steady wedge separated flow with hinge line bleed.

66 Effect of hinge line bleed on the mass flow entrainment for an unsteady separation growth.

67 Effect of the assumed dead-air temperature on the predicted lags in unsteady separation growth. Measured, and modelled, steady separation lengths matched.

68 Comparison of fully laminar, and fully turbulent, asymptotic shear layer velocity profiles. Local freestream flow conditions matched to those that occur adjacent to the shear layer with the fixed flap angle of 35 degrees, no side plates.

A4.1 Simulated effect of gauge erosion on the measured surface heat transfer rate.

A4.2 Variation of measured heat transfer coefficients during the test period, with a fixed flap angle of 35 degrees.

A8.1 Example application, and verification, of the numerical filter.

List of Tables.

1 Interference heating correlations taken from the review of Hung (1973).

2 Tunnel operation for the low freestream Reynolds number.

3 Low freestream Reynolds number conditions.

4 Liquid crystal formulation temperature - colour bandwidths.

5 Resistivities of 0.1 μm thick metal films.

Acknowledgements.

The author would like to express his thanks to the following:-

Prof. R A East for his supervision of this student, and particularly for the support, and understanding, provided during its difficult periods.

Tim Roberts for his advice in many aspects of this research project during its initial stages.

Zia ul Haq for his practical advice with the liquid crystal thermographic technique, and many useful discussions.

Paul Clarke, and Geoff Thomas, for operating the ILPT hypersonic test facility.

Dave Hill, and the staff of the machine workshop, for the manufacture of the test models.

Geoff Hutt for his shared supervision of this student during the early part of this project.

Dave Baxter, Graham King, and Dr G T Roberts, for their general advice, and technical support.

The financial support of Dassault Aviation for funding this investigation as part of the Hermes research and development program.

List of Symbols.

a	speed of sound.
A	area.
c_f	skin friction coefficient.
c_{p_p}	plateau pressure coefficient.
c	specific heat capacity.
c_p	gas specific heat capacity at constant pressure.
c_v	gas specific heat capacity at constant volume.
C	capacitance.
c'	capacitance per unit length.
C	Chapman-Rubesin constant.
C_T	sum of capacitance values in an RC analogue line.
D	diameter.
f	frequency.
G_d	integrated mass flow rate from the shear layer into the separation.
G_{reatt}	reattachment shear layer mass flow rate.
h	heat transfer coefficient.
h	specific enthalpy.
h_o	stagnation value of the specific enthalpy.
H	boundary layer form factor.
i	current.
k	reduced frequency parameter.
k	RC analogue line electrical length.
k	thermal conductivity.
l_i	viscous-inviscid interaction length locally about the separation point.
l	thin film gauge thickness.
L_{sep}	length of separated flow, measured from the hinge line to the separation point.
L_{ds}	length of the dividing streamline.
M	Mach number.
M_R	reattachment Mach number necessary on the dividing streamline.
m_d	mass of separated flow.
n	ratio of momentum thickness just before separation to the momentum thickness just after separation.
n	number of sections in an RC analogue line.
N	reattachment pressure rise parameter.

p static pressure.

Pr Prandtl number.

q dynamic pressure = $1/2\ \rho u^2 = 1/2\ \gamma p M^2$.

q heat flux.

r′ resistance per unit length.

R resistance.

R gas constant.

Re Reynolds number.

R_{in} first resistor element in an RC analogue line.

s Laplace operator.

St Stanton number = $\dfrac{q_s}{\rho_\infty u_\infty c_p (T_{aw} - T_{wall})}$

t time.

T temperature rise in heat conduction theory.

T absolute temperature in flow theory.

T_{wall} wall temperature.

T_{aw} adiabatic (recovery) temperature.

u,v velocity components in x,y directions.

u_{av} average reverse flow velocity.

V volume.

V voltage.

$\bar{V}$ correlation parameter for flat plate leading edge viscous interaction effects on skin friction, and heat transfer = $M_\infty \sqrt{\dfrac{C}{Re_{\infty_x}}}$

w ratio of local stagnation enthalpy to adjacent inviscid flowfield value.

W total incompressible shear layer thickness.

x distance from plate leading edge.

x,y orthogonal coordinate system in analytic flow models,
- x - measured in direction along test model surface, or along the the dividing streamline,
- y - measured normal to test model surface, or normal to the dividing streamline.

x,y orthogonal coordinate system for heat conduction model,
- x - depth below gauge surface,
- y - distance along surface.

x_r distance from the hinge line to the reattachment point.

X,Y transformed flowfield orthogonal coordinate system in an incompressible flow plane.

Z impedance.

α thermal diffusivity = $k/\rho c$

α_R thin film gauge temperature coefficient of resistance = $\frac{1}{R_o}\frac{dR}{dT}$

β Mach number function = $(M^2 - 1)^{1/2}$

β resistance ratio in an RC analogue line = R_{in}/R_1

β_s separation shock wave angle.

γ ratio of gas specific heat capacities = c_p/c_v

δ boundary layer thickness.

δ^* boundary layer displacement thickness.

δ_1 incompressible boundary layer thickness just before separation.

δ_2 incompressible boundary layer thickness just after separation.

δ_3 incompressible boundary layer thickness at end of reattachment process.

δ_l incompressible shear layer thickness below the dividing streamline.

δ_u incompressible shear layer thickness above the dividing streamline.

Δt increment of time.

Δx element of this thickness.

θ momentum thickness.

θ_f flap angle.

θ_s deflection angle of the shear layer at separation.

μ coefficient of viscosity.

ν kinematic coefficient of viscosity.

ρ density.

ρ_R resistivity.

ϕ velocity ratio.

ϕ_r necessary velocity ratio for flow reattachment.

φ acoustic time lag term.

$\bar{\chi}$ viscous interaction parameter = $M_\infty^3 \sqrt{\frac{C}{Re_{\infty_x}}}$

$\bar{\chi}_L$ viscous interaction parameter with Reynolds number based on length L.

ω circular frequency = $2\pi f$.

Subscripts.

1 inviscid flow region above the plate (see Fig.58).

1 thin film resistance gauge material layer.

2 inviscid flow region downstream of the separation point (plateau region) (see Fig.58).

2 substrate material beneath the thin film resistance gauge.

3 inviscid flow region downstream of reattachment (see Fig.58).

a based on speed of sound.

av average value.

d in dead-air region.

ds on dividing streamline.

e at edge of boundary layer.

in input to an RC analogue line.

j evaluated on the dividing streamline in Cooke's analytic model.

l shear layer region below the dividing streamline.

L based on the plate length.

o beginning of the separation interaction.

o initial value of temperature dependent parameters.

o stagnation value.

out measured output voltage.

p wall measurement in the separated flow plateau region.

r at, or, to reattachment point.

s surface.

s at, or, from separation point.

undist. undisturbed value which occurs at the hinge line in the absence of separation.

u shear layer region above the dividing streamline.

wall determined at the model wall.

x at distance x from the plate leading edge.

x at depth x below the surface.

x_o based on length from leading edge to beginning of separation interaction.

∞ freestream values.

Superscripts.

* evaluated at the reference temperature.

– (barred quantities) Laplace transforms.

1. General introduction.

A hypersonic vehicle can experience many regions of flow separation, which might be locally generated by its geometrical features, or by the impingement on its surfaces of shock waves that originate from other parts of its structure. These separations occur when the low momentum fluid contained in a boundary layer is unable to penetrate an adverse pressure gradient, or fails to follow an abrupt drop in the wall geometry. At supersonic, and hypersonic, Mach numbers the separation of a boundary layer is associated with a complex viscous - inviscid coupling of the flow which generates a shock wave - boundary layer interaction.

The separation of flow can represent a significant departure from the inviscid, or ideal, flow model. This must be seriously considered when determining overall vehicle performance, or locally assessing control effectiveness. At high freestream Mach numbers a more important practical consideration is the modification in the surface heat transfer distribution that separation causes. In the hypersonic flight regime the heat fluxes, and surface gradients in heat flux, can be extremely high in flow reattachment regions. In the design of thermal protection systems these levels of local heating must be predicted both in location, and magnitude.

A substantial database of experimental, and theoretical, research has been accumulated over the last 30 years for separated hypersonic flows induced by fixed geometries, or fixed impinging shock waves, in steady flow. A particular example is the trailing edge flap geometry which is a favoured control concept for many types of vehicle. These investigations have collectively covered a wide range of conditions that may be encountered in flight. At high Mach numbers the stability of laminar boundary layers increases substantially, and in the low Reynolds number hypersonic flow regime fully laminar separations may occur. Investigations of these are particularly relevant to re-entry type spacecraft configurations. High Mach number cruise vehicles will encounter much higher Reynolds numbers, and the interactions here will be predominantly turbulent. For the fully laminar interaction case there has been considerable development in modelling the flowfield. It is now possible to numerically solve the full Navier Stokes equations with the potential to accurately predict fully the details, and scale, of hypersonic laminar separated flows. For hypersonic turbulent separated flows the understanding is less complete, although sufficient experimental data has been obtained to apply empirical correlations for some design purposes.

The unsteady development of separated hypersonic flows has received much less attention. Evidence from the available data indicates that the assumption of a quasi-steady flow response to rapid changes in geometry, or freestream flow, based on frequency parameters incorporating freestream velocity, can be incorrect when the flow is separated. Consideration of this may be relevant to a vehicle in unsteady flight, with its many regions of embedded separation, and also during the actuation of control surfaces. In addition to vehicle performance, another concern is the modification to surface heat transfer distributions that may occur within an unsteady separated flow. This aspect has received almost no previous investigation, although it may be potentially the most important in the hypersonic flow regime. Studies of unsteady separated flows are also relevant with respect to aiding the validation of separated flow experiments made in very short duration hypersonic facilities, and for the development of criteria for experimenters that would apply dynamic testing as a means of generating multiple points of data with the assumption that the flow is everywhere quasi-steady.

The objectives of the present work were to determine the adjustment mechanisms contained in the unsteady response of a separated hypersonic flow, induced by a rapidly actuated control surface, and their effects on the surface heating. This is the first recorded experimental investigation of the heat transfer distribution throughout an unsteady separated flow induced by a rapid change in a model geometry. The model configuration selected was a sharp edged flat plate with a trailing edge flap, deflected at velocities approaching 3000 degs./s. This was tested in a short duration hypersonic wind tunnel, operated at a freestream Mach number of 6.85. The freestream Reynolds number was reduced to a minimum in an attempt to obtain fully laminar separated flows, for which the interpretation of mechanisms contained in the dynamic response were expected to be simplest. The principal experimental measurements consisted of surface heat flux distributions along the centre line chord of the plate, and flap. A substantial amount of time was spent by this author in developing suitable high quality instrumentation for this purpose. These measurements were complemented with schlieren flow visualisation of the separated flow structures, and surface thermography using a liquid crystal technique. The separated flow unsteady response was interpreted by comparing the measurements obtained at instantaneous dynamic flap angles with those of the steady separations induced at corresponding fixed flap angles. To support the experimental work, simple analytic models of the unsteady separated flow response were developed, based on separate

fundamental flow adjustment mechanisms.

PART I

LITERATURE REVIEW AND PERSPECTIVE OF THE PRESENT INVESTIGATION.

2. General characteristics of steady separated hypersonic flows.

2.1 Geometries of separation.

The investigation of shock wave - boundary layer interactions has proceeded by concentrating on specific types of model geometry, or incident shock. These have evolved as ideal examples of the variety of interactions that might be generated on a real vehicle (Fig.1). The principal two-dimensional test cases are illustrated in Fig.2. Bogdonoff & Vas (1962) classified the separated flows generated by these geometries into the categories of wedge, cavity, and mixed type. The wedge type includes the ramp, and incident shock, induced separations. In these, neither the separation, or reattachment, points are explicitly fixed by the model geometry, but instead are determined by the local interactions at separation, and reattachment, together with conservation of mass, momentum, and energy within the separation. For the cavity type, both a separation, and reattachment point are explicitly fixed by the wall geometry. This is the only type of separated flow across which there can theoretically be zero change in pressure. The mixed type can be conceived as a combination of the other two, and includes both the forward, and the rearward, facing steps. In these, a separation, or reattachment, point is determined by the wall geometry, while the other extreme of the separated flow is wedge type. The separated flow geometries, and shock structures, for these types of interaction are shown in Fig.2.

For the wedge type, and forward facing step, an adverse pressure gradient originates from the change in wall geometry, or location of the incident shock. The magnitude of this gradient determines whether the approaching flow separates.

If the flow remains unseparated by a compression corner, or incident shock, then the observed shock system is similar to that for an inviscid flow. A pressure rise from the origin of the disturbance is propagated upstream through the subsonic portion of the attached boundary layer, causing it to thicken. The displacement effect of this creates a compression fan in the adjacent supersonic flow, and this in turn imposes a pressure distribution on the boundary layer. This process is a complex mutual interaction which continues until there is an equilibrium between the induced pressure distribution, and the shear forces in the boundary layer. The generated compression waves increase in strength, and reduce their inclination to the freestream, as they are refracted outwards through the supersonic boundary layer region. In the hypersonic flow regime, the compression fan may coalesce

to form a shock before the outer edge of the boundary layer. A single shock wave is observed for an attached flow over a compression corner, and this originates from the corner region. For a flow that remains attached when subjected to an incident shock, there appears a regular reflection of this shock from near the wall.

The peak pressure that can be tolerated before separation is much less for the forward facing step than for the compression corner (Sterrett & Emery 1960), and the flow will separate unless the step height is only a small fraction of the approaching boundary layer thickness. For the rearward facing step, separation is associated with an inability to follow an abrupt drop in geometry, and a breakaway of the flow. This breakaway separation is accompanied by the generation of a Prandtl-Meyer expansion fan.

The limit between attached and separated flow is termed the incipient separation condition. This is defined as a flow in which there exists a single point of zero wall skin friction, being positive at all other locations. If the adverse pressure gradient caused by the change in wall geometry, or incident shock, is increased beyond this, the low momentum fluid in the boundary layer region is unable to penetrate this, and is separated. The flow geometry and shock structure that occurs is a significant departure from the inviscid flow pattern.

For the separated compression corner flow, the separation geometry is similar to a double-wedge configuration (Figs.2 & 3). The first wedge corresponds to an initial turn of the inviscid flow at separation, and the second wedge to the final turn at reattachment. Each process is associated with the generation of a shock wave. The effective displacement surface is formed by the separated flow, and a separated shear layer that divides this from the inviscid region.

The incident shock induced separation is geometrically more complex (Fig.2). A shock wave originates from upstream of where the incident shock would first meet the wall in an inviscid flow. This is induced by the initial deflection of the inviscid flow at separation. Where the incident shock meets the effective displacement surface there occurs an expansion fan. This is created by a constant pressure boundary, due to the inability of weak shear forces within the separated subsonic flow to support a discrete pressure rise. The incident shock, and expansion fan, turn the inviscid flow and free shear layer back towards the wall. This is followed by a final turning of the flow when it reattaches, and turns parallel to the wall, which generates a reattachment shock wave.

Locally, in the region where a boundary layer separates in response to an adverse pressure gradient, there is a mutual viscous-inviscid interaction which generates the separation shock. A pressure rise originates upstream of the separation point, being propagated through the subsonic boundary layer flow. Downstream of the separation point the boundary layer is lifted from the surface, and develops as a separated shear layer. A dividing streamline originates from the separation point, and for steady flow it is this streamline that must reattach (Fig.3). This is a necessary condition for the conservation of mass within a separation region that does not have a continual mass addition, or bleeding.

If the reattachment process is a wedge type, it is the reattachment process that then principally determines the scale of the separation. The flow on the dividing streamline is accelerated by the action of viscosity as the separated shear layer grows. This flow must achieve a sufficient momentum to be just able to overcome the reattachment pressure rise, and reattach. The flow beneath the dividing streamline possesses insufficient momentum to reattach, and is reversed by the pressure rise. This reversed flow will eventually be scavenged by the developing free-shear layer to form a continuously recirculating region of relatively slow flow (Fig.3). Conversely, flow in the shear layer above the dividing streamline is able to continue through the reattachment process, and develop downstream. Shortly after reattachment, the boundary layer develops a local minimum, the neck, before eventually asymptoting to a flat-plate type profile far downstream of the interaction. In the region of a wedge type reattachment, the flow is turned, generating a reattachment shock that originates from the inner edge of the supersonic viscous flow.

In the hypersonic flow regime the Mach wave angle is small. As the compression fans at separation, and reattachment, develop in the supersonic regions of the boundary layer, their inclination to the surface becomes small. This can cause large normal pressure gradients through the boundary layer, in addition to those that occur in the freestream direction. Because of the small shock wave angles in hypersonic flow, the separation, and also possibly the leading edge shock, may intersect with the reattachment shock above the wedge near the model surface. A strong expansion fan originates from this shock-shock interaction, which is directed onto the wedge surface downstream of reattachment.

Although geometrically different, the compression corner, and incident shock, generated separations are very similar (Hankey & Holden 1975). When the

compression corner angle is twice that of the incident shock generator, the interaction strengths caused by these different mechanisms is the same (neglecting viscous interaction effects near leading edges).

There also exist similarities between the forward facing step, and the separation interaction generated upstream of a transverse jet. The former has sometimes been used as a simple model of the jet interaction (Spaid & Cassel 1973).

2.2 Transition.

The location of transition is a very important parameter in the study of separated flows. One of the first sets of experiments to identify this was that of Chapman et. al. (1958) for both subsonic and supersonic separations. It was noted that transition was the single most important parameter that affected both the scale, and the properties of a separation. Subsequently, separated flows were classified according to the location of transition:-

(i) Pure Laminar - a laminar separation, with transition not occurring before the end of the reattachment process.
(ii) Transitional - transition beginning between the separation, and the reattachment points.
(iii) Turbulent - Transition complete, and an equilibrium turbulent boundary layer developed before separation.

Transition Reynolds number increases rapidly with freestream Mach number (see for example Anderson 1989). The consequence of this is that in the hypersonic flow regime there is a practical Reynolds number range where stable fully laminar separation may be experienced.

When transition does occur at high Mach number, then the length of the transition process can be considerable (Holden 1977; Holden 1986). It is thus possible for transition to begin upstream of separation, and for the flow to still be in a state of transition at separation. Although this condition is not explicitly defined by the above categories, it should be classed as a transitional type. The importance of transition on separated flows has been subsequently observed by many experimenters in the hypersonic flow regime (e.g. Sterrett & Holloway 1964; Needham & Stollery 1966b; Hung 1973; Hankey & Holden 1975; Newmann 1987).

Laminar flows are characterised by their weak resistance to separation, and when this does occur the separation scales can be extensive. This is in contrast to turbulent flows, which can withstand far larger pressure gradients

before separating due to the much fuller velocity profile in the inner regions of the approaching boundary layer. Turbulent separations are an order of magnitude smaller than the equivalent laminar separations that would be induced by the same configurations (Korkegi 1971). The separation shock wave originates from deeper within the boundary layer for the turbulent flow. This becomes more firmly embedded within the boundary layer with increasing freestream Mach number, and at very high Mach numbers it is possible for this shock wave to be completely contained within the turbulent boundary layer until it coalesces with the reattachment shock wave (Holden 1972; Holden 1977).

If the freestream Reynolds number is increased, with an initially fully laminar separation, then transition in the separated flow first occurs in the reattachment region. A consequence of this is a significant reduction locally in the x-wise scale of the reattachment process. As the Reynolds number is further increased, the beginning of transition moves forward along the free shear layer until eventually transition is complete ahead of the separation point. Within the transitional separation regime, the separation length is particularly sensitive to changes in freestream Reynolds number, and reduces as this is increased. This is in strong contrast to the behaviour for the adjacent regions of fully laminar, and fully turbulent separated flow (Needham & Stollery 1966b; Lewis et al 1968; Johnson 1970), (see also § 2.5.3).

If the strength of the disturbance inducing separation is increased, with constant freestream conditions, then the transition Reynolds number is reduced. This is observed as a movement of transition location towards the separation point as the separation length increases (Johnson 1970).

The occurrence of transition within the separated flow has been found to introduce a strong unsteadiness (Chapman et al 1958). This self-induced unsteadiness persists with increasing freestream Reynolds number through to the fully turbulent regime, where it is less severe, but still significant. In fully turbulent flows, oscillations of the separation point have been measured of one third the local boundary thickness about a mean position, with frequencies in the range 1 kHz to 10 kHz (Hankey & Holden 1975).

In addition to the scale effects of transition, and the introduction of unsteadiness, there also occur changes in the form of the pressure, and heat transfer distributions (Sterrett & Holloway 1964; Lewis et al 1968; Todisco & Reeves 1969; Johnson 1970; Chpoun 1989), (see also § 2.4). These first occur locally in the region of transition, and persist downstream. The occurrence of transition dramatically increases the peak reattachment heat transfer (Hung

1973; Chpoun 1989). This is a very important consideration in the hypersonic flow regime.

Although laminar flows become more stable with increasing freestream Mach number, the separation of flow is a highly disturbing process, and can create an effective boundary layer trip. Transition Reynolds numbers in free shear layers are typically an order of magnitude less than those for attached flat plate boundary layers (Johnson 1970; Newmann 1987).

The transitional regime of separations is the most difficult to define precisely. Correlation of data from these experiments is difficult (e.g. Roberts 1970). The development of successful analytical or numerical theories to compare with transitional separation experiments, free from semi-empirical input, have not been developed. For these reasons, most experimenters have the objective of examining the characteristics of fully laminar, or fully turbulent, separated flows. This requires a careful examination of experimental data to determine that it is free from transitional effects. Both fully laminar, and fully turbulent, separated flows are difficult to achieve experimentally. For the fully laminar separated flows, a combination of low Reynolds number and high freestream Mach number are required. These experiments must be thoroughly scrutinised to discount transition effects in the reattachment region. For the fully turbulent separations it is often difficult to achieve an equilibrium turbulent boundary layer ahead of separation. This is because of the combination of severe model scale restrictions, usually imposed in hypersonic test facilities, and the limit of freestream Reynolds number that can be generated. Some experimenters have used artificial techniques to overcome this problem. These include the use of boundary layer trips, and tunnel wall boundary layers. A comparison of the results using these different artificial methods has led to some controversy (see § 2.5.3). The number of experiments that have successfully achieved natural flat plate transition to fully developed equilibrium turbulent boundary layers well ahead of the interaction on mounted models is few (e.g. Holden 1977).

The undetected influence of transition in assumed fully laminar, and fully turbulent, separated flows has led to incorrect conclusions, and problems of correlation. It is therefore very important to detect if transition is present. Several methods have been proposed for this:-

(i) The variation of separation length with freestream Reynolds number - A separated flow is transitional if it exhibits a strong trend of the separation

length reducing with increasing freestream Reynolds number, while maintaining the other dependent parameters constant (Needham & Stollery 1966b; Lewis et al 1968; Johnson 1970). The application of this technique requires the ability to independently vary the freestream Reynolds number in sufficiently small increments to give an accurate determination of the separation length trends about the condition of interest. A difficulty in applying this method is the accurate location of the separation, and reattachment, points. Often these are inferred from flow visualisation techniques such as schlieren, but this is not precise in determining these positions.

(ii) Flow visualisation. - Some investigators have inferred the location of transition from the optical flow visualisation techniques of shadowgraph, and schlieren, which observe spatial derivatives of density variations in the flowfield. A particular change in appearance of the free shear layer is associated with the onset of transition. For the shadowgraphs this is the termination, or convergence towards the surface, of the white line characteristic of a laminar boundary layer that first develops adjacent to the model surface (Chapman et al 1958). With the schlieren flow visualisation, transition is accompanied by the occurrence of fuzziness in the free shear layer, and the appearance of weak waves originating from this region (Johnson 1970). A local deflection of the free shear has also been used as a criterion for transition location (Gray 1964). At high Mach numbers the transition length increases, and the observed changes in the character of the free shear layer accompanying transition become less abrupt than in supersonic flow. Indications of the transition location derived from these flow visualisation techniques at high Mach number then tend to be nearer the end of the transition region (Potter & Whitfield 1960; Johnson 1970), and less pronounced. If transition occurs near the end of the reattachment process, then the above criteria for detecting transition would be obscured by the strong density variations occurring with recompression of the free shear layer.

(iii) Pressure Distribution - The location of transition has been found often to correlate with an abrupt rise in pressure (Chapman et al 1958). This is not always the case, and conversely, an abrupt pressure rise does not always indicate transition. This rise becomes less distinct with increasing freestream Mach number. If transition is in the region of reattachment, then the pressure rise associated with transition is obscured by the reattachment pressure rise.

Chapman (1958) measured a pressure in the separated flow (plateau pressure), and found that a change in the dependence of this parameter with freestream Reynolds number accompanied the change from a pure laminar to transitional flow regime. This criterion was modified by Ginoux (1969a) who instead measured a pressure in the separation, and reattachment regions. In these there exists a trend reversal of pressure variation with Reynolds number following the onset of transition. This is a more sensitive detector than a measure of the change in dead air pressure.

(iv) Heat Transfer - Transition in the free shear layer is accompanied by a local rise in wall heat transfer below this region, analogous to flat plate boundary layer transition (Sterrett & Holloway 1964; Todisco & Reeves 1969; Johnson 1970; Chpoun 1989). Sterrett & Holloway (1964) observed this rise to occur from a value less than the attached flat plate heat transfer to a value above (see § 2.4.2). If transition is in the reattachment region then any local rise in heat transfer is obscured by the very high heat transfer gradients that always prevail in this region.

Transition has the effect of greatly increasing the peak reattachment heat transfer (Sterrett & Holloway 1964; Johnson 1970; Hung 1973; Chpoun 1989). This peak value is very sensitive to Reynolds number variation in the transitional regime (Hung 1973), which provides another indication of transition onset.

(v) Noisy Signals - The transition from laminar to turbulent flow is associated with the onset of flow unsteadiness, which is observed as flow noise on recorded signals within the separated flow on the model surface (Lewis et al 1968; Batham 1972).

2.3 Free-interaction.

Experimenters in the supersonic flow regime were first to observe that the flowfield locally at a wedge type separation was independent of the downstream disturbance, provided a sufficiently large separation existed. This was termed by Chapman et al (1958) as a free-interaction, the process of which was determined by the interaction between local inviscid, and viscous flows. A simple order of magnitude analysis was developed by Chapman et al using this concept of a coupled interaction. The boundary layer equation was applied at the wall, and the linearised equation of supersonic flow was used for the adjacent inviscid flow. The analysis was equally applicable to laminar, and turbulent, separations, and led to the derivation of correlation equations for

the pressure rise through the interaction, and also the local length scale of the separation process.

$$\frac{p - p_o}{q_o} \propto \frac{\sqrt{c_{fo}}}{(M_o^2 - 1)^{1/4}} \tag{1}$$

$$\frac{l_i}{\delta^*} \propto \frac{1}{\sqrt{c_{fo}}\ (M_o^2 - 1)^{1/4}} \tag{2}$$

Chapman et al compared these equations with adiabatic experimental data generated with wedges, incident shocks, curved compression surfaces, and forward facing steps, over a Mach number range from near unity to 3.6. Specifically, the separation point, and plateau pressure rises (if existing, see § 2.4.1) were compared with the trends predicted by these equations. Simple incompressible relationships for laminar, and turbulent, skin friction coefficients were used. These particular pressure rises have been used by many later experimenters as a test for free-interaction.

The most important aspect of Chapman et al's analysis was to stress the mutual interaction between the viscous, and inviscid, flows. This concept has formed the principal component of successful subsequent models of laminar boundary layer separation (see § 2.8).

Chapman et al found that for the laminar separations, the separation pressure rise, and the pressure rise to the plateau were correlated correctly with Mach number, and Reynolds number, by this theory. A scaling of the data with parameters for pressure rise, and interaction length, produced a single curve up to the plateau region. This clearly demonstrated that such separations were locally free.

For the turbulent separations, a scaling of the data showed that the pressure rise up to the separation point was free, but the pressure rise following this appeared to exhibit a dependence on the particular geometry inducing the separation. The only turbulent separations that exhibited a well defined plateau were those induced by forward facing steps. The simple order of magnitude analysis predicted the correct dependence of the separation pressure rise on Mach number, and Reynolds number.

The agreement of Chapman et al's theory with their experiments was surprisingly good over a large Mach number range, considering the number of simplifying assumptions used. No precise definition was given in this work of

the required scale of separation such that the local interaction would be free. For the laminar separations a qualitative criterion that a well defined plateau pressure should exist was used.

Correlation equations for pressure rises in free-interactions have been derived subsequently in other work. These analyses have had varying degrees of complexity, but the derived equations generally have a similar dependence on freestream flow properties, and skin friction, as has the simple analysis of Chapman et al, (e.g. Hakkinen et al 1959; Erdos & Pallone 1962). Erdos & Pallone (1962) also used an order of magnitude analysis, but introduced the concept of universal scaling functions. In this way they also accounted for normal pressure gradients in the boundary layer. The effect of wall temperature was assumed to be accounted for in the skin friction term. This analysis obtained the same form of equations as Chapman et al, and in fact used Chapman et al's experimental data to obtain the constant in their equation for the separation, and plateau, pressure rises.

Correlations of this type have been used by many subsequent investigators for laminar separations, collectively covering a large Mach number range (e.g. Sterrett & Emery 1960; Miller et al 1964; Putnam 1965; Needham & Stollery 1966b; Hoelmer 1967; Lewis et al 1968; Harvey 1968). Although these theoretical considerations suggest the dependent parameters, the constants are often derived empirically from each experiment. The free interaction theory has sometimes been used as a guide for establishing other empirical correlation laws. For example, Needham & Stollery (1966b) were able to correlate plateau pressures from a large number of previous experiments with the equation,

$$\frac{p_p - p_o}{q_o} = \frac{3\sqrt{c_{fo}}}{M_o^{3/4}} \qquad (3)$$

This covered an extensive Mach number range, $2 \leq M_o \leq 16$, and included the geometries of incident shock, wedge, and forward facing steps. The success of such correlations further support the concept of free interactions in separated laminar hypersonic flows, which have the additional influence from upstream of a strong leading edge viscous interaction.

Lewis et al (1968) noted some of the inadequacies in the assumptions with the simple analysis of Chapman et. al. (1958) when applied to hypersonic flows. A particular example was the use of the linearised supersonic flow equation. By replacing this with a second order analysis they demonstrated an

additional dependence of such correlations on the viscous interaction parameter.

An important effect of wall temperature was also demonstrated by Lewis et al (1968) when they attempted to use Chapman et al's (1958) scaling parameters for both cooled wall, and adiabatic, separated hypersonic laminar flows. Although this analysis correctly correlated the level of pressures for both temperature limits, the scaling of the interaction length was inadequate. The effect of wall cooling reduced the scaled interaction length. This discrepancy was solved by rescaling the data with additional parameters suggested by Curle (1961).

For turbulent separations the degree of free interaction is less clear. Chapman et al (1958) found a free interaction only up to the separation point, although the degree of similarity downstream of this point increased with increasing freestream Mach number. However, some experimenters have found a free-interaction downstream of separation to a plateau level, where the separation is sufficiently large to develop such a region (Bogdonoff & Kepler 1955; Holden 1972; Holden 1977). Holden (1977) was able to correlate the turbulent plateau pressure rise from a number of independent experiments using different geometries, covering a Mach number range from 2.3 to 13. However, Holden (see Hankey & Holden 1975) earlier noted that at very high Mach numbers, where the length of interaction is small compared with the initial boundary layer thickness, there appears to be a dependence of the pressure distribution in the separated flow on the particular geometry inducing the separation. The conditions for the occurrence of a free-interaction plateau pressure in turbulent separations are therefore not clearly defined.

2.4 Surface measurements in compression corner interactions downstream of sharp edged flat plates.

2.4.1 Pressure distributions.

The undisturbed pressure distribution on a flat plate in hypersonic flow is determined by the strength of a viscous interaction in the leading edge region, which can be considerable in high Mach number, low Reynolds number flows (see § 11 & 13.1). This creates local increases in the flat plate pressure distribution towards the leading edge. The pressure distribution then asymptotes towards the undisturbed freestream static pressure as the distance downstream of the leading edge is increased.

When the compression corner interaction strength is insufficient to

separate a laminar boundary layer, the wall pressure begins to rise a little upstream of the hinge line. The pressure continues to rise downstream of this, and reaches a level near the inviscid wedge value. As the Mach number is increased, the upstream influence ahead of the corner reduces considerably, and the rise in pressure is displaced further downstream along the wedge surface (Needham 1965a; Hankey & Holden 1975; Holden 1978).

As the interaction strength is increased for laminar flows, both the upstream influence, and the pressure level attained on the wedge surface, increase. If the interaction strength exceeds the incipient separation pressure rise, then the pressure distribution develops a kink (knee) in its profile. With further increase in the interaction strength, this knee broadens out, and if the separation is sufficiently large this develops into a constant pressure plateau region in which an approximately straight shear-layer develops. Typical forms of pressure distributions are illustrated in Fig.4. The initial pressure rise, above the undisturbed flat plate value, starts at the beginning of the viscous-inviscid interaction, which is ahead of the separation point. This rise continues through the separation point to the plateau pressure, or to a region of reduced pressure gradient if no plateau region has developed in the distribution. Downstream of this, near the corner, the pressure begins to rise steeply as the reattachment process commences. The pressure rises through the reattachment point, and continues to a peak before falling to a value near the inviscid wedge pressure level. The rise in pressure to a value in excess of the single shock inviscid wedge solution is associated with the compression of the flow through a multiple shock system, which is a more efficient compression process. The strong expansion wave, which is directed onto the wedge from the separation shock - reattachment shock interaction, reduces the peak pressure to a value near the inviscid wedge solution.

The change in character of the pressure distribution as the flow separates becomes abrupt as the freestream Mach number is increased to very high values (Holden 1978). This is in contrast to supersonic, and low hypersonic, flows where this change is more gradual.

Comparisons of the pressure distributions in laminar separations with other flow measurements, such as visualisation of flow structures, pitot traverses, and measured skin friction distributions, have been used to locate the separation, and reattachment, points on the pressure profile. The separation point has often been identified with the first inflexion point in the pressure rise to the plateau level (e.g. Needham 1965a; Chpoun 1989). At

higher Mach numbers, Holden (1971a) found the separation point was just downstream of this inflexion point, at 0.6 of the pressure rise to the plateau level. The reattachment point has been located as a fraction of the pressure rise from the plateau level to the peak pressure. Holden (1971a) found a value of 0.6 for this parameter, which compared with a value of 0.37 found earlier by Needham (1965a) at lower freestream Mach numbers.

When the approaching boundary layer is fully turbulent there is practically no upstream influence ahead of the wedge corner when the flow remains attached. For well separated turbulent flows, the pressure distribution exhibits the same general features that evolve for a laminar separation, but extending over a smaller scale (Holden 1972; Batham 1972; Elfstrom 1972). The pressure rise to the plateau is much higher (typically by a factor of 5, Delery & Marvin 1986), and the gradients in the separation, and reattachment regions, are greater than for equivalent laminar flows. These differences are associated with the increased resistance of turbulent boundary layers to separation. The smaller scales of turbulent separated flows are often insufficient to develop a plateau region. The peak pressures in turbulent separations, following reattachment, can be very pronounced (Elfstrom 1972; Coleman & Stollery 1972).

If transition occurs in the free shear layer, the pressure gradient at reattachment increases from the laminar value, and the pressure overshoot following reattachment also increases (e.g. Lewis et al 1968). If transition occurs sufficiently upstream of the reattachment process, then a discrete pressure rise may be observed within the pressure distribution (Chpoun 1989). This is caused by a local thickening of the free shear that accompanies transition, which deflects the adjacent inviscid flow. The transition process becomes less discrete as the freestream Mach number is increased, and distinct local pressure rises become more difficult to discern.

Kuehn (1959) used the changes that occur in the character of the pressure distribution as the flow separates as a criterion for determining the laminar incipient separation condition. The occurrence of incipient separation is accompanied by the onset of three inflexion points (a knee) in the pressure profile. This has been used by many other investigators as an incipient separation criterion for laminar flows, spanning a large Mach number range (e.g. Sterrett & Emery 1960; Needham 1965a; Hankey & Holden 1975). Holden (1978) compared the application of this criterion with direct measurements of the skin friction distribution, and found that this could be inaccurate at very high Mach numbers. In these flows it is possible for a small region of

separated flow to first develop before an apparent change in the form of the pressure distribution was observed.

The application of this criterion for determining incipient separation of turbulent boundary layers has been critisised as inaccurate for both supersonic, and hypersonic flows (Green 1970; Holden 1972; Elfstrom 1972; Spaid & Frishnett 1972). Elfstrom (1972) proposed an incipient separation criterion for turbulent separations based on the development of a pressure overshoot following reattachment.

2.4.2 Heat transfer distributions.

For attached laminar flows at moderate hypersonic Mach numbers, the heat transfer starts to dip below flat plate values ahead of the hinge line as the boundary layer is thickened by the adverse pressure gradient (Holden 1966a). A minimum value of heat transfer occurs near the hinge line, which is followed by a rise along the wedge to a maximum value as the boundary layer is thinned, and its density increased, by the compression process. As the freestream Mach number is increased, the upstream influence diminishes. At very high Mach numbers, the influence of the interaction on the flat plate heat transfer distribution ahead of the hinge line may be negligible, until the incipient separation condition is approached (Holden 1966b; Holden 1967; Holden 1978). Attached laminar flows then display a minimum heat transfer near the hinge line which is cusp like in form (Needham 1965b; Holden 1966a; Holden 1966b; Holden 1967).

When the interaction strength is sufficient to induce a laminar separation, the form of the heat transfer distribution changes. Typical forms of heat transfer distributions are shown in Fig.4. The heat transfer begins to fall at the beginning of the interaction, upstream of the separation point. The cusp-like minimum heat transfer profile, typical of attached laminar flows, changes to a rounded concave form (Needham 1965b; Holden 1966a; Holden 1967; Holden 1978). The heat transfer begins to rise within the separated flow, ahead of the hinge line, and on the wedge there is a rapid increase to a pronounced peak value. The location of the maximum heat transfer is at the neck of the reattaching boundary layer, which is downstream of the reattachment point (Holden 1966a; Holden 1967; Holden 1978).

The very high heating that is experienced with reattachment makes this region the most important from a practical viewpoint in studies of the heat transfer characteristics of separated hypersonic flows.

As the wedge angle is increased, the minimum heat transfer reduces, and

there is a considerable increase in the heat transfer in the reattachment region. The distance between the point of maximum heat transfer and the reattachment point then reduces (Holden 1966a).

Miller et. al. (1964) observed a slight rise in heat transfer upstream of a laminar separation, and a sinusoidal rise in heat transfer to the hinge line from the minimum value in the separated flow. These characteristics have not been found in subsequent investigations of laminar separation heat transfer.

The change in the form of the minimum heat transfer as a laminar flow separates, from a cusp-like minimum to a rounded concave distribution, was used as a criterion for incipient separation by Needham (1965b). However, Holden (1978) found that this criterion was difficult to apply with accuracy at very high freestream Mach numbers.

Several investigators have noted the effects of transition on the heat transfer distributions in separated hypersonic flows (e.g. Sterrett & Holloway 1964; Kaufman et al 1966; Todisco & Reeves 1969; Johnson 1970; Simeonides & Wendt 1991). In the region of transition there is a local rise in heat transfer, which is a departure from the rounded minimum distribution observed for fully laminar separations. Sterrett & Holloway (1964) found that this rise could be abrupt, and their measurements in separations induced by forward facing steps gave,

$$\frac{q_{\text{AVERAGE. SEP.}}}{q_{\text{AV. FLAT PLATE}}} = 0.52 \text{ (laminar), } 2.55 \text{ (transitional)} \qquad (4)$$

If transition occurs near the separation point, then there may not exist an initial drop in heat transfer typical of a laminar separation, but instead, a continuous rise through the separated flow (Todisco & Reeves 1969). Conversely, if transition occurs near reattachment, then its local effects are obscured by the high heat transfer gradients that always exist in this region. Transition causes a dramatic increase of the heat transfer in the reattachment region (e.g. Chpoun 1989).

If the approaching boundary layer is fully turbulent, then for attached flows there is almost no upstream influence on the flat plate heat transfer distribution ahead of the hinge line (Holden 1972; Coleman & Stollery 1972; Holden 1977). The heat transfer increases steadily along the wedge surface as the flow is compressed.

When the turbulent boundary layer separates, then in complete contrast to the laminar separation, the heat transfer increases abruptly in the

interaction region at separation (Holden 1972; Coleman & Stollery 1972; Zakkay & Paolo 1975; Holden 1977). If the separation is sufficiently large, then there is a plateau region of heat transfer which exists following the initial rise. The pressure and the heat transfer distributions are very similar in regions of turbulent separation, and Holden (1972) found that their respective plateau values could be correlated by the equation,

$$\frac{St_p}{St_o} = \left\{\frac{p_p}{p_o}\right\}^{5/8} \tag{5}$$

The heat transfer rises very rapidly in the reattachment region to a peak value, followed by a drop towards the wedge trailing edge. The turbulent reattachment peak heat transfer can be very high, for example, Coleman & Stollery (1972) measured values in excess of those for two-dimensional stagnation point heating. These very high reattachment heat transfer rates correspond to large pressure overshoots that exist in the reattachment regions of turbulent separations (Coleman & Stollery 1972).

Coleman & Stollery (1972) proposed a heat transfer criterion for turbulent separation based on the abrupt rise in heat transfer that occurs just ahead of the hinge line when the flow separates.

The importance of the peak reattachment heat transfer in separated hypersonic flows has led to attempts at simple engineering correlations of its value. Bushnell & Weinstein (1968) presented correlations for laminar, and turbulent, separations. The parameters for these were derived by assuming that a viscous sublayer developed from the reattachment point, which was relatively insensitive to pressure gradients. This concept was first introduced by Holden (1964). The correlation was applied to a range of experimental data in the hypersonic regime. Further support for this correlation was later produced by Matthews & Ginoux (1974) with their theoretical data. A disadvantage of this technique is the requirement for details of the separated flow geometry, and its sensitivity to errors in measuring, or predicting these dimensions, and angles (Zakkay & Paolo 1975).

Measurements of pressure and heat transfer in both laminar, and turbulent, wedge separations have led to correlations of peak heating as a function of the measured, or inviscid, pressure levels (e.g. Hung 1973; Hung & Barnett 1973; Hankey & Holden 1975; Hung & Greenschlag 1976). This includes both the compression corner, and the incident shock, interactions for which

the mechanism of peak heating is the same. The form of these generally incorporates a ratio of peak heating to the undisturbed value, at the hinge line, in the absence of an interaction,

$$\frac{q_{peak}}{q_o} = \left\{\frac{p_{peak}}{p_o}\right\}^{n}_{MEASURED} \quad \text{or} \quad \frac{h_{peak}}{h_{undist.}} = \left\{\frac{p_3}{p_1}\right\}^{n'}_{\substack{INVISCID\ WEDGE \\ PRESSURE\ RISE.}} \tag{6}$$

Correlations of this type usually work well for fully turbulent separations, with values of the exponent differing little between independent experiments (see table 1). These correlations are less successful for laminar separations, and there is a wide scatter in the exponents obtained from different references (see table 1). This scatter has been partly attributed to the undetected influence of transition in some experiments. Hung (1973) extensively reviewed these correlations, and presented revised forms for a laminar separation, with either laminar, turbulent, or transitional reattachment. The greatest increase in heating, expressed as a ratio to the undisturbed heat transfer, exists for transitional separations. i.e. separations that prematurely induce transition that would otherwise be absent for an undisturbed flow.

An alternative correlation form has been developed based on the flow properties downstream of the interaction (Hung 1973; Hung & Greenschlag 1976). This removes the explicit dependence on the pressure rise through the interaction.

$$\left[\frac{St_{Peak}}{St_{undist.}}\right]_{\substack{Based\ on \\ downstream \\ flow\ conditions.}} = \text{Constant.} \tag{7}$$

These correlations have been developed for laminar, transitional, and turbulent separations.

2.5 Effects on the scale of separation.

2.5.1 Flap angle.

The beginning of the separation interaction, and hence the scale of separated flow, is affected significantly if the flap deflection angle is varied, while

holding other geometry and flow parameters constant. Once a flow has been separated, the reattachment process principally determines the scale of separation (Needham & Stollery 1966b). The basic driving mechanism for this is the pressure rise to reattachment, and this increases as the flap angle is increased. Thus, for an established separated flow, increasing the flap angle increases the scale of separation.

Various forms for this basic driving mechanism have been incorporated in simple analytic models which predict the separation length, and in correlations of this length with other parameters (e.g. Chapman et al 1958; Needham & Stollery 1966b; Hakkinen et al 1959; Erdos & Pallone 1962; Putnam 1965). The basic driving mechanism has variously been expressed as,

$$p_{\text{PEAK, FINAL, or INVISCID WEDGE.}} \quad - \quad p_{\text{INCIP., PLATEAU, or UNDISTURBED.}} \tag{8}$$

2.5.2 Freestream Mach number.

For both fully laminar, and fully turbulent, flows experiments have shown that the effect of increasing freestream Mach number, while maintaining a constant wedge angle and freestream Reynolds number, is to reduce the separation length (e.g. Miller et al 1964; Holden 1967; Holden 1972; Elfstrom 1972; Hankey & Holden 1975; Holden 1977), and this is a strong influence. When the separated flow is transitional, then the effect of increasing freestream Mach number is to delay transition in the free shear layer. This would be expected to be a dominant effect, so that the separation length then increases as the Mach number is increased. This variation was observed in the experiments of Kaufman et al (1966), which are believed to be transitional.

Changes in the freestream Mach number affect the plateau pressure rise, the reattachment pressure rise, and the gradients of pressure rise in these regions. The development of the separated shear layer mixing region is also influenced by changes in local Mach number. Statements such as "The Mach number effect may at first appear surprising. It is due however to the greatly increased plateau pressure rise associated with higher Mach numbers" (Wilkinson 1966) are only a partial explanation of the Mach number dependence.

The effects of increasing the freestream Mach number have been found experimentally to increase the incipient separation wedge angle for both laminar and turbulent flows (e.g. Roshko & Thomke 1969; Hankey & Holden 1975).

2.5.3 Freestream Reynolds number.

The effects of Reynolds number on the scale of separation, with constant freestream Mach number and fixed model geometry, have been investigated extensively.

For fully laminar separations it is now generally accepted that increasing freestream Reynolds number increases the scale of separation (Miller et al 1964; Needham & Stollery 1966b; Holden 1967; Lewis et al 1968; Harvey 1968; Hankey & Holden 1975). The Reynolds number influence on laminar separations has frequently been explained through its effect of changing the plateau pressure, and consequently the pressure rise to reattachment (e.g. Miller et al 1964; Needham 1965a). However, there is also an influence of local Reynolds number on the pressure gradients, and on the development of the separated shear layer. The theoretical results of Lees & Reeves (1964) show that the effect of increasing the freestream Reynolds number is to increase the required velocity on the dividing streamline to overcome a given pressure rise to reattach. i.e. a larger length of separated flow is required ahead of the reattachment process to accelerate the fluid on the dividing streamline to a higher velocity as the freestream Reynolds number is increased.

In the transitional regime, the effect of increasing the Reynolds number is to promote transition earlier in the free shear layer. This energising of the separated flow allows the reattachment process to be overcome with a shorter separation length. Thus, increasing the freestream Reynolds number in the transitional regime reduces the separation length, and the sensitivity to changes in freestream Reynolds number is much greater than that in the fully laminar, and fully turbulent, flow regimes (Chapman et al 1958; Kaufman et al 1966; Todisco & Reeves 1969; Johnson 1970). Some investigators have attributed apparent contradictions in the observed variation of laminar separation length with freestream Reynolds number to the undetected influence of transition in separations that were thought purely laminar.

The dependence of fully turbulent separations on freestream Reynolds number is still not fully resolved. The difficulty of achieving natural transition at high freestream Mach number on mounted models, within the restrictions of scale and freestream Reynolds number capability, has led to the application of different experimental techniques to produce a turbulent boundary layer ahead of the separation interaction. These have included the use of tunnel wall boundary layers for experiments (Hammitt & Hight 1959; Roshko & Thomke 1969; see also the review by Green 1970), and the use of boundary layer trips on mounted models (Chapman et al 1958; Kuehn 1959).

Boundary layers at high Mach number are very difficult to trip, and experiments that have attempted to do this may not have had fully turbulent boundary layers in the interaction region.

Experiments that used the tunnel wall boundary layer generally indicated the effect of increasing freestream Reynolds number was to reduce the length of separated flow. However, comparisons of experiments in different facilities, under nominally identical conditions, have produced different results, suggesting that the combination of particular tunnel wall, and model, was an important parameter (Holden 1972). Experiments on mounted models have generally been at much lower absolute Reynolds numbers, based on local boundary layer thickness, and these experiments have indicated an opposite influence of freestream Reynolds number (e.g. Chapman et al 1958; Kuehn 1959; Sterrett & Emery 1960; Todisco & Reeves 1969; Batham 1972; Elfstrom 1972; Coleman & Stollery 1972; Holden 1972; Zakkay & Paolo 1975).

The number of experiments that have been able to produce local Reynolds numbers, based on boundary layer thickness, on mounted models, which are comparable to the experiments on tunnel walls, has been very few. An example was an investigation by Holden (1977) to determine whether the value of absolute Reynolds number was responsible for this difference in the dependence of separation length with freestream Reynolds number. A reversal of dependence was indeed found within the expected range of absolute Reynolds number. This change has been attributed to a change in the structure of the turbulent boundary layer as the Reynolds number is increased in this regime. The more recent experiments of Disimile & Scaggs (1989) investigated freestream Reynolds number effects on a mounted model at conditions comparable to the wall measurements of Todisco & Reeves (1969). The effect of freestream Reynolds number appeared negligible, contradicting the results of Todisco & Reeves, and Disimile & Scaggs concluded that a critical state in the Reynolds number dependence had been achieved.

Although the Reynolds number dependence of fully turbulent separations has still not been fully explained, the various observed effects are generally much weaker than the Reynolds number influence on fully laminar separations (Korkegi 1971).

When the effect of increasing the freestream Reynolds number has been to increase the length of separation, then its effect on the wedge angle for incipient separation, when observed in the same experiment, has been to reduce this.

2.6 Three-dimensional influences in nominally two-dimensional experiments.

All nominally two-dimensional experiments are subject to three-dimensional influences. An important consideration in this respect is the model aspect ratio, or, the aspect ratio based on the separation length and model span. Increasing these reduces the influence of end effects, particularly lateral venting, on the region of flow about the centre line.

Lateral venting is an outflow induced by the pressure differential between the separated flow, and the flow adjacent to the model edges in this region. The effect of this continual outflow is to reduce the separation length below the true two-dimensional value (e.g. Holden 1971a), and for fixed model dimensions, this becomes more significant as the separation length increases.

A technique which has often been applied to prevent lateral outflow is the application of side plates. These plates are fixed at the model edges, and contain the separated flow. However, these have been found to introduce other three-dimensional effects which can increase the separation length (e.g. Popinski & Ehlrich 1966; Lewis et al 1968). A solution that has been proposed to obtain two-dimensional distributions is to systematically increase the model aspect ratio until a change in the edge condition, for example applying side plates, has no effect on the distribution of separation properties in the centre line region (Holden 1967; Lewis et al 1968). The flow about the centre line is then considered to be the correct two-dimensional phenomenon. However, Rudy et al (1991) found that a comparison of experimental measurements obtained in this way with numerical predictions compared poorly assuming two-dimensional flow, but had excellent agreement with a three-dimensional computation allowing for edge effects. If confidence is placed in these particular numerical results, then the question is raised as to whether it is possible to practically obtain truly two-dimensional experimental data.

It is important to note that measuring locally two-dimensional distributions about the centre line, with no test of end effects, is not a sufficient condition to define that these end effects have no influence in the centre line region (Holden 1967; Lewis et al 1968).

Other edge effects, which originate from the corners of the plate leading edge, are the generation of vortices and Mach cones. In these regions, a pressure differential between the upper and lower surfaces causes a flow around the longitudinal edges of the plate. The vortices that this generates are shed downstream, and are contained within the Mach cones. These disturbances can have a strong local effect on the character of the downstream

separated flow (Popinski & Ehlrich 1966). Disturbances of this type are minimised with a large model aspect ratio, and/or the application of skirts attached to the model sides, which prevent flow between the upper and lower surfaces.

Surface flow visualisation, and quantitative measurements of pressure, and heat transfer, in reattachment regions of separated high speed flows have revealed the existence of spanwise spatially periodic variations of flow properties (e.g. Miller et al 1964; Ginoux 1969b; Kipp & Helms 1985; Simeonides & Wendt 1991). These variations have been identified with the existence of streamwise counter-rotating vortices within the reattaching boundary layer. It has been proposed that these originate from disturbances created initially at model leading edges, which are then selectively amplified through the separated flow (Ginoux 1969b). The local curvature in the reattachment region is sufficient to support the hypothesis that the method of generation is similar to that for Görtler vortices on concave walls (Miller et al 1964). The effect of these vortical structures on the mean separated flow properties is small if the freestream Reynolds number is sufficiently low, but they can have a destabilising influence that tends to promote transition (Ginoux 1969b). The existence of these vortices has been observed to persist in both transitional, and fully turbulent reattaching flows (Kipp & Helms 1985; East & Smith 1993), where their characteristic wavelength is reduced. A particularly important consideration is the enhanced heating effect, with attendant very high heat transfer gradients, these vortices produce as observed from surface thermographs (e.g. East & Smith 1991; East & Smith 1993).

These spanwise variations can be a source of error if discrete single spanwise measurements are made in the reattachment region, which may coincide with a local maximum or minimum value.

2.7 Relationship of experiments to a real hypersonic vehicle.

The experiments that have been described are ideal test cases, free from many of the influences that would be encountered by control surfaces on a hypersonic vehicle. For example, actual controls do not experience a clean freestream flow, but are immersed in a local inviscid, and viscous, flow that is created by the upstream geometry of the parent vehicle. Practical considerations will also influence the design of hypersonic controls, and their integration within a vehicle. These influences have been considered experimentally by examining the effect of each such influence individually on

the ideal model. A few examples include: Leading edge bluntness (Holden 1971a), Finite span effects (Putnam 1965), Finite flap chord effects (Ball 1969a), Hinge line bleed (Ball 1969a; Ball & Korkegi 1968), and Wall cooling (Lewis et al 1968).

2.8 The development of theoretical models of shock wave - boundary layer interaction.

The development of methods for predicting regions of separated supersonic, and hypersonic, flow have been reviewed extensively in the literature (e.g. Chilcott 1967; Holden 1967; Murphy 1969; Charwat 1970; Hankey & Holden 1975; Adamson & Messiter 1980; etc), and only a very brief description is included in this section. One of the most significant early contributions to this problem was the work of Crocco & Lees (1952). Their numerical solution of the free-interaction between a laminar boundary layer, and the adjacent external flow, incorporated the use of velocity profiles with a form characterised by a free parameter that was determined as part of the solution. This parameter, which allowed for the description of reverse flow velocity profiles, was a semi-empirical term based on the rate of mass entrainment from the external flow. This semi-empirical weakness of the Crocco-Lees theory was later removed, and a self consistent model developed, through the work of Tani (1954), Honda (1958), Abbott et al (1962), and Lees & Reeves (1964) (see Hankey & Holden 1975). The analysis of Lees & Reeves (1964) was the first capable of accurately predicting the size and properties of a shock-induced laminar separated flow (over an adiabatic wall) at moderate supersonic freestream Mach numbers, without the requirement for semi-empirical input. Holden (1967) extended this theory to include the simultaneous solution of the laminar boundary layer energy equation, which then allowed for the prediction of heat transfer to cooled walls in hypersonic freestream flows. A further improvement by Holden (1970) (see Holden & Moselle 1970) was the inclusion of the normal pressure gradient term across the interacting boundary layer. This model was able to avoid the use of an artificial condition in the numerical solution that had been previously required called the supercritical - subcritical jump.

With the advent of more powerful computing facilities, numerical solutions of the full Navier Stokes equations for the complete flowfield became possible (e.g. Hung & MacCormack 1976), avoiding the simplifying assumptions implicit in the boundary layer equations, and the method of coupling these to the external inviscid flow. Rapid progress has occurred in

this field of computational fluid dynamics (CFD) for both laminar, and turbulent, shock wave - boundary layer interactions, for which an endless list of references could now be supplied. The use of CFD codes requires very thorough validation before they can be generally applied for the prediction of flowfields (e.g. Rudy et al 1991), and then only within the bounds of validation. This requirement is now a useful stimulus for demanding very high quality experimental measurements, with precisely defined freestream flows, and model boundary conditions.

3. Review of unsteady separated flows.

The accumulated past research on the subject of the dynamic response of separated hypersonic flows is very limited. It is, however, sufficient to indicate that when regions of separation occur, the usual assumption of a quasi-steady response of hypersonic flows over rapidly displaced surfaces may be incorrect (Wilkinson 1966; Roberts 1989). Related to this subject are studies of the establishment processes of separated flows in nominally steady state experiments, and the adjustment mechanisms of separated flows to rapid transients in freestream flow conditions, both of which are additionally reviewed in this chapter.

3.1 Definition of unsteady separation.

When there exists a relative velocity between the wall geometry, and the point of separation, the separation point is displaced into the boundary layer away from the wall surface. Under these conditions Prandtl's classical definition of separation is inadequate,

$$\frac{du}{dy} = 0 \quad \text{at} \quad y = 0 \tag{9}$$

A criterion was independently suggested by Sears, Moore, and Rott, for the case of separation in steady flow occurring over a downstream moving wall (see Koromilas & Telionis 1980),

$$\frac{du}{dy} = 0 \quad \text{at} \quad u = 0 \tag{10}$$

With a simple transformation of this problem, the case of unsteady separation moving forwards over a fixed wall is realised. The above criterion for separation may then be applied by defining this in a coordinate system moving with the point of separation. Separation is then described as the appearance of a stagnation point, and a dividing flow trajectory between the boundary layer, and the separated flow.

In subsonic flows at low Reynolds numbers, there can exist significant dynamic effects locally in the region of an unsteady separation point (Koromilas & Telionis 1980). However, in supersonic flows these do not appear significant, and the principal concern has been associated with the overall

scale effects of unsteady separation adjustment.

3.2 Mechanisms of unsteady separation adjustment.

Three characteristic times of separated flow adjustment were identified by Ihrig & Korst (1963) in their studies of the response of separated turbulent base flows to transient freestream conditions:

(i) Acoustic characteristic time, $\Delta t_a = \frac{L}{a}$ (11)

(ii) Mass entrainment characteristic time, $\Delta t_m = \frac{L \sigma}{u_a I_{1j}}$ (12)

(iii) Heat transfer characteristic time, $\Delta t_H = \frac{L}{u_a St}$ (13)

with,

L - characteristic length dimension of the wake.
a - reference acoustic velocity.
σ - mixing parameter (turbulent shear layer).
I_{1j} - mass flow integral.
u_a - flow velocity in the freestream adjacent to the mixing region.
St - Stanton number for the mixing region.

The acoustic time characterised the adjustment of the separation due to pressure waves. This is a traverse time for pressure disturbances, travelling at combined local acoustic and convective velocities, to propagate through the separation region. The second distinct mechanism of adjustment, due to mass transfer, has a characteristic time defined as the mass of the dead-air region divided by an integral of the mass flow rate in the free shear layer (below the dividing streamline), which represents the ability of an unsteady separated flow to exchange mass. For heat transfer adjustment, the characteristic time was defined as an internal energy term of the dead-air region, divided by an energy transfer rate across the mixing region.

For the particular example of a turbulent separation behind a downstream facing step in supersonic flow, Ihrig & Korst (1963) determined these characteristic times from simple analytic models, and obtained a ratio of the mass transfer to acoustic characteristic time of 30. However, it was noted

that the longest adjustment time would be for steady heat transfer, associated with the attainment of steady temperatures in the wake region.

As a consequence of these order of magnitude considerations, Ihrig & Korst developed a model of the dynamic adjustment of the separation region geometry, based on an integration of mass flow from the free shear layer into the separation region (Fig.5). It was assumed that pressure equalisation throughout was instantaneous, and that time derivative terms in the momentum equation for the free shear layer could be neglected. An implication in this model is that although characteristic times of heat transfer may be the longest, the rate of separation geometry adjustment is controlled principally by mass transfer, and that the attainment of equilibrium temperatures in the separated flow has little further influence on the separation geometry. A comparison of the results of this model of the separated flow adjustment compared well with experimental measurements, with the unsteady separation induced by a rapid change in the freestream stagnation pressure.

The thermal adjustment of bulk wake temperatures in separated supersonic turbulent base flows has been investigated by Battin (1963). The specific objective of this work was to determine whether steady state heat transfer measurements within separated flows could be obtained in facilities such as shock tubes, and shock tunnels, with extremely limited test duration. These concerns were prompted by preliminary experiments in a high enthalpy subsonic flow, which indicated that the thermal adjustment time in a wake was significantly longer than that required for the pressure adjustment which accompanied the attainment of the steady separated flow geometry. This was consistent with the simple order of magnitude considerations discussed by Ihrig & Korst (1963).

Battin proposed a theoretical model of the bulk wake temperature adjustment, solving the transient energy balance equation with the separated flow treated as an essentially closed system (Fig.6). This assumed, as an approximation, that the wake separated flow geometry was instantaneously established. The contributing components of energy transfer were:- the energy transfer through the mixing region, the wake region wall heat transfer, and the effect of the wall boundary layer ahead of the step. The sum of these components was equated to the rate of change of the wake internal energy, which then determined the rate of adjustment of the bulk wake temperature. The derivatives of each energy transfer mechanism with time were neglected. The results of this model were compared with experimental measurements of the wake temperature as a separated flow established behind a rearward facing step in a

shock tube flow. The good agreement found between theory and experiment gave support to the mechanisms proposed. It was concluded that the relatively slow thermal adjustment time should be considered for the correct interpretation of heat transfer measurements in separated flows. Even though the wall heat transfer coefficients in the separated flow may be established with the separated flow field geometry, the slow adjustment of the wake bulk temperature will be the controlling factor for the wall heat transfer rates.

Holden (1971b) correlated the times for steady separations to establish in uniform hypersonic freestream flows from a large number of tests. These were defined as the times for pressure, and heat transfer, within the separated flow to reach 98 % of their final steady mean values. Experimental measurements on spheres indicated that these establishment times for large laminar base separations were significantly greater than an acoustic propagation time. These times were directly proportional to the size of separated flow, and decreased with increasing freestream velocity. Steady pressure measurements required just under 30 body lengths of flow to stabilise,

$$\frac{U_\infty \, t_{(\text{steady pressure})}}{D} = 27.9 \qquad (14a)$$

D - diameter of sphere

This non-dimensional time (Eq.14a) was found to be only a weak function of freestream Mach number, and Reynolds number, over the range tested. It was concluded that for these separated flows, the establishment of viscous mixing in the free shear layer was the dominant mechanism in attaining flow equilibrium. Heat transfer measurements took the longest to stabilise, approximately twice the time for steady pressure readings.

$$\frac{U_\infty \, t_{(\text{steady heat transfer})}}{D} = 70 \qquad (14b)$$

However, it was noted that changes in the fine structure within the separation during the attainment of steady heat transfer, after the base pressure had stabilised, had no significant influence on the gross properties of the separation. These observations are similar to those of Ihrig & Korst (1963), and Battin (1963), for supersonic turbulent base separations.

Turbulent wakes were observed by Holden (1975) (see Hankey & Holden 1975) to establish significantly faster than the corresponding laminar flows. This

difference was attributed to inherently higher turbulent mixing rates. No additional time for the stabilisation of heat transfer within the separated flow, after the separation geometry had established, was noted, in contrast to the laminar wakes in hypersonic flows, and the supersonic turbulent base separation studied by Ihrig & Korst.

For the slender laminar separations induced by shock boundary layer interactions, which have much smaller volumes of dead-air than the base flows, Holden (1971b) found the additional time to achieve equilibrium beyond the acoustic propagation time was small. This time was calculated using the local speed of sound based on the wall temperature, and the total length of the interaction region. Measurements indicated that the establishment of separated flow over these models was associated with the establishment of flow in the streamwise plane, perpendicular to the model, and not a phenomenon associated with lateral outflow. The leading edge of these separations was observed to propagate forward with a velocity close to that of the local speed of sound at the wall. No additional time for the stabilisation of heat transfer in these wedge type separated flows was noted. In these slender separations, the concept of a bulk thermal adjustment time for a dead-air region is probably inappropriate. The establishment time of turbulent shock boundary layer separations of comparable size was 3 to 4 times faster (Holden 1977).

These measurements suggest that for a particular test model configuration, the location of transition may be the most important single parameter that influences the dynamic behaviour of the separated flow.

Needham & Stollery (1966b) examined the initial establishment of a wedge separated flow in a gun tunnel experiment using ciné schlieren flow visualisation, and its subsequent response to changes in freestream flow fluctuations during the early part of the test period. At the start of the tunnel run the separated flow geometry was seen to establish within 0.6 ms. Comparisons of the subsequent changes in separation length with a freestream pitot pressure trace indicated that the initial response of the separated flow to changes in freestream flow was faster than that of the probe itself. From these observations it was concluded that the establishment time of the wedge separated flow was sufficiently short to justify the use of shock tunnels with running times of the order of 5 ms.

3.3 Response of separated flows to changing wall geometries.

Wilkinson (1966) studied the response of a separated hypersonic flow to rapid oscillating changes in the wall geometry inducing separation. This is the

first recorded investigation of an unsteady separation response to wall geometry in either supersonic or hypersonic flow. The model was a forward facing step, the height of which was oscillated sinusoidally about a mean position, with freestream Mach numbers of between 8.4 and 12.5. Wilkinson defined a reduced frequency parameter based on the oscillating step frequency, the mean separation length, and the velocity on the dividing streamline at the end of the mixing process,

$$k = \frac{\omega L_{sep}}{u_{ds}} \tag{15}$$

Chapman's (1950) value for the velocity on the dividing streamline was used in evaluating this parameter, which assumes an asymptotic development of a laminar free-shear layer. Experimental measurements by Wilkinson included both pressure, and heat transfer, at a point within the separation, together with ciné schlieren photography of the changing flow geometry. Care was taken to determine whether transition occurred. For fully laminar separations, it was found that for values of k in excess of 0.02 the separation length response was not quasi-steady. For values of k equal to 0.1 there existed phase lags between the separation length and the step motion of up to 40 degrees, although this phase lag was not constant through a cycle. The measurements of pressure, and heat transfer, in the dead-air region indicated significant unsteady variations. When transition occurred near reattachment, the measured phase lags were reduced considerably.

Wilkinson (1966) modelled the dynamic response of this separation, based only on mass exchange considerations (Fig.7), with the order of magnitude analysis of Ihrig & Korst (1963) as justification for this. The formal mass balance equation for the dead-air region was written as,

$$\frac{d}{dt}(\rho_d V_d) = m_{in} - m_{scav.} \tag{16}$$

with,

ρ_d - dead-air density.

V_d - dead air volume.

m_{in} - mass flow rate in the free shear layer, beneath the reattaching streamline, reversed back into the separation region.

$m_{scav.}$ - mass flow scavenged by the developing free shear layer ahead of the reattachment process.

This equation equated the instantaneous net rate of change of mass within the separation region to the difference between the mass reversed into this by the reattachment pressure rise, and the mass scavenged by the free shear-layer mixing process. In the mass transfer model developed by Ihrig & Korst (1963), the term on the right of Eq.(16) was determined completely by an integration of the flow in the free shear layer by choosing appropriate streamlines. Wilkinson used a different, approximate method, for determining the mass scavenged term. Both models used a quasi-steady analysis of the free shear layer growth, determined at any instant by the local external flow, and the point of separation, with a dead-air region assumed below. Wilkinson's measurements of pressure, and heat transfer, within the unsteady separation subsequently suggested that the assumption of a dead-air region for this may not be valid. In Wilkinson's model of the separation adjustment the phase lag was approximated as constant. A comparison of the results of this mass transfer theory with the experimental measurements of the unsteady separation lengths showed reasonable agreement.

This theoretical model was subsequently applied by Wilkinson to the example of the separation response induced by an oscillating trailing edge flap. The phase lags predicted for this geometry were an order of magnitude less than those predicted for the step, with similar separation lengths. However, it was noted that even if the mass transfer lag is small, there may still be large fluctuations in the unsteady separated flow heat transfer. The example of a rapidly deflected flap was suggested by Wilkinson as a future subject of investigation.

This configuration of a rapidly actuated flap control surface was studied by Roberts (1989), and is the most closely related work to the present investigation described in this thesis. The model consisted of a sharp edged flat plate, with a trailing edge flap rapidly deflected from 0 to 35 degrees in about 20 ms. The centre line pressure distribution was measured along the plate, and flap, with flush mounted miniature pressure transducers. The condition of the separated shear-layer was thought predominantly laminar in these experiments, although transition may have occurred near reattachment. The pressure measurements, and ciné schlieren flow visualisation, indicated a lag in growth of the unsteady separation compared to the steady separation lengths that would be generated at corresponding fixed flap angles. The separation geometry, and shock structure, for the unsteady flow maintained the same form as that observed for wedge type steady separations. The steady separated flows in these experiments were corrupted by nozzle exit compression

wave interference. An estimate of lags in unsteady separation growth from dynamic flap deflections upwards, and downwards, gave a maximum value equivalent to 2.7 degrees of flap deflection, occurring with a maximum flap velocity of 51 rads./s at a flap angle of 35 degrees. It was observed that there existed an increased level of pressure fluctuation within the separation region for the unsteady condition. The effect of the dynamic response on the force, and moment coefficients, was to increase these, but by no more than 3.8% above the steady state values at the same flap angles. A model of the dynamic response, based only on the limitation of acoustic propagation of pressures through the length of separation, gave good agreement with the experimental results.

A numerical solution for the flow development over a rapidly deflected short flap in supersonic flow was presented by Kazakov (1981), using the method of matched asymptotic expansions. This technique divides the flow into three regions:- a laminar sub-layer adjacent to the wall, an inviscid rotational flow which covers most of the boundary layer in which viscous forces can be neglected (flow essentially driven by pressure and inertia forces), and the irrotational inviscid flow adjacent to the boundary layer. The solutions presented were valid for very high Reynolds numbers, with the further assumptions that the flap deflection angle, separation scale, and time of deflection, were of the order of the Reynolds number to the power of minus one quarter. The flap was deflected from zero to the maximum value using a sine function time dependence. The results showed the time required to establish rarefaction flow at the flap trailing edge was appreciably shorter than the time required for the flow to establish in the separation region. The modelled response of the separated flow indicated a dynamic effect of increasing the lift and moment coefficients at the instant the flap reached its maximum deflection angle, compared to the stabilised flow at the same angle. More importantly, the maximum heat transfer in the flow reattachment region was higher than the steady value obtained at corresponding fixed flap angles, and this difference increased with an increase in the rate of flap deployment, and maximum angle. It was concluded that such a phenomenon may play an important part in the aerodynamic heating of flaps deflected through large angles at a high angular velocity.

3.4 Numerical solutions.

With the advent of accurate numerical solutions to the full time dependent Navier-Stokes equations, information can be obtained from these for the

establishment times of separated hypersonic flows. Rudy et al (1991) compared predictions of several codes with the experimental test case of a nominally two-dimensional compression corner, with freestream Mach number of 14.1 (Holden & Moselle 1970). Results using four different numerical codes, assuming two-dimensional flow throughout, were all in close agreement, but significantly overpredicted the experimentally measured separation scale for the largest flap angle of 24 degrees. Effective times for the codes to establish a steady state separation were in excess of 12 ms, compared with an experimental establishment time of 4 ms. The numerical prediction was repeated with a single code, modelling the interaction fully in three dimensions. This gave excellent agreement with the experimental data, and the effective steady state establishment time for this code was approximately 4 ms, also in very close agreement with the experiment. Rudy et al described the difference in establishment time between the two-dimensional, and three-dimensional, results as quite surprising. However, the time for the two-dimensional code to establish a separation size equal to the three-dimensional centre line separation length was only about 3 ms. This is not expected to be the same as the 4 ms for the three-dimensional case, since for the two-dimensional flow at this point the separation is still rapidly growing, with the mechanism that determines the final scale of separation still strong. For the three-dimensional case, the solution has approached its final steady value, with the mechanism driving the increase in separation scale becoming progressively weaker towards its steady solution. The comparison of the two-dimensional, and three-dimensional, solutions in this context indicates that the dominant parameter that determines the difference in establishment times of these separated flows is the scale of the final separation, and that other three-dimensional effects on the establishment time are not strong. This dependence of the establishment time on the scale of separation is expected, due to acoustic propagation and/or mass entrainment requirements.

Lee & Lewis (1993) numerically simulated the establishment of base separated flows over a number of test model configurations placed within a hypersonic shock tunnel nozzle flow. It was emphasised that establishment times were an important consideration for properly designing experiments, and interpreting data, using very short duration impulse hypersonic test facilities. The entire flowfield within the nozzle, including the aerodynamic model, was solved with a two-dimensional code. The establishment time for these numerically simulated separations was defined as that required for all the pressures in this region to reach 98 % of their final steady values (as

also defined by Holden 1971b), minus the time for the tunnel starting process to pass the test model. The model configurations examined included a circular cylinder, a thick double wedge, a thin double wedge, a biconvex aerofoil, and a flat plate. The establishment times, presented in the non-dimensional form of Eq.(14a), were strongly dependent on the particular model geometry. The longest non-dimensional time was found for the circular cylinder, with a value of 46. This compares with a value of 27.9 measured by Holden for a sphere geometry. It was also verified from these numerical results that the dependence of the absolute establishment time was inversely proportional to the freestream velocity, as found experimentally by Holden (Eq.14a).

3.5 Discussion.

The dominant characteristic adjustment time appears to be determined by the geometry of separation, and hence, the size of the dead-air region. For the base separations this region is large, and the requirement to entrain additional mass into this is the restriction that determines the rate of response. Boundary layer separations induced by compression corners generally have much smaller volumes of separated flow than the base type. The very limited data concerning the response of these suggests that their establishment, and adjustment, can be predicted with analytic models based on the propagation of pressure changes, and not mass transfer adjustment.

Transition is generally accepted as the single most important parameter in steady separations, and this may also extend to the dynamic response of separated flows.

The most neglected measurements in the investigation of the dynamic response of separated flows are clearly heat transfer. This may be the most important consideration in the hypersonic flow regime, where any mechanisms that could potentially increase the peak reattachment heat transfer must be seriously considered. This is the principal subject of investigation in the present work described in this thesis.

PART II

EXPERIMENTAL SET-UP AND MEASUREMENT TECHNIQUES.

4. Introduction to the experimental work.

The objectives of the experiments described in this thesis were to investigate the dynamic response of a laminar separated hypersonic flow, induced by a rapidly actuated control surface, and measure the effects of this on the heat transfer distribution. These dynamic effects have been studied by comparing measurements of the unsteady separation development with those for the steady separations induced at corresponding fixed flap angles.

The test configuration chosen for these experiments was a two-dimensional trailing edge flap model, with a sharp leading edge. An alternative configuration that could have been chosen was an axisymmetic flare model. Although this is free from end effects it is much more difficult to practically implement in a dynamic mode.

The experiments were performed in the University of Southampton isentropic light piston compression tube hypersonic wind tunnel, using a contoured nozzle with a measured exit freestream Mach number of 6.85. The principal measurements made on the trailing edge flap model were of the centre line surface heat transfer distributions. A large amount of time was spent by the author in manufacturing appropriate heat transfer gauges for this, integrating these with the test model, and in arranging high quality supporting instrumentation, and data reduction methods. These heat transfer measuring techniques are described in detail in this part of the thesis.

During the period of this research, some developments were also made by this author in the application of liquid crystal surface thermography for hypersonic testing, particularly with respect to the use of multi-layer substrate models (Smith & Baxter 1989). The liquid crystal thermography technique was applied in the present tests specifically for the qualitative assessment of three-dimensional influences in the nominally two-dimensional fixed flap experiments.

Schlieren photography was used to examine the flow structure, and the scale, of both the instantaneous dynamic, and the steady, separated flow regions.

5. The isentropic light piston compression tube (ILPT) hypersonic wind tunnel.

The ILPT hypersonic wind tunnel is a facility that was specifically designed for the investigation of unsteady aerodynamic phenomena, capable of providing extremely steady flow conditions for run durations of typically 0.5 s. A lack of this combination of high flow quality and duration in test facilities such as gun tunnels, shock tunnels, arc heated facilities, and their derivatives, is reflected in the relatively few previous investigations of unsteady separated flows in the hypersonic regime.

The principles of isentropic light piston compression, and its application to this facility, have been extensively documented (Jones et al. 1973; Qasrawi 1977; East & Qasrawi 1978). A brief description of the operation of this facility is given below, with reference to Fig.8.

A light piston, driven by a high pressure reservoir choked at a restrictor, compresses a test gas initially contained in the tube. The piston velocity is relatively low, and the gas is compressed isentropically (neglecting the gas heat loss to the tube, and viscous effects). When the nozzle diaphragm ruptures at the stagnation pressure, the important feature of operation is the matching condition. This requires the volume flow rate of driver gas into the tube to equal the volume flow rate of test gas out of the tube, adjacent to the nozzle entry. Correct matching produces extremely steady flow conditions. The driver gas, and the test gas, used in this facility are commercial nitrogen.

A wave damper - baffle plate assembly is incorporated following the driver gas inlet to the compression tube. This matches the unsteady viscous flow through a baffle plate to the flow behind the non-steady expansion wave that originates from the nozzle opening. This eliminates this wave, extending the run duration to much greater times than would otherwise result with a mode of operation as a Ludweig tube using isentropic compression (Oldfield et al 1973).

The compression tube is preheated electrically to an elevated temperature, with a temperature gradient superimposed on this along its length (see table 3). In large length:diameter ratio tubes there are significant heat losses during the compression stage. This is due to the formation of a vortex ahead of the piston, containing cooler gas from the wall boundary layer. This heat loss is compensated by the temperature gradient along the compression tube, maintaining a uniform stagnation temperature. The initial elevated

temperature added to this effectively increases the run duration by reducing the amount of compression heating required, maintaining a sufficient stagnation temperature to prevent gas condensation. The final 15% to 20% of the run contains cool gas that originates from the formation of another vortex when the piston accelerates to the matching velocity at the instant the nozzle opens. This loss of the last part of the run period is inherent in this type of facility, and is accepted as unavoidable.

The test gas is expanded through a contoured nozzle, with a design Mach number of 7, and exit diameter of 0.21m. The test section flow is of the open jet type (Fig.9), which is collected by a convergent-straight-divergent diffuser, leading to a large chamber (the dump tank). This chamber, and the test section, are initially evacuated to a very low pressure, and remain in this condition until the nozzle diaphragm is ruptured. The open jet length is adjustable to accommodate different model geometries, and minimise flow spillage. The freestream Reynolds number range that had been previously achieved in this facility before the present tests was 4.1×10^6/m to 40.3×10^6/m, with a calibrated freestream Mach number of 6.85. This variation of Reynolds number is accomplished by changing the stagnation pressure (nozzle diaphragm burst pressure), while maintaining a stagnation temperature of about 600 K.

5.1 Low freestream Reynolds number operation of the ILPT facility.

In the present experiments the facility was operated at a low freestream Reynolds number, in an attempt to maintain fully laminar separated flows.

In the mode of operation initially used, variations in stagnation pressure of up to 20% occurred from run to run. For low Reynolds number operation, the stagnation pressure of the flow is reduced. This is achieved with a weaker diaphragm at the nozzle entry, in conjunction with a reduced initial test gas pressure in the tube before piston compression. The reservoir (driver) pressure was maintained at its standard value, and with the low initial charge pressure this produced high piston velocities. The effective gas stiffness is much less with the low stagnation pressure, and coupled with the higher piston velocity, the piston dynamics become significant. The piston dynamics are affected by piston friction, and this was believed to be the cause of poor repeatability between runs.

To improve the operation of the tunnel for a low freestream Reynolds number, the reservoir pressure was reduced from 17.339×10^6 N/m^2 to 3.549×10^6 N/m^2 (absolute pressure), and the initial temperature distribution along the

compression tube adjusted to compensate for an increased compression time. This significantly improved the tunnel repeatability. During a run, the variation in stagnation pressure over a period of 0.3 s was less than 2%, and within 5% for the mean pressure level between runs. The freestream stagnation temperature was deduced from the measurements of flat plate laminar heat transfer (see § 11). During the period of the flow in which the dynamic tests were performed, and the steady data reduced, the peak fluctuations of freestream stagnation temperature were less than ±2.5%. The variation between runs for the average stagnation temperature over this period was within 5%. The test section Mach number was calibrated at the nozzle exit plane. A value of 6.85 was measured at the centre, with a spatial variation within the inviscid flow core of +0.8%. The freestream Reynolds number was calculated to be 2.45×10^6/m. The freestream properties, and details of tunnel operation, at this Reynolds number are contained in tables 2 & 3.

6. Dynamic / Fixed trailing edge flap model.

A single two-dimensional trailing edge flap model was designed for both the dynamic, and the steady, separation heat transfer measurements. The final configuration, and its dimensions, are illustrated in Figs.10 & 11. The plate, and the flap, had chords of 155 mm, and 51 mm respectively, with a uniform model span of 102 mm. Many of the features of this model, including the plate and flap dimensions, flap driver mechanism, and the method of dynamic flap angle measurement, were based on a model developed by Roberts (1989) for the measurement of pressures within unsteady separations, tested in the same ILPT hypersonic test facility.

The plate was machined from gauge steel, with a sharp leading edge. This leading edge thickness was measured with a travelling microscope to be less than 0.02 mm. Aluminium was selected for the flap material to maintain its inertia to a minimum for the dynamic experiments. The dimensions of the plate, and the flap, were decided with consideration for the following requirements (Roberts 1989):-

(i) A large extent of two-dimensional separated laminar flow induced at the highest flap angle.
(ii) Reattachment of the flow well within the flap chord.
(iii) Maximum possible model span for the requirement of two-dimensional flow.
(iv) The overall model size to be within the limit set by wind tunnel blockage.

The maximum flap deflection angle was set to 35 degrees. The dimensions of the model were then a compromise to satisfy conditions (ii) and (iii) within the constraints of (iv). If the model size is too large, then the tunnel freestream flow will be unable to correctly establish, and blockage will occur (Qasrawi 1977).

The flap was hinged to the plate to allow for its motion. These hinges were flush with the plate and flap sides to prevent disturbance to the flow, and to allow for the attachment of side plates for some tests. It was not practical to seal the plate-flap junction, and simultaneously allow for the unconstrained motion of the flap. The gap that existed was made as small as possible, and independent of the flap angle, by using concentric radii of the same direction for the plate trailing edge, and the flap leading edge. The plate, and flap, assembly were supported in the test flow with a hollow centre support.

For the dynamic tests the flap was rapidly driven by a powerful spring - lever arrangement, with a restraint set at an angle of 35 degrees to stop its motion. The springs were placed in a position outside the test flow, and the lever arms, constructed from thin plate metal, presented only a small disturbance to the flow beneath the model. With this arrangement, a deflection of the flap to 35 degrees was obtained within 20 ms, with flap velocities approaching 3000 degrees/s. A single rate of deployment was used for all the dynamic tests. This was thought to be the maximum rate that could be tolerated without risk of damage to the model, or the heat transfer gauges, through the mechanical shock generated at the end of the flap motion.

The release mechanism was activated with a solenoid, and incorporated a fine adjustment to set the flap to zero degrees prior to its release. This solenoid was screened with Mu metal to prevent any electrically induced interference to the heat transfer signals during the flap deployment. The changing flap angle was measured with a potentiometer, attached to the flap through a linkage. This potentiometer output was initially calibrated against the flap angle using a clinometer (accurate to $\pm$ 1 minute of arc). The flap motion, after release in the freestream flow, was found to be extremely repeatable, with no measurable differences observed between the potentiometer signals of repeated tests.

For the fixed flap experiments, the driver springs were replaced with a locking screw mechanism.

Heat transfer measurements were made with gauge inserts mounted flush in the model along the plate, and the flap, centre line. A separate plate, and flap, of the same dimensions were constructed for the liquid crystal thermography tests (see § 8.5). The model span was sufficiently large to prevent the Mach cones generated at the leading edge corners interfering with the centre line heat transfer measurements along the plate and the flap lengths.

6.1 Design of side plates.

The aspect ratio of this model plate was 0.67. This was substantially less than the value of 2 found necessary by Holden (1967) to achieve two-dimensionality in the centre line region of large laminar separated flows without side plates. For this reason, all tests both dynamic, and fixed, were performed with, and without, side plates attached. This was necessary to determine whether any observed non-quasi-steady dynamic response could be attributed to edge effects.

A single set of side plates was designed, capable of containing the largest separated flow generated with the maximum flap angle of 35 degrees, at the lowest freestream Reynolds number used. For flap angles less than this, the side plates extended beyond the separation point. This is usually avoided for fixed flap experiments, since any viscous interaction with the supersonic flow on the inner edge of the side plates may introduce undesirable three-dimensional influences. However, for these experiments the principal objective was a comparison of steady, and dynamic, separations, which only required a consistent use of the same side boundary conditions.

To correctly contain the largest separated flow, the top edge of the side plates should be aligned with the outer edge of this separated flow free shear layer. This edge can be approximated as a straight line originating from the separation point. The angle of this is then equal to the deflection of the inviscid flow that produces a pressure rise equal to that measured in the separated flow plateau region. The deflection angle of the free shear layer for any separation point was determined from a correlation of the low Reynolds number test data of Roberts (1989), in the form of Eq.(1), and with the use of simple oblique shock wave equations.

With the addition of side plates, the steady separation lengths may increase, and side plates designed to contain the size of separation generated with a flap at 35 degrees, without side plates, may then not be sufficiently large. The side plates were designed to accommodate a separation size 75% of the plate length. These were constructed from thin metal plate, 2 mm thick, each with a chamfer of 10 degrees on the outer side, normal to a sharp leading edge. The side plates were rigidly attached to the plate, with a length extending past the undeflected flap. The flap was able to move between these, against their inner sides. The friction in this had a negligible influence on the flap motion compared to that obtained without the side plates attached.

7. Heat transfer instrumentation.

7.1 Introduction.

The accurate measurement of heat transfer in regions of shock wave - boundary layer interaction is a particularly challenging problem for thermal instrumentation. In reattachment regions of separated hypersonic flows there exist large gradients of heat transfer. A high density of individual measurements is needed here to accurately locate, and determine, peak heating levels. These large gradients may induce significant lateral heat conduction within the model surface and the thermal instrumentation. If this occurs, distributions of measured heating will be distorted, and therefore inaccurate. Instrumentation incorporating insulating substrates to minimise this problem may produce locally high surface temperatures. This is undesirable in that a discontinuous surface temperature boundary condition may effect the development of the measured flowfield, and may also lead to thermal stress failure of the instrumentation. Conversely, within regions of recirculating separated flow, the heat transfer levels can be very low, and the thermal instrumentation must then have a high sensitivity, yet be capable of measuring heat transfer throughout the separated flow which may typically vary in value by two orders of magnitude.

Hypersonic test facilities are generally limited to short duration testing. The measurement of heat transfer in a transient facility is actually advantageous in that it limits surface temperature rises, maintaining a more nearly isothermal wall condition, and reduces the occurrence of undesirable thermal conduction losses that would require correction. The thermal instrumentation used in these wind tunnels must have a sufficiently rapid response, determined either by the run duration for steady experiments, or the requirement to measure an unsteady phenomenon within the test period.

In the experiments of the present research, the objective was to measure the heat transfer distributions generated by a rapidly actuated flap, displaced through an angle of 35 degrees in about 20 ms. It is necessary that the thermal instrumentation has a response time which is much less than this deflection time to avoid the introduction of complex data reduction. This response time requirement was a very significant factor in the selection of the appropriate thermal instrumentation for these experiments.

Distributions of heating produced with a dynamic flap had not been previously studied. It was therefore necessary to instrument this model with a high spatial resolution of measurements throughout its length, to accurately

resolve any form of unsteady separation development that might have occurred. This was an extension of the usual requirement for dense instrumentation locally in reattachment regions for steady shock wave - boundary layer interactions.

7.2 Heat transfer gauges.

Surface heat transfer is a quantity which cannot be measured directly. However, its effects are observable through changes in gauge temperatures, and this is the principle on which heat transfer measurement is based. The measured changes of temperature are related to the surface heat transfer through simplified analytic solutions of heat conduction, consistent with the thermal boundary conditions embodied in the gauge design, and its integration within the model.

Three conceptual methods of heat transfer measurement have been identified by Thompson (1981), examples of which have been extensively reviewed by Neumann (1988). These classes are:-

(i) Heat flux may be related to the temperature gradient set up in a thin material layer.
(ii) Heat may be captured within a thermal mass which acts as a calorimeter, and whose transient temperature change can be related to heat flux.
(iii) A heat balance in steady state may be established between incoming aerodynamic heating, and a calibrated heat removal process.

The response time required of the thermal instrumentation in these experiments restricts the appropriate selection to a class (ii) type of gauge, in which a temperature sensor is applied at the surface. The gauge response time is then only limited to the thermal diffusion time of the temperature sensor. In class (i), class (iii), and some class (ii) gauges (for example the often used thin-skin calorimeter technique) the gauge response time is increased substantially by a necessary thermal diffusion time across a material layer in addition to the temperature sensor.

A suitable class (ii) gauge that has been extensively developed is the semi-infinite thermal model. This gauge captures the heat pulse within its thermal mass, operating for times less than the thermal diffusion time of the heat pulse through the substrate. The gauge material may be a thermal insulator, or a conductor, the selection of which is determined by the particular application, including considerations of test duration, lateral heat conduction, and thermal integration of the gauge within the test model.

The instantaneous surface heat flux is then related to the surface temperature history through a solution of the unsteady heat conduction problem, with the assumption of one-dimensional heat conduction, and an unchanged substrate rearface temperature.

A requirement for the surface temperature sensor is that it does not interfere with the heat conduction thermal model applied to the substrate. i.e. it must have a negligible thermal mass. The two types of sensor that have been used most successively for point measurements with the semi-infinite thermal model are the thin film resistance element, and the surface thermocouple. The thermocouple has the advantage of a constant calibration factor for all gauges, which is unaffected by flow abrasion. No external power supply is needed to activate the gauge. This sensor has been applied to both insulator, and conductor, substrates. The thin film resistance gauge is a powered gauge, in which a voltage is applied across the surface resistance element. These sensors must be applied to electrically insulating substrates, which has restricted their application to thermal insulators. These gauges must be individually calibrated, and are susceptible to flow abrasion problems. The use of thermally insulating substrates produces higher temperature rises than for a conductor, and hence larger electrical signals. The sensitivity of the thin film resistance gauge is also typically in excess of ten times that for the thermocouple, making them suitable for the measurement of very low heating levels. The construction of resistance gauges is relatively straight forward, and a high density of measurements on an insulating substrate is achievable, providing excellent spatial resolution with minimal distortion through lateral conduction. Both the surface thermocouple, and the thin film resistance element, can be deposited in extremely thin layers, providing a very rapid response, and minimal interference with the thermal conduction model for the substrate.

The thin film resistance gauge has been selected for the experiments of this research project as the most suitable technique that satisfies the necessary requirements throughout the flow interaction region. The application of this method for measuring heat transfer distributions in regions of shock wave - boundary layer separation at high Mach number has been well established, as demonstrated, for example, in the very thorough experiments of Holden (1964, 1966a, 1967, 1971, 1972, 1977).

7.3 The thin film resistance heat transfer gauge.

7.3.1 Thermal model.

The surface heat transfer is related to the surface temperature rise through a solution of the unsteady heat conduction equation in one-dimension, with a homogeneous substrate, and appropriate boundary conditions. The differential equation which governs this conduction process is:

$$\frac{\partial^2 T}{\partial x^2} = \frac{1}{\alpha}\frac{\partial T}{\partial t} \tag{17}$$

where T is the temperature rise at a depth x below the surface at time t. The boundary conditions for this problem are:

$$-k\frac{\partial T}{\partial x} = q_s \qquad \text{at} \quad x = 0$$

and,

$$T = 0 \qquad \text{at } x = \infty$$

Eq.(17) is solved using standard Laplace transform techniques (Schultz & Jones 1973),

$$\bar{T}_x = \frac{1}{\sqrt{\rho c k}}\frac{\bar{q}_s}{\sqrt{s}}\exp.\left\{-x\sqrt{\frac{s}{\alpha}}\right\} \tag{18}$$

where s is the Laplace operator, and the barred quantities are the transformed variables. At x = 0, Eq.(18) is inverted to give a solution for the surface heat transfer as a function of the surface temperature rise, or vice versa.

$$q_s = \frac{\sqrt{\rho c k}}{\sqrt{\pi}}\int_0^t \frac{\frac{dT}{d\tau}}{(t-\tau)^{1/2}}\,d\tau \tag{19}$$

$$T_s = \frac{1}{\sqrt{\pi}\sqrt{\rho c k}}\int_0^t \frac{q_s(\tau)}{(t-\tau)^{1/2}}\,d\tau \tag{20}$$

The effect of the surface temperature sensor on this heat conduction process

has been assumed negligible.

The second boundary condition for this solution, T = 0 at x = ∞, cannot be physically implemented, and so a criterion must be established for the necessary substrate thickness for this analysis to be accurately applied. For a step in surface heat transfer, the solution of the unsteady heat conduction equation at a depth x can be solved from Eq.(18) (Schultz & Jones 1973). The solution expresses the temperature rise, or heat flux, at a depth x, as fractions of their respective surface values,

$$\frac{T_x}{T_s} = e^{-(x^*)^2} - \sqrt{\pi}\, x^*\, \mathrm{erfc}(x^*) \tag{21}$$

$$\frac{q_x}{q_s} = \mathrm{erfc}(x^*) \tag{22}$$

$$\text{where } x^* = \frac{x}{\sqrt{4\alpha t}}$$

The penetration depth for both these fractions to be 1% at time t are very similar, and this defines a thickness of substrate for which losses from the rear face are negligible for test durations of this time. This thickness is described as the semi-infinite thickness, which is evaluated for a required test duration, and with the relevant substrate thermal properties. For insulator type materials the thermal diffusivity α is small, and the semi-infinite depth required for a given test time is much less than for a conductor.

7.3.2 Measurement of surface temperature with thin film gauges.

The thin film resistance element is deposited as a very thin metal element on the surface of the substrate. The variation of the resistance of this element with temperature can be assumed linear over a substantial temperature range with high accuracy,

$$R = R_o\, (1 + \alpha_R (T - T_o)) \tag{23}$$

The suffix o refers to the initial conditions, and α_R is the gauge temperature coefficient of resistance defined by this equation. The gauge is initially biased with a steady voltage V_o, and the current then maintained at a constant value during operation. The temperature rise of the gauge, and hence substrate

surface, is then given by,

$$V - V_o = V_o \alpha_R (T - T_o) \tag{24}$$

The measurement of this voltage change is the basis of the operation of this temperature gauge.

A figure of merit for the film metal has been defined as,

$$\alpha_R \sqrt{\rho_R} \tag{25}$$

This term is proportional to the gauge sensitivity of different metals dissipating the same power. On the basis of a comparison of this figure for different metals, and because of its stability, platinum has been used most extensively as the gauge material. Each thin film gauge must be calibrated for the coefficient of resistance α_R.

7.3.3 Evaluation of the surface heat flux from a temperature signal.

There are two commonly applied methods for obtaining the surface heat flux from the surface temperature signal. If this temperature signal is recorded digitally at a constant sampling frequency, then a numerical integration of this may be easily applied to obtain the surface heat flux. This may cause an undesirable delay between testing and evaluating the heat transfer, and an alternative is to use an analogue network to directly obtain a record of the surface heat flux in real time. Both numerical, and analogue, techniques have been applied during the development of suitable instrumentation for this project:-

(i) Numerical integration.

The surface heat flux is related to the surface temperature rise through Eq.(19). Direct application of this is undesirable when the heat transfer rate is not constant, because the derivative term in the integral introduces excessive computational noise. A more convenient form is obtained by expanding this equation with an integration by parts (Schultz & Jones 1973).

$$q_s = \frac{\sqrt{\rho c k}}{\sqrt{\pi}} \left[\frac{T(t)}{\sqrt{t}} + \frac{1}{2} \int_o^t \frac{T(t) - T(\tau)}{(t - \tau)^{3/2}} \, d\tau \right] \tag{26}$$

Several methods have been proposed for the numerical evaluation of the integral term in Eq.(26), inparticular for dealing with the singularity at τ =

t. An example is the method of Cook & Felderman (1966). The recorded temperature in this method is approximated as a piecewise linear function between data points,

$$T(\tau) = T(t_{i-1}) + \frac{T(t_i) - T(t_{i-1})}{\Delta t} (\tau - t_{i-1}) \qquad (27)$$

$$\text{for } t_{i-1} \le \tau \le t_i$$

where Δt is the time period at which the signal was sampled. With this representation, the singularity in the integral at $\tau = t$ tends to zero. Substitution of this representation into the integral gives an equation for the surface heat flux at any instant, which can then be obtained from the recorded temperature signal.

$$q_s(t_n) = \frac{\sqrt{\rho c k}}{\sqrt{\pi}} \left[\frac{T(t_n)}{\sqrt{t_n}} + \sum_{i=1}^{n-1} \left\{ \frac{T(t_n) - T(t_i)}{(t_n - t_i)^{1/2}} - \frac{T(t_n) - T(t_{i-1})}{(t_n - t_{i-1})^{1/2}} + 2 \frac{T(t_i) - T(t_{i-1})}{(t_n - t_i)^{1/2} + (t_n - t_{i-1})^{1/2}} \right\} + \frac{T(t_n) - T(t_{n-1})}{\sqrt{\Delta t}} \right] \qquad (28)$$

The accuracy of this method improves with a higher sampling frequency of the recorded temperature signal, and also for larger periods of time with a constant sampling frequency. The time required to perform this integration increases very rapidly with the number of points, and for a high sampling frequency can be very substantial.

(ii) Analogue networks.

An alternative to the numerical integration procedure is to use an analogue network, from which the heat transfer signal may be obtained directly during the experiment. The operation of the analogue is based on an analogy that exists between the flow of heat into a semi-infinite substrate, and the flow of current into a semi-infinite transmission line with distributed resistance

and capacitance. This analogy is seen from a comparison of the differential equations that govern these two diffusion processes:-

Heat flow.	Current flow.
$\frac{\partial q}{\partial x} = -\rho c \frac{\partial T}{\partial t}$	$\frac{\partial i}{\partial x} = -c' \frac{\partial V}{\partial t}$
$-q = k \frac{\partial T}{\partial x}$	$-i = \frac{1}{r'} \frac{\partial V}{\partial x}$

(29)

where c', and r', are the capacitance, and resistance per unit length. The equivalent terms are therefore:-

$$q \equiv i\,, \qquad T \equiv V\,, \qquad k \equiv \frac{1}{r'}\,, \qquad \rho c \equiv c'$$

The solution for each of these equations, at $x = 0$, is obtained in Laplace transforms (see Eq.18) as,

$$\bar{i}_{in} = \sqrt{\frac{c'}{r'}}\ \sqrt{s}\ \bar{V}_{in} \tag{30}$$

$$\bar{q}_s = \sqrt{\rho c k}\ \sqrt{s}\ \bar{T}_s \tag{31}$$

The boundary conditions for these equations are:-

$$T = V = 0 \quad \text{for} \quad t = 0, \qquad \text{and} \quad T = V = 0 \quad \text{for} \quad x = \infty$$

It is not practical to construct a continuous resistance - capacitance transmission line, and in practice this is approximated with discrete resistance, and capacitance elements in sections, while maintaining the ratio of resistance to capacitance a constant for each section. The conventional application of an analogue line with the thin film gauge temperature signal is illustrated in Fig.13. The thin film gauge signal is applied to the analogue circuit, so that the input signal to this is,

$$V_{in} = \alpha_R V_o T_s \qquad \text{i.e.} \quad \bar{V}_{in} = \alpha_R V_o \bar{T}_s$$

From the solution for the analogue line (Eq.30), an input current will occur, given by,

$$\bar{i}_{in} = \sqrt{\frac{c'}{r'}}\ \sqrt{s}\ \alpha_R V_o \bar{T}_s \qquad (32)$$

Eliminating $\bar{T}_s$ via Eq.(31), the input current and the heat transfer are related through,

$$q_s = \sqrt{\rho c k}\ \sqrt{\frac{r'}{c'}}\ \frac{1}{\alpha_R V_o}\ i_{in} \qquad (33)$$

In the conventional instrumentation arrangement, the input current is determined from the measured voltage across the first resistor element in the analogue line, R_{in} (Fig.13).

7.3.4 Correction for temperature effects on the substrate thermal properties.

The value of the surface heat flux that is determined from a thin film gauge temperature history, and application of the semi-infinite thermal model (numerically, or through the RC analogue transmission line), assumes that the thermophysical properties of the substrate, inparticular the thermal product ρck (see Eq.19), do not vary with changes in temperature. This assumption may be incorrect if there are significant elevations in the surface temperature during the test period. The magnitude of temperature induced changes in the thermal product, and hence the necessary corrections to compensate for this, will depend on the particular substrate material used. Methods developed to correct for these temperature induced variations in the substrate thermal product are discussed in detail in appendix 2. The particular correction that was applied in the present experiments is illustrated in Fig.16. For the fixed flap experiments, at large deflection angles, corrections of up to 10 % of the measured heat transfer were necessary. The temperature rises for these fixed flap conditions are greater than for the dynamic flap tests where the model surface is exposed to high heat fluxes for only a very short duration. In the plotted heat transfer distributions the corrected heat transfer data are only illustrated where the temperature effects on the substrate are significant.

In the experiments the initial model temperature varied between 19.3°C to 24.3°C. The small variation in pyrex ρck that may occur from test to test with this difference in initial temperature has not been corrected for. This is

because the scatter in the calibrations of pyrex ρck from different sources (see Schultz & Jones 1973) is much greater than the change in ρck over a 5 degree interval, and a sufficiently accurate correction could not therefore be applied. For the presentation of the dynamic flap data, the results have been presented in a form non-dimensionalised with respect to the first plate gauge measurement of heat transfer in each test. This removes the influence of the model initial temperature on the substrate ρck, although corrections must still be applied for the temperature rises that occur during the test period when these are substantial.

Each surface temperature rise in these experiments has been determined from an integration of a measured heat transfer signal. This relationship is based on the same thermal model effectively used by the analogue line, but applied in reverse. The original surface temperature signal from the thin film gauge is therefore recovered without a source of error from the temperature variation of the pyrex thermal product ρck.

7.3.5 Construction methods for analogue lines.

If a sinusoidal signal of frequency ω is applied to the analogue input, and the output measured across the first resistor component in the line, R_{in} (Fig.13), then the magnitude of the analogue gain when it is operating correctly is obtained from the Laplace solution (Eq.30) as,

$$\frac{V_{out}}{V_{in}} = R_{in}\sqrt{\frac{c'}{r'}}\sqrt{\omega} \qquad \text{with,} \quad |Z_{in}| = \sqrt{\frac{r'}{c'}}\,\frac{1}{\sqrt{\omega}} \tag{34}$$

In practice, there will be a lower frequency, and an upper frequency, of the analogue operation between which the gain is correctly represented by Eq.(34). If each R-C stage of the analogue line is designed as a T section (Fig.13), and the total resistance and capacitance of stage one are R_1 and C_1, then the lower frequency limit of the analogue operation is (see appendix 3),

$$\omega_1 = \frac{C_1}{R_1}\,\frac{1}{C_T^{\,2}} \qquad \text{with} \quad \frac{r'}{c'} = \frac{R_1}{C_1} \tag{35}$$

For this T section construction, if $R_{in} = \beta R_1$, (Fig.13), the upper frequency limit of the analogue operation is given by (see appendix 3),

$$\omega_2 = \frac{1}{R_1 C_1} \frac{1}{\beta^2} \tag{36}$$

Eqs.(35) & (36) define the frequency limits of operation of an RC analogue line. In practice, the upper frequency limit will be specified by requiring a sufficient analogue response for the particular phenomenon to be measured, while the lower frequency limit is set to ensure that the analogue line remains semi-infinite for the test duration.

The electrical length of an analogue line is defined as,

$$k = \frac{\sum_{i=1}^{n} C_i}{C_1} = \frac{C_T^2}{C_1} \tag{37}$$

where n is the number of sections in the analogue line, and C_T is the sum of all the capacitor elements in the analogue line. A required frequency range of the analogue operation determines the necessary electrical length, which then determines the number of T sections in the analogue line for a particular method of construction,

$$\frac{\omega_2}{\omega_1} = \frac{1}{R_1 C_1} \frac{1}{\beta^2} \frac{R_1}{C_1} C_T^2 = \frac{k^2}{\beta^2} \tag{38}$$

When the frequency limits have been set, then the analogue line can only be uniquely designed when the first resistor has been specified. In a conventional application (Fig.13), this resistor should be high enough to prevent loading of the thin film gauge circuit, yet low enough for a high signal to noise ratio. If the output is measured directly across the first resistor, then the analogue sensitivity is proportional to this resistance value. A value of typically 50 times the thin film gauge resistance is satisfactory. If this resistor instead forms the first component of a current to voltage converter and amplifier, then this condition is not necessary, and any loading effects on the gauge bias circuit can be subsequently compensated for (see § 7.4.2).

There are three techniques that have been developed for the construction of analogue lines:-

(i) Constant section line.

In this analogue, all T sections of the line each have the same values of resistance, and capacitance. Hence,

$$C_T = \sum_{i=1}^{n} C_1 = C_1 n \qquad (39)$$

The electrical length k is therefore equal to the number of sections in this analogue line. Each T section of the analogue is arranged symmetrically, giving a value of $\beta = 0.5$. For a large operating frequency range, the number of sections required can be excessive. A more efficient construction technique is to increase the resistance, and capacitance per section, while maintaining their ratio, R/C, for each section at a constant value. This method is used in both the arithmetic, and logarithmic, design methods.

(ii) Arithmetic line.

In this analogue, the resistance, and capacitance values for each T section follow an arithmetic progression, maintaining R/C = constant throughout. It is necessary that the first three sections of this line are identical to improve the high frequency response (Schultz & Jones 1973). Hence,

$$C_T = C_1 \left(1 + 1 + 1 + (1+\delta) + (1+2\delta) + (1+3\delta) + ... + (1+(n-3)\delta) \right) \qquad (40)$$

where δ is the additional fraction of C_1 added at each section. Each T section is again arranged symmetrically. The electrical length is then given by,

$$k = n + (n-2)\delta \left\{ \frac{(n-2)}{2} - 1 \right\} \qquad (41)$$

For a specified operating frequency range, the number of sections required is less than for the constant section design.

(iii) Logarithmic Line.

This is the most efficient design method for an analogue line requiring a large operating frequency range, and is the technique which has been used for the instrumentation used in the experiments of this research. In this design, the values of resistance, and capacitance, are arranged in a geometric progression. If α is the ratio of successive values of capacitance in each T section, then

$$C_T = C_1 \left(1 + \alpha + \alpha^2 + \alpha^3 + ... + \alpha^{n-1} \right) = C_1 \frac{1 - \alpha^n}{1 - \alpha} \qquad (42)$$

Therefore,

$$k = \frac{1 - \alpha^n}{1 - \alpha} \tag{43}$$

For ease of manufacture, the capacitors used are preferred values, defining $\alpha = 10^{1/3}$. For correct matching, the distribution of resistance components about each T section should be such that the resistance values on either side of the capacitor element also lie in a geometric progression, as well as their total section values (Burd & Doe 1980). This defines,

$$\beta = \frac{1}{1 + \sqrt{\alpha}} = 0.4052 \tag{44}$$

The logarithmic design method dramatically reduces the number of sections required, with a quality of response equal to that of the other construction techniques (Burd & Doe 1980). In the final instrumentation configuration used in this research project, logarithmic lines with a frequency response of 0.02Hz to 100kHz were used, each constructed with 9 sections. The same frequency response with an arithmetic, and constant section, line would require 48, and 1068 sections respectively !

7.3.6 Analogue time response.

The finite time required for an analogue to operate correctly, in response to a step in heat transfer, can be obtained by considering the size of a slab of thermal substrate equivalent to the first discrete R-C section of the analogue line (Meyer 1960). In the analogy, equivalent terms are:

$$c' \equiv \rho c \quad , \qquad r' \equiv 1/k$$

The values of the first analogue section are R_1, and C_1. If this is considered equivalent to a thickness of thermal substrate Δx, then for consistency of the analogy,

$$R_1 = r'\Delta x = \frac{\Delta x}{k} \tag{45}$$

$$C_1 = c'\Delta x = \Delta x \, \rho c \tag{46}$$

hence,

$$R_1 C_1 = \frac{\Delta x^2}{\alpha} \qquad (47)$$

If the analogue is assumed to operate correctly when the electrical pulse just passes the first section i.e. the first section now acts as a distributed line, then this time is equal to the thermal diffusion time through thickness Δx. This is approximately the time at which

$$\frac{q_x}{q_s} = 1\% \qquad \text{for } x = \Delta x$$

For the logarithmic circuits used, this gives a response time of 0.7 μs. Schultz & Jones (1973) quote a rise time for an analogue equal to the time constant of the first resistor, and capacitor, elements ($= \beta R_1 C_1$). This gives a time of 4 μs. Both criteria give a very rapid response time, which reflects the upper frequency limit of 100 kHz.

Meyer (1960) determined that for a constant section line, the analogue would reproduce a step function in heat transfer to within 1.4% for a duration of,

$$t = 0.2n^2 R\ C \qquad (48)$$

With R, and C, the values in each T section of the line. This time can be determined for the arithmetic, and logarithmic, designed analogue lines by establishing the equivalent number of sections that would be necessary in a constant section line with the same operating frequency range. R, and C, are then the values used in the first analogue T section. For the logarithmic lines used in the present tests (range 0.02 Hz to 100 kHz), this gives a time of 9 seconds.

7.3.7 Thin film gauge manufacture.

There are two types of technique that have been developed for depositing thin film resistance elements on substrate surfaces:-

(i) Painting and firing.

(ii) Vacuum deposition.

In the painting technique a thin layer of a solution of a metal suspended in an organic solvent is applied to the surface of a substrate, which is then fired in a furnace. These gauges have the advantage of a very strong resistance to abrasion, but suffer from a lack of control over the gauge thickness and uniformity. Gauges constructed using vacuum deposition

techniques (such as sputtering, and electron beam evaporation) may have accurately controlled dimensions, and hence final resistance, but are unable to match the robustness of painted gauges.

Although precautions are taken to ensure the operation of the ILPT facility is clean, some measure of fine dust contamination in the flow is inevitable. During fracture of the diaphragm, discrete particles of its material are introduced into the flow during the starting process, and another source of particle contamination is piston wear during operation. The test flow environment can therefore be a severe test of a gauge abrasion resistance, especially in shear layer reattachment regions. The construction technique of painting and firing was chosen for this reason.

All gauges used in these experiments were manufactured by the author. The gauge paint used was the commercially available "Liquid Bright Platinum, Hanovia 05-X" (Englehard Industries Ltd), applied to the substrate surface with a fine brush. Pyrex was chosen as the gauge substrate, and a single insert was used along the plate centre line, and also a single insert in the flap. Pyrex is an easily workable substrate, and was found able to withstand the severe mechanical shock at the end of the dynamic flap motion without fracture. The disadvantage of this material is that its thermal properties may vary between manufactured batches, and pyrex has an undesirable sensitivity of these thermal properties to temperature change (Schultz & Jones 1973, see also appendix 2). Care was taken to ensure that in the final model configuration the pyrex inserts for the plate, and for the flap, were taken from the same supply batch.

The firing cycle for the painted gauges is shown in Fig.14, which is typical of those recommended by previous investigators (e.g. Schultz & Jones 1973; Holden 1964). The upper furnace temperature limit should be as high as possible, without distorting the substrates, which were supported in a stainless steel block within the furnace. There is a degree of diffusion of the platinum gauge material into the substrate surface, which increases with peak firing temperature, and this effect very much improves the abrasion resistance. The annealing part of the baking cycle is important to relieve any internal stresses within the substrate. All the gauges manufactured were very stable, and no increase in resistance due to stress relief was observed. Single layer films only were manufactured, to maintain the thin film thickness to a minimum. The final resistance of all the gauges, at room temperature, was between 35 to 45 ohms.

The edges of the platinum gauges were at least a distance from the sides

of the pyrex substrate equal to the semi-infinite depth, to prevent interference of the assumed one-dimensional thermal diffusion model from edge conduction effects.

The connections to the gauges should be thermally inert, with negligible resistance. On the surface of the substrate, thin film gold connections were applied to each gauge end (Hanovia liquid bright gold). Gold has a much lower resistivity than platinum, and several layers were separately painted, and fired, to reduce these connections to a very low resistance. The temperature response of a thin layer is proportional to the resistance of the element (Eq.23), and by maintaining the connection resistances to a minimum, the thermal sensitivity of the gold becomes negligible. The use of thin film gold connections prevented any disturbance to the local surface flow. Thicker silver paste layers (Johnson Matthey E8140 + E8150) were applied, and fired, at the pyrex sides, round to the rear surface, where soldered connections were made.

In the initial experiments, a single gold connection on either side of each gauge was used. This restricted the number of gauges possible on each insert due to the physical limitations on the space available for the connections. It was found with this arrangement that insufficient spatial resolution was obtained of the reattachment heat transfer distribution. Sets of gauges were re-manufactured, designed with a common gold connection on either side of successive groups of gauges (Fig.12). This allowed a substantial increase in the number of gauges that could be accommodated. In the final configuration, 39, and 17, platinum thin film elements were deposited on substrate inserts for the plate, and the flap, respectively.

During the period of this study two sets of plate thin film gauge inserts were manufactured. For the flap, six sets of gauges had to be made. These different sets corresponded to six attempts at obtaining the dynamic, and fixed, flap configuration data. These repeated attempts were due to problems of tunnel repeatability, gauge fitting in the model, lack of spatial resolution, excessive erosion caused by the use of an inappropriate material for the tunnel piston, and nozzle exit compression wave interference.

7.4 Heat transfer instrumentation arrangements.

7.4.1 Conventional gauge signal - analogue arrangement.

Initial heat transfer measurements were made by directly applying the voltages from the temperature signals to the analogue lines (Fig.13), and deducing the

currents from measurements of the potential across the first resistor component of each line. The gauge bias unit was a reproduction of a design for shock tube heat transfer measurements, providing a constant current for the gauge operation, with a moderate amplification of the temperature signal prior to the analogue input. These analogues were designed logarithmically, with a frequency range of 1 Hz to 10 kHz. Each analogue line was calibrated with a sine wave generator for its transfer function (see § 7.5).

Both the heat transfer signal, and the temperature signal, were measured simultaneously. The heat transfer signal was also reconstructed from the recorded temperature signal using the method of Cook & Felderman (1966), as a further check of the analogue operation, and also in an attempt to determine which method gave the best quality heat transfer signal. An example of a comparison of these two methods is shown for a gauge on the moving flap in Fig.15, from which it can be seen that there is very good agreement of these two techniques. The noise level is less for the numerically deduced heat transfer, although both methods fail to provide a sufficiently high quality signal to measure the initial flat plate heat transfer values. It was decided that a new instrumentation set up would have to be applied to provide the capability to accurately measure the heat transfer throughout the interaction regions, for both attached, and separated flows.

7.4.2 Low noise instrumentation.

A thin film gauge heat transfer unit was found to be commercially available, based on a design from the University of Oxford for measuring a large range of heat transfer, specifically down to very low values. This unit was considered appropriate for the present work, and an eight channel unit was purchased.

Each channel contains a constant current supply, an analogue network, a two stage amplifier of very high gain, and a final filter stage (Fig.17). A separate power supply is used for each channel, and these are individually screened to minimise noise interference.

The constant current supply is based on the characteristics of a single transistor. This current is adjusted through the base voltage, and the current is then determined by this value, irrespective of thin film resistance changes in the collector section. The gauge temperature signal is fed directly to the first capacitor in the analogue line. Instead of measuring the potential across the first resistor of the analogue line with a high impedance device, this resistor forms the first resistor element of an amplifier stage.

Following each analogue line, there is a film resistance compensation

unit preceding the amplifier circuits. The first resistor in each analogue line has a low resistance value, to maintain low noise levels, and the compensation unit is included to compensate for loading effects that occur on each thin film gauge constant current supply. It can be shown that the current flow into each analogue is given by,

$$i_{in} = \frac{V_o}{R_{o,gauge}} \quad \frac{R_{gauge}}{(Z_{in} + [\delta R + R_{gauge}])} \tag{49}$$

where V_o is the initial voltage across a gauge, Z_{in} is the input impedance of an analogue line, and δR is the film compensation resistance. This equation reduces to that with zero loading of the gauge current circuit when,

$$\delta R + R_{gauge} = 0 \qquad \text{i.e. } \delta R \approx -R_{o,gauge}$$

The appropriate value of δR is set for each gauge with the compensation unit.

The first amplifier stage can be considered as a current to voltage converter. There is a second stage amplifier that follows this, and a final filter of 10 kHz (not shown in Fig.17).

The heat transfer value is related to the measured output voltage of a channel through Eq.(33), with inclusion of the two stage amplifier gain,

$$q_s = \sqrt{\rho c k} \; \frac{1}{R_{in}} \sqrt{\frac{r'}{c'}} \; \frac{1}{\alpha_R V_o} \; \frac{1}{(Gain)} \; V_{OUT} \tag{50}$$

The signal quality with this mode of interconnection was far superior to that in which the voltage across the first analogue resistor is measured with a high input impedance device, as also noted previously by Schultz and Jones (1973).

7.4.3 Evaluation of the surface temperature rise when using the low noise arrangement.

With the low noise instrumentation arrangement there is no facility for recording the surface temperature rise, which is a necessary parameter for properly reducing the heat transfer signal to coefficient values. However, the information necessary to construct a temperature signal is fully contained in the heat transfer signal (Eq.20). Unlike the conversion of temperature to heat transfer, the reverse procedure does not include a derivative term in the

integral, so that the evaluated surface temperature trace will be smooth. A simple linear piecewise fit between the measured data points was used to evaluate this integral,

$$q_s(\tau) = q_s(t_{i-1}) + \frac{q_s(t_i) - q_s(t_{i-1})}{\Delta t}(\tau - t_{i-1}) \qquad (51)$$

$$\text{for} \quad t_{i-1} \le \tau \le t_i$$

This leads to the solution,

$$T_s(t_n) = \frac{1}{\sqrt{\pi}} \frac{1}{\sqrt{\rho c k}} \sum_{i=1}^{n} \left\{ 2\, q_s(t_{i-1}) \left\{ \sqrt{t_n - t_{i-1}} - \sqrt{t_n - t_i} \right\} \right.$$

$$+ \left\{ \frac{q_s(t_i) - q_s(t_{i-1})}{\Delta t} \right\} \left\{ \frac{4}{3}(t_n - t_{i-1})^{3/2} - \frac{4}{3}(t_n - t_i)^{3/2} \right.$$

$$\left. \left. - 2\,\Delta t\,(t_n - t_i)^{1/2} \right\} \right\} \qquad (52)$$

7.5 Calibrations of the heat transfer instrumentation.

There are three calibration procedures that must be applied with the heat transfer gauges and instrumentation described above. Each thin film platinum element must be calibrated for its coefficient of resistance, the value of the substrate thermal properties for separate pyrex inserts must be measured, and each analogue must be calibrated for its transfer function.

(i) Thin film gauge coefficient of resistance α_R.

The coefficients of resistance (Eq.23) were determined from steady-state measurements of each platinum gauge resistance at temperatures within the expected operating range,

$$\alpha_R = \frac{1}{R_o} \frac{dR}{dT} \qquad (53)$$

The first method applied to determine these coefficient values measured the resistance of a gauge with an accurate multi-meter, with the substrate

immersed in heated water, and the temperature measured with a mercury thermometer. This simple arrangement only supported a single gauge for each calibration procedure, and accurate measurements of resistance change, in order to check the assumed linearity of the resistance - temperature relationship, was difficult over small temperature differences.

An automated arrangement was constructed to improve the quality and efficiency of this calibration. Constant current supplies were applied to individual gauges, and from a measurement of the voltage change across each gauge, resistance changes were determined. The substrate was placed in a heated silicon oil bath, and the temperature of this was monitored with an iron-constanton thermocouple. The thermocouple, and gauge potentials, were continually measured using a transient data recorder. The oil bath was allowed to cool from a high temperature, with continual stirring, and at predetermined temperatures the gauge resistances were automatically recorded. This arrangement had the capacity to simultaneously calibrate seven thin film resistance elements. Each constant current supply was calibrated prior to each routine using an upper, and lower, standard resistance value.

For the plate insert, the gauges were calibrated from room temperature to 50°C, and the flap gauges calibrated up to 70°C. The coefficients of linear regression obtained using the resistance - temperature relationship of Eq.(23) were typically greater than 0.9999 for both temperature ranges, demonstrating excellent linearity. The repeatability of the calibration procedure was found to give coefficient values for the same gauge to within ± 2 %.

(ii) Substrate thermal properties.

The calibration for the pyrex thermal product was made using an electrical discharge technique. The circuit developed for this is shown in Fig.18, which was based on a design described by Schultz & Jones (1973). A gauge is initially balanced in the bridge. The current for this is kept low by the 51 kΩ resistor. The capacitor is then charged with the mercury switch open, and subsequently discharged across the bridge circuit. The discharge current is much greater than that for balancing, and creates significant ohmic heating within the thin film, producing a change in its resistance. The useful test period for this discharge is restricted to the first 0.5 % of the time constant $C(R_s+R_2+R_{o,gauge})$, (see Fig.18), during which time the current is constant to within 0.5 %. The ohmic heating at the gauge is equivalent to a step in surface heat flux during this time. This electrical discharge test is first performed with the gauge in a vacuum (or still air), and then repeated

with the gauge immersed in a fluid of known thermal properties. It can be shown that the gauge substrate (pyrex) thermal product is then given by (Schultz & Jones 1973),

$$\sqrt{\rho c k}_{pyrex} = \frac{\sqrt{\rho c k}_{liquid}}{\frac{V_1}{V_2} - 1} \qquad (54)$$

where V_1, and V_2, are the out of balance bridge voltages measured after the same time following the capacitor discharge, with the test in air, and fluid, respectively. The fluid used was glycerine as recommended by Maulard (1969) (see Schultz & Jones 1973). An improvement in the accuracy of this calibration can be achieved if the bridge signal is measured throughout each discharge test, and the voltage levels in Eq.(54) replaced by the respective square roots of the least squares fitted slope of the voltage signal squared plotted against time.

When this technique was applied for the present experiments, the repeatability of measurements for the thermal product at the same gauge location was no better than ±10 %. The cause of this poor repeatability was believed to be due to an insufficient accuracy in initially balancing the bridge. This problem could have been reduced with a better selection of resistance values in the circuit of Fig.18, together with an increase in the discharge voltage level. There was insufficient time for further improvement of this circuit in the present tests. This calibration is the most significant source of error in absolute heat transfer measurement in these experiments.

This discharge circuit also provides a test of the correct operation of a thin film gauge. With a properly deposited thin film, the out of balance bridge voltage should be parabolic in form when plotted against time, in response to the constant ohmic heating (see Eq.58). An incorrectly deposited thin film is clearly evident from a step type voltage response to the discharged current. This is probably caused by small regions beneath the thin film where the generated heat is unable to diffuse into the pyrex, caused by a failure in manufacture for the platinum to properly bond to the substrate in these locations. All the gauges on all the substrates were tested with this method. To obtain the fully working set of 39 thin films on a single substrate for the plate required four attempts at manufacture.

(iii) Analogue transfer function.

Each analogue line must be calibrated for its transfer function (see Eq.50),

$$R_{in}\sqrt{\frac{c'}{r'}} \tag{55}$$

This may be determined by applying a sinusoidal input to the analogue, with frequencies throughout its operating range, and measuring the gains across the first resistance element, R_{in} (see Eq.34). This procedure was used for the separately constructed analogue lines.

For the low noise heat transfer instrumentation, the analogue sections are an integral part of a complete circuit, and the application of a sinusoidal input to the analogue in isolation cannot be achieved. This calibration may, however, be obtained with an equivalent numerical procedure, using accurately measured values of the resistance, and capacitor, components in each analogue line. Referring to Fig.19, the impedances at each frequency are,

$$Z_i = R_i + \frac{Z_{i+1}}{1 + j\omega C_i Z_{i+1}} \tag{56}$$

and,

$$Z_n = R_n + \frac{1}{j\omega C_n} \tag{57}$$

The total input impedance, and hence the gain across the first resistor element, is determined by summing the impedance contributions from the last analogue section through to the first using these equations.

7.6 Sources of error.

Potential sources of error in applying this heat transfer measuring technique include:-

(i) The value of the substrate thermal properties.
(ii) The gauge coefficient of resistance.
(iii) The RC analogue transfer function.
(iv) Finite lead resistance.
(v) Power dissipation in the thin film.
(vi) Erosion of the thin film resistance element during testing.
(vii) Lateral heat conduction effects.

Only some of these terms contribute significantly to the overall error in heat transfer measurement. These are considered in appendix 4, from which an error band of ± 13.5 % in absolute heat transfer measurement, and ± 3.5 % scatter in distributions of heating for relative comparison, are established. Further experimental sources of error in the heat transfer measurement include the response time of the gauge in the dynamic tests, electrical noise on signals, and the error in reducing heat transfer values to Stanton numbers. These are considered in the relevant subsequent sections of this thesis.

8. Liquid crystal thermography.

8.1 Introduction.

The accurate resolution of complex two-dimensional, or three-dimensional, surface heating patterns is difficult with discrete point measurements. This particularly applies to hypersonic testing, where models are usually constrained to a very small scale. An alternative to point measurements is the use of a survey test method such as liquid crystal thermography.

Liquid crystals have been developed as a tool for aerodynamic testing over the last twenty years. Such tests have attempted to employ the shear sensitive, or temperature sensitive, properties of certain liquid crystal formulations e.g. Klein & Margozzi (1969), den Ouden & Hoogendoorn (1974). In these liquid crystals (classed as cholesteric, or chiral nematics) the alignment of successive layers of molecules trace out a helical path. When the liquid crystal formulation is applied to a surface in a thin layer, and when the helical pitch length is of the order of the wavelength of visible light, it selectively reflects bright, almost pure colours. The pitch length, and hence the reflected colour, is sensitive to many influences including temperature, and surface shear. This temperature dependence of the liquid crystal is reversible.

The first attempted application of liquid crystals for surface thermography in aerodynamic testing was made by Klein (1968). The primary objective was to determine regions of boundary layer transition in a supersonic flow, characterised by a change in the adiabatic wall temperature, and hence, different reflected colours. However, attempts to obtain quantitative data were unsuccessful due to the influences of flow induced shear stress, and contamination, on the liquid crystal reflection.

A later development in the application of liquid crystals was the process of microencapsulation, in which tiny droplets of the liquid crystal are surrounded by a wall coating to give small capsules. An early use of this by McElderry (1970), in an experiment similar to that of Klein, successfully observed boundary layer transition with the influence of surface shear removed with the liquid crystal in this form. The application of microencapsulated chiral nematic liquid crystals for surface thermography in hypersonic flows has now been used in several transient facilities (e.g. Scholer & Banerji 1984; Smith & Baxter 1989; Haq et al 1989; Haq et al 1991).

In liquid crystal formulations the reflected colour changes from clear to red at a low temperature, and as the surface temperature increases the

reflected colour passes through the visible spectrum to blue/violet, and then eventually to clear again. A large range of formulations is now available, with red start temperatures between -30°C to 100°C, and colour bandwidths from 0.5°C to greater than 20°C. It is thus possible to obtain high resolution colour thermographs of a model surface over extensive test conditions, revealing phenomena such as separation, reattachment, vortex development, and transition, each characterised by its local heat transfer profile. The advantages of the liquid crystal technique compared to the earlier use of temperature sensitive colour change paints are the reversibility of the colour dependence of the liquid crystals, and the much greater variety of colour change.

8.2 Liquid crystals as a surface thermometer.

The development of techniques applying liquid crystals directly as a surface thermometer for quantitative heat transfer measurements have been successful for low to moderate values of heat flux (< 1000 W/m^2) e.g Ireland & Jones (1986). These techniques have applied the liquid crystal layer to a semi-infinite substrate. The solution of Eq.(20) for constant heat transfer is,

$$T_s = \frac{2\, q_s}{\sqrt{\pi}} \sqrt{\frac{t}{\rho c k}} \qquad (58)$$

The assumption of constant heat flux at any point will be valid if uniform flow conditions exist, and the change in the difference between recovery and wall temperature is negligible. For the condition of a constant heat transfer coefficient with a changing wall temperature, a modification of Eq.(58) has been derived (Schultz & Jones 1973). In both cases, a measurement of the temperature rise at a single point in time is sufficient to determine the heat flux, or heat transfer coefficient, at any location on the model surface. Direct application of Eq.(58), or its modified form, is often used in the application of survey techniques to determine the heat flux from a temperature rise measurement at a single time instant. An accurate knowledge of the substrate thermal properties is required in this calculation. Consideration must also be given to the accuracy of the surface temperature measurement, and the response time of the sensor.

The insulative properties of a liquid crystal layer, and its finite thickness, may make its influence on the thermal conduction process

non-negligible. A numerical, or analytic, solution of the unsteady heat conduction process (Smith & Baxter 1989) reveals a temperature gradient through the liquid crystal layer which is proportional to the surface heat flux. Where application of the liquid crystal layer for directly determining the surface temperature rise has been successfully applied, the errors that occur from a neglect of this gradient, and the liquid crystal response time, have been small. However, when this technique is applied in the hypersonic flow regime, the temperature gradient may become very large (Fig.20). In these circumstances the direct application of the liquid crystal static calibration of colour change with temperature is inappropriate. To infer the model surface temperature by applying this calibration directly to the observed thermograph may incur a considerable error.

The response time of a liquid crystal layer as a surface thermometer has two contributing components. Firstly there is a finite conduction time through this surface layer, and secondly, there is a lag in response associated with adjustment of the liquid crystal molecular structure. The thermal conduction time is that required to raise the liquid crystal layer, or part of it, to a colour transition temperature. This time will depend on the applied surface heat flux, the liquid crystal layer thickness, the base substrate material(s), the model initial temperature, and the liquid crystal colour-temperature bandwidth. Several experimenters have attempted to measure the liquid crystal molecular adjustment time (Parker 1971; Ireland & Jones 1987; Zhang et al 1989), and found values of the order milliseconds. This is consistent with experiments in the Southampton ILPT hypersonic wind tunnel by Smith (1987), and the flow visualisation achieved within the 20ms run duration of the University of Southampton gun tunnel facility (e.g. Westby 1988). The significance of the response time will depend on the run duration of the facility, and hence, the time at which the thermograph is recorded. In short duration hypersonic facilities this response time may be a significant percentage of the available test time, and under these circumstances any method directly applying liquid crystal surface temperature measurements to determine heat transfer must consider this time in the subsequent analysis.

8.3 Development of a liquid crystal technique for measuring heat transfer in short duration hypersonic test facilities.

An accurate evaluation of the effect of a large temperature gradient on the liquid crystal colour reflection, and an assessment of the response time for the full range of flow conditions likely to be encountered on all model

geometries would be very difficult! To avoid these sources of error, an alternative engineering method of heat transfer measurement has been developed by the author of this thesis (Smith & Baxter 1989). This is a reference type method, similar to those that have been applied for quantitative measurements with temperature sensitive paints (e.g. Sartell & Lorenz 1964). The reference model used is a flat plate, with a sharp leading edge, and liquid crystal thermographs obtained on this are compared with Eckert's reference enthalpy prediction of flat plate laminar heat transfer. This forms a colour - heat transfer calibration to be applied to the test model. The details of this technique are fully described in the published paper (appendix 10). This work involved extensive numerical analysis (by this author) of unsteady heat conduction both in one-dimension, and two-dimensions, for multi-layered substrates. A simple conceptual model of the effects of a temperature gradient on colour reflection was also developed. More recent work by Haq et al (1989, 1991) has further developed application of liquid crystal thermography for quantitative heat transfer measurements.

8.4 Application of liquid crystal thermography to the present trailing edge flap model.

Liquid crystal thermography has been applied in the present research for a qualitative assessment of the separated flow structures occurring with fixed flaps.

A microencapsulated chiral nematic liquid crystal, contained in a water soluble binder, was sprayed on the model surface (diluted 1:7 with distilled water for TCF binder, 1:2 for TCS binder). An optimum intensity of the reflected light is obtained with a layer about 10 microns thick when dry (BDH 1988). The optical properties of the liquid crystal layer produce a reflected intensity of about 5% of that of the incident white light. It is necessary to prevent excessive reflection from the model surface which would swamp the liquid crystal display, and this is achieved by applying the liquid crystal layer to a blackened model surface.

There is a sensitivity of the observed colour to the viewing angle, and both the incident light source, and the observation angle, should ideally be as near normal to the model surface as possible. The process of microencapsulation reduces this sensitivity, and experience suggests deviations of as much as 30 degrees from the normal are acceptable.

The instant of recording the surface thermograph is determined with precise triggering of a flash illumination in a darkened test section room,

with a single photographic record obtained for each tunnel run.

8.5 Model construction for surface thermography.

Models manufactured for surface thermography in transient facilities are usually machined from insulating substrates, which then provide a sufficiently high surface temperature rise within a short period. This type of substrate may place a restriction on the complexity of a model, associated with the difficulties of manufacture, or the lack of strength or rigidity.

A multi-substrate model construction has been applied for the present experiments, initially developed in conjunction with the quantitative application of the liquid crystal technique (Smith & Baxter 1989). This is a two substrate model, produced by spraying a thin black paint layer on a metal surface. By reference to the established theory for unsteady heat conduction through such a model (Doorly & Oldfield 1987), it is seen that the surface temperature rise has two distinct regions (Fig.21). Initially the surface temperature rise is rapid, which is a property of the insulative paint layer. This is followed by a much reduced rate of surface temperature rise, which is a characteristic of the metal, but with an initial offset caused by the presence of the paint. The division between these rates of temperature rise occurs in the region of a switch point, which physically relates to the time following that at which the heat pulse penetrates the metal substrate. It is the initial rapid surface temperature rise caused by the presence of the thin paint layer that makes this model construction suitable for liquid crystal thermography. For typical thicknesses of paint (approx. 60 microns), the switch point occurs at about 40 ms after a step in surface heat transfer. In regions of very high heating, the use of a multi-substrate construction can be advantageous in limiting excessive surface temperature rises.

The application of a liquid crystal layer to a painted surface actually produces a three substrate model. The liquid crystal layer is itself an additional insulating layer, and extends the initial rapid rise in surface temperature (Fig.20). The thermal properties of the liquid crystal formulation, and the paint, are very similar.

A separate model was constructed for the flap model surface thermography tests, with the same overall dimensions as that used with the thin film heat transfer measurements. Reattachment heat transfer can be very high, and for these experiments the flap of the surface thermography model was constructed by painting a base metal substrate. On the plate the heat transfer rates are much less, and a semi-infinite insulative insert (black acetal polymer

material, tradename Delrin) was used, which was positioned as near the leading edge as possible, and extending to the hinge line.

8.6 Liquid crystal formulations.

The microencapsulated liquid crystal formulations that were used are commercial preparations obtained from Merck Ltd (formerly BDH Ltd.). Type TCF552 were applied to the plate, and type TCS416 for the flap. The respective colour-temperature bandwidths are listed in table 4. The TCF, and TCS, prefixes refer to the binder mechanism. Type TCS is the latest development, and the most robust. No problems of erosion occurred with either formulation.

9. Schlieren flow visualisation.

A conventional single pass schlieren system, Fig.22, was used for the visualisation of the separated flow structures (e.g. see Liepmenn & Roshko 1957). Regions of the flowfield with different density gradients cause the light passed through the test section to be refracted differently, and these are then intercepted at the knife edge location by varying amounts. The black and white image focused at the camera then appears with regions of different light intensity corresponding to changes in the flowfield density gradients. The illumination used for these schlieren tests was an argon spark source with a duration of about 0.5 μs, producing a flow visualisation which is effectively instantaneous. The knife edge was placed horizontally which produces a schlieren visualisation sensitive to changes in the component of density gradients which are normal to the test model plate surface.

The camera film conventionally used with the spark source illumination is a Polaroid film with an ASA rating of 3000. This was replaced with a Kodak T-Max negative film with an ASA rating of 3200. This allowed the subsequent pictures to be enlarged with much better resolution, requiring no alterations to the spark source intensity, or duration.

For some of the high freestream Reynolds number tests in these experiments, the knife edge was replaced with a graduated cut-off filter. This provides a sensitivity which increases as the density gradient in the flow increases. This helped remove some of the flow noise in the nozzle exit boundary layer which surrounds the inviscid test core flow. The use of the negative film, and the graded filter, were both shown by this author to significantly improve the quality of the schlieren flow visualisation obtained in the ILPT facility. Unfortunately, there was insufficient time available to repeat the low freestream Reynolds number tests using a graduated cut-off.

PART III

STEADY SEPARATED FLOW EXPERIMENTS.

10. Introduction to the steady separated flow experiments.

The results of the experiments with the model in its fixed flap configuration are presented in this section. The separation lengths, and heat transfer distributions, obtained from these tests form a basis for comparison with the dynamic flap measurements, from which the separated flow unsteady response has been interpreted. These steady measurements also help establish the general characteristics of the separations induced by this trailing edge flap model configuration, including the significance of finite span, and chord, effects, and whether transition occurs within these regions.

Liquid crystal thermographs, and schlieren flow visualisation, were obtained for fixed flap angles from 0 to 35 degrees, at 5 degree increments. Measurements of the centre line heat transfer distribution using the thin film resistance gauges were made at each of these conditions, except for the 5, and the 10, degree fixed flap settings. All these tests were repeated with the addition of side plates. These experiments were made with the tunnel operated at its lowest freestream Reynolds number of 2.45×10^6/m. Some additional schlieren photographs were obtained at higher freestream Reynolds numbers.

The heat transfer signals required a further filtering stage to achieve an acceptable signal:noise ratio for the low values that occurred within the separated flow. Simple R-C low pass analogue filters, with a 1.1kHz cut-off, were applied to all the heat transfer signals. This achieved a level of electrical noise that allowed the measurement of heat transfer as low as 0.8 kW/m^2, with a minimum signal:noise ratio of 7. For these steady separations, each heat transfer value was obtained by averaging the analogue voltage signal over a period of 50 ms. This was particularly necessary for the gauges on the flap, and near the hinge line, where substantial flow noise existed within large separated flows. In regions of high heat transfer, an error may occur by averaging an analogue signal over a finite time, during which the increasing wall temperature reduces the heat transfer level. For the highest heat transfer measured in the reattachment region, the surface temperature difference during this interval was less than 1 degree about the central point of the period within the tunnel run at which this data was reduced. When presented in Stanton number form, the error from this is only $\pm$ 0.27%.

The restriction of eight thin film gauge instrumentation modules required measurements from separate wind tunnel runs to be combined to obtain a complete heat transfer distribution. In each tunnel run the heat transfer at the first gauge on the plate was measured as a reference, from which the

freestream flow properties could be inferred (see § 11). The remaining 7 channels were assigned to gauges widely dispersed along the plate, and the flap. This gives a better representation of the data scatter in a complete heat transfer distribution than the combination of measurements from tests in which the biased gauges have been adjacent, or in very close proximity.

The heat transfer measurements for both the steady, and the dynamic tests, were reduced for the period of the freestream flow where the steadiest stagnation conditions existed within each tunnel run. The variations in the freestream test flow conditions were interpreted from changes in flat plate laminar heat transfer signals (e.g. Fig.31). The highest quality flow existed typically between times of 400 ms, and 700 ms, after the flow start. The expected cooling effects of vortex developments in the compression tube for this tunnel operation are apparent in the heat transfer signals for the final 30% of the tunnel run duration. There also appears a region of relatively cool flow during the first 16% of the run period.

11. Determination of the stagnation temperature.

To reduce the measured heat transfer values to Stanton numbers, it is necessary to measure, or infer, the stagnation pressure, and the stagnation temperature, in each test. It was assumed that Mach number variations between tests at a nominal operating condition were negligible. The freestream velocity, density, and the recovery temperature, can then be calculated. A flat plate laminar recovery temperature was used in reducing all the heat transfer measurements to Stanton numbers. In the subsequent comparison of the flap heat transfer distributions between the fixed, and dynamic, conditions, a flat plate turbulent recovery temperature was also used.

The pressure rises that occur in the compression tube during the tunnel operation were measured with a transducer mounted near the nozzle entry. These measurements were then added to the absolute charge pressure initially contained in the tube, before the piston compression, to determine the stagnation pressure during the run period (Fig.31). A thermocouple in this location would have an insufficient thermal response time to accurately measure the stagnation temperature throughout the run period. This quantity is instead typically measured with a probe mounted in the freestream flow (East & Qasrawi 1978). However, the use of a probe in each test would introduce lengthy operational procedures, and it would be difficult to locate this in a position where it did not interfere with the test model flowfield.

For the present experiments, a method was developed for determining the stagnation temperature from the measurements of heat transfer on the test model. The first gauge on the flat plate is ahead of the separation interaction at all the flap angles, and therefore measures a laminar flat plate heat transfer. With this measured heating as the solution of Eckert's (1955) reference enthalpy prediction of flat plate laminar heat transfer, the flow properties in this equation were substituted as functions of the unknown stagnation temperature. A simple iterative numerical scheme was then used to solve for this stagnation temperature.

The reference enthalpy method is an accurate prediction of surface heat transfer, provided there is a negligible influence of any pressure gradient in the streamwise direction (accurate to within 6% compared with numerical solutions over an extensive range of hypersonic freestream flows, Eckert 1955; Hayes & Probstein 1959). However, in real hypersonic flows, the large laminar boundary layer thickness on a flat plate has a displacement effect on the adjacent inviscid flow. This generates a viscous-inviscid interaction from the

leading edge region. The effect of this is to increase pressures above the freestream static values, and create a negative pressure gradient that increases towards the leading edge. The form of the pressure distribution induced by this interaction is characterised by the parameter $\bar{\chi}$, where,

$$\bar{\chi} = M_{\infty}^{3} \sqrt{\frac{C}{Re_{\infty,x}}} \tag{59}$$

Since $\bar{\chi}$ includes a Reynolds number, based on distance from the leading edge, it is then a function of x at a fixed set of freestream conditions. For large $\bar{\chi}$ (»1) the interaction is termed strong. In this regime, the displacement effect of the boundary layer on the inviscid flowfield is strong, and the changes this induces then feedback to influence the boundary layer development. The interaction is thus mutual, and continues until an equilibrium state is achieved. As $\bar{\chi}$ is reduced, the rate of growth of the boundary layer, and its influence on the inviscid flow, become less. For $\bar{\chi}$~o(1) the interaction may be defined as weak, and the changes induced in the local inviscid flow are then considered only as small perturbations superimposed on the uniform freestream flow.

At the first gauge location on the plate, $\bar{\chi}$ = 1.05 at Re_{∞}= 2.45x10^{6}/m, which is in a region of weak viscous interaction. Lees & Probstein (1952) (see also Hayes & Probstein 1959) presented an analysis of the boundary layer development in the weak interaction regime, and determined that there was no first order effect on the heat transfer due to the self-induced pressure gradient. To first order in $\bar{\chi}$, the heat transfer is then identical to the zero pressure gradient result. Lees & Probstein's (1952) theory indicated that this was an accurate assumption for values of $\bar{\chi}$ as high as 5. Similarly, to first order in $\bar{\chi}$, the recovery temperature is unaltered by weak viscous interaction (Probstein & Lees 1953). Vidal et al (1963) also proposed a solution for the heat transfer in the weak interaction regime, based on the assumption of local flat plate similarity (see appendix 5). Application of this approximate analysis to the present experiments, at the first thin film gauge location, indicated that the effect of the interaction was to increase the heat transfer by only 1.8% above the zero pressure gradient value.

In the present experiments the Reynolds number, based on the plate leading edge thickness, is 50. This satisfies the criterion proposed by Hayes & Probstein (1959) that this Reynolds number should be less than 100 for

bluntness effects to have a negligible downstream influence on the leading edge viscous interaction.

To further support the use of the reference enthalpy prediction of heat transfer for inferring the stagnation temperature in the present tests, the discrepancy between experimental measurements of flat plate heat transfer, and zero pressure gradient predictions, have been examined in previous investigators work. The correct parameter for correlating weak, and strong, viscous interaction effects on flat plate heat transfer coefficients is $\bar{V}$ (Anderson 1989), where,

$$\bar{V} = M_\infty \sqrt{\frac{C}{Re_{\infty,x}}} \tag{60}$$

In the experiments of Cheng et al (1961), and Holden (1964, 1966a), comparisons of measured flat plate heat transfer in the weak interaction regime with zero pressure gradient predictions agree well for $\bar{V} \leq 0.034$, and $\bar{V} \leq 0.026$ respectively ($\bar{\chi} \leq 1.6$, and $\bar{\chi} \leq 2.57$). The scatter between the measured, and predicted, heat transfer is then $\leq 15\%$ for Cheng et al, and $\leq 10\%$ for Holden's data. These discrepancies result from errors in measuring heat transfer, and the freestream flow properties, approximations in the prediction methods, and second order $\bar{\chi}$ viscous interaction effects on heat transfer. For the present experiments, $\bar{V} = 0.022$ at the first gauge location ($\bar{\chi} = 1.05$), which is within both of the above regimes. For the present experiments, an error band of $\pm$ 25 % has been assumed for the possible difference between the measured heat transfer, and the reference enthalpy prediction of heat transfer that would be calculated with the freestream flow conditions. This includes $\pm$ 13.5 % error in the absolute heat transfer measurement (appendix 4), $\pm$ 6 % error in the accuracy of the reference enthalpy prediction, and $\approx \pm$ 5 % to allow for freestream Mach number gradient effects (see § 12) and noise on signals. With this error band, the subsequent uncertainty in determining the stagnation temperature using the inverse reference enthalpy method was found to be $\pm$ 9.7 %. The error in determining the absolute Stanton numbers have been considered in appendix 4 for particular examples. For the highest heat transfer measured at a flap angle of 35 degrees, the maximum possible error band in the reduced Stanton number is - 15 % to + 28 %. The actual errors are believed to be considerably lower than this example, as reflected by the low scatter apparent in *all* the Stanton number

distributions. This method of determining the stagnation temperature provided a repeatable technique for each test, which was particularly important when data had to be combined from different tunnel runs to obtain each complete heat transfer distribution for both the steady, and the unsteady, separated flows.

This method of determining the stagnation temperature in each test was compared with an approximate technique based on the equations for the operation of an isentropic light piston tunnel, using the measured run duration, and the measured stagnation pressure (appendix 6). Applying this analysis to a particular tunnel run, the mean stagnation temperature calculated for the complete run was 583 K, and for the period 400 ms to 700 ms, where the freestream flow conditions were reasonably constant, the stagnation temperature calculated was 617 K. This latter value compares with a value of 607 K determined using the inverse application of the reference enthalpy method, a difference of only 1.6 %.

For the original low Reynolds number operation of the wind tunnel facility, a measurement of the freestream stagnation temperature from a stagnation probe had been made (Baxter 1990). This gave a value of 660 K for the central period of the run. The determination of the stagnation temperature over a substantial number of tunnel runs at this original low Reynolds number operation, using the inverse reference enthalpy method, gave average values for the central period of the test flow varying between 657K, and 684K for different runs (associated with variations in stagnation pressure of up to 20%). There was insufficient time available to re-calibrate the modified low Reynolds number condition with the stagnation probe.

The close agreement of stagnation temperatures determined with the inverse reference enthalpy method, and the alternative techniques, further supports the use of this method in the present experiments.

12. Model position.

The first complete set of fixed flap measurements were made with the model located in a position with the leading edge just downstream from the nozzle exit plane. The last contribution to these measurements were the liquid crystal thermographs. These indicated the introduction at large flap angles of very high heating near the flap trailing edge corners, evident from the colour transition to blue, and adjacent clear regions where the liquid crystal had passed above its colour bandwidth (Fig.23a). There also appeared significant three-dimensional features on the plate thermograph within the separated flow region. These effects are now attributed to interference from the nozzle exit compression waves. The presence of this had not been initially suspected from either the centre line heat transfer measurements, or the schlieren photographs, in which the separated flows were thought typical of a transitional wedge type.

Roberts (1989) observed separations on the same scale fixed model geometry in the University of Southampton ILPT hypersonic facility that grew throughout the run duration. Although the impingement of nozzle compression waves on the model was one explanation proposed, there was no direct experimental evidence for this. The model used in the present tests was placed at a lower position within the inviscid test flow than the location used by Roberts. This presented less flow blockage, and the contraction of the nozzle exit waves was therefore less. Steady separations were observed in the present tests at all the fixed flap angles. However, the liquid crystal thermographs clearly indicate that the single condition of steady separations is insufficient to define an experiment free from nozzle compression wave influences.

To remove this interference effect, it was necessary to move the model forward, and place the diffuser as close as possible to the model trailing edge. This reduced the open jet length, minimising flow spillage from the diffuser, and hence the contraction of the nozzle exit waves. The model was finally located in a forward position where no evidence of this interference could be observed from the surface thermographs with the flap at its highest angle of 35 degrees. With the model in this position, the leading edge penetrated the last 5 cm of the nozzle length. In hypersonic contoured nozzles, the Mach number gradient in the exit region is small. For this particular nozzle geometry, at a higher unit freestream Reynolds number operation (32.4×10^6/m), it has been estimated that the change in the centre

line Mach number along the final 5 cm is 0.05 (East 1992). All the liquid crystal, schlieren visualisation, and thin film heat transfer measurements, for the all the fixed flap angles were repeated with the model in this position.

With the model in this forward position, the interference effects previously observed at high flap angles disappear, and the heating pattern on the plate is much more two-dimensional (compare Figs.23a & 23b). For flap angles of 20 degrees, and less, the details of the thermographs are the same with the model in the two positions (Figs.23c & 23d).

The schlieren photographs of these flow structures have been compared for the two model positions. When the nozzle waves interact with the model flowfield, the scale of the separation is increased, and the reattachment process is less clearly defined (Figs.24a & 24b). The shear layer also then appears to have more prominent irregular edges, suggesting a more transitional - turbulent flow. This observation is supported by the first set of fixed flap heat transfer measurements (see Smith & East 1991). An unawareness of these tunnel interaction effects for the steady separations presented in this reference led to the determination of a response time of the unsteady separated flows which is now known to be incorrect.

The compression waves exiting the nozzle appear as a thin white line above the model in the schlieren pictures. The position of these which is visible is that in the central vertical plane of the flow, where the density gradient normal to the knife edge is strongest. The direct impingement of the nozzle exit compression waves on the flap trailing edge corners is not clear in these schlieren pictures. The normal density gradient of the nozzle shock surface at these locations is small, and this is obscured by the reattachment process of the free shear layer.

The separation lengths with the model in its forward, and original position, are plotted against the flap angles in Fig.26. These lengths are the distance from the hinge line to the separation points (see § 13.1). With the model in the forward position, the separation length remains nearly linear with flap angle throughout the deflection range up to 35 degrees. A comparison of the separation lengths for the two model positions shows that for flap angles up to 20 degrees, the separation lengths with the model moved forward are slightly less. For flap angles greater than this there is a strong increase in the rate of separation length growth for the model downstream of the nozzle exit plane. This abrupt divergence from the separation lengths obtained with the model moved forward is believed to be due to the nozzle exit

waves impinging on the flap when the model is in this position. This hypothesis is consistent with the liquid crystal thermographs which indicate interference effects at a flap angle of 25 degrees for the model downstream of the nozzle. The small discrepancies in separation lengths up to 20 degrees for the two model positions may be explained by a slight expansion of the freestream flow downstream of the nozzle exit, caused by an off-design performance of the contoured nozzle at this low Reynolds number operation. A comparison of the flat plate heat transfer distributions, ahead of the separation interactions, Fig.32, shows a slightly greater rate of reduction of heating with distance from the leading edge for the model in the downstream location. This suggests an increased expansion of the freestream flow for the model in this position. The results that are subsequently presented within this part of the thesis indicate that the fixed flap separated flows are transitional. This type of flow separation is particularly sensitive to small changes in the freestream flow. An increase in the freestream Mach number, and consequent reduction in unit Reynolds number, will delay transition, and increase the scale of this separated flow type. This is consistent with the comparison of separated flow lengths for the two model positions for flap angles below 20 degrees.

To formulate a more specific criterion for interference free separated flows, the height of the nozzle exit compression wave, visible in the schlieren photographs, above the projected nozzle centre line at the flap trailing edge position, has been taken as a measure of the flow blockage. The value obtained with the model in the downstream location, with a flap angle of 20 degrees, has been taken as the limit for the maximum test core contraction, beyond which tunnel interference effects may occur. When this criterion is applied with the model moved forward (Fig.27), these separated flows are seen to comfortably satisfy the imposed condition for interference free tests for all the flap angles.

As the flap angle is increased, the trailing edge moves closer to the nozzle centre line height, where the inviscid flow core is expected to be widest for a given contraction rate. For the same height of the nozzle exit compression waves above the nozzle centre line, interference is therefore less likely when the model is forward with high flap angles, than for the model in its original downstream location at the lower deflection angles, from which the criterion was established.

The linearity of separation length increase with flap angle for the forward model position is additional strong evidence that these separated

flows are free from tunnel interaction effects (Fig.26). The fixed flap results presented in the following sections are for the model in this forward position.

This author believes that some previous experimenters, without the benefit of a high resolution thermal mapping technique such as liquid crystal thermography, or who have not used surface oil flow visualisation, may have been unaware of similar interference effects in their tests. The data from the present experiments demonstrates that this interference can have a significant influence on the scale of the separation interaction, and its properties, even though these may still appear typical of the expected flowfield type. The results also reinforce the observation made by previous experimenters that the model position should be maintained invariant when transition occurs within the flowfield.

13. Steady separated flow results and discussion.

13.1 Separated flow lengths.

A method that has been used by previous investigators for determining the separation point from schlieren photographs is to assume that this occurs at the location where the separation shock intersects with the visible edge of the boundary layer (e.g. Putnam 1965). To support the use of this method in the present experiments, application of this criterion, and that for determining the separation point from measured pressure distributions, were both applied to the data of Putnam (1965), Miller et al (1964), and Needham (1965a). The separation locations determined with these two criteria were in good agreement within each of these experiments.

At the low freestream Reynolds number of 2.45×10^6/m, without side plates, a separation, and reattachment, shock are visible for flap angles down to 10 degrees. The separation lengths have been determined from the schlieren photographs using the above criterion, and these are plotted against flap angle in Figs.26 & 28. The separation length, defined as the distance from the separation point to the hinge line, increases nearly linearly with flap angle. This is a characteristic that has been previously observed for laminar wedge separations (Putnam 1965). An extrapolation of this line to zero separation length gives an estimate of the incipient separation wedge angle, which for these freestream conditions gives a value of 6.4 degrees. This is in close agreement with a value of 6.5 degrees predicted with a laminar incipient separation correlation by Holden (see Hankey & Holden 1975).

The leading edge shock wave, generated by viscous interaction, did not interfere with the wedge flowfield for any of the flap angles studied.

With the side plates attached, the details of the flowfield adjacent to the model are obscured in the schlieren photographs, and it has been necessary to use another method to determine the separation point locations. The ratio of the separation point heat transfer coefficient to its equivalent laminar attached flow value was determined for each flap angle, without side plates, and plotted against the position of the beginning of the separation interactions. Each interaction start occurs where the heat transfer begins to depart from its flat plate distribution, which has also been found to be well approximated by the intersection of an extrapolation of the separation shock to the plate surface. The variation of the separation point heat transfer ratio with the interaction start location was then applied to the heat transfer distributions produced with side plates to determine the separation

points for these. This assumes that the fraction of flat plate heat transfer at the separation point is only a function of the position of the separation interaction, and is not influenced by the edge boundary condition.

The effect of adding the side plates increases the separation lengths substantially at low flap angles (Fig.28). At the high flap angles the percentage increases are less. The schlieren photographs show that the side plates are not quite large enough to completely contain the separated flow at the highest angle of 35 degrees. This may contribute slightly to the reduction in separation length increase at the high angles when side plates are added. More significantly, for the large separated flows the beginning of the separation interaction follows from a region of negative pressure gradient, induced by the leading edge viscous interaction, and this gradient increases towards the leading edge. This tends to suppress substantial increases in separation length when side plates are added with the flap at large angles. At the low flap angles, the side plates extend well ahead of the separation point, and the potential for viscous interaction on their inner edges, which may influence the scale of separated flow, is greatest. These adverse effects of side plates, which tend to increase the separation length beyond its true two-dimensional value, may be a reason for the substantial effects of side plates on the scale of separation at the low flap angles.

The separation lengths at higher freestream Reynolds numbers, for flap angles from 15 to 35 degrees, have also been determined with schlieren photography, and are shown in Fig.28. The effect of increasing freestream Reynolds number is seen to consistently reduce the separation length at each of these angles (see also Fig.25). This is sufficient to define these higher Reynolds number conditions as transitional separations. For the lowest freestream Reynolds number condition, the reduction in separation length as the freestream Reynolds number increases would occur if these were transitional. However, with a smaller increment in the freestream Reynolds number, some of these separation lengths may initially increase before transition is introduced at the higher freestream Reynolds numbers of these other tests. To be able to determine the separation types at the low Reynolds number using this criterion, it would be necessary to additionally measure the separation lengths at a reduced freestream Reynolds number. If the separated flows were then transitional at $Re_\infty = 2.45 \times 10^6$/m, the reduction in Reynolds number would increase the separation lengths, and if laminar at some flap angles, those separation lengths would reduce.

The linearity of the increase of separation length with flap angle is

still observed at the higher Reynolds numbers, where the separations are transitional. An extrapolation of these lines indicates that the effect of increasing freestream Reynolds number from the lowest value of 2.45×10^6/m to 6.4×10^6/m increases the separation lengths for flap angles of about 10 degrees, and less. The separated flows for these angles, at the low freestream Reynolds number must then be laminar. The effect of this increase in freestream Reynolds number is to reduce the incipient separation wedge angle, which is a characteristic expected in the laminar regime. At the highest freestream Reynolds number of 9.7×10^6/m, the incipient separation angle is much higher. Heat transfer measurements on the model for this freestream flow have shown that flat plate transition occurs ahead of the hinge line (East & Smith 1990), which accounts for the increased resistance to separation.

The separated flow length measurements at the three freestream Reynolds numbers, without side plates attached, have been added to the correlation proposed by Needham & Stollery (1966b) (Fig.29a). To apply this correlation it is necessary to evaluate, or measure, the local inviscid flow properties at the beginning of the separation interaction. These will not be equal to the freestream flow values because of leading edge viscous interaction. The wall pressure distribution has been estimated using the second order weak interaction analysis of Hayes & Probstein (1959), which for a Prandtl number of 0.725 gives,

$$\frac{p_{wall}}{p_\infty} = 1 + \gamma\, d_\infty\, \bar{\chi} + \frac{\gamma\,(\gamma + 1)}{4}\, d_\infty^2\, \bar{\chi}^2 \qquad (61)$$

where,

$$d_\infty = \frac{1}{2}\left\{ \frac{1.937}{M_\infty^2}\,\frac{T_{wall}}{T_\infty} + 0.578\left\{\frac{\gamma - 1}{2}\right\} - \frac{0.207}{M_\infty^2} \right\}$$

The required local flow properties are evaluated from this pressure distribution using tangent wedge theory. The separated flow pressure terms in the length correlation have been estimated from the flow geometries, using simple oblique shock wave equations. For the plateau pressures, the deflection angles are those of the separated shear layers, measured from the schlieren photographs. The accuracy of the schlieren photographs was determined by comparing the measured flap angle in these pictures with the values set in the experiments using the potentiometer calibration. The difference between these

did not exceed 1.4 %, which occurred at the highest flap angle of 35 degrees. The peak pressures at reattachment have been assumed equal to that achieved with the two shock compressions of the separated flows. The finite thickness of the shear layer makes the determination of its effective wedge angle subject to error, particularly for the small separated flows. An error band of ± 0.5 degrees was assigned to the measurement of this angle, and this is illustrated for each point on the correlation. It has been assumed that a developed plateau pressure exists for all the separated flows. This assumption may be incorrect for the small separated flow at the flap angle of 10 degrees. The separated flow length defined in this correlation is equal to the distance along the shear layer between the origins of the separation, and reattachment, shock waves. The origin of the reattachment shock was difficult to define in the schlieren visualisation for some of these tests, particularly for the small separated flows.

All the lowest freestream Reynolds number data points lie about the laminar region of this correlation. At the high flap angles these points are slightly below the laminar line, and at low angles they are above. However, in both limits the data is within the scatter of the previously correlated laminar data. At the higher freestream Reynolds numbers, the data points move clearly into the region of transition, and towards the turbulent separation regime. In this correlation there is no direct account taken of wall cooling effects, or the pressure gradient that may be generated by leading edge viscous interaction. This may account for some of the scatter in this correlation of laminar data from different experiments.

The present low freestream Reynolds number separation lengths have also been added to the fully empirical laminar correlation of Popinski & Ehlrich (1966) (Fig.29b). The agreement with this correlation is very good. However, the data correlated by Popinski & Ehlrich was not rigorously examined for transition effects, and the results should be interpreted with caution.

A separated flow length correlation proposed by Erdos & Pallone (1962) has not been used because of the scatter in applying this which has been found by previous investigators (e.g. Giles & Thomas 1966).

13.2 Plateau pressures.

The correlation of plateau pressure coefficients has been used by many investigators as a test of the free-interaction principle (see § 2.3). The plateau pressures for the low freestream Reynolds number tests, Re_∞ = 2.45×10^6/m, without the side plates attached, have been correlated with data

from other experiments in the form originally suggested by Chapman et al (1958) (Fig.30). This correlation has been successfully applied for separated flows in the hypersonic flow regime by other investigators (e.g. Erdos & Pallone 1962; Sterrett & Holloway 1964; Needham & Stollery 1966b; Hoelmer 1967; Harvey 1968). Although the present separations may be influenced by lateral venting, the experiments of Putnam (1965) indicate that this does not influence the plateau pressures, which are still correlated by terms derived from a two-dimensional free-interaction analysis. Some investigators have attempted to correlate plateau pressures with a Reynolds number term instead of the skin friction coefficient (e.g. Hill 1967). This, unlike skin friction, does not account for Mach number effects, wall cooling, or the leading edge interaction. This is particularly important when correlating high Mach number data from different sources. The apparent large scatter in Fig.30 for high Mach number data is due to a log scale effect which significantly amplifies differences between ordinate values when these values are small.

To apply this correlation to the present data, the local skin friction coefficient must be determined, allowing for the effects of leading edge viscous interaction. The favourable pressure gradient this interaction produces increases the skin friction coefficient above the zero pressure gradient value. In the weak interaction regime, an additive correction term is applied to the zero pressure gradient prediction (Hayes & Probstein 1959) which for a Prandtl number of 0.725 gives,

$$c_f = \frac{0.664\sqrt{C}}{\sqrt{Re_x}} + 2\sqrt{\frac{C}{Re_x}}\left\{\frac{0.9685}{M_\infty^2}\left\{\frac{T_{wall}}{T_\infty}\right\} + 0.289\left\{\frac{\gamma - 1}{2}\right\} - \frac{0.1035}{M_\infty^2}\right\}^2 \bar{\chi} \qquad (62)$$

In the correlation of the free-interaction process, both the plateau pressure, and the skin friction coefficient, should be non-dimensionalised with the local inviscid flow properties at the interaction start. The plateau pressure values for the present experiments were determined by calculation from the shear layer angle measured from the schlieren photographs, and will therefore

suffer from the inaccuracies already described (§ 13.1). These sources of error are indicated with error bars added to the highest, and lowest, correlated data points for the present data. Included in this correlation are the experimental measurements of Holden (1971a, 1978), which agree well with the measurements from other sources. For these hypersonic data the skin friction was directly measured.

The correlation of the present low Reynolds number data is seen to be within the scatter of the other laminar separation measurements, and the various correlation equations. An estimate of the plateau pressures that would occur if these separations were fully turbulent has been determined by applying a turbulent plateau pressure correlation proposed by Sterrett & Holloway (1964). To plot this in the form of Fig.30 the appropriate skin friction value was estimated using Eckert's (1955) reference enthalpy method for a fully turbulent boundary layer, with interaction start locations between the limits of those measured in the low Reynolds number experiments. The turbulent plateau pressure estimate is seen to lie well above the measured plateau pressures (Fig.30).

13.3 Three-dimensional effects.

For the tests without side plates, the liquid crystal thermographs indicate that edge effects, which include lateral venting, cause only small departures from a substantially two-dimensional flowfield at all flap angles (Figs.23b, 23d, & 23e). Of course, these separations may not be the true two-dimensional flow geometries which would occur with a model of infinite aspect ratio. In comparing the liquid crystal thermographs in Fig.23 it should be noted that these were obtained with slightly different model initial temperatures.

At low to moderate flap angles, without side plates, there is a narrow heating pattern adjacent to both edges of the plate, which appear to originate from near the leading edge corners (e.g. Fig.23d). These have been attributed to the development of vortex structures, where a pressure differential created by the plate underside compression surface at the leading edge induces a lateral flow. The heating pattern indicates that these vortices are deflected outwards by the pressure rise that occurs in the separation region. At the higher flap angles, the separation pressure rise occurs earlier, and evidence of this vortex structure diminishes.

An example of the effect of adding side plates can be seen with a comparison of Figs.23e & 23f, with the flap at 30 degrees. The addition of these appears to introduce additional three-dimensional disturbances. On the

plate, adjacent to the inner edge of the side plates, and originating from their leading edge, there is a region of relatively low temperature. These regions extend beyond the thermal penetration depth from each plate side, and cannot therefore be attributed to a thermal conduction affect associated with the side plate structures. The thermograph on the flap is less two-dimensional than without side plates, with zones extending from the side plates where the rate of heat transfer rise is less than for the centre line region. No leading edge vortex heating effects are visible when the side plates are attached.

An observation at all the flap angles, both with, and without side plates, are heating striations in the reattachment region (Fig.23). This disturbance is spatially periodic across the complete flap span, with an approximately uniform wavelength. These effects are consistent with the generation of counter-rotating streamwise vortices within the reattaching boundary layer (Miller et al 1964; Ginoux 1969b; Kipp & Helms 1985; Simeonides & Wendt 1991 etc). The spanwise variation of heating in the reattachment region that this phenomenon induces has been estimated by applying the equation of surface temperature rise for a two layer substrate, with the second layer semi-infinite, and assuming a time invariant surface heat flux (Doorly & Oldfield 1987). Neglecting the effects of the temperature gradient that exists through the liquid crystal layer (Smith & Baxter 1989), an application of this simple analysis to Fig.23f (flap angle = 30 degrees, plus side plates), with periodic changes of colour from blue to clear (above the colour bandwidth) across the reattachment region, the spanwise variation in heat transfer is about 30%. This simple estimate neglects local two-dimensional conduction effects, which have been predicted to occur with the high heat transfer gradients created by this particular vortex phenomenon. The consequence of this neglect is to underestimate the spanwise variation in heat transfer. The spacing of the striation patterns is approximately 6 mm.

Although the schlieren system is focused along the model centre line, it is sensitive to density gradients across the complete span. The presence of small variations in separation length across this width creates a non-planar separation shock surface, which then appears in a schlieren spark image photograph (duration approx. 0.5 μs) as irregularities in the shock thickness. Such irregularities are visible for the separation shock generated with the large separated flows (e.g. Fig.24). The origin of separation length variations may be associated with edge effects. They may also be due to transition in the free shear layer, which may introduce both irregularities and unsteadiness that are not uniform across the complete model span.

13.4 Heat transfer distributions.

The heat transfer distributions which were measured without the side plates fitted are discussed first in this chapter, presented in the form of Stanton numbers. The effects of adding side plates are subsequently considered in § 13.4.1.

The heat transfer profile (in Stanton number form) with the flap at zero degrees has a laminar form along both the plate length, and the flap length, with no indication of transition (Fig.32). The comparison with Eckert's (1955) reference enthalpy prediction of laminar flat plate heating, fitted to the first thin film gauge, is good, although there is a slight deviation near the hinge line. This is probably caused by a small disturbance in the flow introduced by the flap leading edge. This is difficult to avoid in a geometry that must allow for the rapid displacement of this surface. The slightly greater rate of reduction in heating with distance from the leading edge for the model in the downstream location has been attributed to an increased expansion of the freestream flow for this length of open jet (§ 12). The scatter in the flat plate heat transfer distributions is within ± 6% of a mean curve, which is representative of that obtained at all the fixed flap angles. This is attributed to measurement errors (appendix 4), noise on signals, and effects of variations in flow conditions between tunnel runs.

At 15 degrees, the heat transfer distribution is typical of a laminar separation (Fig.33a). At the start of the interaction there is a fall in heat transfer, which continues to a minimum value just upstream of the hinge line. The heat transfer rises rapidly on the flap, and a peak value is attained just ahead of the trailing edge. The heat transfer in the separation region has a smooth rounded form. A local rise in heat transfer at the beginning of the interaction, which was observed by Miller et al (1964), is not present in this distribution, and was not found at any of the flap angle settings. This is consistent with the measurements of many other investigators since Miller et al.

As the flap angle increases, the beginning of the interaction, apparent with the departure from the flat plate heating distribution, moves upstream. At all the flap angles there is a fall in heat transfer below the attached laminar value, indicating an initially laminar interaction. The location of the separation point, determined from the schlieren photographs, occurs with a heat transfer between 0.5 to 0.65 of its equivalent attached flat plate value. This is consistent with other investigators measurements at similar freestream flow conditions, where separation locations have been determined using oil

flow visualisation (e.g. Johnson 1970).

A pronounced peak in the heat transfer distribution develops on the flap at angles larger than 15 degrees. The value of this increases rapidly with flap angle, and moves towards the hinge line.

As the flap angle increases above 15 degrees, there is a change which occurs in the form of the heat transfer profile in the separation region on the plate (Figs. 33b & 33c). The rise in heat transfer from the minimum value begins to occur substantially ahead of the hinge line, and there is a slight step in this rise. These features become more apparent as the separation length increases. The departure from a smooth rounded heating distribution, expected for laminar separations, is believed to be associated with the beginning of transition in the separation region, as similarly observed by previous experimenters (e.g. Johnson 1970; Sterrett & Holloway 1964). The distance between the separation point, and the minimum heat transfer from where transition is believed to originate, reduces slightly as the flap angle is increased. As a percentage of the shear layer length, this rise occurs much earlier as the flap angle, and separation size, increase. At the positions where the heat transfer profiles display this stepped type distribution, the noise levels on the heat transfer signals begin to increase (Fig.34). For the large separated flows, where this step becomes more pronounced, the noise levels become substantial within the remainder of the separated flow region. This supports the supposition from the form of the heat transfer profiles that transition occurs within the separated flows for flap angles greater than 15 degrees.

A centre line heat transfer distribution, schlieren flow visualisation, and liquid crystal thermograph, are compared in Fig.35 for the example of a flap angle of 30 degrees. The low heating levels, and rapid increase to a high peak value on the flap, can be clearly identified with the separation, and the reattachment process in the schlieren photograph. The peak value of heat transfer is seen to occur after the flow has reattached. The separation, and reattachment, regions are also accurately located in the qualitative features of the liquid crystal thermograph. The low heating levels in the separated flow are visualised with a colour change only to red, and the peak heating, and high heat transfer gradients at reattachment, are indicated with a colour change throughout the liquid crystal colour spectrum within a narrow region on the flap.

13.4.1 Effects of side plates.

The increase in separation length that the addition of side plates produces is clearly apparent when the heat transfer distributions with, and without, side plates are compared (Figs. 33a, 33b, 33c). The general form of the heat transfer distributions remain unchanged with the side plates attached. The location of the beginning of the heat transfer rise downstream of the separation is slightly delayed at flap angles between 20 to 30 degrees when side plates are fitted, but this difference is very little at the highest angles. This observation must be interpreted with caution, because the separation point locations for the tests with side plates were not determined directly, but from a method using the data without side plates attached. The local rise in heat transfer within the separated flow occurs further upstream of the hinge line with the side plates attached, corresponding to the longer separated flow lengths.

A comparison of the peak heat transfer values obtained with, and without side plates, only show differences which are within the experimental scatter. The most significant influence of the side plates on the scale of separation occurs at a flap angle of 25 degrees, for which the difference in peak heating that the side plates produce is only 1.6%.

13.4.2 Peak heat transfer.

At flap angles of 15 degrees, and greater, a peak develops in the reattachment heat transfer profile. A comparison of these with the schlieren photographs indicates that the peak heating locations are downstream of reattachment, in the region of the boundary layer neck. The distance between reattachment, and peak heating, reduces continuously as the flap angle is increased, and at 35 degrees this is small. At the high flap angles, the maximum measured values of the reattachment heating may be less than the true peak levels because of the limited thin film gauge spatial resolution in these regions of very high heat transfer gradient.

The measured peak heating values, non-dimensionalised by the laminar flat plate value at the hinge line, have been plotted against the single shock inviscid pressure rise for the flap at each angle (Fig.36). These data points have been compared with the peak heating correlations for fully laminar separated flows determined by Holden (see Hankey & Holden 1975),

$$\frac{q_{peak}}{q_o} = \left\{ \frac{p_{peak}}{p_o} \right\}^n_{measured} = \frac{h_{peak}}{h_o} \qquad (0.5 < n < 0.85) \qquad (63)$$

and Hung (1973),

$$\frac{h_{peak}}{h_{undist}} = \left\{ \frac{p_3}{p_1} \right\}^{0.7}_{inviscid} \qquad (64)$$

In applying the correlation of Eq.(63), the required pressure ratio term was estimated from the separation geometries, with a two shock compression of the inviscid flow. Hung's correlation curve is seen to lie within the limits of those of Holden (Fig.36). The present experimental measurements have been reduced to heat transfer coefficients using a laminar flat plate recovery temperature throughout. These data are seen to lie well above the laminar correlations at all these flap angles. This is believed to be due to the occurrence of transition in the free shear layer ahead of, or at, reattachment.

If transition does occur in the reattachment region, then the recovery temperature will be higher than the laminar value, and the peak heat transfer coefficients will have been overestimated. This is only likely to account for a small fraction of the difference between the data points, and the upper limit of the fully laminar correlation curves.

The peak heat transfer measurements have also been added to the laminar, and turbulent, correlations of Bushnell & Weinstein (1968), (Fig.37). The parameters for this are based on the assumption of a sub-laminar boundary layer growing from the reattachment point. In applying this correlation, an expression for the reattaching free shear-layer thickness must be included, assuming the flow is either fully laminar, or fully turbulent, from the plate leading edge. Both of these conditions have been applied in correlating the measurements, to provide limits between which transitional data would occur. The definition of the heat transfer coefficient is not explicit in this reference. In correlating the present data the stagnation temperature has been used, which is consistent with some of the source references for experimental data used by Bushnell & Weinstein. This produces a lower limit for the calculated heat transfer coefficient values. All the correlated points for the

present data (15 to 35 degrees) lie above the fully turbulent correlation curve. This would be expected for separations with transition to a turbulent type velocity profile in the reattachment region. For this condition, the normal velocity gradients are larger than for a fully turbulent separation, in which the reattaching shear layer thickness would be greater. Without a substantial variation in the unit Reynolds number for each of the fixed flap angles, it is not possible to determine whether the flows are turbulent, or still transitional, at reattachment for the present experiments.

The use of the transitional peak reattachment heating correlation of Hung & Barnett (1973) fails when applied to the present data. This is because the transition Reynolds numbers that occur in the present experiments are less than that assumed in the correlation, and a consequent extrapolation of the transitional heating equation to these Reynolds numbers then predicts peak reattachment heating levels that are lower than those expected for a fully laminar separation. This emphasises the difficulties of correlating transitional data.

A three-dimensional influence on the measured peak heat transfer is the presence of the striations in this region, which produce local spanwise variations of heat transfer across the finite gauge width. However, at the high flap angles, the wavelength of this phenomenon, $\approx$ 6 mm, is very similar to the gauge width, 5.5 mm, and therefore the thin film gauge measurements of heat transfer are close to the mean spanwise value of the peak heating in this region.

13.5 Transition.

A variety of criteria have been applied to these fixed flap experimental data to determine whether transition is present within the separation region. The variation of separation length with Reynolds number suggests that transition might be present, but this is not conclusive because the appropriate freestream Reynolds number range could not be applied. When the separation lengths are correlated with measurements from previous investigations, they are within the scatter of previously defined laminar measurements. The plateau pressures of these separations are also typical of the laminar regime. However, Chapman et al (1958) found this to be a poor indicator of transition onset, finding that laminar plateau pressures occurred in separated flows when transition was close to reattachment.

The interpretation of transition location from irregularities in the schlieren photographs of the free shear layers is very subjective, and

therefore difficult to apply. At the highest flap angles there is some fuzziness at the shear layer edges, but the origins of this are not clear. For flap angles in excess of 20 degrees, non-uniformities exist in the wedge flow following reattachment, which may be evidence of transition.

The qualitative aspects of the heat transfer measurements, including the form of the heat transfer profiles, and the noise levels, suggest the occurrence of transition for flap angles of 20 degrees, and larger. However, by far the most sensitive detector of transition appears to be the correlation of the peak heating in the reattachment region. This indicates values which are very much greater than those expected for fully laminar separations at flap angles of 15 degrees and greater.

13.6 Influence of hinge line bleed.

In allowing for the rapid displacement of the flap in this model configuration, it is not practical to completely seal the hinge line gap. A small leakage of the separated mass flow will be induced through this, which may reduce the separation lengths below those that would occur with a sealed hinge line (Ball & Korkegi 1968; Rhudy et al 1970).

For steady separated flows, the continual removal of mass flow across the hinge line must be balanced by a supply. This can only come from the flow in the free shear layer above the separation streamline, which then allows a higher momentum region of this viscous flow to reattach to the wedge surface. This then reduces the length of separated flow.

At low wedge angles, where the separation length is small, the effect of mass flow removal has an additional viscous accelerating effect. This energises the flow in the separation region, enhancing the sensitivity of its length reduction to hinge line bleed.

To assess these effects for the present experiments, several correlations of the data of Ball & Korkegi (1968) were attempted by the present author. The most successful is shown in Fig.38a. For the small separated flows, i.e. large (mass flow):(separation length) ratio, this correlation works less well. This is believed to be due to the increased sensitivity to hinge line bleed for small separated flows. The mass flow bleed rate parameter was determined with the assumption of choking of the flow at a throat in the hinge line passage. The stagnation pressure was assumed equal to the plateau pressure, and the wall temperature taken as representative of the stagnation temperature. Calculations based on these assumptions were found by Ball & Korkegi (1968) to compare very well with measured hinge line mass flow rates. In the present

experiments, the estimated pressure ratio across the hinge line at all flap angles is sufficient to choke the flow at its minimum cross section, and the above assumptions have been used.

The results of applying this correlation to the present data are shown in Fig.38b. The reduction in separation length for flap angles greater than 15 degrees is very small. This correlation has been derived with data from presumed laminar separations. The effects of transition in the present experiments would be expected to reduce the sensitivity of separation length to hinge line bleed, since the fuller velocity profile in the free shear layer would supply the necessary mass flow rate with less change in velocity to the reattachment streamline. The results in Fig.38b should then be taken as an upper limit on the effects of hinge line bleed in the present tests.

13.7 Effect of finite flap chord length.

If the model flap surface has an insufficient chord length, experiments have demonstrated an influence of the trailing edge expansion fan that reduces the peak reattachment pressure, and the length of the separated flow (Harvey 1968; Ball 1969a; Ball 1969b). Holden (1966a) determined that this expansion fan will have a negligible influence on the distribution of properties in the separated flow if it occurs at a distance from the reattachment neck greater than approximately twice the local boundary layer thickness. This is comfortably satisfied at all the flap angles in the present tests. Another proposed criterion for avoiding the influence of the trailing edge expansion on the separated flow length is a correlation proposed by Ball (1969b), (Fig.39). The present data have been added to this, and for flap angles greater than 15 degrees the trailing edge effects appear negligible. At angles below this the correlation predicts an influence of the trailing edge expansion fan, although the very small separation geometry angles for this condition may distort the accurate application of this criterion.

With transition induced in the reattachment region, the height of subsonic flow adjacent to the wall within the boundary layer is much less than for a laminar reattachment. This is expected to reduce the upstream influence of the trailing edge expansion for the present tests.

13.8 Summary.

At the low freestream Reynolds number of 2.45×10^6/m, the steady separated flows in the present experiments display length scales, and plateau pressures, which are typical of the fully laminar regime. However, measurements of peak

reattachment heat transfer indicate that transition is present for flap angles of 15 degrees, and larger. Liquid crystal thermographs show that these separated flows are substantially two-dimensional, particularly without side plates fitted. Applied correlations suggest that the effects of hinge line bleed, and the flap trailing edge expansion, have only a small, or negligible, influence on these flowfields.

PART IV

DYNAMIC FLAP SEPARATED FLOW EXPERIMENTS.

14. Introduction to the dynamic flap experiments.

All the dynamic flap experiments were made at the lowest freestream Reynolds number of 2.45×10^6/m. Measurements included schlieren photography, and centre line heat transfer distributions. Liquid crystal thermography was not applied because its finite response time, estimated to be a significant fraction of the flap deflection period, would introduce uncertainties in relating the observed colour pattern to the instantaneous unsteady flow. To obtain the complete heat transfer distributions, data were combined from a total of eight separate tests.

The dynamic separation measurements were made with the model in a position with its leading edge just downstream of the nozzle exit plane. This was prior to the realisation of possible interaction effects from the nozzle exit compression waves.

It was observed from the schlieren flow visualisation that the instantaneous height of the nozzle exit wave above the dynamic flap was greater than at corresponding fixed flap angles, with the same model position, throughout the deflection range. For these unsteady separation tests, the change in blockage when the flap is released requires a finite time to effect a further contraction of the freestream jet to a new stable condition. This time is associated with the rate at which the surrounding test section pressure rises, which is determined by its volume, and the rate of spillage from the diffuser. As the test section pressure increases, this then feeds back to further contract the freestream jet, and this interaction continues until a stable condition is achieved. The application of the established criterion for separated flows to be free from nozzle wave interference (§ 12), based on the nozzle wave height above the flap trailing edge, was satisfied at all the dynamic flap angles during the rise from 0 to 35 degrees (Fig.27). There was insufficient time available to repeat the dynamic flap tests with the model in the forward position.

15. Unsteady measurement considerations.

15.1 Schlieren flow visualisation.

Spark source schlieren photography was applied for the visualisation of the separated flow induced by the dynamic flap. This was obtained by synchronising a single spark with the signal for the flap release using a time delay unit. Photographs of the dynamically evolving separation were obtained with instantaneous flap angles between 10.25 to 35.45 degrees over a number of tunnel runs. Schlieren photography of the separated flows induced with a fixed flap (model moved forward) were repeated at each of these angles to give the appropriate comparison. An alternative visualisation technique, used to investigate unsteady flow structures, is cine schlieren photography. This method produces a continuous film record of the schlieren flow visualisation, but the quality of resolution is inferior to that obtained with a spark illumination. This is the primary reason why cine schlieren was not used in the present experiments.

15.2 Heat transfer measurements.

To produce each unsteady heat transfer distribution, the instantaneous value of the heating at each gauge location was obtained from the recorded signals when the flap was at the required angle (e.g. Fig.49). Simple linear interpolation was used when these instants (determined from the calibrated flap potentiometer signal) lay between sampled data points. For these experiments it was necessary that the thin film gauges had an adequate response time. Also, care must be taken when digitally sampling unsteady heat transfer signals, and in the use of analogue and numerical filtering.

15.2.1 Thin film gauge response time.

The presence of a finite thin film gauge thickness introduces a modification to the ideal single substrate unsteady heat conduction process, and this causes the heat transfer measured via an RC analogue transmission line to differ from the actual surface value. This effect has been considered in detail (Schultz & Jones 1973) by analytically modelling the unsteady heat conduction in one-dimension through the two layer model of the gauge on a base substrate, in response to a step function in the surface heating. The solution demonstrates that the measured heat transfer asymptotes to the surface value after a sufficient time, with the discrepancy between these at any instant being less with thinner gauges. A simple relationship for the heat transfer

actually measured (due to a gauge of thickness l), valid for times when this approaches the value of the applied step in surface heating, (Schultz & Jones 1973) is,

$$\frac{q_{s\ meas.}}{q_{s\ actual}} = 1 - \frac{1}{z\sqrt{\pi}} \left\{ \frac{1}{a} - \frac{a}{2} \right\} \qquad (65)$$

$$\text{where, } z = \frac{\sqrt{\alpha_1 t}}{l}, \text{ and, } a = \left\{ \frac{\rho_2\ c_2\ k_2}{\rho_1\ c_1\ k_1} \right\}^{1/2}$$

Conversely, the time for the measured value to be within a required tolerance of the surface heat transfer can be determined from this equation, which is a response time for the thin film gauge to a step function in surface heating.

To evaluate this response time, a measurement, or estimate, of the thin film gauge thickness must be made. In an attempt to measure this dimension from a surface profile, a special set of thin film gauges was manufactured, in which the maximum furnace temperature was reduced to 500 K. This cycle is sufficient to deposit a thin platinum film on the pyrex surface, but below the temperature at which it will start to diffuse into the base substrate. At the usual maximum firing temperature of 700 K, substantial diffusion of the platinum material into the pyrex substrate occurs, but the gauge width, and length are negligibly changed from its dimensions when the gauge is deposited on the substrate surface at 500 K. The change in resistance between these firing cycles was small, and it was therefore assumed that the platinum layers deposited on the pyrex surface at 500 K had thicknesses close to those of the thin film gauges used in the wind tunnel experiments. An alpha step meter was used to measure these. This is a surface profilometer, used in micro-electronics processing, with an adequate resolution to measure changes in surface height of an order well below 0.1 μm. This instrument, although able to discern very small changes, is unable to follow rapid variations. Only a single measurement, across two thirds of a gauge width, was successful (Fig.40). This indicated an uneven surface profile, with a *peak* thickness of 0.13 μm. The difficulties of thickness measurement were due to almost certain contamination of the gauge surface with dust, non-uniformities in the pyrex surface, and the uneven deposited platinum film. These problems are not unexpected with hand painted, and fired gauges, where the conditions and

controls on manufacture are not as strict as might be imposed in the manufacture of micro-electronics circuitry! The failure to successfully measure a complete gauge profile, and the lack of checks for repeatability in this, reduced confidence in the thickness measurement.

An estimate of the *average* gauge thickness was made, based on the typical measured gauge resistance, dimensions, and platinum bulk resistivity (corrected for thickness effects).

$$\text{gauge thickness} = \frac{\text{Pt resistivity x gauge length}}{\text{gauge width x gauge resistance}} \qquad (66)$$

The resistance of metal films is always higher than would be predicted from the bulk resistivity of the material, due to changes in the electronic free path. Experimentally determined increases in resistivity for 0.1 μm thick layers of various metals, which is of the order of thickness for the present experiments, deposited on glass, or pyrex (Berry et al 1968; Winding et al 1955), are contained in table 5. These indicate increases for thin film resistivity above the bulk value of between 13 % to 44 %. Large increases in resistivity do not generally occur until the thickness is reduced below about 0.02 μm (Winding et al 1955). No referenced experimental value for a 0.1 μm platinum film could be found. However, the increase in resistivity is expected to be of the same order as for the metals tabulated (this includes palladium, and nickel, which are contained in the same periodic group as platinum). To determine the gauge thickness from Eq.(66), a high estimate for the resistivity of a layer ~ o(0.1 μm) thick, giving an upper limit on the calculated average thickness and response time, is an increase above the bulk value by 500 %. For the typical gauge resistances, and dimensions, this gives an average thickness for the platinum layer of 0.1 μm. This is similar to the thickness that was directly measured, and consistent with the lower limits of values that have been previously found for painted gauges (e.g. Hartunian & Varwig 1962; Holden 1964; Schultz & Jones 1973).

A uniform 0.1 μm layer platinum thin film gauge on a pyrex substrate has a response time, determined from Eq.(65), of 0.0117 ms for the measured heat transfer to be within 3 % of the surface value. The response time to a step input of heat transfer is an upper bound on the lag between the actual occurrence of values of a general unsteady surface heating, and the times when these levels are measured by the gauge. To determine the errors in the present

experiments due to the gauge response time, examples of the measured unsteady heat transfer signals on the plate, and flap, (filtered numerically to 500 Hz, see § 15.2.2) were uniformly shifted forward in time by 0.0117 ms. At any time instant, the difference in heat transfer between the measured and shifted signals represents an error in measurement due to the finite gauge response. For these heat transfer signals this error was no more than 0.6 %. Since the response time was defined here as that required to measure within 3% of the actual surface heating, the total maximum error in heat transfer measurement due to the finite gauge response is a lag of about 3.6 %.

It must be noted that with painted, and fired, thin film gauges, the diffusion of platinum into the pyrex substrate may create a region of non-homogeneous material below the surface. This introduces an uncertainty in the accuracy of a response time determined from an analytical model which assumes distinct homogeneous materials.

The surface temperature rises in these experiments have been determined from a numerical integration of the measured surface heat transfer rates. This numerical conversion of heat transfer to temperature is based on the same thermal model effectively used by the RC analogue line, but applied in reverse. The thin film gauge mean temperature, and hence the instantaneous model surface temperature, will therefore be recovered from the heat transfer signal without a time lag error. The difference between the surface temperature of the thin film gauge, and its mean temperature, has been assumed negligible for this 0.1 μm thick thermally conducting metal element.

15.2.2 Data sampling and filtering.

To determine the necessary sampling rate, and appropriate analogue filtering, an estimate of the frequency content of the unsteady heat transfer signals was required. These signals were expected to consist primarily of changes associated with the dynamically increasing scale of separation. Superimposed on these might be transition noise, plus possible additional fluctuations induced by the dynamic response. The variable separation geometry effects on heating were of primary concern in these experiments, and these were expected to consist of frequency components contained below some upper limit. Transition noise, and other fluctuating components, may have frequencies distributed throughout a very wide bandwidth. The measurements of Roberts (1989) showed only small lags introduced in a dynamic separation growth with a rapidly displaced, and then oscillated flap, compared to the instantaneous quasi-steady length scales. There were also no significant dynamic effects

observed on the character of the unsteady separated flow geometry, which remained typical of the wedge type throughout its growth. These results have been confirmed with the schlieren flow visualisation of the dynamic separation evolution produced in the present tests (§ 16.1). It was therefore anticipated that the underlying changes in heat transfer, induced by the increasing separation length, would not depart largely from the quasi-steady profiles that could be constructed from measurements at fixed flap angles between the limits of the dynamic flap deflection. Implicit in this assumption was that any additional mechanisms in the dynamic response that may effect a change in the level of heat transfer, distinct from flow noise, were not strong. An *approximate* prediction of the expected order of frequency content of the underlying unsteady heat transfer signals could then be determined from quasi-steady heat transfer profiles.

Quasi-steady profiles were constructed from the measured fixed flap heat transfer rates, combined with the dynamic flap motion obtained in still air. The maximum gradients of changing heat transfer were found to exist for the flap gauge number 9, which was subsequently used for the frequency analysis. A fast Fourier transfer (FFT) algorithm was applied to this signal to determine its frequency content (appendix 7). Simple quadratic and exponential curves were fitted between the discrete measured quasi-steady values, from which a 128 point data file was generated (Fig.41). The fast Fourier transform of this had a resolution of 52 Hz. A Hanning window was applied to the data file, before the frequency analysis, to reduce the far spectral leakage (appendix 7). Although this introduced slight near spectral leakage, the primary concern was to determine an upper limit for the frequency content, and not to observe strong discrete frequency components within the spectrum. The resulting power spectrum indicated that the major content of this signal was contained in frequencies well below 500 Hz (Fig.42). This compared with a value of 400 Hz used by Roberts (1989) as a final cut-off for filtering unsteady pressure signals in a similarly induced dynamic separation. The subsequent frequency power spectrum of the measured unsteady heat transfer signals confirmed the accuracy of this estimate (Figs.41 & 42). This indicated an underlying power spectrum which closely coincided with the estimated distribution, with flow noise superimposed throughout.

For the measurement of the unsteady heat transfer signals it was decided to continue with the 1100 Hz low pass analogue filters, previously used for the steady separation measurements. Although the low pass cut-off frequency could be reduced below this, the phase lags introduced by an analogue filter

near its cut-off frequency can be substantial, requiring large corrections to the measurements to compensate for this.

When the sampling frequency is set, the primary consideration first applied is to avoid aliasing. If this phenomenon occurs, then the characteristics of the low frequency components in a signal are corrupted by high frequencies, and further frequency analysis of the signal, such as numerical filtering, cannot be applied. To avoid aliasing, the sampling theorem states that the minimum acceptable sampling frequency must be twice the highest frequency component in the signal at the analogue to digital stage, requiring a minimum value of 2200 Hz for the 1100 Hz low pass analogue filters. The sampling frequency should actually exceed this in the present experiments, because the simple RC filter has a slow roll-off in signal attenuation about the -3dB point. A further consideration was to achieve an adequate time resolution, for which the sampling frequency should be about five times the highest component contained within the signal (Richards 1977). In the present experiments a sampling frequency of 6.7 kHz was used. The transient data store had the capacity to sample up to twice this value. However, the sampling time with this recorder is fixed throughout the duration of measurement, and is the same on all channels. Unnecessarily high sampling frequencies would have then lead to excessive data storage, with difficult data management, and very large times for subsequent numerical analysis of the measurements.

A numerical filtering algorithm was written to remove frequency components above 500 Hz in the recorded signals (Fig.43). A simple non-recursive method was used (appendix 8). The advantage of this design technique is the ability to easily produce a filter with the desired cut-off frequency, and transition bandwidth between pass and stop, with zero phase changes introduced by the numerical filtering process in the pass band.

The numerically filtered signals must finally be corrected for the small phase lags initially introduced by the 1100 Hz low pass analogue filter. Since the principle of superposition applies to this filter, the original input heat transfer signal from the gauge can be considered to consist separately of the required signal with frequencies up to 500 Hz, plus those above. The numerical filtering removes the undesired component, and the resulting signal is then equivalent to that which would be obtained if the components up to 500 Hz had been passed alone through this low pass analogue filter. A method of phase lag correction was applied to the numerically filtered signals (appendix 9), based on a simple finite difference scheme. The procedure of numerically filtering,

and then correcting for the analogue filter phase lag, was applied to all the dynamic flap heat transfer signals.

A comparison of a gauge signal numerically filtered to 500 Hz, and at a 250 Hz cut-off, showed the same underlying changes in heat transfer, with small differences attributable to the respective amounts of flow noise removed. A signal from the same gauge at nominally identical conditions in a different wind tunnel run compared similarly. These results confirmed that a cut-off frequency of 500 Hz was well above the underlying changes in heat transfer induced by the unsteady changing separation geometry. It was also apparent, as indicated in the frequency power spectrum, that flow noise could not be completely removed without interfering with the required signal. This flow noise was an additional source of scatter in the dynamic separation heat transfer distributions.

16. Dynamic separation results.

16.1 Schlieren flow visualisation.

Examples of the schlieren flow visualisation of the separation evolution obtained by rapidly displacing the flap, and comparisons with the separated flow structures induced at corresponding fixed flap angles, are shown in Fig.46. These indicate that at any instant the geometrical form of the dynamic flap separated flow is the same as the steady wedge type, with the development of a separation shock, shear layer, and reattachment shock.

The separation lengths were determined from these schlieren photographs, and are plotted against the flap angle in Fig.47. At deflection angles up to 18.5 degrees the instantaneous separation lengths for the dynamic flap are coincident with those produced by corresponding fixed flap angles with the same model position. Because of the tunnel interaction effects, the dynamic separation must be compared with the fixed flap measurements obtained with the model moved forward for the majority of the flap deflection range (flap angles $\geq$ 20 degrees), (§ 12.). At deflection angles below 20 degrees, these fixed flap measurements have separation lengths slightly less than those obtained with the same fixed model geometries moved downstream of the nozzle exit plane (Figs.26 & 47). The differences between the two fixed flap data sets at these angles have been previously attributed to small changes in the freestream flow, and the subsequent influence on transition occurrence. The fixed flap separation lengths with the model in the forward position are therefore slightly smaller than the steady measurements which should ideally be compared with the dynamic flap induced separation evolution. A correction to account for this affect is discussed in part V of this thesis.

At flap angles up to 20 degrees, the difference between the fixed (model forward), and dynamic, flap separation lengths remains a small displacement (Fig.47), and is attributable to the model position influence. At higher flap angles, the rate of the dynamic flap separation length increase reduces below that for the fixed flap. At a flap angle of 30 degrees the dynamic separation length is less than that obtained with the corresponding fixed flap, even though this comparison is with the results obtained with the fixed flap model geometry in the forward position with respect to the nozzle exit plane. As the flap angle continues to increase, the lag in the development of the dynamic separation length, compared to those obtained at the same instantaneous fixed flap angles, increases. At the highest deflection angle for which a schlieren photograph of the instantaneous dynamic flap separated flow was obtained of

35.45 degrees, the measured separation length is 8.7 mm less than that produced by the same fixed flap angle.

The schlieren photographs of the dynamic flap separated flow structures indicate that the separated shear layer remains approximately straight along its length between the separation, and reattachment points. The deflection angle of this surface has been measured for each dynamic flap angle, and plotted against the separation lengths (Fig.48). The comparison of these measurements with those for the fixed model geometries indicates that within the accuracy of this measurement (± 0.5 degrees) there appears to be a negligible effect of the dynamic response on the shear layer angle, other than indirectly at high flap angles through a lag effect on the separation length, and hence the value of the local Reynolds number at the beginning of the interaction. The shear layer deflection angle is a parameter that determines the separated flow plateau pressure, and this is a characteristic of the free-interaction process at separation. The measurements from the schlieren photographs therefore indicate that during the growth of the separation induced by this dynamic flap, the free-interaction process remains essentially unaltered. An examination of the pressure measurements of Roberts (1989) show the plateau pressures for a positively, and negatively, rapidly displaced flap surface are the same when the separation points are close. These accurate pressure measurements were made with similar flap velocities, and therefore support the conclusion from the present tests that the free-interaction process remains unaltered by rapidly displacing this wedge surface at these velocities. These results also indicate that differences in the freestream flow for the two model positions are not sufficiently strong to produce significant differences in the shear layer deflection angles through the free-interaction process.

An examination of the details of the shear layer development show that the fuzziness which occurs along its edges for separated flows induced by moderate to large fixed flap angles is also present in the dynamic flap separated flows. This characteristic indicates transition within the shear layer, although as previously discussed this is not precise in locating its origin. Comparing the fixed, and dynamic, flap separated flows, the qualitative features in the shear layer development are very similar for these. Differences that exist in edge irregularities are likely to be caused by unsteady flowfield fluctuations, which can be substantial when the separation is transitional. This may also account for small differences in the detail of the reattachment regions when the dynamic, and fixed, flap induced

separated flows are compared. An estimate of any differences in the respective locations of the origin of shear layer fuzziness between the dynamic, and fixed, flap separated flows from the schlieren photographs is a very subjective interpretation, and has not been attempted.

Further evidence of transition in the dynamic flap separated flows is the presence of non-uniformities in the separation shock appearance, similar to those that were observed in schlieren photographs of the fixed flap separated flows. These are believed to be primarily associated with spanwise variations in the separation length induced by the irregularities, and unsteadiness, of the separation caused by transition, but there is also a possible contribution from edge effects.

A further indication in the schlieren pictures of a lag in the unsteady separation growth at high flap angles is the difference in the relative positions of intersection of the bow shock, and separation shock, with the reattachment shock, compared to that which occurs for the steady separated flows.

16.2 Heat transfer distributions.

For the comparison of the dynamic, and fixed, flap heat transfer distributions, the measurements have been presented as a Stanton number ratio with division by the first plate gauge measurement in each test (Figs.50, 51, 52, & 53). This reduces the scatter caused by small run to run variations in the absolute heating levels.

The flat plate parts of the dynamic flap heat transfer distributions were determined from averages of the gauge signals over a finite time interval to reduce scatter, but only when it was clear that these gauge locations were ahead of the separation interactions. The small differences in the flat plate heat transfer distributions between the fixed, and dynamic, flaps ahead of the separation interactions are due to the model position influence as discussed in § 12.

At the lowest investigated dynamic flap angle of 15 degrees (Figs.50a & 51a), the heating distributions for the dynamic, and fixed, flap appear coincident up to the occurrence of the minimum heating level within the separated flow. The spatial resolution of the thin film gauges, and the scatter in the dynamic separation results, obscure the slight difference in separation length between the dynamic, and fixed, flap conditions caused by the model position.

As the flap angle is increased, without side plates fitted, there is no

clear evidence of a difference in the scale of the separated flows on the plate between the dynamic, and fixed, flaps for deflection angles less than 30 degrees. This is consistent with the schlieren data. These heating distributions also indicate that the response time of the thin film gauges is sufficient to accurately follow the rates of change in the heat transfer that occur on the plate. Any measurement lag effects that are present are sufficiently small to be obscured by the data scatter.

At 30 degrees, without side plates (Fig.50d), there may be a slight displacement of the initial drop in heat transfer between the two interaction start locations, but the differences are of the order of the scatter in the data. When the flap is at 32.5 degrees (Fig.50e), there is clear evidence of a lag in the dynamic separation growth compared to the same fixed flap induced separation, with the fall in heat transfer near the separation point occurring further from the leading edge for the dynamic condition. Because the gradients in heat transfer in this region of the separation interaction are substantial, this slight displacement of the two separation locations produces significant differences in the two heat transfer distributions. At the flap angle of 32.5 degrees the difference in respective heating levels at each gauge location in this region is between 20 % to 25 %. This is certainly larger than the experimental scatter in the heat transfer measurement. At 35 degrees (Fig.50f), this difference in the displacement of the interaction start location between the dynamic, and fixed flap conditions is increased to about 8.3 mm. The accuracy of this measurement is limited principally by the scatter in the data, but this displacement again appears to be consistent throughout the drop in heating to the minimum values. The lag for the dynamic flap separated flow length at 35 degrees measured from the heat transfer distribution, and that measured from the schlieren photographs at 35.45 degrees, 8.7 mm, are in close agreement. This indicates that the location of separation relative to the fall in heat transfer at the interaction start is unaffected when a lag in the dynamic flap separated flow is established.

When the side plates are fitted, the same trends are observed with a comparison of the heat transfer distributions for the dynamic, and fixed flap conditions (Fig.51). However, the displacements between the beginning of the interaction starts, and subsequent displacement of the initial fall in heat transfer on the plate to a minimum value within the separated flow, is less both at 32.5 degrees (Fig.51e), and 35 degrees (Fig.51f), than for the condition without side plates. At 35 degrees, with side plates, this displacement in the location of the heat transfer fall for the separation

induced with the dynamic flap compared to the same fixed flap angle is a lag of about 6 mm.

The coincidence over a large range of the flap deflection, before lag effects become significant, of the dynamic, and fixed, flap heat transfer distributions for the fall in heat transfer to its minimum value support the conclusion that dynamic effects on the free-interaction for this geometry, and flap deployment rates, are negligible.

The heat transfer distributions within the dynamic separated flows following the minimum heating location generally exhibit considerable scatter when the flap angle is in excess of 20 degrees, both with, and without, side plates attached (Figs.50b to 50f, & 51b to 51f). This corresponds to the regions of high noise level observed for the fixed flap separated flows, caused by transition (Fig.34). For the fixed flap separations, these noise levels are averaged out at each gauge location in the data reduction, but this is not possible with the dynamic separation measurements. When the distributions of heat transfer in this region are compared between the conditions of the dynamic, and fixed, flaps there are no consistent differences that are observed to develop throughout the flap deflection, either with, or without, the side plates fitted. The noise levels measured in the fixed flap tests at each position (due to both flow noise, and electrical noise for these low heat transfer fluxes) have been compared with the scatter in the dynamic flap heat transfer distributions at corresponding flap angles, and gauge locations. Throughout the flap deflection range, any slight differences in the position of local rises in heat transfer on the plate (indicating transition) with respect to the interaction start position that are apparent between the dynamic, and corresponding fixed, flap conditions are well within the possible data scatter.

At the low flap angles where the noise levels within the separated flow region are least, both with, and without, side plates attached, there are no significant differences in the dynamic, and fixed, flap heat transfer levels that indicate a different transition location caused by the changed model position. This is probably because this effect is small, and at the low flap angles is confined to a region of high heat transfer gradient near reattachment. The differences in the magnitude of the flat plate heat transfer levels, due to the different model positions and respective expansions of the freestream flow, are not consistently observed throughout the separation region ahead of transition on the plate. It is likely that these small differences are obscured by the data scatter in the dynamic flap results.

The heat transfer distributions on the flap have been re-reduced using a flat plate turbulent recovery factor, and are separately illustrated in Figs.52 & 53. This recovery factor is more appropriate in this region because of the transitional - turbulent nature of these separated flows near reattachment.

The heat transfer measurements for the dynamic flap, and fixed flap, tests were made with different thin film gauge inserts in the flap. The magnitude of experimental errors when determining differences between the dynamic, and fixed, flap heating distributions are therefore greater than on the plate where a single gauge insert was used for all the test conditions.

At flap angles up to 32.5 degrees, the dynamic, and fixed, flap heat transfer distributions for the rise in heating from the hinge line have differences that can be attributed to the general scatter in the dynamic flap data, both with, and without, the side plates attached. Of particular interest is a comparison of the magnitude of the peak heating levels. Throughout the majority of the flap deflection range, both with, and without, side plates, this shows that the measured peak dynamic flap heat transfer levels are generally slightly greater than the fixed flap values (corrected for ρck changes). However, these differences are certainly within the possible experimental measurement errors, and are also typical of the general scatter within each dynamic flap distribution. The noise levels measured in the steady experiments have been compared with the differences between the dynamic, and fixed, flap peak heat transfer levels. The measured dynamic effects on peak heat transfer for flap angles up to 32.5 degrees were found to be contained within the possible flow noise at these gauge locations, both with, and without the side plates fitted to the model. Estimates of the location of the true peak heating levels from the distributions appear about the same for the dynamic, and fixed, flap conditions over this deflection range. It must again be noted that the accuracy of the measurement of both the peak heating levels, and their positions, are restricted by the gauge spatial resolution, and it is quite probable that at the higher flap angles these levels are only approximately measured, and located.

At a flap angle of 35 degrees, without side plates attached (Fig.52), the peak heating level on the dynamic flap is substantially above the fixed flap level, with an increase of 10 %. This is still less than the combination of experimental errors, and possible flow noise, but this peak level appears to be consistent with this complete dynamic flap heat transfer distribution. This peak level is displaced towards the hinge line compared to that which occurs

with the fixed flap, and the heat transfer gradients to the dynamic peak level are higher. At the same flap angle with side plates attached (Fig.53), the dynamic peak heat transfer is again substantially above the fixed flap value, with an increase of 15 %. The true location of this peak heating appears possibly slightly ahead of that for the fixed flap, but this is only an interpretation from the heat transfer gradients. The actual measured peak level for this is at the same gauge location as for the fixed flap, probably because of the limited gauge spatial resolution.

The heating distributions for the dynamic, and fixed, flaps downstream of the peak levels are similar at all flap angles up to 30 degrees, with, and without side plates. However, at 32.5 degrees, and 35 degrees, a local increase in the heat transfer towards the flap trailing edge is measured for the dynamic condition. This increase is measured by the last 3 gauges without side plates, and by the last 2 gauges when side plates are attached.

The surface temperature rises on the flap surface at high fixed deflection angles are 30 to 40°C greater than for the dynamic condition, while temperature differences on the plate surface are negligible. To ensure that any flap wall temperature effects on the scale of the steady separated flows, and its properties, are negligible, the heat transfer distribution for the largest fixed flap angle of 35 degrees was re-evaluated from the measurements in a time period nearer the start of the freestream flow, where surface temperature rises are less. The run to run repeatability of the freestream conditions in this earlier part of the test flow are not as good, and the *average* value of the unit freestream Reynolds number is 4 % greater. This earlier period of the test flow is 0.25 s after the flow start, compared to about 0.66 s used before, and the surface temperature rises are approximately 40 % less. Maximum surface temperature rises on the flap surface were 26, and 43, degrees respectively. The heat transfer distribution obtained from this earlier period is compared with the previously measured data in Fig.54. There appear no significant differences between these heat transfer distributions on the plate, although there is a slight increase in the data scatter for the earlier flow period as expected. The heat transfer distributions on the flap, corrected for ρck changes, are close, although the peak level appears slightly nearer the hinge line for the earlier time period. This may be the influence of data scatter, although each peak level appears consistent with its respective flap heat transfer distribution in this region. Differences may also be due to the slightly higher freestream Reynolds number, although there is no significant effect apparent on the plate heat transfer distributions.

Another possible effect of a higher wall temperature is an increase in the interaction length in the reattachment region, similar to wall temperature effects on the free-interaction length at separation.

The results indicate that there are no measurable flap wall temperature effects on the separated flow on the plate, and therefore the comparison of the dynamic, and fixed flap tests is valid in this region. On the flap there may be a slight wall temperature effect, but the agreement between dynamic, and fixed, flaps for the peak heating location at moderate flap angles when lag effects are negligible suggest that this influence is not strong.

16.3 Summary.

The schlieren photographs, and the heat transfer measurements, both indicate a lag develops in the dynamic flap separated flow growth at high flap angles. The heat transfer measurements indicate that the size of this lag is influenced by the side boundary condition imposed. The free-interaction at separation appears to be negligibly influenced by the separation growth in response to this rapidly displaced flap. At low to moderate flap angles, where differences in the separation length between the dynamic, and fixed, flaps are negligible, the evidence of transition within these separated flows appears similar. At the highest flap angle of 35 degrees there is a significant increase in the measured peak heat transfer for the dynamic flap, both with, and without side plates attached. There also occurs a local increase in heat transfer towards the flap trailing edge for the dynamic flap separated flows at high deflection angles.

It may be postulated that the differences between the dynamic, and fixed, flap induced separated flows that become apparent at large deflection angles may be caused one, or more, of the following mechanisms:-

(i) Dynamic effect on transition.
(ii) Separation growth rate restricted by a mass entrainment requirement and / or,
(iii) Separation growth rate restricted by communication times of pressure changes through the separated flow.
(iv) Dynamic influence of the side boundary condition.
(v) Dynamic response affected by the hinge line bleed.
(vi) Possible tunnel interaction effect for the dynamic flap tests at high deflection angles.

The possibility of mechanism number (vi) has been investigated extensively, and Figs.27 & 47 strongly support tunnel interaction free experiments. Further, the measurement of a separation length lag for the dynamic flap condition is not consistent with the observed effect of a tunnel interaction, which tends to increase the scale of a separated flow above its true value. However, the complete absence of tunnel interaction influences cannot be totally discounted without repeating the dynamic tests in a more forward model position, which would also eliminate model position effects on transition. It has always been acknowledged by this investigator that the model position is a parameter that should be maintained invariant. However, the tunnel interaction phenomenon for the fixed model tests was an unforeseen problem, and there was insufficient time to repeat both the fixed, and dynamic, flap experiments.

The coincidence of the fixed, and dynamic, flap test heat transfer distributions at the lowest flap angle (for both conditions with, and without, side plates), indicate that it is possible for a small difference in transition occurrence to exist, caused by the different model positions, which is not clearly apparent in the comparison of these measurements. However, in this case the influence of the difference in transition occurrence on the separation length is so slight that this is also not clear in the comparison of these heat transfer distributions between the dynamic, and fixed, flap conditions. At the flap angle of 32.5 degrees (both with, and without, side plates), the difference in separation lengths between the dynamic, and fixed, flap conditions is substantially larger than the model position effect, but the form of the heat transfer distribution on the plate, and the flap heating profiles (including the peak level) remain very similar, with no evidence of a dynamic effect on transition. This suggests that mechanism number (i) does not significantly contribute to the difference in separation length between the dynamic, and fixed, flaps that is observed to develop at high deflection angles. However, the measurements with different model positions at low flap angles indicate that a small dynamic effect on transition occurrence cannot be completely discounted from the evidence of these heat transfer measurements alone.

Possible dynamic effects that could potentially influence the occurrence of transition include the unsteady motion of the separation point, disturbances in the reverse flow which is then scavenged by the developing separated shear layer, and the moving flap surface locally in the reattachment region. The majority of these effects might be expected to be most significant when the rate of separation growth is greatest. From Figs.45 & 47 the

separation point velocity was determined to be 9.2 m/s at a flap angle of 20 degrees, which then reduces continuously as the flap angle increases to a value of 5.7 m/s at a flap angle of 35 degrees. The rate of separation growth is therefore most rapid in a region where there are negligible dynamic effects on the separation length. The greatest separation point velocity is less than 1% of the freestream velocity, and the perturbation pressure created by the moving flap surface is less than 1% of the shock recompression pressure rise at reattachment for all the flap angles. These comparisons further suggest any dynamic influence on transition is negligible, in support of the evidence from the heat transfer distributions.

The postulated mechanisms number (ii) to (v) are examined in part V of this thesis.

PART V

SIMPLE ANALYTIC MODELS OF THE DYNAMIC FLAP SEPARATED FLOW RESPONSE.

17. Separation growth.

The unsteady separation growth induced by the rapidly actuated flap has been predicted with simple analytic models of the flow adjustment, based on the separate constraints of pressure wave communication, and mass entrainment.

17.1 Separation adjustment with respect to pressure waves.

In this model of the separation adjustment it is assumed that the rate of separation growth is only constrained by the propagation time of pressure disturbances.

The pressure rise at reattachment is the boundary condition in the pressure field that effectively determines the scale of a steady separated flow. If a flap surface is deflected impulsively to a new angle, then the time required to establish a new pressure field, and hence separation length, will be approximately equal to that required for the pressure waves to traverse a distance between the reattachment point, and the final steady separation point, travelling at combined local acoustic and convective velocities. For a continuously deflected flap surface, the separated flow will then develop a lag in its growth compared to the quasi-steady separations, due to the pressure communication times. The magnitudes of these lags will depend on the lengths of steady separated flow, their rate of increase with flap angle, and the flap deflection rates.

An instant during the unsteady separation development induced by the moving flap surface is illustrated diagrammatically in Fig.55. A reattachment pressure rise that occurs at an instantaneous flap angle θ_f will be communicated through the unsteady separated flow, and after a time interval of φ will induce a separation length equal to the steady value that would be generated by a fixed flap of the same angle θ_f. Each value of φ, corresponding to a different θ_f, is determined from the equation,

$$\varphi(\theta_f) \simeq \frac{L_{ds}(t)}{(u_{av} + a_{av})} + \frac{1}{(u_{av} + a_{av})} \int_{t}^{t+\varphi} \frac{dL_{ds}}{dt}(t)\, dt \qquad (68)$$

where u_{av}, and a_{av}, are the average convective, and acoustic, velocities respectively in the separated flow, and $L_{ds}(t)$ is an instantaneous distance between the separation, and reattachment points (Fig.55). Solving the integral in Eq.(68) then leads to the result,

$$\varphi(\theta_f) = \frac{L_{ds}(t+\varphi)}{(u_{av} + a_{av})} \qquad (69)$$

From the definition of $\varphi(\theta_f)$, $L_{ds}(t+\varphi)$ is the distance between the separation and reattachment points for the steady separated flow length associated with the particular θ_f. In this simple model of the separation response, the reverse flow velocities have been neglected, and the communication distances between the reattachment and separation points have been measured along the dividing streamline (Fig.55). For an imposed flap deflection history, the variation of the quasi-steady separation length with time is known, and the corresponding unsteady separation length development can be determined by an evaluation of φ at each flap angle (with associated steady separation length), (see Fig.56).

The experimentally measured lags in the unsteady separation growth (part IV) have been determined from a comparison of the dynamic tests with the model downstream of the nozzle exit plane, and the fixed flap measurements with the model moved forward. As described in § 16.1, the steady separation lengths with the model in the forward position are slightly less than those that should ideally be compared with the dynamic separation growth. To correct for this model position effect, the difference in the steady separation lengths for the two model positions with a fixed flap angle of 20 degrees (determined from the schlieren measurements of the separated flow without side plates, Figs.26 & 47) has been added to all the measured lags.

The acoustic model has been applied to predict the unsteady separated flow response throughout the flap deflection range when side plates are not attached. These results are compared in Fig.57 with the corrected experimental measurements, and the acoustic prediction for the condition with side plates fitted, determined for the region of high dynamic flap angles.

The appropriate temperature for the determination of an acoustic velocity should be the average value within the separated flow. An approximation, valid when there are low levels of skin friction on the plate surface in this region, is to assume that this temperature is equal to the nearly isothermal wall temperature ahead of the hinge line. The effect of increasing the assumed temperature for the propagation of pressure disturbances is illustrated by an example included in Fig.57.

The predicted lags in unsteady separation growth with this model, based

only on pressure communication times, become substantially less than those measured at flap angles of 30 degrees and greater. At lower flap angles there is a lag in growth predicted where none was measured experimentally, but these are small enough to be contained within the measurement errors, and subsequent data scatter. These lags are also less than the influence of the model position on the scale of the steady separated flows.

17.2 Mass transfer adjustment of the wedge separated flow.

The unsteady growth of a fully laminar wedge separated flow, induced by the rapidly displaced flap surface, has been modelled with a response determined by the constraints based on mass transfer capability. This mass entrainment mechanism of separation adjustment has been previously described by Ihrig & Korst (1963).

An analytic model of the steady wedge separated flow is required in both determining this unsteady response of the wedge separated flow, and for evaluating the appropriate lags in its growth. A consequence of this is that the modelled fully laminar steady separation lengths are not correctly matched in size to those obtained in the experiments. Consideration of this effect on the unsteady response of the separated flow, and a solution which incorporates the correct lengths of steady separation, are subsequently examined. The influence of hinge line bleed, and transition in the shear layer, on the unsteady separated flow response are considered in later sections.

17.2.1 Steady wedge separation solution.

The method of Cooke (1963) has been used to model the steady laminar wedge separated flows. This is a Chapman-Korst type of analytic model (e.g. see Charwat 1970), extended to include the effects of a finite boundary layer at separation. This theory was developed to predict both wedge separated supersonic flows, and those formed downstream of backward facing steps. The principal elements of this model are illustrated in Fig.58. The reverse flow velocities within the separation are neglected, and this region is considered to consist of dead-air. The shear-layer is assumed straight, and is modelled analytically as a free viscous layer developing in a constant pressure region, without interaction with the external supersonic flow. A solution for the velocity profile in this viscous layer is obtained, with its initial conditions determined from the flat plate boundary layer, and simplifying assumptions at the separation point.

The mass flow entrained from the internal region must be returned to it

in the recompression process, thereby satisfying the conservation of mass. This defines a continuous single dividing streamline joining the separation to the reattachment point. The Chapman-Korst type model assumes that the recompression process along the dividing streamline is isentropic, so that the pressure at reattachment equals the stagnation pressure of the flow on this streamline where the reattachment process begins. An empirical condition determines the pressure rise to reattachment. The separation length is then calculated by requiring a sufficient viscous acceleration of the flow along the dividing streamline to achieve a stagnation pressure at the beginning of the reattachment process that is equal to the pressure at the reattachment point.

An additional unknown that must be solved for in Cooke's model for the wedge separated flow is the origin of the separation point. This requires an iterative solution to solve for its location, determined by repeatedly estimating a position for its occurrence until the requirement for the reattachment condition is precisely obtained. Some of the more important additional assumptions in Cooke's model of the separation include:-

(i) The pressure rise at separation is modelled at a single location, across which the boundary layer thickness changes discontinuously. The effect of pressure gradients upstream, and downstream, of the separation point are neglected.

(ii) The form of the velocity profile immediately after separation is unchanged from that on the flat plate ahead of the interaction.

(iii) The constant pressure region in which the free shear layer develops continues as far as the wedge corner, from which the reattachment process is assumed to begin.

(iv) Reattachment takes place half way up the pressure rise from the plateau to the peak value on the wedge.

Although the details of Cooke's model of the separated flow have been described comprehensively in many previous references (e.g. Cooke 1963; Needham 1965a; Merritt 1964) a summary of this theory is included here to allow a full discussion of its extension for the subsequent model of the unsteady separation growth. The description of this theory is divided into separate sections associated with each region of the flow development from the plate ahead of the interaction to that downstream of reattachment. This piecewise description of the flow model, parts (a) to (d) below, reflects the nature of the solution. The subscripts 1, 2, and 3, refer to the inviscid flow regions defined in Fig.58.

(a) Flat plate boundary layer.

The development of the flat plate boundary layer is solved after the x-y coordinate transformation to X-Y, defined by,

$$Y = \int \frac{\rho}{\rho_1} dy , \qquad X = Cx \tag{70}$$

This assumes the use of a linear temperature-viscosity law of the form,

$$\frac{\mu}{\mu_1} = C_1 \frac{T}{T_1} \quad , \text{where} \quad C_1 = \frac{\mu_{wall}}{\mu_1} \frac{T_1}{T_{wall}} \tag{71}$$

This transformation reduces the compressible equations of motion to incompressible equations when the pressure, and external velocity are constant, even with heat transfer, and a general Prandtl number. The same transformation is also used to solve for the free shear layer development, but with the local freestream conditions of region 1 substituted with those of region 2 in Eqs.(70) & (71), and with μ_{wall} and T_{wall} replaced with the conditions assumed for the dead-air region.

The incompressible solution for the boundary layer thickness at the separation point is obtained using a Polhausen method, with a sine function assumed for the form of the incompressible velocity profile.

$$\phi = \frac{u}{u_1} = \sin\left(\frac{\pi}{2}\frac{Y}{\delta}\right) \tag{72}$$

This form was used to maintain consistency with the sine functions adopted for the subsequent solution of the free shear layer, which were decided after reference to previous calculations by Lock (1951) for the incompressible mixing of two streams. These showed particularly good agreement between the exact solution, and a Polhausen solution with this type of sine function velocity distribution. There is no consideration of leading edge viscous interaction, or the pressure gradient upstream of separation, in this calculation of the plate boundary layer.

If separation occurs a distance x_1 from the leading edge, then the incompressible flat plate boundary layer thickness at this location is,

$$\delta_1 = 4.795 \sqrt{\frac{\nu_1 C x_1}{u_1}} \qquad (73)$$

(b) Boundary layer separation.

The separation of the boundary layer is assumed to occur with a step change in pressure, neglecting the gradients that actually exist upstream, and downstream of this location. The deflection angle of the free shear layer at this point is obtained from a correlation of the free-interaction plateau pressure rise (see 2.3, Eq.1), and simple oblique shock wave theory. In the present application of Cooke's model, the use of a free-interaction correlation of the form Eq.(1) was substituted for with a direct curve fit of the measured shear layer deflection angle dependence on the separation length. This simplifies the subsequent equations derived for the mass transfer dynamic separation response, and does not contradict earlier remarks about these separations being of the free-interaction type. A simple cubic function was found to accurately represent the variation of shear layer deflection angle with separation length,

$$\theta_s \text{ (degs.)} = 3.245 + 19.216\ L_{sep} - 64.257\ L_{sep}^2 + 1820.9\ L_{sep}^3 \qquad (74)$$

It is assumed that the form of the shear layer velocity distribution immediately after separation is unchanged from that on the plate. The experimental measurements of Hakkinen et al (1959) in the supersonic flow regime support this assumption, but its validity in the hypersonic flow regime is perhaps questionable because of the increase in normal pressure gradients within the boundary layer in the region of the separation point that occurs at high Mach numbers. Cooke uses a relationship derived by Kirk (1959) to relate the momentum thicknesses downstream and upstream of the separation point,

$$\frac{\theta_2}{\theta_1} = 1 + \left\{ \beta - \frac{1 + H}{\beta} \right\} \theta_s = n \qquad (75)$$

with the incompressible form factor H = 2.66. The shear layer separation angle θ_s is defined as negative in this equation for a compression process. With the same form for the velocity profile in these two regions, this equation also

gives the ratio of the boundary layer thicknesses immediately downstream to that upstream of separation (= δ_1/δ_2). If the shear layer thicknesses above, and below, the dividing streamline are δ_u and δ_l respectively, then the initial conditions after separation for the shear layer development are,

$$\delta_u = 4.795\ n \sqrt{\frac{\nu_1 C\ x_1}{u_1}}\ , \qquad \delta_l = 0 \tag{76}$$

(c) Shear layer development.

The viscous mixing region that develops following separation is modelled as a free shear layer, neglecting the effect of finite reverse flow velocities in the separation region. The local inviscid freestream is assumed uniform, and is determined from oblique shock theory with a deflection of the upstream flow through the effective wedge angle formed at separation. Physical coordinates x,y, and transformed coordinates X,Y, are measured along, and normal, to the dividing streamline respectively. The assumed incompressible velocity profiles in the shear layer are (following Lock 1959),

$$\phi_u = \frac{u_u}{u_2} = \phi_j + (1 - \phi_j) \sin\left(\frac{\pi\ Y}{2\ \delta_u}\right) \qquad \text{above the dividing} \tag{77}$$

$$\phi_l = \frac{u_l}{u_2} = \phi_j - \phi_j \sin\left(\frac{\pi\ (-Y)}{2\ \delta_l}\right) \qquad \text{below the dividing streamline} \tag{78}$$

where ϕ_j is the velocity ratio u/u_2 on the dividing streamline. To satisfy the requirement for continuity of shear stress on the dividing streamline,

$$\delta_u = W\ (1 - \phi_j), \quad \text{and} \quad \delta_l = W\ \phi_j, \quad \text{where} \quad W = \delta_u + \delta_l \tag{79}$$

The simultaneous solution of the momentum integral equation both above, and below, the dividing streamline then leads to the results,

$$l + b\ \phi_j - c\ \phi_j^2 = \frac{l\ \delta_2}{W} \tag{80}$$

and,

$$\frac{x\ \nu_2\ u_1\ C_2}{x_1\ \nu_1\ u_2\ n^2\ C_1} = \frac{2\ l^2\ k\ 4.795^2}{(e+f)^3\ \pi\ c^2}\left\{ 3ef\ \log\frac{e-\phi_j}{f+\phi_j} - \frac{f^3\ (e+f)}{2\ (\phi_j+f)^2} + \right.$$

$$\left. \frac{e^3\ (e+f)}{2\ (e-\phi_j)^2} + \frac{e^3}{e-\phi_j} - \frac{f^3}{f+\phi_j} + \text{constant} \right\} \qquad (81)$$

with,

l = 0.13662, m = 0.09014, k = 0.22676, b = m - l, c = m + k
e = 0.5873, f = 0.7338

The value of the constant in Eq.(81) is determined from the boundary condition that $\phi_j = 0$ when x = 0. The inclusion of the ratio of the Chapman Rubesin constants C_2/C_1 in Eq.(81) is an addition to the original equation derived by Cooke which was in error.

Eq.(81) is an implicit solution for the dividing streamline velocity ratio as a function of the distance along the dividing streamline. The velocity on this streamline accelerates, through viscous action, from zero at the separation point, increasing with distance along the dividing streamline towards an asymptotic value of 0.587 of the local freestream velocity. This is the constant value that is obtained for the dividing streamline velocity ratio with a self-similar development of a laminar free shear layer with zero initial boundary layer thickness (Chapman 1950). To evaluate the dividing streamline velocity ratio for a given distance x, the method of Newton-Raphson was used in the present work for the solution of Eq.(81), with an initial guess for the velocity ratio of 0.58. This gave rapid convergence to an accurate result for all values of x.

(d) Reattachment process.

The peak pressure rise on the wedge is determined from oblique shock theory, with a deflection of the inviscid flow equal to the difference between the flap, and shear layer angles. The pressure rise at the reattachment point occurs somewhere along this peak pressure rise, and is determined from an empirical reattachment parameter N, defined by,

$$N = \frac{p_r - p_2}{p_{3\,(peak)} - p_2} \tag{82}$$

Cooke assumes N = 0.5 in all cases of laminar separation. This result was based on limited experimental data, and an argument that the separation process is similar to that at reattachment, for which the pressure rise to separation is about half that of the plateau pressure. Of course, the reattachment process is not a free interaction, and it has been observed in subsequent separation experiments that the value of the parameter N is not constant, but varies with the scale of the separated flow (Naysmith 1962; see also Holden 1978). There is no simple correlation for this parameter, and, accepting its inadequacies, a constant value of N = 0.5 has been used in applying this theory. This is probably a reasonable average value throughout the flap deflection range. The simplification of the reattachment region is *one* of the major weaknesses in this model of the separated flow.

The pressure rise to reattachment along the dividing streamline is approximated as an isentropic process, neglecting the effects of viscosity. i.e. $\partial\tau/\partial y$. This defines a necessary stagnation pressure on the dividing streamline at the beginning of the reattachment process that is equal to the reattachment pressure. It is necessary to determine the Mach number on the dividing streamline to calculate its total pressure, which requires a relationship for the temperature variation through the free shear layer as a function of the velocity. Cooke uses the enthalpy profiles derived by Carriére & Sirieux (1961),

$$h_o = w\, h_{o,2}\,, \qquad \text{with} \quad w = w_m + \phi^2\,(1 - w_m) \tag{83}$$

where h_o is the stagnation enthalpy on a streamline within the shear layer,

$$h_o = c_p T + \frac{u^2}{2} \tag{84}$$

and w_m is the value of w in the dead-air region where $h_o = c_p T_d$. For a pressure rise to reattachment of p_r/p_2, this then defines a necessary value of the velocity ratio on the dividing streamline, above the hinge line (where the reattachment process is assumed to begin), necessary to reattach to the flap surface, given by a solution of the equation,

$$\frac{p_r}{p_2} = \left\{ \frac{1}{1 - \dfrac{\frac{\gamma-1}{2} M_2^2 \phi_j^2}{\left(w_m (1 - \phi_j^2) + \phi_j^2 \right)\left(1 + \frac{\gamma-1}{2} M_2^2 \right)}} \right\}^{\frac{\gamma}{\gamma - 1}} \tag{85}$$

Alternative temperature - velocity relationships that can be used through the free-shear layer include Crocco's equation (Pr = 1),

$$T = T_d + \left\{ T_2 - T_d + \frac{u_2^2}{2 c_p} \right\} \frac{u}{u_2} - \frac{u^2}{2 c_p} \tag{86}$$

and Monaghan's (1953) approximate relationship as used by Merritt (1964) in applying Cooke's analytic model to a separated hypersonic flow formed behind a downstream facing step,

$$T = T_d + Pr^{1/3}(T_{aw} - T_d)\frac{u}{u_2} - Pr\, T_2 \left(\frac{\gamma-1}{2} \right) M_2^2 \left(\frac{u}{u_2} \right)^2 \tag{87}$$

where,

$$T_{aw} = T_2 \left(1 + \frac{\gamma-1}{2} \sqrt{Pr}\, M_2^2 \right)$$

These two relationships, Eqs.(86) & (87), are identical for unity Prandtl number, and lead to the following equation with general Prandtl number for the velocity ratio on the dividing streamline necessary to satisfy the imposed reattachment criterion,

$$\frac{p_r}{p_2} = \left\{ 1 + \frac{1}{\dfrac{1 + \frac{\gamma-1}{2} Pr^{1/2} M_2^2}{\frac{\gamma-1}{2} M_2^2 \phi_j^2} \left\{ \dfrac{T_d}{T_{aw}} \left(1 - Pr^{1/3}\phi_j \right) + Pr^{1/3}\phi_j \right\} - Pr} \right\}^{\frac{\gamma}{\gamma-1}} \tag{88}$$

Monaghan's equation does not satisfy the boundary condition that $T \Rightarrow T_2$ as $u \Rightarrow u_2$ for arbitrary Prandtl number. This approximate relationship is therefore only valid for the inner regions of the shear layer near the dividing streamline (equivalent to the wall region for an attached boundary layer).

In applying Eq.(85) or (88), a temperature must be assumed at the lower edge of the free shear layer mixing region. The low levels of heat transfer in fully laminar separated flows indicate that the normal temperature gradients in the recirculating flow adjacent to the plate surface are small. As an approximation, the dead-air temperature was set equal to an isothermal wall temperature of 293 K.

The following calculation procedure is used for determining the steady separated flow geometry with this analytic model:-

1) Estimate a location for the separation point, and calculate the flat plate boundary layer.

2) Apply a correlation of the separation interaction to determine the shear layer deflection angle.

3) Determine the shear layer development, and the velocity ratio on the dividing streamline above the hinge position.

4) Determine the reattachment pressure rise, and hence the necessary value of the dividing streamline velocity ratio at the beginning of the reattachment process.

5) If the velocity ratio calculated on the dividing streamline is less than the necessary value to overcome the reattachment pressure rise, then estimate a larger separation length, and repeat the above calculations. If this comparison is vice-versa then estimate a smaller separation length.

6) Repeat this procedure until the correct velocity on the dividing streamline is obtained for the reattachment process.

The steady separation lengths predicted with this analytic model are presented in Fig.59, where they are compared with the experimental measurements. At low flap angles there is good agreement between the theory and the experiment when the enthalpy profiles of Carriere & Sirieux are used. There has been no account taken of hinge line bleed in the analytic model, although the application of a correlation of these effects suggest that its influence on the experimental measurements is small (see § 13.6). Lateral venting will also influence the separated flows observed in the experiments. At low flap angles where the aspect ratio of the separated flow is high this effect is likely to

be weak. There is a sensitivity to the particular temperature - velocity relationship used, although the effect of Prandtl number in Eq.(88) is only slight. The rate of separation length increase from this theory is larger than that measured experimentally, particularly when Monaghan's, or Crocco's, equation is used. This is expected because of the influence of transition, and lateral venting, in the experiments.

The agreement between experiment and theory at the lowest fixed flap angle is better than that previously found by Needham (1965a) for small to moderate wedge angles with a freestream Mach number of 9.7. However, Needham's derivation of Eqs.(85) and (88) both contained errors, which may have accounted for the strong discrepancy between the results of this analytic model, and his experimental measurements. It should be noted, however, that the success of the analytic model here may be due to, for example, a cancellation of inaccuracies in over-simplifying the separation region, and the reattachment process.

17.2.2. Dynamic response.

This two-dimensional model of the separated flow dynamic response is based on the ability of this growing region to entrain additional mass. Pressure equalisation throughout the separated flow is assumed instantaneous, and the dead-air temperature (assumed equal to an isothermal wall temperature), and therefore its density, are approximated as uniform. Any possible dynamic effects on the shear layer growth are neglected, and therefore its development is modelled as in the steady separation calculations. Ihrig & Korst (1963) described their model of separation adjustment with the same assumptions as "quasi-steady". For application to their base separated flow, these assumptions were justified by the much larger characteristic time for mass transfer adjustment compared to that for pressure waves (ratio of 30). For the present wedge separated flow the ratio of these characteristic times is less, particularly at low flap angles, and these assumptions are less easily justified. In this present model, the free-interaction process at separation is assumed unaltered.

A further requirement for validating the use of a quasi-steady shear layer model, not discussed by Ihrig & Korst, is the consideration of diffusion times for momentum, and heat transfer, across this viscous region. Moore (1951) formulated criteria for attached boundary layers to determine whether there unsteady response would be quasi-steady. These required that the ratio of the time to diffuse across the boundary layer a unit proportional change in

a freestream flow parameter should be much less than the time for this imposed change to occur. Specifically, for a boundary layer response to a change in adjacent freestream flow velocity to be quasi-steady, the following parameter must be much less than unity,

$$\frac{\delta^2}{\nu}\ \frac{1}{u_e}\ \frac{du_e}{dt} \tag{89}$$

where u_e is the local freestream flow velocity. This parameter has been evaluated for the present experimental conditions, using a typical shear layer thickness δ, and average dynamic viscosity ν, with the rate of change of local velocity determined from the separated shear layer deflection angle changes that occur as a function of time. This gives a typical value for the parameter of Eq.(89) equal to 1.5×10^{-6}. This then justifies the assumption that the shear layer response in this respect is quasi-steady. With a Prandtl number of 0.74, the adjustment times for diffusion of momentum, and heat transfer through the shear layer are of the same order.

The separated flow geometry is approximated as a triangular section, with a mass of recirculating flow m_d (Fig.60). As the separation length increases, so does this mass of flow. The source for this increase is an entrainment mechanism from the free shear layer, which is illustrated in Fig.60. There exists a streamline in the shear layer that originates from the separation point, which for the steady separated flow is the continuous dividing streamline that eventually reattaches on the flap surface (Fig.58). If it is supposed that a lag in the growth of the unsteady separated flow develops, then the velocity on the separation streamline at the beginning of the reattachment process will be less than that for the steady separation generated by the same instantaneous fixed flap angle, since the accelerating effect of the shear layer will have acted for a shorter length. The separation streamline will therefore have insufficient momentum to be able to overcome the reattachment pressure rise, and will be reversed back into the recirculation region. The reattachment streamline must then originate from a higher momentum region of the free shear layer, which will be above the separation streamline. This produces a net rate of mass transfer to the separated flow, G_d, equal to,

$$G_d = \int_{y_s}^{y_r} \rho u \, dy \tag{90}$$

where y_s is the streamline in the shear layer originating from the separation point, and, y_r is the streamline that eventually reattaches on the flap surface. This integral is evaluated at the beginning of the reattachment process (Fig.60), which for the wedge separated flow is assumed to occur at a location in the shear layer above the hinge line. This description of the unsteady separated flow development suggests that it must develop a lag in its growth in order to entrain additional mass. If then the scale of a dynamically separated flow does appear quasi-steady, this implies that a negligible lag in growth is sufficient to entrain a high enough rate of mass flow to maintain this lag at a negligible level with further growth of the unsteady separation.

For a mass flow rate entrained from the free-shear layer at any instant equal to G_d, conservation of mass in this two-dimensional separated flow requires,

$$G_d = \frac{dm_d}{dt} \tag{91}$$

For the triangular section (unit depth),

$$m_d = \frac{p_2}{2 R T_d} \left\{ L_{sep}^2 \cos\theta_s \sin\theta_s + \frac{L_{sep}^2 \sin^2\theta_s}{\tan(\theta_f - \theta_s)} \right\} \tag{92}$$

Differentiation of this then gives,

$$\frac{dm_d}{dt} = \frac{1}{2 R T_d} \frac{dp_2}{d\theta_s} \frac{d\theta_s}{dL_{sep}} \frac{dL_{sep}}{dt} \left\{ L_{sep}^2 \cos\theta_s \sin\theta_s + \frac{L_{sep}^2 \sin^2\theta_s}{\tan(\theta_f - \theta_s)} \right\} +$$

$$\frac{p_2}{2 R T_d} \left\{ \frac{dL_{sep}}{dt} \left\{ 2L_{sep} \cos\theta_s \sin\theta_s + \frac{2L_{sep} \sin^2\theta_s}{\tan(\theta_f - \theta_s)} + L_{sep}^2 (\cos^2\theta_s - \sin^2\theta_s) \frac{d\theta_s}{dL_{sep}} \right.\right.$$

$$+ \frac{2L_{sep}^2 \sin\theta_s \cos\theta_s}{\tan(\theta_f-\theta_s)} \frac{d\theta_s}{dL_{sep}} + \frac{L_{sep}^2 \sin^2\theta_s}{\sin^2(\theta_f-\theta_s)} \frac{d\theta_s}{dL_{sep}} \Bigg\} \Bigg\} -$$

$$\frac{p_2}{2 R T_d} \frac{L_{sep}^2 \sin^2\theta_s}{\sin^2(\theta_f-\theta_s)} \frac{d\theta_f}{dt} \qquad (93)$$

where the identities,

$$\frac{d\theta_s}{dt} = \frac{d\theta_s}{dL_{sep}} \frac{dL_{sep}}{dt}, \quad \text{and,} \quad \frac{dp_2}{dt} = \frac{dp_2}{d\theta_s} \frac{d\theta_s}{dL_{sep}} \frac{dL_{sep}}{dt}$$

have been incorporated. This derivative of the separated flow recirculating mass is equated to G_d, and then rearranged to solve for the rate of separation length increase,

$$\frac{dL_{sep}}{dt} = \frac{G_d + \frac{p_2}{2 R T_d} \left(\frac{L_{sep}^2 \sin^2\theta_s}{\sin^2(\theta_f-\theta_s)} \right) \frac{d\theta_f}{dt}}{Z} \qquad (94)$$

where

$$Z = \frac{1}{2 R T_d} \frac{dp_2}{d\theta_s} \frac{d\theta_s}{dL_{sep}} \left(L_{sep}^2 \cos\theta_s \sin\theta_s + \frac{L_{sep}^2 \sin^2\theta_s}{\tan(\theta_f-\theta_s)} \right) +$$

$$\frac{p_2}{2 R T_d} \Bigg\{ 2L_{sep} \cos\theta_s \sin\theta_s + \frac{2L_{sep} \sin^2\theta_s}{\tan(\theta_f-\theta_s)} + L_{sep}^2 (\cos^2\theta_s - \sin^2\theta_s) \frac{d\theta_s}{dL_{sep}}$$

$$+ \frac{2L_{sep}^2 \sin\theta_s \cos\theta_s}{\tan(\theta_f-\theta_s)} \frac{d\theta_s}{dL_{sep}} + \frac{L_{sep}^2 \sin^2\theta_s}{\sin^2(\theta_f-\theta_s)} \frac{d\theta_s}{dL_{sep}} \Bigg\}$$

The solution of Eq.(94) requires the evaluation of the following parameters:-

(i) $dp_2 / d\theta_s$

The rate of the plateau pressure change with the effective wedge angle is determined from simple oblique shock theory, using,

$$\frac{dp_2}{d\theta_s} = \frac{dp_2}{d\beta_s}\,\frac{d\beta_s}{d\theta_s}$$

Differentiation of $p_2 = f(p_1, M_1, \beta_s)$, and the implicit θ-β-M relationship gives,

$$\frac{dp_2}{d\theta_s} = \frac{A}{B}\,\frac{4\gamma\, p_1 M_1^{\,2}}{(\gamma+1)}\,\sin\beta_s\cos\beta_s \qquad (95)$$

where,

$$A = \sec^2\theta_s \tan^2\beta_s \left(M_1^{\,2}\gamma + M_1^{\,2}\cos 2\beta_s + 2 \right)^2$$

$$B = 4\, M_1^{\,2}\sin^2\beta_s \left(M_1^{\,2}\gamma + M_1^{\,2}\cos 2\beta_s + 2 \right) +$$

$$\left(2 - 2\, M_1^{\,2}\sin^2\beta_s \right) \left(\left(M_1^{\,2}\gamma + 2 + M_1^{\,2}\cos 2\beta_s \right) \sec^2\beta_s - 4\, M_1^{\,2}\sin^2\beta_s \right)$$

(ii) $d\theta_s / dx_s$

This parameter is determined by direct differentiation of the correlation equation $\theta_s = f(L_{sep})$, Eq.(74).

(iii) $d\theta_f / dt$

This is a boundary condition which is chosen to match the experimental conditions at each flap deflection angle (Figs.44 & 45).

(iv) G_d

Using the compressible–incompressible transformation, the entrained mass flow rate may be re-written in incompressible coordinates as,

$$G_d = \rho_2 \int_{Y_s}^{Y_r} u\, dY \qquad (96)$$

The separation streamline Y_s, which is the dividing streamline for the steady separated flow, occurs at $Y = 0$, where the velocity ratio $\phi = \phi_j$. The reattachment streamline Y_r is determined at each instant as part of the unsteady solution. Substitution of the incompressible velocity profile above the dividing streamline into Eq.(96), and integrating between the limits,

$$G_d = \rho_2 u_2 \left\{ \phi_j Y_r + \frac{2\,\delta_u}{\pi}\left(1 - \phi_j\right)\left(1 - \cos\left(\frac{\pi\, Y_r}{2\,\delta_u} \right) \right) \right\} \qquad (97)$$

The velocity on the separation streamline ϕ_j is determined for a given length x of free-shear layer ahead of the hinge line, from a solution of Eq.(81) with the Newton-Raphson method. The incompressible height of the free-shear layer above the separation streamline δ_u at this location is determined from Eqs.(80) & (79).

The reattachment streamline Y_r must contain sufficient momentum to just overcome the reattachment pressure rise, with the deceleration of flow along this streamline again assumed isentropic. The reattachment pressure rise is determined primarily by shock compression, with a value of N = 0.5. There is, however, an additional perturbation pressure caused by the translational motion of the moving flap surface at the reattachment point. The magnitude of this additional pressure has been determined from the solution of the simple acoustic wave equation (e.g. see Liepmann & Roshko 1957), from which the perturbation pressure is,

$$dp_r = + \rho_r a_r du_r = \frac{p_r}{R\,T_r}\sqrt{\gamma R T_r}\, du_r = p_r \sqrt{\frac{\gamma}{R\,T_{wall}}}\, \frac{d\theta_f}{dt}\, x_r \qquad (98)$$

where the suffix r refers to conditions at the reattachment point. In evaluating this, it has been assumed that the appropriate temperature is the flap wall temperature since the perturbation pressure originates from this surface. The translational velocity is determined from the angular rate of flap deflection, and the distance from the hinge line to the reattachment point x_r, where

$$x_r = \frac{L_{sep} \sin\theta_s}{\sin(\theta_f - \theta_s)} \qquad (99)$$

The magnitude of this perturbation pressure is less than 1% of the shock recompression pressure rise at all angles.

For the assumed isentropic compression along the reattaching streamline, a necessary Mach number on this at the beginning of the reattachment process above the hinge line is,

$$M_R^2 = \frac{2}{\gamma-1}\left\{\left\{\frac{p_r + dp_r}{p_2}\right\}^{\frac{\gamma-1}{\gamma}} - 1\right\} \tag{100}$$

With the enthalpy profiles of Carriere & Sirieux the necessary velocity ratio on the reattachment streamline at this location is then,

$$\phi_r^2 = \frac{\dfrac{M_R^2\, w_m\, h_{o2}}{c_p}}{\dfrac{u_2^2}{\gamma R} - M_R^2\left\{(1-w_m)\dfrac{h_{o2}}{c_p} - \dfrac{u_2^2}{2c_p}\right\}} \tag{101}$$

and with Monaghan's or Crocco's (Pr = 1) temperature-velocity relationship,

$$\phi_r^2\left[u_2^2 + M_R^2\gamma R T_2 \frac{Pr}{2}(\gamma-1)M_2^2\right] - \phi_r\,\gamma R M_R^2 Pr^{1/3}(T_{aw} - T_d) - \gamma R M_R^2 T_d = 0 \tag{102}$$

The combination of Eqs.(100) & (101), or (100) & (102), is equivalent to Eqs.(85) and, (88) respectively, with $\phi_r \equiv \phi_j$, and $p_r/p_2 \equiv (p_r + dp_r)/p_2$. With ϕ_r determined, the reattachment streamline Y_r is obtained from the incompressible velocity profile,

$$Y_r = \frac{2\,\delta_u}{\pi}\sin^{-1}\left(\frac{\phi_r - \phi_j}{1 - \phi_j}\right) \tag{103}$$

The solution for the unsteady separation growth, Eq.(94), was calculated with a simple finite difference numerical scheme,

$$L_{sep}(t+\delta t) = L_{sep}(t) + \delta t\left\{\frac{G_d + \dfrac{p_2}{2RT_d}\left(\dfrac{L_{sep}^2 \sin^2\theta_s}{\sin^2(\theta_f - \theta_s)}\right)\dfrac{d\theta_f}{dt}}{Z}\right\} \tag{104}$$

with the bracketed term evaluated at time t. Care was taken to use a sufficiently small time increment for an accurate solution. It was necessary to start the unsteady solution of the separation growth from an initially established steady separated flow, at an angle below which the accumulated lag effects can be considered negligible. The initial condition set was a steady separated flow predicted with a 10° flap angle, from which the flap was subsequently deflected instantaneously, with the flap velocity v's flap angle matched throughout to the experimental conditions (Figs.44 & 45).

The results of this modelled unsteady response are illustrated in Fig.61, and compared with the measured dynamic separation lags in Fig.62. These measured dynamic separation lags have again been corrected for the model position effect.

The predicted establishment of a lag in the dynamic separation growth, based on this mass adjustment model, occurs at a smaller flap angle than is observed experimentally, and throughout the flap deflection range the predicted lags in separation growth are much greater than those measured. Factors that may contribute to this discrepancy are considered below:-

(i) Steady separation scale.

The predicted steady separation lengths increase more rapidly with flap angle than those measured in the experiments, and therefore contain more recirculating mass. This increases the mass transfer characteristic time of the unsteady separation adjustment, which increases the lags in its growth with respect to the instantaneous quasi-steady separation lengths. Therefore, an important parameter to match to the experimental conditions in modelling the unsteady separation growth is the steady separation length at each flap angle. This requirement has been incorporated in the model of the unsteady separation growth by formulating a new reattachment criterion for the Mach number required in the shear layer above the hinge line.

Altering the reattachment criterion does not affect the basic driving mechanism for the mass reversal in the shear layer, which is the lag that develops between the dynamic, and steady, separated flows at each instantaneous flap angle. The magnitude of this lag is determined by the values of the steady separation length at each angle, and the shear layer velocity profile.

The dependence of the measured steady separation lengths on the flap deflection angle, without side plates fitted, is closely approximately by the equation,

$$L_{sep} = 0.00321\ \theta_f(\text{degrees}) - 0.0201 \qquad (105)$$

At 0.1 degree increments in the flap angle, between 10 to 35 degrees, steady separation lengths were obtained from this equation, and for each of these the Mach number on the dividing streamline above the hinge line was calculated using Cooke's model of the shear layer development. The corresponding reattachment pressure rise for each of these steady separation lengths was determined, assuming a value for the reattachment parameter N = 0.5. These values of Mach number v's pressure rise were used as a new reattachment criterion in the mass exchange model of the unsteady separation growth, thereby matching the modelled steady separation lengths to the experimental measurements. Linear interpolation was used in applying this reattachment criterion when instantaneous values of the reattachment pressure rise lay between its discrete values.

For this two-dimensional model of the unsteady separation growth, the predicted steady separation lengths should ideally be matched to the experimental measurements that were made with the side plates attached. However, it was not possible to accurately measure these separation lengths from the schlieren photographs with the side plates fitted. The measurements of the steady separation lengths without the side plates attached still provide a significant improvement in matching the modelled steady separation lengths to the appropriate scale.

The results of the modelled unsteady separation growth with the correctly matched steady separated flow lengths are shown in Figs.63 & 64. The predicted lags in growth are substantially less than those previously obtained with the larger steady separated flow geometries, as expected. These lags are still greater than the measured values throughout this flap deflection range. However, at the largest flap angle of 35 degrees the modelled response is of the correct order compared to the experimental measurements.

The results of this modelled dynamic separation growth were found to be negligibly influenced by the choice of temperature–velocity relationship, provided the same relationship was used in formulating the reattachment criterion, and for the subsequent model of the unsteady separation growth. The sensitivity to the choice of the reattachment parameter was examined by using a value of unity in formulating the reattachment criterion, and in the dynamic model of the separation growth. This did not significantly influence the magnitude of the predicted dynamic separation lags compared with those

obtained using N = 0.5.

(ii) Hinge line bleed.

In the experiments there is a mass bleed across the hinge line gap during the dynamic separation development, which has been neglected in the mass exchange model of the separated flow response. If the effective stagnation pressure for this choked flow across the hinge line gap is the plateau pressure, and the stagnation temperature is assumed to be the wall temperature, then the magnitude of this mass bleed is determined by the instantaneous separation length. If the free-interaction remains unaltered for the dynamic separation, then with respect to the instantaneous separation length the hinge line bleed is a quasi-steady term.

The experiments indicate that there is a negligible lag in the unsteady separation growth when the angle of the moving flap is less than 20 degrees. For a quasi-steady separated flow, the mass bleed across the hinge line gap must be precisely balanced by a continual entrainment of mass flow from the shear layer (Fig.65). If a lag in the dynamic separation growth does develop then the *net* mass entrainment from the shear layer for the separation growth that this induces, evaluated at the beginning of the reattachment process, must come from above that streamline below which there is a mass flow to balance the hinge line bleed (Fig.66). Since the hinge line bleed is a quasi-steady term, this lower streamline that defines a boundary for the net mass entrainment is also the streamline that would reattach to the wedge surface for a steady separation equal in length to the instantaneous dynamic separation length. The streamline that defines the upper boundary for the net mass flow entrained is that which satisfies the reattachment criterion for the instantaneous flap angle. The velocity on this streamline at the beginning of the reattachment process is approximately equal to that on the reattaching streamline of the steady separated flow that would be induced by this instantaneous flap angle (neglecting the slight differences in the respective shear layer deflection angles). This means that the mechanism that drives an increase in net mass entrainment into the unsteady separated flow as a lag in its growth develops is the difference in length of the instantaneous quasi-steady separated flow, and the instantaneous dynamic separation. i.e. the lag in dynamic separation growth. This mechanism is precisely the same as that which occurs during the separated flow growth without hinge line bleed.

Differences in the separated flow response with, and without, hinge line bleed, will be associated with the rate of increase in the net mass

entrainment rate from the shear layer as a lag establishes in the dynamic separation growth, and the instantaneous respective masses of recirculating separated flow. Some of the influences of hinge line bleed on these are discussed below.

Fig.66 illustrates an instant during the unsteady separation development in which there is a lag in growth, x_{lag}, and u_T, and u_B, are the upper, and lower, bounds respectively for the net rate of mass entrainment at the beginning of the reattachment process. This is shown for conditions both with, and without, hinge line bleed. The velocity u_B is then also equal to the reattachment value necessary at the beginning of the reattachment process for a steady separation equal in length to the dynamic separation L_{sep}, and u_T is approximately the reattachment criterion for the steady separated flow (length $L_{sep} + x_{lag}$) that would be generated by the instantaneous flap angle. If the variation of the steady separation lengths with the flap angle is known from experiment, then from the derivative of this dependence, the change in flap angle necessary to produce an increase in steady separation length from L_{sep} to $L_{sep} + x_{lag}$ can be estimated as,

$$\delta\theta_{flap} \simeq \frac{x_{lag}}{\left\{\frac{dL_{sep}}{d\theta_{flap}}\right\}_{\text{at } L_{sep}}} \qquad (106)$$

The effective change in reattachment angle of the free shear layer that accompanies this increase in steady separation length is then $\delta\theta_{flap} - \delta\theta_s$, where $\delta\theta_s$ is the increase in shear layer angle with the change in separation length L_{sep} to $L_{sep} + x_{lag}$. The change in the steady separation reattachment criterion, $u_T - u_B$ (which are the approximate bounds for the net mass entrainment caused by x_{lag} in the unsteady separation growth), is caused by an increase in reattachment pressure rise, which is effectively induced by this increase in reattachment turning angle of the shear layer. i.e.,

$$u_B - u_T = f(\delta\theta_{flap} - \delta\theta_s) \qquad (107)$$

The influence of hinge line bleed on the steady separation lengths for flap angles above 20 degrees is small (§13.6, Fig.38b). There is a slight increase in the derivative of steady separation length with respect to the flap angle, compared to a sealed hinge gap, producing a corresponding reduction in $\delta\theta_{flap}$

in Eq.(106). However, with hinge line bleed, the separation lengths are less, and therefore the rate of increase in θ_s with increasing separation length is less, reducing $\delta\theta_s$. Therefore the displacement of the boundaries for the *net* rate of mass flow entrainment increase at about the same rate with the development of a lag in dynamic separation growth for both conditions with, and without, hinge line bleed.

The mass flow rate entrained for given bounds u_T, and u_B, in the shear layer will be influenced by the form of the shear layer velocity profile (see (iv) below). This profile will be slightly less developed at the beginning of the reattachment process when there is hinge line bleed, because of the reduction in steady separation lengths. Assuming a linear shear layer velocity profile, which is typical in the laminar hypersonic regime, the change in slope of this is approximately proportional to a ratio of the square roots of the respective separation lengths measured from the hinge line. The differences in steady separation lengths with, and without, hinge line bleed, for flap angles in excess of 20 degrees are only a few percent, and with a dependence of the velocity profile on the square root of the separation length, this effect of hinge line bleed on the net mass entrainment rate is negligible.

The limits u_T, and u_B, are both further from the separation streamline when there is hinge line bleed (Fig.66). If the shear layer is fully laminar, with a nearly linear velocity profile, then this will have little effect on the net mass flow entrained. However, the shear layer in the experiments is transitional, and for this condition the shear layer becomes fuller above the separation streamline. This increases the y displacement of the velocity limits for mass entrainment when there is hinge line bleed, and hence the net rate of mass entrainment. This effect will tend to reduce the experimentally measured lags in dynamic separation growth compared to those that would be measured if the hinge line had been sealed.

The reduction in steady separation lengths with hinge line bleed lowers the angle of the separation shear layer at each flap angle, compared to those that occur with a sealed hinge. The turning angle of the free shear layer at reattachment is therefore slightly greater with hinge line bleed for a given flap angle, and hence u_B is also slightly larger. This means that the net mass entrained for the dynamic separation growth will come from a region of higher velocity in the shear layer when there is hinge line bleed. This region of higher velocity is also a region of higher density, since the viscous dissipation is less, and this effect of hinge line bleed tends to increase the

rate of mass flow entrainment if a lag in dynamic separation develops, compared to that for a sealed hinge line.

A consequence of the reduced steady separation lengths with hinge line bleed is a reduction in the mass of separated flow, and this tends to lower the characteristic mass adjustment time. This reduction is enhanced by both a smaller shear layer angle, and a reduced rate of increase of the shear layer angle with respect to separation length.

The various influences of hinge line bleed on the dynamic response are therefore several, some of which tend to reduce the response time of the dynamically separated flow, and some of which increase it. However, in conclusion, the effects of the particular magnitude of hinge line bleed in the present experiments on the scale of steady separation for flap angles above 20 degrees is so small, that the contribution from each of the influences described above is likely to be negligible. The sensitivity of the separation growth rate is also less than directly proportional to the changes in the net mass entrainment rate (see Eq.94). The experimentally measured response of this unsteady separation is therefore expected to be little different from that which would be obtained with a sealed hinge line.

(iii) Recirculating flow region.

In modelling the steady, and dynamic, separations it has been assumed that the region beneath the shear layer can be considered to consist of dead-air. In fact, the three regions of external flow, recirculation, and shear layer, must mutually interact so that their matching at each interface depends on the complete solution. If the reverse flow velocity significantly influences the shear layer velocity profile then the model of the unsteady separation response will be in error. This effect can only *potentially* be precisely determined from a numerical solution of the complete Navier-Stokes equations for this flowfield. Experimental measurements from pitot pressure traverses (Needham & Stollery 1966a), and investigations of the sensitivity of separation geometries to changes in the wall profile at the corner (Needham & Stollery 1966a), suggest that the dead-air assumption is reasonable in the hinge line region of well developed wedge separated hypersonic flows.

Another approximation in the unsteady separation model is that the mass of separated flow m_d has uniform properties. This is not strictly correct, because even if the assumption is valid that the flow beneath the shear layer is dead, the mass m_d still includes the lower part of the shear layer (Fig.60). Due to viscous dissipation in this region, the average temperature

of the mass m_d will be greater than the wall temperature. The effect of increasing the assumed recirculating flow average temperature on the modelled dynamic separation response has been examined, and the results are illustrated in Fig.67. The most significant influence of increasing this temperature appears to be the reduction it creates in the average density of the separated flow, which reduces the rate of steady separated flow mass increase with flap angle. This reduces the lag in the unsteady separation growth. The magnitude of this influence is not sufficient to account for the difference between experimentally measured lags, and those predicted.

(iv) Transition.

The mass entrainment rate, and therefore the unsteady separation response, is sensitive to the form of the shear layer velocity profile. The fuller this profile is, the more mass flow rate will be entrained for a given lag in separation growth. This is because the temperature, and therefore the Mach number, and density profiles, are functions of the velocity in the free shear layer. For a particular reattachment Mach number, and therefore reattachment velocity, the fuller the shear layer profile the greater the y displacement for the velocity bounds of net mass entrainment. The integrated mass flow rate (Eq.90) is therefore larger.

The separated flows in the experiments are transitional, and will therefore have a more rapid unsteady separation response than that predicted with the fully laminar model. An indication of the effects of transition on the free shear layer development is illustrated in Fig.68, which compares velocity profiles calculated with analytical models for the examples of an asymptotic laminar free shear layer, and an asymptotic turbulent free shear layer, with typical local freestream flow conditions that occur in the present experiments. The turbulent velocity profile was calculated following the theory of Korst (1956), with the jet spread factor determined from an empirical equation incorporated by Childs et al (1966) in their model of turbulent wedge separated flows. It is clear that the velocity profile about the separation streamline becomes much fuller for the turbulent condition.

(v) Lateral venting.

The modelled separation response is for a two-dimensional flow that does not consider the influence of lateral venting. The experiments show that the lags in dynamic separation growth at high flap angles are reduced with side plates attached. This reduction is typically by 20% (e.g. see Fig.62). The slight

leakage of flow past the side plates for the highest fixed flap angle of 35 degrees is not believed to have a strong influence on the measured dynamic separation lag in growth at this angle. For the lower flap angle of 32.5 degrees, the measured lag in dynamic separation growth with the side plates attached is still significant. The rate of increase in this lag with flap angle when the side plates are attached appears similar to that which occurs when the lateral venting is unconstrained.

The driving potential for lateral venting of the recirculating flow is a pressure difference between the flow adjacent to the model outer edges, and the separated flow pressures on the model, which include the plateau pressure, and pressure rises to reattachment. This lateral venting is an additional mass transfer term in the separation unsteady growth. Its various sources of influence on the dynamic separation response are the same as those described for the hinge line bleed, although the effect of lateral venting on the scale of the steady separations is greater. Also, this influence increases for larger separated flows, in contrast to hinge line bleed. If a lag develops in the unsteady separated flow growth, then compared to a steady separated flow of the same instantaneous length, the lateral venting is larger for the dynamic separation because of its higher flap angle. This increase in lateral venting as the dynamic separation grows is a non-quasi-steady effect that will tend to increase the lags in its growth.

The effect of lateral venting on the scale of the separated flow at high flap angles causes a large reduction in the mass of separated flow, strongly reducing the characteristic mass adjustment time. The simultaneous effect on the shear layer development through the reduction in separation length is less significant because of the asymptotic nature of its development for large lengths. The reduction in the mass transfer characteristic time of adjustment caused by lateral venting at moderate to high flap angles might be expected to be most significant, and therefore reduce the measured lags in the dynamic separation growth compared to that with side plates fitted. However, this contradicts the experimental measurements.

The measured differences in separation response with, and without, side plates fitted, are believed to be associated with transition occurrence. The increase in shear layer lengths with the side plates attached is likely to promote transition further ahead of the hinge line, producing a fuller velocity profile. This will reduce the mass transfer response time of an unsteady separation. A comparison of the measured heat transfer distributions for both the steady separations, and for the dynamic separations (Figs.33, 50,

& 51), clearly indicate that the local increase in heat transfer on the plate that characterises transition onset occurs further ahead of the hinge line when the side plates are attached. However, it must be noted that it is not clear if the transition location measured on the plate surface corresponds directly to the position of its occurrence in the shear layer.

17.3 Discussion.

The two models of unsteady separation growth are based on a number of simplifying assumptions, and are therefore only expected to indicate the correct order of response compared to experiment. This particularly applies for the prediction of mass transfer adjustment, which requires a detailed model of the shear layer development. The experimentally measured lags required a correction for the model position effects. The method used of adding a constant is only approximate, and could be an underestimate of the position effects at the highest flap angles. The comparison of the experimental measurements with the results of these two models indicates that at low flap angles the assumption of pressure wave adjustment is most suitable, and that at high flap angles mass entrainment becomes dominant. An evaluation of the ratio of characteristic times for mass transfer adjustment to that for pressure waves (as defined by Ihrig & Korst 1963, see § 3.2) for this wedge separated flow gives 0.84 at a 10 degree flap angle, to 3.05 for a flap angle of 35 degrees. Both these values are much lower than the ratio of 30 obtained by Ihrig & Korst (1963), which was subsequently used to justify a mass transfer model of separation adjustment. This suggests that simple models of separation adjustment, based on a single dominant mechanism, will not be accurate for the present configuration, where there is instead likely to be a response characterised by a strong interaction between both pressure wave, and mass entrainment, mechanisms. However, the analytic models that have been developed do provide a useful description of the physical mechanisms contained within this separation adjustment.

18. Dynamic effects on heat transfer.

18.1 Separated flow region.

Any mechanisms within the separated flow dynamic response that influence the wall heat transfer rates will be associated with unsteady effects on the local heat transfer coefficients in this region, and / or, on the temperature differences between the wall and the flow adjacent to the local boundary layer.

At any instant, energy is transferred to the separated flow along its upper boundary through shear work, and heat conduction. The mass convected into the growing separated flow does work, and also convects kinetic, and internal, energy into this region. Energy transfer out is through heat conduction to the model walls, and the work done in moving the boundaries of the separated flow region. During the unsteady separated flow development, these rates of energy transfer will change as the details of the flowfield adjust.

Thermal changes that occur in the local conditions at the edge of the separated flow region will be both diffused, and convected, through the flowfield. The rate at which these transport mechanisms occur determines whether the instantaneous energy exchanges to, and within, the separated flow during its unsteady development can be considered quasi-steady, or whether the rates at which these vary with time are important. The thermal diffusion process in one-dimension through an initially uniform fluid at rest is characterised by the equation (e.g. see Choudhury 1970),

$$\frac{\partial T}{\partial t} = \frac{k}{\rho\, c_p} \frac{\partial^2 T}{\partial y^2} \qquad (108)$$

which is the same as that for unsteady one-dimensional heat conduction in a solid (see § 7.3.1). A solution of this equation determines the necessary time for the effect of a change in boundary temperature to diffuse to a depth δ, and begin to change the temperature at this location (by 1% of the boundary temperature change),

$$t = \frac{\delta^2}{16 \left\{ \frac{k}{\rho c_p} \right\}} \qquad (109)$$

Eq. (109) has been evaluated for the conditions of the unsteady separated flowfield to determine its characteristic time of thermal diffusion. In calculating this, the maximum height of the separated flow above the plate has been used as a representative length dimension of the separated flow, which is a direction across which convective transport of energy is a minimum. The value of laminar thermal conductivity which occurs at the wall temperature has been used in determining these times. This temperature is less than the average value for the separated flow, and consequently the calculated times of laminar diffusion are an upper limit. At instantaneous dynamic flap angles of 10, 20, and 35 degrees, this characteristic time of thermal diffusion is 6.25 μs, 0.16 ms, and 0.6 ms respectively. The transitional / turbulent effects that occur in the experiments have not been considered in these calculations. These substantially reduce the thermal diffusion times by introducing much larger effective thermal conductivities due to eddy motion.

An evaluation of the characteristic time for thermal convection requires an estimate of the reverse flow velocities, which has not been attempted here. However, within the separated flow region above the plate these will generally be small, and thermal adjustment will occur most rapidly by diffusion. A comparison of the calculated diffusion times with the time for unit proportional changes in the local freestream temperature, and velocity, adjacent to the unsteady separated shear layer occurring in the present tests gives ratios of 3×10^{-6} to 3.8×10^{-3}. This suggests that lag effects associated with the transport of energy across the separated flow will be negligible.

The concept of a separated flow bulk thermal adjustment time has been discussed by Battin (1963) for the example of a wake formed behind a downstream facing step. This is associated with the time necessary for the whole mass of separated flow to heat up to its steady (equilibrium) temperature distribution. The heat transfer to the wall in the separated flow is driven by the difference between the wall temperature and that of the local flow adjacent to the boundary layer. This therefore varies continuously until there is a simultaneous achievement of steady separated flow temperatures, and of the energy transfer rates into and out of this region. The bulk thermal adjustment time is effectively determined by the separated flow mass (i.e.

internal energy), and the temperature differences between its initial, and final, states. For the slender wedge separated flows, the mass of recirculating flow is generally much less than that for a wake. The low levels of heat transfer in laminar wedge separated flows indicate that the separated flow temperatures in this region are not much greater than that at the wall, and do not vary significantly as the scale of the separated flow is increased. These properties of wedge separated flows suggest that any bulk thermal adjustment times will be much less than for the wake type of separated flows, and that if such an effect is present it is only likely to occur at the larger flap angles.

During the growth of the dynamic separation, additional mass is entrained into the separated flow from the shear layer, which contains regions of relatively higher viscous dissipation, and consequently higher temperature, than the bulk of the separated flow. This could potentially increase the wall heat transfer in a dynamic separation compared to the corresponding steady flowfield. The significance of this will depend on the the rate of entrainment of high energy flow compared to the instantaneous mass of separated flow.

In addition to unsteady influences on the separated flow temperature distribution, there may be an effect on the local heat transfer coefficients. For example, if a lag develops in the dynamic separated flow growth, then the pressure gradient along the flap in this region will be greater than that for the steady separation. This increased pressure gradient increases the reverse flow velocities in this region, which will increase the local heat transfer coefficients. Any unsteadiness introduced into the separated flow by its dynamic response may also generally increase the heat transfer coefficients throughout the separated flowfield.

The significance of the dynamic influences described above on the wall heat transfer rates cannot be accurately predicted with simple analytic models. However, the experimental measurements throughout the flap deflection range, both with, and without side plates, (Figs.50 & 51) generally show very close agreement between the heating distributions on the plate for the dynamic, and the steady, separated flows. The dynamic effects in the present experiments therefore have a negligible influence on the wall heat transfer rates in this region. At the highest flap angle of 35 degrees there appears a slight increase in the measured heat transfer gradient along the flap, which would correspond to an increase in the pressure gradient along this surface when a significant lag in the unsteady separated flow growth develops.

18.2 Peak reattachment heat transfer.

The high heat transfer rates that occur in reattachment regions of separated hypersonic flows makes it particularly important to understand any mechanisms in a dynamic response that may increase these levels. In the present experiments, increases in peak reattachment heat transfer of up to 15% have been measured for the dynamic flap conditions compared to those for the corresponding steady separated flows.

During the unsteady separated flow growth, the requirement to entrain mass may cause a reduction in the reattaching shear layer flow rate, and its thickness. A lag in unsteady separation growth would also cause an increase in the effective turning angle at reattachment, due to its reduced shear layer deflection at separation. Both of these dynamic effects might lead to a more severe necking of the boundary layer on the wedge surface downstream of reattachment, which would produce an increase in the peak heating level in this region. An assessment of the significance of these effects has been attempted by applying Holden's (1964) model of laminar peak reattachment heating to both dynamic, and steady, wedge separated flow geometries occurring in the present experiments.

Holden's prediction of peak heating incorporates an extension of Cooke's (1963) analytic model of laminar wedge separation, from which the mass flow rate in the shear layer above the dividing streamline at the beginning of the reattachment process is evaluated. It is assumed that any mass entrained by the shear layer during the reattachment process is negligible, so that this flow rate is then contained in the wedge boundary layer at the end of the reattachment pressure rise. The wedge boundary layer at this location is assumed to have a sine function velocity profile after transformation to the incompressible plane (using equations of the form Eq.70). This is consistent with the form of the incompressible velocity profiles used in Cooke's model for the attached boundary layer, and separated shear layer. The total mass flow rate contained in this boundary layer is then determined by an integration of mass flow rate across its height,

$$\int_0^{\delta} \rho u \, dy = \rho_3 \int_0^{\delta} u \, dY = \rho_3 u_3 \int_0^{\delta} \sin\left(\frac{\pi Y}{2 \delta_3}\right) dY = \frac{2 \rho_3 u_3 \delta_{3(incomp)}}{\pi} \quad (110)$$

The subscript 3 refers to conditions at the end of the reattachment process

(see Fig.58), and δ_3 is the boundary layer thickness at this point after the transformation to incompressible flow. If the mass flow rate above the dividing streamline in the shear layer at the beginning of the reattachment process is G_{reatt}, then for conservation of mass,

$$\frac{2\rho_3 u_3 \delta_{3(incomp)}}{\pi} = G_{reatt} \tag{111}$$

from which δ_3 can be determined. This boundary layer thickness is assumed to grow from a virtual origin as a flat plate laminar boundary layer, with local freestream conditions the same as those that occur at the peak heating location. If the effective length of growth to achieve a thickness δ_3 is x_3, then,

$$\delta_3 = 4.795 \sqrt{\frac{\nu_3 C x_3}{u_3}} \tag{112}$$

From Eqs.(111) & (112),

$$x_3 = \frac{u_3}{\nu_3 C_3} \frac{1}{4.795^2} \left\{ \frac{\pi G_{reatt}}{2 \rho_3 u_3} \right\}^2 \tag{113}$$

The peak heat transfer rate is then calculated using a laminar flat plate reference enthalpy method, with freestream conditions equal to those at the end of the reattachment pressure rise, and a length of development x_3,

$$q_{peak} = \frac{0.332 \, Pr^{*-2/3} \, \rho^* u_3 (h_{aw} - h_{wall})}{\sqrt{Re^*_{x_3}}} \tag{114}$$

The superscript * refers to temperature dependent parameters evaluated at a reference temperature for the flow conditions at this location. Although not explicitly described by Holden as such, this method effectively uses local flat plate similarity to calculate the peak heat transfer rate. Because of the number of simplifying assumptions required to predict wall heat transfer from such a complicated flow structure, the validity of this model can only be

truly substantiated by comparison with experimental measurements. Comparisons by Holden (1966a) of peak heating predictions with this theory, and experimental measurements on fixed wedge geometries in a Mach 10 freestream flow, showed agreement to within 20% for flap angles up to 35 degrees.

This method of predicting laminar peak reattachment heat transfer has been applied to the present experimental conditions for both the dynamic, and fixed, flap separated flow geometries that occur at 35 degrees without side plates, for which there is a lag of 8.3 mm (measured from the heat transfer profiles) in the unsteady separation growth (not corrected for model position effects). The reattaching mass flow rates from the shear layer have been determined using Eq.(96). For the steady separated flow, the limits of integration for this are $Y = 0$, and $Y = \delta_2$. For the dynamic separation, the lower limit is replaced with the height of the reattaching streamline. This streamline has been determined by applying the correlation of reattachment Mach number against reattachment pressure rise that was formulated from the steady separated flow length measurements without the side plates attached (see § 17.2.2). The results of this model predict that a 2.5% increase in peak heat transfer would occur for the dynamically separated flow for the condition of a fully laminar flowfield. This is substantially less than the measured difference of 10% when there are no side plates, and that of 15% with the side plates attached. No consideration of the transitional / turbulent nature of the flow in the reattachment region has been considered in this model. Some of the discrepancy between the predicted, and measured, dynamic effects on peak heating could also be attributed to the experimental measurement errors. However, it is also possible that the dynamic effects described above are not accurately predicted with this simple analytic model.

PART VI

GENERAL DISCUSSION AND CONCLUSIONS.

19. General discussion.

The measurements of the steady separated flows produced in the low freestream Reynolds number tests have been thoroughly examined to determine their flowfield characteristics. These steady separated flows are believed to be of the transitional type. Of the various established criteria applied to the data to check for transition, the most sensitive by far has been the correlation of peak reattachment heat transfer with respect to the undisturbed flat plate value. Although transition does occur, the lengths, and plateau pressures, of these separated flows appear more typical of the fully laminar regime. The liquid crystal thermographs indicate flowfields which are substantially two-dimensional in character, particularly without the side plates attached, although neither side boundary condition is believed to produce separated flows equivalent to those which would occur with an infinite model span. Effects of the hinge line bleed, and the flap trailing edge expansion, on these transitional separations are believed to be only very small. The heat transfer distributions measured at these fixed flap angles form a high quality transitional separated flow data set. This is perhaps a contradiction in that the occurrence of transition would generally be avoided. However, this flow regime may in practice be encountered by hypersonic vehicles, and even though the development of general correlations of transitional data from different tests is extremely unlikely, a knowledge of its effects is important. Particularly apparent from these tests were the extremely high peak heating values that occurred, in excess of those obtained from correlations of fully turbulent interactions.

The considerations required in making the unsteady heat transfer measurements, and the care necessary in properly reducing these, illustrate the substantial increase in difficulty compared to steady, or time averaging, measurement methods. These considerations also emphasise the important factors that should be considered when attempting to make accurate steady heat transfer measurements in very short duration facilities.

The consequence of using different model positions in these experiments for the fixed, and dynamic, flap data sets to avoid the influence of nozzle wave interference is believed to have been substantially corrected for. If there had been sufficient time available this inconsistency would have been removed. The difference in model positions is a clear criticism of this work.

The schlieren flow visualisation shows that at any instant the geometrical form of the dynamic flap separated flow displays the same features

that occur in the steady wedge type. The comparison of the fixed, and dynamic, flap experimental measurements of heat transfer, and schlieren photography, are consistent in illustrating the development of a lag in the unsteady separation growth at high flap angles compared to the quasi-steady separated flow lengths. This lag in the unsteady separation growth increases as the flap angle increases. The magnitude of these lags is affected by the side boundary condition imposed. This has been attributed primarily to the effect of side plates on transition location in the steady separated flows, and not significantly due to a dynamic lateral venting phenomenon. A significant influence of the hinge line bleed on the dynamic response has also been discounted in the present experiments.

There is no consistent evidence from the heat transfer distributions of a significant unsteady separated flow effect on the location, or process, of transition in the shear layer. This is supported by considerations of the variation of the separation point velocity with flap angle, and the relative magnitude of disturbances associated with the unsteady separation. However, a small dynamic effect on transition, with an associated effect on the heat transfer distributions which is within the scatter in these measurements, cannot be totally discounted. This uncertainty illustrates the complexities that can be introduced by the occurrence of transition, and why ideally this flow regime should be avoided in experiments.

It has been concluded that the lag in unsteady separated flow growth is due principally to the finite rate of fundamental flow adjustment mechanisms within the separation, in a steamwise plane perpendicular to the model surface. The comparison of the experimentally measured lags in unsteady separation growth with simple analytic models of its adjustment indicate that both acoustic, and mass entrainment, requirements are important in determining the response of this particular wedge separated flow. The interaction between these distinct mechanisms involves the propagation of pressure disturbances which influence instantaneous mass entrainment rates, and vice-versa, throughout the region. As the scale of the separated flow increases the mass entrainment requirement appears to become more important in determining the rate of growth.

Previous investigators have generally predicted the response, or establishment, of wedge type separated flows with an acoustic model. The present tests appear to contradict the accuracy of this. The discrepancies between the present data, and that obtained by Roberts (1989) for the same model configuration, is almost certainly due to the lack of steady separated

flow data in Robert's experiments with which to form a correct basis for comparison with the dynamic flap separated flows. Holden (1971b) concluded that the establishment time of wedge type separated flows could be estimated with an acoustic model, although the measured times in these experiments were consistently slightly greater than this approximate prediction (by up to 20 %). This acoustic time was based on a communication distance equal to the complete interaction length, and the speed of sound evaluated at the wall temperature. In the present tests, the interaction lengths were difficult to estimate from the schlieren photographs, but at high flap angles these do not appear to be much larger than the lengths of the dividing streamline. To account for the experimentally measured lags at high flap angles in the present tests with only an acoustic model, the interaction lengths assumed would have to be about 4 times larger than the lengths of the dividing streamline! The wedge separated flow establishment time measurements of Holden (1971b) were made at much higher freestream Mach numbers than the present tests, although throughout the Mach number range examined of 12 to 20 the acoustic model provided a good estimate of the establishment time. The freestream Mach number of the present results is much less than the lower limit tested by Holden. At these lower freestream Mach numbers the deflection angle of the separated shear layers is greater, and the amount of separated flow occupied by the shear layer is much less. These effects would tend to increase the mass adjustment times. The conclusions from the present data suggest that it is inappropriate to generalise which adjustment mechanism is important for a particular type of model configuration at all freestream conditions, and for all scales of separated flow.

Within the accuracy of these measurements, there appears to be a free-interaction at separation during the unsteady separated flow development. This conclusion is supported by both measurements obtained from the schlieren flow visualisation, and the form of the heat transfer profiles in the separation region. In general, the criterion that determines whether the interaction about an unsteady separation point remains free is expected to depend on the rate of movement of this location compared to the time necessary to establish the viscous-inviscid free-interaction in this region. The establishment time of the free-interaction will be associated with pressure communication times across the boundary layer, and more significantly, diffusion times for the local adjustment of the boundary layer in this region. The observation in the present tests of a free-interaction during the unsteady separated flow development contradicts the earlier measurements of Wilkinson

(1966) for an oscillating step, and that by Holden (1967) for the establishment of a wedge separated flow, in which it was observed that the plateau pressure reduced slightly as the separation grew. In Holden's experiments the rate of movement of the separation point was close to the speed of sound at the wall. In the present tests, the propagation of the separation point is much less than this, ≈ 7 m/s. The separated flows examined in Wilkinson's experiments were much smaller than those of the present tests, and the oscillation frequencies of the moving step where up to 700 Hz. In these separations, the propagation velocity of the separation point was also higher than that of the present experiments, although substantially less than the local speed of sound.

The present tests show that there are no significant unsteady separated flow heat transfer effects on the plate surface. This is apparent throughout the flap deflection range, both with, and without, the side plates attached. This supports the hypothesis that the bulk thermal adjustment time for these slender wedge type separations is much less than for the base type separated flows, and that the thermal diffusion times across the separated flow are very rapid compared to the rate of this unsteady separation growth.

For flap angles up to 32.5 degrees, there appears no significant dynamic effect on the level of the peak reattachment heat transfer. However, at the highest flap angle of 35 degrees there was a substantial increase in the peak value measured for the dynamic flap both with, and without, the side plates attached, compared to the levels that occurred at the corresponding fixed flap conditions. Although the potential sources of data scatter can account for these differences, the peak levels measured do appear consistent with their respective heat transfer distributions along the flap surface. The modelled unsteady separated flow effects of a reduced shear layer thickness reattaching to the flap surface, caused by the requirement for mass entrainment, together with an increase in the reattachment turning angle due to the lag in growth, only account for a fraction of the measured increases in peak reattachment heat transfer for the dynamic flap at this angle. The analytic model of the reattachment heat transfer process was very simple, and it is possible that the dynamic effects described were not correctly predicted.

The results of this study indicate that separated flows can exist for which the establishment times are not accurately predicted using criteria developed from simple analytic flow models. For the purposes of designing, or checking the feasibility, of proposed fully laminar interaction experiments in short duration facilities, the prediction of separated flow establishment

times using computational fluid dynamics (CFD) appears promising, as in the example of Lees & Lewis (1993). These laminar times also provide an upper limit appropriate for flowfields in which transition may occur. For fully turbulent separated flows the establishment times will be much less than for laminar interactions induced by identical test model configurations. In most cases these times are not expected to be significant. However, when the test flow duration is extremely limited, and / or, the expected separation is large (for example wake separated flow regions), the establishment times are best predicted, when possible, by reference to previous experimental measurements for the same type of model geometry in a similar flow regime. Accurate predictions of these turbulent flowfields using CFD methods are at present unreliable. Within any test, the flow duration should always be sufficiently long for steady measurements to be obtained well within the available test time, and a check of this is the only satisfactory criterion to ensure flowfields have properly established.

There has been no formal attempt in the present work at studying the scale effects of a separation on its dynamic response, although it is clearly apparent that both pressure propagation times, and mass adjustment times, will both increase. The mass transfer adjustment time appears to be particularly sensitive to increases in the separation length when the interaction is fully laminar, as was apparent in the development of the mass entrainment model of the dynamic flap separated flow. For the few scenarios where an unsteady separated flow adjustment could potentially be an important practical consideration for full scale hypersonic vehicles, as possibly in the control of a missile type projectile, an accurate prediction of the significance of this appears to be possible only within the framework of computational fluid dynamics for the fully laminar interaction regime. When the flow is turbulent it is unlikely that these full scale dynamic effects will be important.

20. Recommendations.

In general, the unsteady response of a separated hypersonic flow will be determined by the particular model geometry, freestream flow, and changing boundary condition. The development of criteria from experimental investigations of this, when possible, are unlikely to be generally valid outside the range of flow conditions, and model configurations, tested. The present experiments have highlighted the mechanisms of separated flow response, and discussed possible sources of unsteady effect. These will be most significant for fully laminar interactions, and for the future assessment of the significance of these in any particular example it appears the best potential lies in the use of computational fluid dynamics. Further verification of this numerical method is recommended by comparison of CFD predicted establishment times with high quality experimental data.

21. Conclusions.

(1) The separated flows in these experiments are transitional.

(2) Peak heat transfer levels have been measured in the fixed flap tests which are in excess of those predicted with fully turbulent heating correlations.

(3) The unsteady separated flow induced by the rapidly actuated flap maintains the wedge type geometry, but develops a lag in growth with respect to the steady separations induced at corresponding fixed flap angles.

(4) The lag in unsteady separated flow development occurs both with, and without, side plates attached.

(5) The lag in the unsteady separated flow growth at high flap angles becomes substantially larger than can be attributed to pressure propagation times through this region. This is believed to be due to the requirement for mass entrainment into the growing separated flow.

(6) The largest corrected difference in separated flow lengths between the dynamic, and fixed, flap conditions in the present tests is equivalent to a phase lag with respect to the flap angle of 3.8 degrees.

(7) Within the accuracy of the measurements made, the free-interaction is maintained locally about the unsteady separation point.

(8) There appears no significant unsteady separated flow effect on the transition location, or process, as interpreted from the heat transfer measurements.

(9) Unsteady separated flow effects on the plate heat transfer within the separated flow are negligible.

(10) There is an unsteady separated flow effect apparent at the highest flap angle which increases the peak heat transfer.

(11) There is a local increase in heat transfer towards the flap trailing edge that occurs at high dynamic flap angles.

APPENDICES

APPENDIX 1.

Tables.

Table 1. Interference heating correlations taken from the review of Hung (1973).

$$\frac{h_{Peak}}{h_{undist.}} = \left(\frac{p_3}{p_1}\right)^n \quad \text{(INVISCID PRESSURE RISE)} \qquad \text{or} \qquad \frac{q_{peak}}{q_o} = \left(\frac{p_{Peak}}{p_o}\right)^n \quad \text{(MEASURED PEAK PRESSURE RATIO ACROSS INTERACTION)}$$

AUTHOR (S)	n	PRESSURE TERM
TURBULENT.		
Hung & Barnett	0.80	p_3/p_1
Markarian	0.85	p_3/p_1
Markarian	0.85	p_{Peak}/p_o
Newmann & Burke	0.80	$p_{Peak}/p_{o.}$
Popinski	0.71	p_3/p_1
Haslett et al	0.80	p_{Peak}/p_o
Holden	0.85	$p_{Peak}/p_{o.}$
Sayano	0.80	p_{Peak}/p_o
LAMINAR		
Hung & Barnett	1.13	p_3/p_1
Newmann & Burke	0.80	$p_{Peak}/p_{o.}$
Markarian	1.30	p_3/p_1
Markarian	1.29	p_{Peak}/p_o
Markarian	0.97	p_3/p_1
Haslett et al	0.80	p_{Peak}/p_o
Haslett et al	0.70	p_{Peak}/p_o
Popinski	0.88	p_3/p_1

Table 2. Tunnel operation for the low freestream Reynolds number.

Reservoir (driver) pressure = 3.549×10^6 N/m^2 (absolute)
Compression tube charge pressure = 377.2 kN/m^2 (absolute)
Diaphragm = Melinex, 1.5/1000 inch thick.
Restrictor diameter = 3/8 inch diameter.
Valve delay = 0 s.
Tube temperature settings (pre-compression): 270, 270, 250, 240, 240, 240, 215, 220, 210, 215, 225.

Table 3. Low freestream Reynolds number conditions.

$M = 6.85$
$P_o = 551600$ N/m^2
$T_o = 610$ K
$\rho_o = 3.04$ kg/m^3
$p = 153$ N/m^2
$T = 58.74$ K
$\rho = 0.008764$ kg/m^3
$u = 1070$ m/s
$Re = 2.45 \times 10^6$/m

Table 4. Liquid crystal formulation temperature - colour bandwidths.

	Temperature / °C	
Colour onset.	TCF552 (Plate)	TCS416 (Flap)
Visible	23.4	28.1
Red	23.6	28.5
Green	25.2	32.4
Light blue	27.2	38.7
Clear	41.4	46.3

Table 5. Resistivities of 0.1 μm thick metal films.

Metal	% increase in resistivity above the bulk value.
Palladium	18
Nickel	44
Copper	18
Aluminium	18
Silver	20
Gold	13

APPENDIX 2.

Correction to the measured heat transfer rates for the temperature effects on the pyrex substrate thermal properties.

When there are significant elevations in surface temperature it is necessary to correct heat transfer measurements that have been made with the assumption that the substrate thermal product ρck is constant.

Experimental measurements of the temperature variation of substrate thermophysical properties indicate that this sensitivity is particularly strong for pyrex, being substantially larger than for the other commonly used thin film gauge substrate materials quartz, and MACOR (Hartunian & Varwig 1962; Schultz & Jones 1973; Miller 1981). Comparisons of the measurements of the temperature dependence of the pyrex thermal product from independent experiments show considerable differences, even though most have used essentially the same technique of an electrical pulse calibration (see Schultz & Jones 1973). The data which has been generally incorporated into subsequent models correcting for pyrex substrate ρck variation on the measured heat transfer is that produced by Hartunian & Varwig (1962). Miller (1981) later re-correlated this experimental data with additional specific heat capacity measurements. The results differed little from the original Hartunian & Varwig results, and the heat transfer correction subsequently applied did not incorporate this improved data set. The ρck data produced by Hartunian & Varwig was generated with painted and fired thin film gauges. Because this gauge manufacturing technique may introduce particular modifications to the pyrex substrate bulk thermal properties, the results of these tests are particularly relevant to the present experiments.

Both analytical, and numerical, corrections have been derived to account for the effect of varying substrate thermal properties with temperature on the measured surface heat flux. Hartunian & Varwig (1962) presented an analytical solution, incorporating the assumption that the effects of temperature on the thermal diffusivity could be neglected. This solution provided a correction to the measured surface heat transfer as a function of the surface temperature rise, determined for the boundary conditions of a step in surface heating, and a step in the surface temperature. For the condition of a constant surface heating, the correction is strictly appropriate if the heat transfer had been determined from a single measurement of surface temperature, and application of Eq.(58).

A method of determining the surface heat transfer from a general surface temperature measurement, allowing for temperature dependence of the substrate

thermal product, was developed by Cook (1970). This was a finite difference scheme that incorporated the temperature variations of the substrate thermal properties determined by Hartunian & Varwig (1962). The results obtained by Cook were in excellent agreement with particular exact theoretical solutions for special cases of thermal property variation, thereby verifying the accuracy of the numerical technique. This method was subsequently applied with the independent variation of the substrate thermal properties, and the two boundary conditions of the surface temperature varying in proportion to root time, and with a step in surface temperature rise. The error in heat transfer measurement if constant thermal properties had been assumed for these two boundary conditions was then determined as a function of the surface temperature rise. With a step in surface heat transfer, and with varying substrate thermal properties, the surface temperature rise would not be expected to depart largely from the root time boundary condition. The effects of the ρck variation for this boundary condition that were determined by Cook therefore provide an accurate correction factor for measurements of constant surface heating which have been made with the assumption of constant ρck. The comparison of the correction by Cook with that obtained by Hartunian & Varwig for the condition of a constant surface heat transfer differ significantly. Cook suggested that these differences were due to Hartunian & Varwig not properly accounting for the temperature effect on the thermal diffusivity in their analytical solution. The correction factors predicted by Hartunian & Varwig have also been critisised by Reece (1966), who determined a lower value at a surface temperature rise of 150 degrees, which is coincident with the numerical result of Cook (see Schultz & Jones 1973).
(N.B. the correction curves of Cook for the two boundary conditions are labelled incorrectly in reverse order in the reference Schultz & Jones 1973).

For the condition of approximately constant surface heat transfer, the correction factors determined from Cook's results have been generally used by subsequent investigators (e.g. Miller 1981). Miller (1985) simultaneously measured stagnation point heat transfer with thin film gauges on three different substrate materials of pyrex, quartz, and macor. Surface temperatures up to 570 K were experienced (rise $\approx$ 275 K), and the subsequent maximum corrections for ρck variation were 16 %, 33 %, and 59 %, for MACOR, quartz, and pyrex respectively. Within the test period in the Mach 10 facility, $0.5\ s \leq t \leq 1.4\ s$, the variation in the reduced heat transfer coefficients was less than $\pm$ 2.5 % for the MACOR and quartz substrates, and less than $\pm$ 5 % for the pyrex. Considering the magnitude of the maximum

corrections applied 1.4 s after the flow start, the relatively small variations in the heat transfer coefficients lends credibility to the correction factors for ρck variation determined by Cook (1970) for a pyrex substrate, and later extended to MACOR, and quartz by Miller (1981).

APPENDIX 3.

Frequency limits of an RC analogue line operation.

If a sinusoidal signal of frequency ω is applied to an analogue input, and the output measured across the resistor R_{in} (Fig.13), then the magnitude of the analogue gain when it is operating correctly is obtained from the Laplace solution (Eq.30) as,

$$\frac{V_{out}}{V_{in}} = R_{in}\sqrt{\frac{c'}{r'}}\sqrt{\omega} \qquad \text{with,} \quad |Z_{in}| = \sqrt{\frac{r'}{c'}}\,\frac{1}{\sqrt{\omega}} \qquad \text{(A3.1)}$$

In practice, there will be a lower frequency of operation. Below this, the impedance of the capacitors will swamp that of the resistors, and the input impedance of the analogue will tend to,

$$|Z_{in}| \simeq \frac{1}{\omega\, C_T} \qquad \text{(A3.2)}$$

where C_T is the sum of the capacitors in the analogue line.

Therefore, at the lower frequency limit of the correct analogue operation,

$$\sqrt{\frac{r'}{c'}}\,\frac{1}{\sqrt{\omega}} = \frac{1}{\omega\, C_T} \qquad \text{(A3.3)}$$

If each R-C stage of the analogue line is designed as a T section (Fig.13), and the resistance and capacitance of stage one are R_1 and C_1, then the lower frequency limit of the analogue operation is,

$$\omega_1 = \frac{C_1}{R_1}\,\frac{1}{C_T^{\,2}} \qquad \text{with} \quad \frac{r'}{c'} = \frac{R_1}{C_1} \qquad \text{(A3.4)}$$

At the upper frequency limit of the analogue operation, the low impedance presented by C_1 shunts the rest of the line, so that the input impedance approaches,

$$|Z_{in}| = R_{in} \qquad \text{(A3.5)}$$

For the T section construction, if $R_{in} = \beta\, R_1$, the upper frequency limit of the analogue is given by,

$$\sqrt{\frac{r'}{c'}}\ \frac{1}{\sqrt{\omega}} = R_{in} = \sqrt{\frac{R_1}{C_1}}\ \frac{1}{\sqrt{\omega}} = \beta R_1 \qquad \text{(A3.6)}$$

Hence, the upper frequency of the analogue operation is,

$$\omega_2 = \frac{1}{R_1 C_1}\ \frac{1}{\beta^2} \qquad \text{(A3.7)}$$

Eqs.(A3.4) & (A3.7) define the frequency limits of operation of an analogue line.

APPENDIX 4.

Heat transfer measurement errors.

(A) Absolute value of the heat transfer.

The potential sources of error in the heat transfer measurement that are listed in § 7.6 are considered below, and their contribution to an error band established.

(i) The value of the substrate thermal product $\sqrt{\rho ck}$.

Any error in calibrating this quantity uniformly affects all gauges on the same substrate insert, and its accurate evaluation is therefore less critical when relative measurements are made with the same set of gauges. For the present tests the same heat transfer gauges were used consistently for all the measurements on the plate surface, although different flap gauge inserts were used for the conditions of fixed, and dynamic deflections. However, all the substrates were obtained from the same manufactured batch, and their respective thermal properties were not expected to differ significantly. The accuracy of the calibration of the thermal product was only to within ± 10 %, and this contributes directly to the error in absolute heat transfer measurement.

(ii) Thin film gauge coefficient of resistance α_R

The accuracy of this calibration for each gauge was to within ± 2 %.

(iii) RC analogue transfer function $R_{in}\sqrt{\frac{c'}{r'}}$.

Within the design operating frequency limits of the RC analogue circuits there exists a slight ripple in the transfer function. The amplitude of these is less than ± 1.5 % of the mean values of each analogue transfer function.

(iv) Finite lead resistance.

Ideally the leads supplying the thin film gauge biasing current should have zero resistance. Any finite lead resistance modifies the gauge operating equation (Eq.24) to,

$$V - V_o = V_o \alpha_R (T - T_o) \frac{R_o}{R_o + R_{lead}} \qquad (A4.1)$$

This directly affects the measured heat transfer. To compensate for the effect of the finite lead resistance the RC analogue outputs are corrected by the factor,

$$\frac{R_o + R_{lead}}{R_o} \qquad \text{(A4.2)}$$

Application of this in the present tests required corrections of no more than 2 %.

(v) Power dissipation.

When a thin film gauge is biased with a steady voltage, prior to the heat transfer measurement, it will dissipate power. This will establish some initial temperature distribution through its substrate. The effect of this on the measured heat transfer rate will depend on the biasing voltage, the gauge area, and the magnitude of the imposed surface heat flux. In the present tests, bias voltages of both 0.5 V and 1 V were used for gauges measuring low heat transfer levels on the plate. The effect of this change in the bias voltage was found to be negligible, therefore discounting a significant influence of the gauge power dissipation.

(vi) Gauge erosion.

The occurrence of a flow erosion of the flap thin film gauges in the present experiments was evident from an increase in their resistances accumulated after a large number of tests. This was most apparent for regions of flow reattachment, with associated high heat transfer, occurring with large flap deflections. When gauge erosion exists, this causes an increase in the gauge resistance in addition to the temperature effects, and is therefore a source of error in the heat transfer measurement. Any discrete particle impacts on the gauges were clearly apparent in the present heat transfer signals, corresponding to the occurrence of spikes, and these test data were discarded. In addition, there existed a continual erosion during the test period due to the fine dust contamination of the flow. This is likely to cause a uniform rate of resistance increase throughout the test period.

All the plate, and flap, thin film gauges were recalibrated after testing, and the effects of erosion on the temperature coefficients of resistance were found to be negligible.

For the example of a step in surface heat flux, the rate of gauge

resistance increase due to temperature is inversely proportional to the square root of time, and hence diminishes throughout the test period. Therefore, the influence of erosion effects, which produce a steady rate of resistance change, should be clearly apparent on the measured heat transfer throughout the test period. This effect was theoretically simulated by adding a uniform rate of resistance change to that which would be induced by a step in heat transfer, and inverting the resulting temperature signal with the numerical method of Cooke & Felderman (1966), (see Eq.28). The conditions chosen were the occurrence of the maximum peak heating that was measured in the experiments for the fixed flap angle of 35 degrees, with the properties of the gauge identical to that used in the experiments at this location. The comparison of the imposed surface heat transfer and that which would be measured (Fig.A4.1) clearly illustrates the influence of erosion, which increases the measured heat transfer throughout the run duration.

To check that the experimental measurements did not display significant erosion characteristics of this form, the peak heat transfer signal measured at a flap angle of 35 degrees was reduced to a heat transfer coefficient at each instant of the test period (Fig.A4.2). The turbulent recovery temperatures were calculated from the freestream conditions inferred from the heat transfer measurement at plate gauge number 1 at each instant, and the surface temperature rises were determined from an integration of the flap gauge heat transfer signal. During the central period of the test flow (200 ms to 700 ms after the flow start), during which the flow conditions are reasonably constant, there is no indication of significant erosion effects. Actually, when the signal is presented in the form of a heat transfer coefficient, if erosion effects are significant then these would be even more apparent than for the heat transfer signal, because any erosion increases both the apparent surface temperature rise, and the heat transfer. It has therefore been concluded that erosion effects in the present tests are not significant.

(vii) Lateral heat conduction.

Implicit in the thermal model for heat transfer measurement is that,

$$\frac{\partial^2 T}{\partial y^2} \ll \frac{\partial^2 T}{\partial x^2} \qquad \text{(A4.3)}$$

For the example of a step in surface heat flux, and using a quasi-one-dimensional model of heat conduction, application of the criterion

in Eq.(A4.3) at the surface requires that,

$$\frac{2\,t}{q_s}\,\frac{k}{\rho c}\,\frac{\partial^2 q_s}{\partial y^2} \ll 1 \qquad \text{(A4.4)}$$

If this condition is not satisfied, then a quasi-one-dimensional analysis is not appropriate, and the heat transfer can only be correctly related to the surface temperature rises through a two-dimensional model of the unsteady heat conduction. For the present trailing edge flap model configuration, lateral conduction effects *may* be significant in the peak heating location. Evaluation of the condition in Eq.(A4.4) is not practical because of the lack of spatial resolution of point measurements about the location of peak heating. If lateral conduction is significant, then its effect will be to cause the measured peak heating to be less than the actual value.

Considering the various sources of error described above, these contribute an error band of ± 13.5 % in absolute heat transfer measurement, and for relative comparisons of heat transfer a scatter of ± 3.5 % in each distribution. Additional scatter in the heat transfer measurements is caused by the presence of electrical, and flow, noise on the measured signals. The scatter apparent in the measured flat plate heat transfer distribution is ± 6 % (Fig.32), and this is considered representative of the total scatter due to measurement error, and sources of noise.

(B) Stanton number.

The sources of error in determining the Stanton numbers arise from both measurement errors in the heat transfer, and any incorrect evaluation of the freestream flow conditions. The uncertainty in the freestream conditions can be evaluated using the inverse reference enthalpy prediction of these (§ 11), with a ± 25 % error band applied to the measured heat transfer. This is the maximum discrepancy established in § 11 between the measured heat transfer at the first plate thin film gauge location, and the heat transfer that would be predicted by the simple reference enthalpy method for the correct freestream flow. Combined with the error in absolute heat transfer that exists at each of these limits, the uncertainty in Stanton numbers can then be determined.

When the maximum error of + 25 % exists between the first plate gauge heat transfer measurement, and the reference enthalpy prediction of heat

transfer, then the error in absolute heat transfer measurement at the first plate gauge is + 10 % caused by an incorrect value for the substrate thermal product, and an additional + 6 % for the scatter. The heat transfer measurement error at other gauge locations will be + 10 % due to the error in the substrate thermal product, plus ± 6 % for the scatter.

At the other limit when the error of - 25 % exists between the first plate gauge heat transfer measurement, and the reference enthalpy prediction of heat transfer, then the error in heat transfer measurement at the first plate gauge is then - 10 % for the substrate thermal product, plus - 6 % due to possible scatter. The heat transfer measurement error at other gauge locations will be - 10 % error in the substrate thermal product, and an additional ± 6 % possible scatter.

The examples considered to determine representative errors in Stanton numbers were the measurements at the first plate gauge, and that on the flap where the maximum heat transfer occurred at a deflection angle of 35 degrees. The Stanton numbers at these locations were re-evaluated at both limits of correction of ± 25 % necessary to the measured first plate gauge heat transfer value to infer the correct freestream flow conditions, and with the corresponding corrections to the absolute heat transfer values that accompany these limits as discussed above. From a comparison of these re-evaluated values with the originally determined Stanton numbers, the representative error bands for these Stanton numbers have been established. For the first plate thin film gauge location, the error band for the Stanton number is only - 2 % to + 4 %. These bounds are small because there is a certain cancellation of an error in the absolute heat transfer value, and the consequent error in the evaluated freestream flow properties. i.e. when the measured heat transfer is higher than the true value, the velocity, and stagnation temperature are also overpredicted, and vice-versa. The error band in the Stanton number at the flap gauge location at which the highest heat transfer in these tests occurs is - 15 % to + 28 %. The much larger error band for locations other than the first plate gauge is due to the possibility of scatter being positive for the first plate gauge, and negative for any other gauge, and vice-versa. On the flap there is also a greater sensitivity of the reduced Stanton numbers to changes in the estimated freestream recovery temperature since the surface temperature rises are higher than for the plate.

These error bands for the reduced Stanton numbers are upper limits. It is believed that for the flap heat transfer measurements the actual errors are considerably less than these. This is supported by the low scatter apparent

throughout *all* the heat transfer distributions.

APPENDIX 5.

Effects of weak viscous interaction on flat plate heat transfer.

If the Howarth-Dorodnitsyn transformation is applied to the governing boundary layer equations (e.g. see Cheng et al 1961), then it is apparent that in the hypersonic flow regime local flat plate similarity may be applied, with an error of the order $\epsilon = (\gamma-1)/(\gamma+1)$. This assumes unity Prandtl number, and a linear temperature-viscosity law. The local heat transfer coefficient is then given by (Cheng et al 1961; Cox & Crabtree 1965),

$$M^3St = 0.332\ \bar{\chi}_L \left\{\frac{p}{p_\infty}\right\} \left\{\int_0^x \frac{p}{p_\infty}\,\frac{dx}{L}\right\}^{-1/2} \qquad (A5.1)$$

where,

$$St = \frac{q_s}{\rho_\infty\, u_\infty\, (h_o - h_{wall})}$$

To account for the effects of weak viscous interaction, Vidal et al (1963) substituted the solution for the induced pressure distribution (Eq.61), neglecting the second order term, into Eq.(A5.1), and integrated to x from the leading edge. With the induced pressure distribution described to first order by (see Eq.61),

$$\frac{p}{p_\infty} = 1 + \gamma d_\infty \bar{\chi} \qquad (A5.2)$$

following Vidal et al (1963) with substitution of this into Eq.(A5.1), the heat transfer coefficient in the weak viscous interaction regime is given by,

$$M^3St = \bar{\chi} \left\{\frac{1 + \gamma d_\infty \bar{\chi}}{\sqrt{1 + 2\gamma d_\infty \bar{\chi}}}\right\} \qquad (A5.3)$$

The flat plate zero pressure gradient solution can be obtained directly from Eq.(A5.1),

$$M^3St = 0.332\ \bar{\chi} \qquad (A5.4)$$

APPENDIX 6.

Estimate of the freestream stagnation temperature from the measured run duration.

An average value for the freestream stagnation temperature can be obtained from the equations for the operation of an isentropic light piston tunnel (Jones et al 1973), using measured values of the run duration, and the average stagnation pressure.

$$\sqrt{T_o} = \frac{x_{ad}\, A}{\beta \sqrt{\gamma R}\, \tau_{run}\, A_a} \qquad \text{(A6.1)}$$

with,

$$x_{ad} = x_{ao} \left\{ \frac{P_{charge}}{P_o} \right\}^{1/\gamma}$$

where,

P_{charge} = initial charge pressure
P_o = mean stagnation pressure
x_{ao} = compression tube length.
x_{ad} = length of tube ahead of piston at diaphragm rupture.
τ_{run} = run duration.
β = function of ratio of specific heats, = 0.578
A = compression tube cross-sectional area.
A_a = nozzle throat area.
T_o = mean stagnation temperature.

The average value of the stagnation temperature is less than that during the useful part of the test period, because it includes the effects of the relatively cool gas created by vortex developments in the compression tube. For the present experiments, the stagnation temperature during the central part of the test duration was related to the average value for the whole run by using the heat transfer voltage signal from the first plate thin film gauge, which is ahead of the separation interactions. Assuming that the changes in stagnation temperature have a negligible effect on the heat transfer coefficient, and that the change in wall temperature is very small, then,

$$V_{analogue} \propto (T_{aw} - T_{wall\ initial}) \qquad \text{for } 0 < t \leq t_{run} \qquad \text{(A6.2)}$$

The stagnation temperature is related to the recovery temperature through the laminar recovery factor, and the freestream Mach number. From the ratio of mean voltage signal to the voltage level during the appropriate run period, the ratio of mean to relevant stagnation temperature can be easily determined. This method uses an analogue voltage signal which has not been reduced to the heat transfer value, and is therefore not subject to errors from the gauge and substrate calibrations. Included in this analysis is an assumption of an isentropic compression in the tunnel operation, which neglects both the heat loss by conduction, and the viscous dissipation mechanisms in the tube. Both of these reduce the stagnation pressure below its ideal isentropic value for a given piston location during the compression process. The effect of this assumption results in an estimate for the stagnation temperature which is larger than the actual value.

APPENDIX 7.

Signal power spectrums.

An estimate of the power spectrum of a discretely sampled time signal can be directly obtained with a fast Fourier transform (FFT) algorithm. The FFT is a fast method of solution for the discrete Fourier transform, that can be applied to a signal containing a power of 2 number of points which has been sampled at a constant rate. The power spectrum of this time signal is then proportional to the distribution of the FFT complex coefficients squared and summed at each frequency (Bergland 1969).

The discrete Fourier transform is most closely related to the exponential form of the Fourier series for continuous signals. Its derivation, properties, applications, and practical implementation in the form of the FFT have been extensively discussed in detail by many authors (e.g. Bergland 1969; Champeney 1973; Broch 1981).

If a data file contains N points (which is a power of 2), recorded at a sampling frequency of f Hz, then a power spectrum of the signal can be obtained with the FFT which has a value every f/N Hz between 0 and f/2 Hz. An implication in using the FFT is that the time series is assumed periodic, with this period equal to the time length of the signal to be analysed. The effect of analysing a finite length record then usually introduces artificial discontinuities in the time series where each cycle is implied to end, and another begin. The effect of this is to introduce a spread (or "leakage") in the true power spectrum (Bergland 1969). To reduce the extent of leakage, window functions (weightings) can be applied to the signal before the FFT process. A commonly applied window, that has been used with the signals analysed in these experiments, is the hammimg weighting function,

$$\omega_k = 0.46 \cos\left\{2\pi \frac{k - (N - 1)/2}{N - 1}\right\} + 0.54 \qquad \text{(A7.1)}$$

$$0 \leq k \leq (N-1)$$

This is a combination of rectangular, and cosine bell, functions. The spectral leakage obtained after applying this function to the time series is much less, although sharp peaks in the true power spectrum become less discrete. This window then significantly reduces far spectral leakage from each frequency within the power spectrum, although some near leakage will *always* occur.

APPENDIX 8.

Numerical filtering algorithm.

A simple non-recursive digital filter (finite duration impulse response, FIR) was designed for the processing of the heat transfer signals. This type of filter is a simple averager, with the k^{th} term of the output defined by the operation,

$$y_k = \sum_{i=-m}^{i=m} c_i \, x_{k-i} \qquad \text{(A8.1)}$$

where c_i are the coefficients of the filter. The principal advantages of this type of numerical filter include the relative simplicity of design for a specified frequency response, and the ability to produce a filter which introduces zero phase change throughout the pass band. However, for a satisfactory rate of signal attenuation about the cut-off frequency, this filter type usually requires a large number of coefficients. This may introduce substantial computing times, but for the application in these experiments, where only small sections of each data file were filtered for the period of the flap deployment, this was not considered a problem.

A Fourier design method (e.g. see Williams 1986) was used to determine the appropriate coefficients for a 500 Hz low pass filter. If the specified frequency response is D(f) (Fig.43), then each filter coefficient is determined from the equation (Williams 1986),

$$c_i = \int_{-\pi}^{\pi} D(\omega) \, e^{jwi} \, d\omega \qquad \text{(A8.2)}$$

with $i = -m,.....,+m$

where ω is a circular frequency appropriate to discretely sampled signals,

$$\omega = \frac{2\pi f}{f_{sampling}} \qquad \text{(A8.3)}$$

The design frequency response for this ideal low pass filter operation is defined by D(f) = 1 for $|f| \leq 500$ Hz, and D(f) = 0 for $|f| \geq 500$ Hz.

The Fourier design method requires an infinite number of coefficients to approach the specified frequency response. If a finite number of coefficients are used, derived directly from Eq.(A8.2), this effectively applies a

rectangular window to the infinite series of possible coefficients. The actual filter performance is then a convolution of the design, and the window frequency responses. The rectangular window introduces an unacceptable rippling effect, and a finite transition width between the pass and the stop bands of the low pass filter frequency response. To reduce the rippling, alternative window functions are applied to the calculated coefficients. The width of the transition region for any window reduces with the number of coefficients used in the filter. The window applied for the present filter was a hamming function, defined for a filter with 2m+1 coefficients by,

$$w_i = 2a \cos(\pi i/m) \qquad \text{for} \qquad |i| \leq m \tag{A8.4}$$

The terms a and b have values optimised for the number of filter coefficients (Chebyshev criterion, see Williams 1986). The rippling in the filter response with this window is negligible. However, the width of the transition region is larger than for the rectangular window. For a filter with 2m+1 coefficients the transition width is,

$$\Delta f = \frac{2 f_{sampling}}{m + 1} \tag{A8.5}$$

This is centred about the design cut-off frequency. For the filter applied in the present analysis, the transition width was ± 55 Hz about the 500 Hz cut-off.

The actual frequency response of this digital filter is determined from (Williams 1986),

$$H(\omega) = \sum_{i=-m}^{m} c_i e^{-jwi} \qquad \text{for} \quad -\pi \leq \omega \leq \pi \tag{A8.6}$$

The real, and imaginary components calculated from this equation provide the gain, and phase, as a function of the frequency. The design, and actual, frequency response for the filter used in this present work are illustrated in Fig.43. An example of the application of this filter to a recorded heat transfer signal is illustrated in Fig.A8.1, together with the FFT's of the unfiltered, and filtered, signals. This demonstrates the attenuation of the signal frequency components to zero at about 550 Hz. The phase of the signal in the filter pass band is seen to be unchanged from the original signal content. There is some small phase change in the transition region, but this

is of no significance because the signal amplitude is strongly attenuated here.

APPENDIX 9.

Phase lag correction for the low pass analogue filtered signals.

The RC analogue filter introduces a phase lag to the measured unsteady heat transfer signals, which must be compensated for with a correction. A method for this has been developed, and applied to the numerically filtered signals. The frequency content of these is contained below a level much less than the analogue filter cut-off, and the lag correction is therefore small.

The relationship between the input, and output, signals for the RC analogue filter can be expressed in the form,

$$V_{in} = V_{out} + RC \frac{dV_{out}}{dt} \qquad (A9.1)$$

This filter has the property of superposition, so that Eq.(A9.1) applies to the transmission of the signal content below 500 Hz, with no influence from higher frequency terms in the originally recorded signal. V_{out} then represents the numerically filtered signal, and V_{in} is the required corrected signal. Eq.(A9.1) can be expressed with a simple finite difference scheme,

$$V_{in}(k) = V_{out}(k) + RC \frac{V_{out}(k+1) - V_{out}(k-1)}{2\,\delta t} \qquad (A9.2)$$

for k = 1 to N-1

The presence of the difference term in this expression may amplify noise. However, the high frequency components have been removed by the numerical filtering, and this was not a problem. This difference equation was applied directly to all the numerically filtered signals (e.g. Fig.49).

To check the accuracy of this method, a different technique of correction was developed. The transfer function of the RC analogue filter is,

$$V_{out} = \frac{1}{e^{t/RC}\,RC} \int_0^t V_{in}\, e^{t/RC}\, dt \qquad (A9.3)$$

The numerically filtered signal was applied as the input to this transfer function, and an output determined. Simple linear interpolation was used between sampled points to increase the accuracy of numerically integrating this function. The difference between the input, and output, signals at each

time was taken as an estimate of the lag effect. These were added to the original numerically filtered signal as the correction. Although this method is only approximate, there was excellent agreement between the results of this method and the finite difference scheme.

APPENDIX 10.

Published papers.

(1) Smith, A.J.D., and Baxter, D.R.J., 1989, "Liquid Crystal Thermography for Aerodynamic Heating Measurements in Short Duration Hypersonic Facilities," In: Proc. of the Int. Congress on Instrumentation in Aerospace Simulation Facilities, Sept., pp.104-112.

(2) Smith, A.J.D., and East, R.A., 1991, "The Dynamic Response of Separated Hypersonic Flows," In: Aerothermodynamics for Space Vehicles, Proc. of the First European Symp., ESTEC, Noordwijk, The Netherlands, May 28-30.

LIQUID CRYSTAL THERMOGRAPHY FOR AERODYNAMIC HEATING MEASUREMENTS IN SHORT DURATION HYPERSONIC FACILITIES

A.J.D. Smith and D.R.J. Baxter

Department of Aeronautics & Astronautics
Southampton University
Hants SO9 5NH
United Kingdom

ABSTRACT

A method has been developed which applies liquid crystal thermography to the measurement of surface heat flux in short duration hypersonic facilities. Flat plate thermographs are compared with Eckert's prediction of surface heat flux, to provide a calibration which replaces the liquid crystal static colour calibration. This allows measurement of high surface heat flux, avoiding sources of error associated with the large temperature gradient through the liquid crystal layer, and its response time. In conjunction with this, a multi-substrate model construction has been used, which allows measurement of surface heat flux on complex configurations. The technique has been successfully applied over a wide range of model scale, and test time.

NOMENCLATURE

A	=	$\frac{1-\sigma}{1+\sigma}$
c	=	Specific Heat Capacity
$erfc$	=	Complementary Error Function
k	=	Thermal Conductivity
Q	=	Constant Heat Transfer Rate
T	=	Temperature Rise
t	=	Time
α	=	Thermal Diffusivity (= $k/\rho c$)
σ	=	$\left[\frac{\rho_2 c_2 k_2}{\rho_1 c_1 k_1}\right]^{\frac{1}{2}}$
ρ	=	Density

Subscripts

1	=	Insulating Top Layer
2	=	Second Layer
s	=	Surface

1. INTRODUCTION

The measurement of surface heat transfer in short

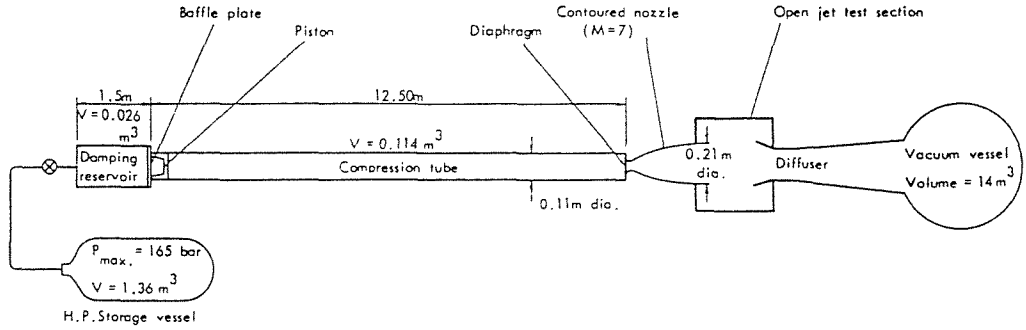

Fig. 1 Schematic of the Isentropic Light Piston Tunnel.

duration hypersonic facilities is often limited with respect to model complexity. Although the established methods are capable of measuring high surface heat fluxes within the short run duration, they are difficult to apply to complex shapes, and lack high spatial resolution. These limitations are exaggerated by the severe constraints on model size that often exist in these facilities.

The liquid crystal technique offers an alternative approach, capable of providing high resolution thermographs on complex configurations. The application of liquid crystals for flow visualisation in these facilities is not a new concept [1]. The extension of this technique for quantitative measurement of high surface heat flux presents a number of problems. The development of such a technique is described in this paper.

Two intermittent hypersonic wind tunnels have been used. Primary experiments were performed in a hypersonic gun tunnel at M = 8.4, with a run duration of 20 ms. This provides a test of the technique, with severe restrictions on model size. Experiments were repeated on a larger scale in the Isentropic Light Piston Tunnel (ILPT). This facility provides an open jet test section with a nozzle exit diameter of 0.21 m, and a flow Mach number of M = 6.85 for flow durations of typically 0.5 s. In both of these, uniform flow conditions exist, so that the model is subjected to a step in heat flux distribution.

2. DEVELOPMENT OF THE LIQUID CRYSTAL TECHNIQUE FOR AERODYNAMIC HEATING MEASUREMENTS

The development of the liquid crystal technique as a tool for aerodynamic testing has occured over the last twenty years. Such tests have attempted to employ the shear sensitive, or temperature sensitive aspect of certain liquid crystal structures [2,3]. This sensitivity is observed as a change in the spectral composition of reflected light, when the liquid crystal is deposited as a thin film on a surface.

With the introduction of liquid crystal microencapsulation, formulations are available that respond only to changes in temperature. It is thus possible to obtain a complete picture of the thermal field of a surface in a given flow, revealing such phenomena as separation, vortex development, and transition, each characterised by its local temperature field.

The development of techniques applying liquid crystals for quantitative measurements have been successful for low to moderate values of heat flux (< 1000 W/m^2) [4]. These techniques have generally used the liquid crystal layer as a surface thermometer applied to a semi-infinite model substrate. The semi-infinite depth is a depth below the model surface at which the heat flux is only a very small fraction of the surface value. This depth increases with time for a step in surface heat flux, and at any instant is a function of the thermal properties of the substrate. Its value is calculated as the depth at which the heat flux is only 1% of the surface value, at the instant the results are recorded. The semi-infinite depth is a practical representation of a theoretical model which assumes an infinite depth of substrate [5]. If uniform flow conditions can be assumed, then a single measurement of surface temperature rise after a measured time will enable evaluation of the surface heat flux. An accurate knowledge of the substrate thermal properties is required in this calculation. This type of technique directly applies liquid crystal measurements. Consideration must therefore be given to the accuracy of surface temperature measurement, and the response time of the liquid crystal layer.

The thermal properties of a liquid crystal layer make it an insulator relative to the substrate upon which it is applied. A numerical or analytical solution of the unsteady heat conduction through this model reveals that a temperature gradient exists through the liquid crystal layer. This gradient is proportional to the surface heat flux. Where direct liquid crystal measurements have been successfully used, the error that results from neglecting the effect of this gradient, and in addition the response time, has been small. However, when this is extended to conditions typical of a hypersonic wind tunnel, this gradient becomes very large. Under these conditions a static calibration of liquid crystal colour against uniform temperature is inappropriate. Thus, to infer model surface temperature from the observed thermograph, and then evaluate

surface heat flux directly is liable to inaccuracy.

The response time of a liquid crystal surface layer has two components. There is a conduction lag through the liquid crystal layer, and then, in addition, any lag in response associated with the liquid crystal structure. The conduction lag can be estimated by applying the theory for unsteady heat conduction through a two substrate model. Several experiments have attempted to measure these two components of response time [6,7]. These results indicate values of a few milliseconds for the conditions of the experiments described in this paper. This has been verified in previous experiments at Southampton University made in the ILPT [8]. Flow visualisation has also been achieved in the Gun Tunnel within the test time of 20 ms [9].

The significance of the response time will depend on the run duration of the facility, and hence the time at which measurements are recorded. In short duration facilities, the response time may be a significant percentage of the available run duration. Under these circumstances a method applying direct liquid crystal measurements must allow for the response time in the subsequent analysis.

3. EXPERIMENTAL TECHNIQUE

An accurate evaluation of the effect of a large temperature gradient on liquid crystal reflection, and the magnitude of the response time is questionable. To avoid these as sources of error an alternative method has been developed.

This method first obtains liquid crystal surface thermographs on a flat plate. These are produced for several flow conditions, but at the same instant during each run. The colour distributions observed are compared with Eckert's reference enthalpy prediction of surface heat flux for the well defined laminar boundary layer.

The flat plate and the test model have the same substrate construction. This ensures that at any instant they have the same temperature profile through the liquid crystal layer, and hence observed colour, when subjected to the same surface heat flux, starting from the same initial temperature.

The test model surface thermographs are obtained at the same point during each run as were the flat plate calibration tests, at the required flow conditions. If the test model and flat plate initial temperature has been a constant throughout all the tests, then direct comparison of colour on the test model with the flat plate, and Eckert's prediction, gives the surface heat flux distribution. This method avoids application of the liquid crystal static colour calibration. The comparison enables evaluation of surface heat flux in regions of different colour shade, as well as colour change. Direct application of this method for the Gun Tunnel experiments was successful [9]. However, with the larger models in the ILPT, control of the model initial temperature proved difficult, necessitating a modification to the above procedure.

For this modification, the colour is replaced by temperature rise in the calibration against laminar boundary layer heat transfer. On the flat plate thermographs the temperature rise is calculated at the junctions between observed colour bands. This is determined from the measured model initial temperature, and application of the static colour calibration to the observed colour change. From the comparison with Eckert's reference enthalpy method at these locations, a new calibration is formed of temperature rise against surface heat flux. When the surface thermographs are obtained for the test model, the surface temperature rise is calculated along colour change contours in the same way. By applying the flat plate calibration, surface heat flux contours are obtained.

For the same apparent colour change to exist on models which were at different initial temperatures, the net temperature rise through the liquid crystal layer differs, and hence, so does the surface heat flux. The temperature distribution through the liquid crystal layer is a function of the surface heat flux. Hence, the static colour calibration is applied to different distributions of temperature through the liquid crystal layer, but which have the same apparent colour change. The significance of this is examined in section 4. Although some errors are introduced by this procedure, the sources of error associated with direct liquid crystal measurements, such as the response time, and accurate knowledge of substrate thermal properties have still been avoided.

An encapsulated chiral nematic liquid crystal has been used for these experiments. This is contained in a PVA binder, which, after dilution with water, is sprayed on model surfaces. Optimum colour intensity is obtained with a layer about 10 microns thick.

The instant of recording the surface thermograph is controlled by triggering a flash illumination in a darkened test section room. A single photograph is obtained for each run.

3.1 Model Construction

Models that are manufactured for surface thermography are usually machined from insulating substrates, which provide the necessary surface temperature rise within a short period. This type of substrate may place a restriction on model complexity, associated with the difficulties of manufacture, or the lack of strength or rigidity.

The optical properties of the liquid crystal layer produce a reflected distribution of light about a particular frequency. The magnitude of the peak frequency is 50% of the same frequency of the incident light. This distribution gives a total reflected intensity of about 5% of the total incident light [10]. It is necessary to prevent reflection from the model surface, which would swamp the liquid crystal display. This is achieved by applying the liquid crystal layer to a blackened substrate surface.

A multi-substrate model construction has been developed for these experiments, which overcomes some of the usual constraints. This is a two substrate model, produced by spraying a black paint layer on a metal surface. By reference to the theory for unsteady heat conduction through such a model [11], it is seen that the surface temperature history has two distinct regions. Initially the surface temperature rise is rapid, and is characterised by the insulating properties of the paint layer. This is followed by a much reduced rate of surface temperature rise, which is a characteristic of the metal, but with an initial offset caused by the paint. The division between these occurs in the region of a switch point, which physically relates to the time at which the heat pulse first penetrates the metal substrate.

For a step in surface heat transfer, the surface temperature rise is given by,

$$T_s(t) = \frac{2Q_s}{\sqrt{(\rho_1 c_1 k_1)}} \left[(t/\pi)^{\frac{1}{2}} + 2 \sum_{n=1}^{n=\infty} A^n \left\{ (t/\pi)^{\frac{1}{2}} \exp\left[\frac{-n^2 a^2}{\alpha_1 t} \right] - \frac{na}{\sqrt{\alpha_1}} \operatorname{erfc}\left(na/(\alpha_1 t)^{\frac{1}{2}}\right) \right\} \right]$$

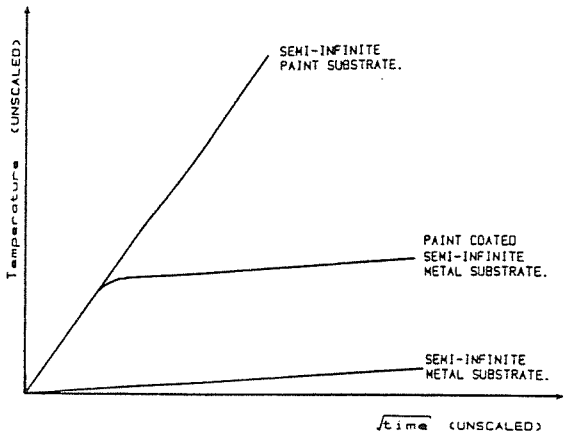

Fig. 2 Surface Temperature Rise for Substrates Subjected to a Step in Surface Heat Flux.

It is the initial rapid surface temperature rise caused by the insulating properties of the paint layer that makes this model suitable for liquid crystal thermography.

The application of a liquid crystal layer to this surface actually produces a three substrate model. This is an additional insulating layer, and extends the initial rapid rise in surface temperature. The thermal properties of the liquid crystal formulation, and the paint, are very similar.

The calibration plate, and the test model were machined from stainless steel. They both have a semi-infinite metal base, and a uniform thin black paint layer applied to the surface. For the same surface heat flux they then produce the same temperature rise.

3.2 Flat Plate Calibration Tests

The calibration model should provide a well defined surface thermograph, against which an established

method of surface heat transfer prediction can be compared.

The colours reflected by the liquid crystal layer are sensitive to the viewing angle if this exceeds about 30 degrees from the normal. This prevents application of a sphere calibration model, which satisfies the other requirements, and which has been successfully applied for this purpose with temperature sensitive paints [12]. An alternative model is the flat plate with sharp leading edge, which has been used in this work.

In a region extending from the plate leading edge the metal depth is less than the semi-infinite requirement. As the distance from the leading edge is increased, this requirement is eventually satisfied. Any calibration results obtained too near the leading edge will have excessive surface temperature rise, and will be a source of error. The leading edge chamfer contains an angle of 30 degrees. This gives the maximum increase in thickness with distance from the leading edge, without producing a detached leading edge shock.

To determine the distance from the leading edge in excess of which calibration results may be recorded without correction, a numerical scheme has been written. This uses an alternating direction implicit (ADI) method. The unsteady two dimensional heat conduction is modelled through the two substrate painted wedge section that exists from the plate leading edge. The effect of the heat transfer to the plate underside is included. The results from this were compared with the ideal one dimensional solution for a painted semi-infinite metal substrate.

As the distance from the leading edge increases, the discrepancy between these reduces. This comparison included both surface temperature rise, and temperature distributions through the paint layer. Calibration results were recorded from the flat plate thermograph only at distances from the leading edge in excess of where these agree.

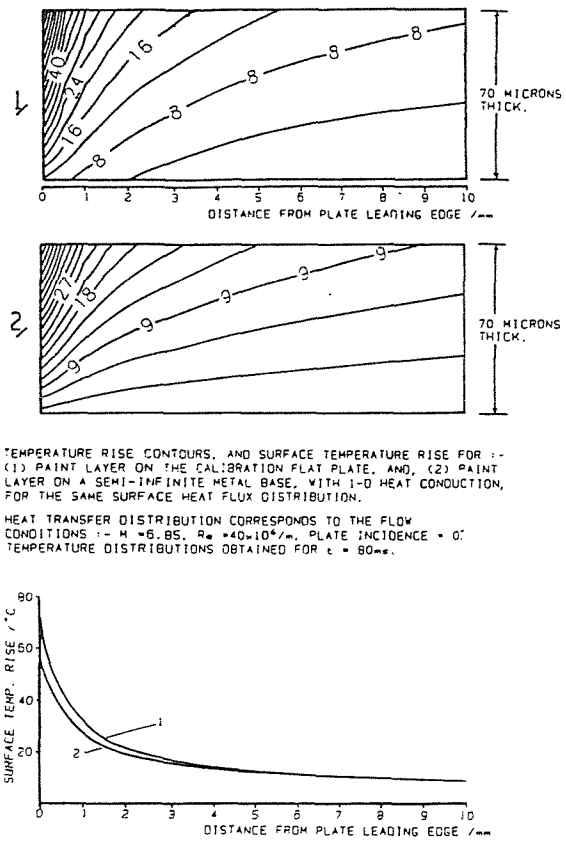

TEMPERATURE RISE CONTOURS, AND SURFACE TEMPERATURE RISE FOR :- (1) PAINT LAYER ON THE CALIBRATION FLAT PLATE, AND, (2) PAINT LAYER ON A SEMI-INFINITE METAL BASE, WITH 1-D HEAT CONDUCTION, FOR THE SAME SURFACE HEAT FLUX DISTRIBUTION.

HEAT TRANSFER DISTRIBUTION CORRESPONDS TO THE FLOW CONDITIONS :- M =6.85, R_e =40×10⁶/m, PLATE INCIDENCE = 0°. TEMPERATURE DISTRIBUTIONS OBTAINED FOR t = 80ms.

Fig. 3 Comparison of the Temperature Distribution through the Paint Layer on the Calibration Flat Plate, with the One-Dimensional Semi-Infinite Solution.

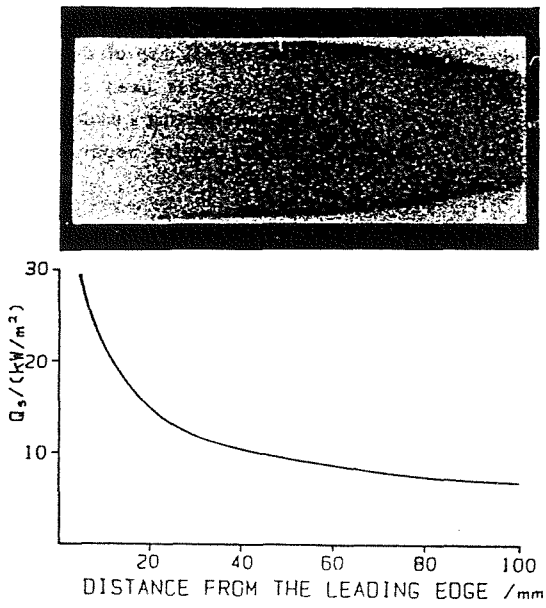

Fig. 4 Comparison of a Flat Plate Thermograph with Eckert's Prediction of Surface Heat Flux.

The direct calibration of colour with surface heat flux is sufficient for the case in which the initial temperatures of the calibration model and the test model are identical.

For the experiments in the ILPT a calibration of indicated surface temperature rise against surface heat flux has been produced from a number of flat plate thermographs. Flow conditions over the plate were varied with changes in freestream Reynolds number, and plate incidence.

The comparison with Eckert's reference enthalpy method is only valid ahead of transition. Previous experimental work at Southampton University has compared liquid crystal thermography with thin film gauge measurements on a flat plate [8]. This has demonstrated that the surface thermographs can precisely indicate transition, evident by a local increase in surface temperature. If transition was evident on the calibration plate thermographs, then results were only recorded upstream of its location.

A comparison of the thin film gauge measurements with Eckert's reference enthalpy method showed excellent agreement.

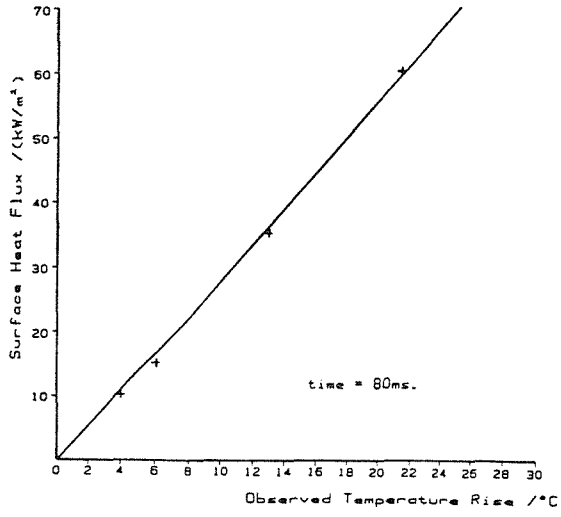

Fig. 5 Calibration of the Observed Liquid Crystal Temperature Rise Against Surface Heat Flux.

3.3 Heat Transfer Measurements

The thermographs obtained on the test models are reduced to surface heat flux regions by applying the appropriate calibration.

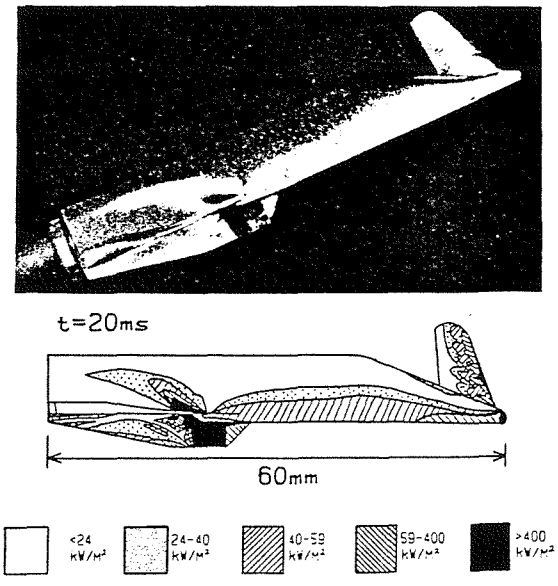

Fig. 6 Liquid Crystal Thermograph, and Surface Heat Flux Contours for a Model in the Gun Tunnel (taken from [9]).

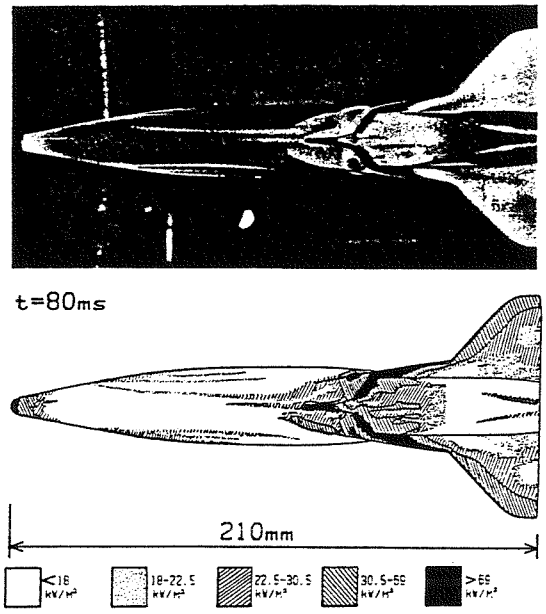

Fig. 7 Liquid Crystal Thermograph, and Surface Heat Flux Contours for a Model in the ILPT.

The test model results are valid within a viewing angle of up to 30 degrees deviation form the normal, and provided there is sufficient depth of metal. The latter may only be a problem in regions of thin wings etc. This problem can be avoided by applying a thicker paint layer, and, or, obtaining flow visualisation for the flat plate and test model earlier in the tests. Both of these reduce the semi-infinite depth of metal required.

It is possible that the time of thermograph recording may be before the paint-metal switch point. In this case there is no thermal conduction in the metal, and its only purpose is to support the paint. For the tests in the Gun Tunnel, surface thermographs were obtained at t = 20 ms. This is at the end of the run duration, but before the paint-metal switch point. The paint is then effectively a single semi-infinite substrate, and flow visualisation is valid over the entire test model surface. Consideration must still be given to the validity of flat plate calibration results in the region of the leading edge, where there will be a heat transfer distribution to the exposed metal underside. The numerical modelling has been applied to assess regions of inaccuracy for all calibration tests.

Even within the severe constraints of model size in the Gun Tunnel, a well defined thermal map of the model surface heat flux distribution has been obtained. Alternative techniques for instrumenting a model of this scale within 20 ms would require sophisticated construction, and instrumentation.

In any one test, the number of heat transfer contours is limited to regions within the liquid crystal colour temperature bandwidth. Additional heat transfer contours can be obtained by repeating the tests at a different initial temperature, and, or, using a liquid crystal formulation with different colour bandwidths. It is thus possible to map the complete surface of a model.

A source of error in these heat transfer measurements is associated with any discrepancies that might exist between the flat plate, and the test model construction. The sensitivity to paint thickness and metal depth has been examined with a one dimensional numerical model of the unsteady heat conduction. This shows that the surface temperature rise, and temperature distribution through the liquid crystal layer is relatively insensitive to metal depth. Even when this is substantially less than the ideal semi-infinite value, the errors in assuming the surface temperature rise is that with a semi-infinite base may be small. For a given depth, the magnitude of this error will depend on the surface heat flux, and the semi-infinite value. The surface temperature rise is directly proportional to the paint thickness. This makes it important that the flat plate and the test model have only a small difference in paint thickness.

The other source of error is a subjective one associated with distinguishing between the different colour bands.

4. TEMPERATURE DISTRIBUTION THROUGH THE LIQUID CRYSTAL LAYER

The temperature distribution through the liquid crystal layer is a function of the model construction, the time for which the surface heat flux has been applied, and its absolute value. In all cases, if the surface heat flux is high, then a large temperature gradient will exist through part, or all of the liquid crystal layer.

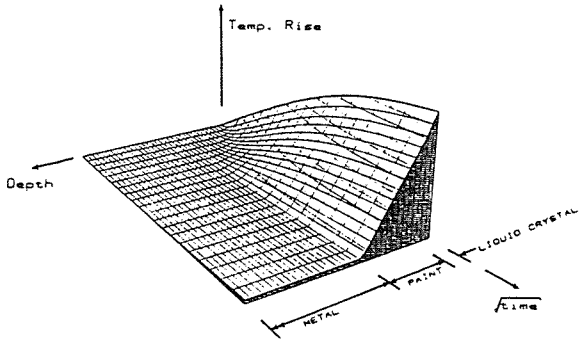

Fig. 8 Temperature Distribution through the Three Substrate Model of Liquid Crystal, Paint, and Metal Base.

Thermochromic liquid crystal formulations generally have a narrow red temperature bandwidth, with broader green, and blue regions. When a large temperature gradient exists through the layer it is only possible for a fraction of this to be in the red bandwidth. The other regions contain green, or are outside the colour bandwidth. This is observed experimentally in situations of high heat transfer rate, with the surface thermographs predominantly green, and blue, with only small, less intense regions of red.

To assess the significance of different initial model temperatures for the experiments in the ILPT, the unsteady heat conduction through the three substrate model of liquid crystal, paint, and metal has been modelled numerically. For these experiments, the thermographs were recorded 80 ms after the flow established. At this time the results of the numerical scheme indicate a uniform temperature gradient throughout the liquid crystal layer. This agrees with the analytical solution in the limit, as the time becomes large,

$$\frac{\partial T}{\partial x} = \frac{Q_s}{k_1}$$

Any error that may be incurred in the experimental method will be associated with the application of the static colour calibration for different temperature distributions through the liquid crystal layer, that produce the same observed colour change. In an attempt to quantify this error, the static colour calibration has been applied at each point through the layer, for the temperature distributions obtained from the numerical procedure. It is assumed that the observed reflected colour is that which occupies the largest fraction of the layer thickness. At a particular initial temperature, this procedure is applied to obtain values of surface heat flux that produce changes in the observed colour. Then, as in the experimental method, the static colour calibration is applied to the observed colour change, to obtain a curve of surface heat flux against temperature rise. This is repeated for a range of initial temperatures.

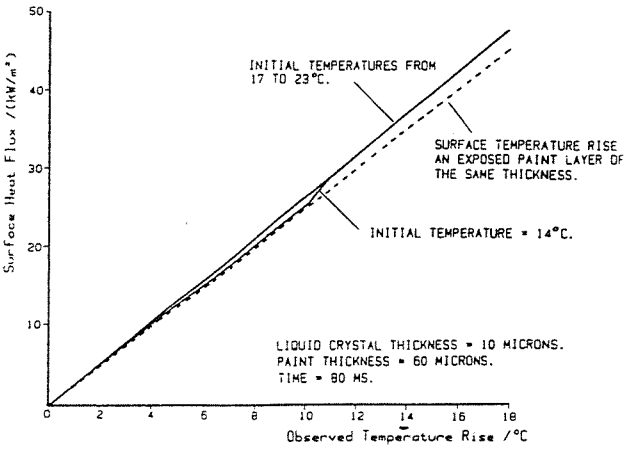

Fig. 9 Predicted Effect of Initial Temperature on the Calibration of Observed Liquid Crystal Temperature Rise against Surface Heat Flux.

Any error in the experiment would be observed as a difference between the above curves, over the range of relevant initial temperature. The results from this analysis indicate a consistent calibration curve within the initial temperature range of 17 to 23 degrees. Outside this range, as indicated by the example for 14 degrees, a significant error may be incurred in applying the static colour calibration to some observed colour changes. The calibration curves obtained are dependent on the temperature bandwidth of each liquid crystal colour. These will determine the range of colours through the layer for a particular initial temperature and surface heat flux. For the range of initial temperatures that provide a consistent calibration

curve, and hence no error, only two colours exist through the layer at an observed colour change. This change then corresponds to an even split of these colours in the layer. When the initial temperature is low, then a higher surface heat flux is required to produce the net temperature rise for the same observed colour change. A larger variation in temperature, and hence colour is produced through the liquid crystal layer. All experiments in the ILPT combined results from different initial temperatures within the range 17 to 23 degrees.

This analysis represents an approximation of the physical behaviour of the liquid crystal layer. A comparision between different initial conditions is expected to give a reasonable assessment, rather than an absolute result.

5. CONCLUSIONS

Thermochromic liquid crystals have been successfully applied to the measurement of surface heat flux in short duration hypersonic facilities. The technique developed has application over a wide range of model scale, and test times, as demonstrated in the two hypersonic facilities used for these experiments. High values of surface heat flux can be measured without difficulty.

The use of a multi-substrate model construction allows application of this thermographic technique to complex model configurations. In addition, many existing metal models can be easily modified for thermographic heat transfer measurement.

REFERENCES

[1] H. Schöler, A. Banerji, "Visualisation of Boundary Layer Transition on a Cone with Liquid Crystals.", DFVLR Internal report, July 1984.

[2] E.J. Klein, A.P. Margozzi, "Exploratory Investigation on the Measurement of Skin Friction by means of Liquid Crystals.", NASA TM X-1774, 1969.

[3] C. den Ouden, C.J. Hoogendoorn, "Local Convective Heat Transfer Coefficients for Jets Impinging on a Plate: Experiments using a Liquid Crystal Technique.", Proceedings of the Fifth International Heat Transfer Conference, Vol. V, AIChE. New York, pp293-297, 1974.

[4] P.T. Ireland, T.V. Jones, "Detailed Measurements of Heat Transfer on and around a Pedestal in Fully Developed Passage Flow.", Proceedings of the Eigth International Heat Transfer Conference, Vol. 3, pp975-980, 1986.

[5] D.L. Schultz, T.V. Jones, "Heat Transfer in Short Duration Hypersonic Facilities." AGARDograph No. 165, 1973.

[6] R. Parker, "Transient Surface Temperature Response of Liquid Crystal Films.", Lawrence Livermore Laboratory, Rept. UCLR-73583, 1971.

[7] P.T. Ireland, T.V. Jones, "The Response Time of a Surface Thermometer Employing Encapsulated Thermochromic Liquid Crystals.", J.Phys.E:Sci Instrum, Vol. 20, 1987.

[8] A.J.D. Smith, "The Response Time of the Liquid Crystal Flow Visualisation Technique and its Application to Heat Transfer Analysis.", B.Eng. Project Report, Dept. of Aeronautics & Astronautics, Southampton Univeristy, 1987.

[9] M.F. Westby, "A Study of the Hypersonic Aerodynamics of a Hotol-Like Re-Entry Vehicle.", B.Eng. Project Report, Dept. of Aeronautics & Astronautics, Southampton University, 1988.

[10] BDH Ltd., "*LICRITHERM Thermochromic* Liquid Crystals", 1988.

[11] J.E. Doorly, M.L.G. Oldfield, "The Theory of Advanced Multi-Layered Thin Film Heat Transfer Gauges.", Int. J. Heat Mass Transfer, Vol. 30, No. 6., pp1159-1168, 1987.

[12] R.J. Sartell, G.C. Lorenz, "A New Technique for Measurement of Aerodynamic Heating Distributions on Models of Hypersonic Vehicles.", Proc. 1964 Heat Transfer and Fluid Mech. Institute, Stanford University Press, p.130, 1964.

THE DYNAMIC RESPONSE OF SEPARATED HYPERSONIC FLOWS

A.J.D. Smith and R.A. East

Dept. of Aeronautics & Astronautics
University of Southampton, England

ABSTRACT

The dynamic response of a separated hypersonic flow to a rapidly actuated trailing edge flap has been investigated. Experimental measurements have shown a lag in the rate of separation growth, which has been attributed, principally, to the requirement for mass entrainment. Measurements of heat transfer for the evolving dynamic separation have an increased level in the reattachment region at high flap angles, in excess of that for equivalent steady separated flows. Simple analytic models have been developed which support the proposed mechanisms of unsteady separated flow adjustment.

Keywords: hypersonic, separated flow, unsteady, two-dimensional

NOMENCLATURE

a	-	local speed of sound
G	-	mass flow rate
L	-	length
m	-	mass
M	-	Mach number
P	-	pressure
q	-	surface heat flux
Re	-	Reynolds number
t	-	time
T	-	temperature
u	-	velocity
V	-	volume
ρ	-	density
θ	-	angle
ϕ	-	phase lag

Subscripts

d	-	dead air
f	-	flap
s	-	separation
∞	-	freestream
ds	-	dividing streamline

1. INTRODUCTION

A hypersonic vehicle is subject to many shock induced separations. The modifications in pressure and heat transfer that result from these have serious implications on design, and performance.

There has been considerable work in the study of separated high Mach number flows induced by fixed geometries, both experimentally, and theoretically. The present investigation has studied the unsteady response of such a separation to a rapidly actuated flap. A study of this phenomenon is relevant to further understanding basic separated flow mechanisms, and in setting criteria for experimenters that would apply 'dynamic' testing as a means of generating multiple points of data with quasi-steady flow. In the context of the application of this work to full scale configurations, consideration must be given to how the flow dynamic response scales from these model tests.

The accumulated research by previous investigators which is relevant to this subject is scarce. Studies in the low supersonic flow regime by Ihrig & Korst (Ref. 1) investigated the response of a turbulent base separation to rapidly changing freestream conditions. They concluded that the time required to entrain mass into a growing separation was the dominant factor that restricted the rate of separation growth. Experimental measurements by Wilkinson (Ref. 2) of the separated flow generated ahead of a rapidly oscillating forward facing step in hypersonic flow also identified mass entrainment as the principal restriction in determining the rate of separation response. However, measurements of the establishment times of laminar separated flows induced by wedges in hypersonic flow indicate that the mass entrainment time becomes less dominant for these slender separations, and that acoustic

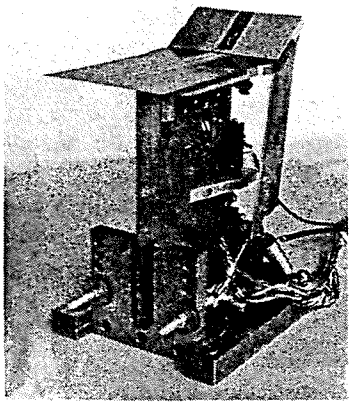

Fig. 1 Dynamic/Fixed flap model.

communication times must be considered (Ref. 3). This has been supported by the recent work of Roberts (Ref. 4). In the study of the dynamic behaviour of separations, heat transfer experiments have been the most neglected. A numerical simulation by Kazakov (Ref. 5) of the separation induced by a rapidly deflected flap in supersonic flow predicted values of reattachment heat transfer in excess of the values obtained for steady separations. Reattachment heat transfer can be very high in the hypersonic regime, so that any mechanism that might further increase this must be seriously considered.

For the experiments described in this paper, a sharp leading edge flat plate with a trailing edge flap was used to simulate a nominally 2-D control surface, in a Mach 6.85 freestream flow. The principal investigation was through heat transfer measurements on the plate and flap centre line. Schlieren flow visualisation has been obtained of the separated flow structures. Dynamic flap measurements have been compared with those obtained at corresponding fixed flap angles.

An analytical model of the separation dynamic response has been developed, and compared with the experimental measurements.

2. EXPERIMENTAL PROGRAM

2.1 Wind Tunnel

The experiments were performed in the Isentropic Light Piston Hypersonic Tunnel at the University of Southampton. This is an intermittent facility which provides an open jet test section of diameter 0.21 m in the nozzle exit plane, at a flow Mach number of 6.85. The principal advantages of this wind tunnel include comparatively long run durations, up to 0.9s, and extremely uniform flow. This high flow quality is especially important for these experiments where a separated flow response is required only to a changing model geometry. These flow conditions cannot generally be achieved for sufficient duration in hypersonic test facilities, and this is perhaps one reason why such experiments have until now been very limited.

2.2 Model

A single model was designed for both the dynamic, and fixed flap tests (Fig. 1). The flat plate has a chord of 156 mm, and a span of 100 mm, fitted with a full span trailing edge flap of chord 51 mm. For the dynamic tests the flap was deflected from an angle of 0 to 35 degrees within 20 ms. The flap angle is measured with a potentiometer, which provides an accuracy to within 0.2 degrees. The facility to add side plates was included. A single set was designed, which was able to contain the largest separated flow.

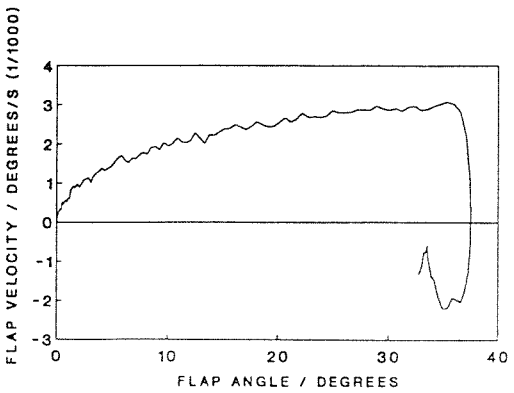

Fig. 2 Dynamic flap motion.

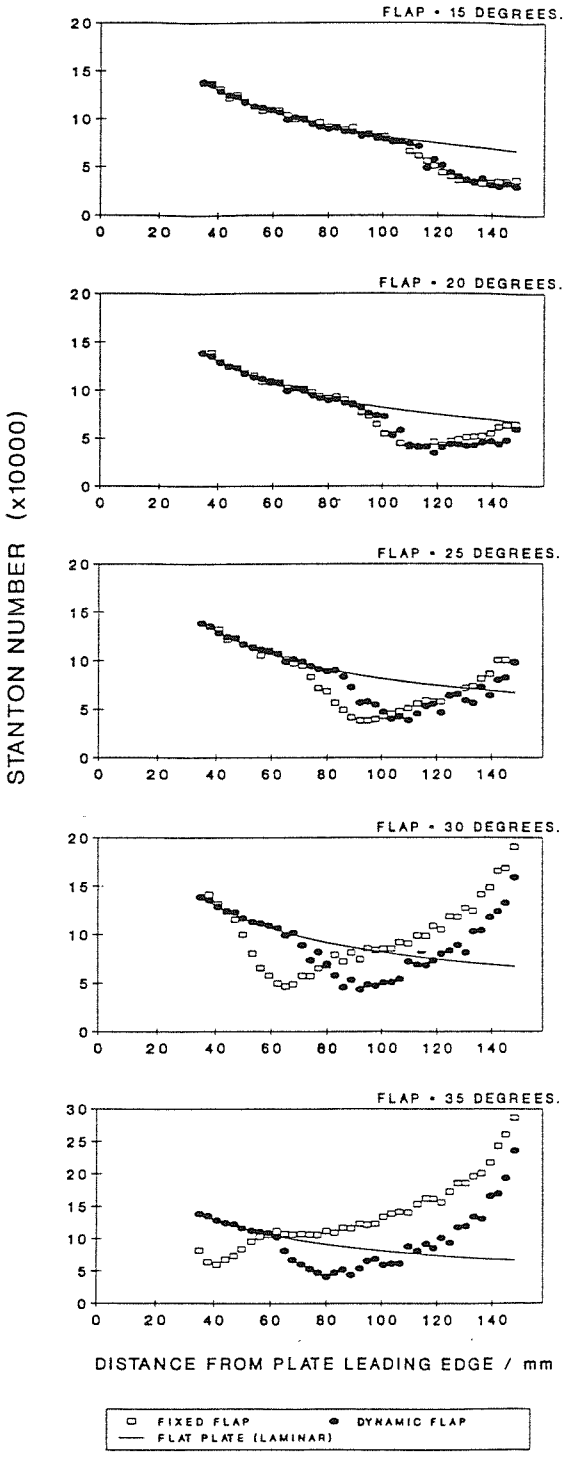

Fig. 3 Heat transfer distributions on the plate for the dynamic and fixed flaps. No side plates. M_∞ = 6.85, Re_∞ = 2.6×10^6/m.

2.3 Heat Transfer Instrumentation

The plate and flap were instrumented with thin film platinum resistance gauges, desposited on pyrex substrates. A single pyrex insert was used along each of the plate, and flap centre lines. The supporting instrumentation for these gauges

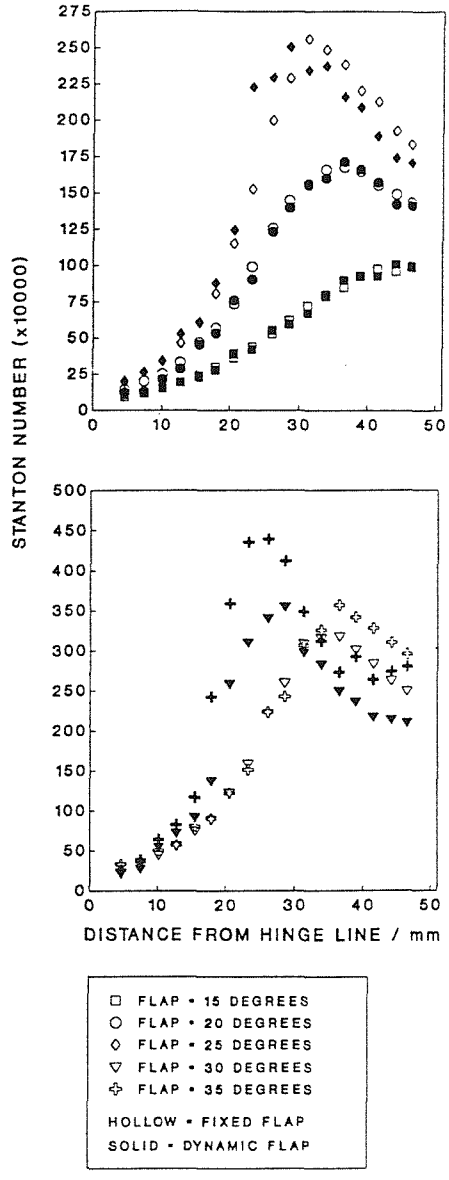

Fig. 4 Heat transfer distributions on the flap for the dynamic and fixed conditions. No side plates. M_∞ = 6.85, Re_∞ = 2.6×10^6/m.

incorporated integral logarithmically matched analogue networks and high gain amplifiers, to give an output directly proportional to the surface heat flux. The temperature rise at each gauge location was obtained from a numerical integration of the recorded heat flux signal. The heat transfer - temperature trace obtained in this way has superior low noise quality (Ref. 6).

2.4 Heat Transfer Measurements

Heat transfer measurements were obtained at the lowest available freestream Reynolds number of 2.6×10^6/m, in an attempt to maintain fully laminar separated flows. A laminar recovery factor was used in the reduction to Stanton numbers.

The measured heat transfer distribution with an undeflected flap was characteristic of a laminar boundary layer over the complete model. The deflection from 0 to 35 degrees within 20ms produces

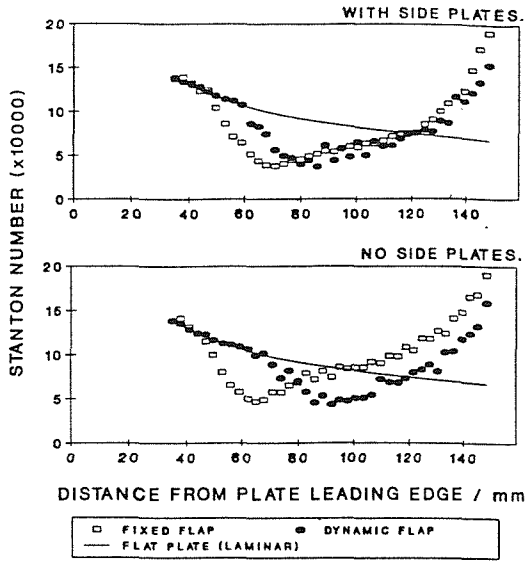

Fig. 5 The effect of side plates on the plate heat transfer distribution. Flap = 30 degrees. M_∞ = 6.85, Re_∞ = 2.6×10^6/m.

flap velocities approaching 3000 degs./s (Fig. 2).

Heat transfer distributions were obtained for various fixed flap angles. These were compared with those obtained at corresponding dynamic flap angles. This comparison, without the use of side plates, is shown in Figs. 3 & 4, from which the following observations are made. At low flap angles the differences between the heat transfer distributions for the steady, and unsteady separations are small. As the flap angle increases, a 'lag' in the extent of separation on the plate develops for the dynamic condition compared to the steady flow. This 'lag' increases at higher flap angles, and at the largest angle of 35 degrees is substantial. For flap angles in excess of 20 degrees there is evidence of transition within the separated flow for both fixed, and dynamic flaps. This is determined from the local increase of separated flow heat transfer on the plate, which is a departure from the rounded distribution characteristic of fully laminar separations (Refs. 7,8). The location of transition, inferred from this criterion, is different for steady and dynamic conditions at the same flap angle. For the dynamic separations the rise in heat transfer is less, suggesting that transition is occurring later, or less abruptly, in the free shear layer compared to the equivalent steady separation. This difference is very clear at the largest flap angle.

The heat transfer distributions on the flap are essentially the same for steady, and dynamic conditions, at low to moderate flap angles (Fig. 4). At the highest angles there is an increase in peak reattachment heat transfer for the dynamic flap in excess of that for the steady flow, and this peak occurs at a more forward location on the flap. This increase is 23% at a flap angle of 35 degrees.

These heat transfer measurements were repeated with the addition of side plates (Fig. 5). Only a small amount of this data has so far been analysed. An example is illustrated for the plate heat transfer distribution with a flap angle of 30 degrees. The 'lag' in the dynamic separation growth is less than that which occurs without side plates. There appears to be a smaller dynamic effect on transition within the separated flow when side plates are added. This addition has affected the local rise in

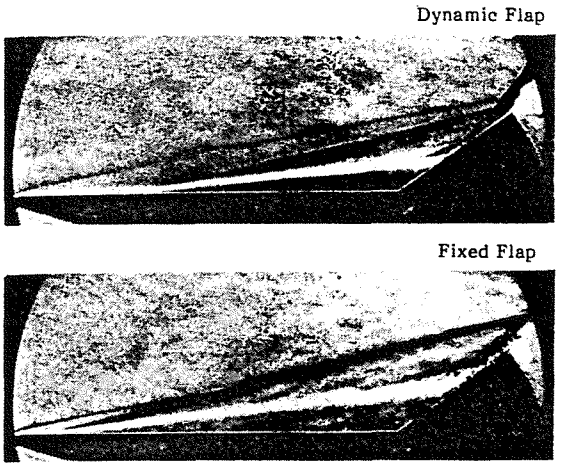

Fig. 6 Schlieren flow visualisation for the fixed and dynamic flaps at 35 degrees. M_∞ = 6.85, Re_∞ = 2.6×10^6/m.

heat transfer on the plate for both the steady, and unsteady conditions when they are compared respectively to those obtained without side plates. The reduced 'lag' in dynamic growth may be due to either, a different influence of the side effects for the evolving unsteady flow, such as reduced lateral venting, or the occurence of transition earlier in the free shear layer for the dynamic separation. It is not clear at this stage which mechanism is responsible. This may be clarified when this data set has been more fully analysed. It is, however, important to note that a significant 'lag' in dynamic separation growth remains, which cannot be attributed to the influence of side effects.

2.5 Schlieren Flow Visualisation

For the fixed flap, schlieren photographs were obtained throughout the range of flap deflection, and at three freestream Reynolds numbers of 2.6, 7.6, and 14.6×10^6/m, both with and without the addition of side plates. Separation lengths were measured from these, defined as the distance from the separation point to the hinge line. The approximate location of separation was taken as the point of intersection of the separation shock with the visible edge of the boundary layer. It was observed that at any fixed flap angle, the separation length reduced with increasing freestream Reynolds number. This is typical of the behaviour expected for transitional separations (Ref. 9). There was only a small effect of the side plates on the steady separated flow geometry.

Spark source schlieren photographs were also obtained of the separated flow generated by the dynamic flap, at the freestream Reynolds number of 2.6×10^6/m without side plates. These were accumulated from a number of tests by varying the time between the flap release, and the spark illumination. Separation lengths were obtained from these, and compared with the fixed flap results for these freestream conditions (Figs. 6 & 7). The observed 'lags' in separation growth for the dynamic flap induced separations are consistent with those inferred from the heat transfer measurements. The appearance of the free shear layer is different than the steady condition (Fig. 6). For the dynamic case, it is more regular in structure, and is followed by a better defined reattachment process. This is also consistent with the heat transfer measurements in indicating that transition is delayed, or less abrupt, for the dynamically separated flows, without side plates.

The measurements of a 'lag' in the growth of the dynamic separation is consistent with finite times to entrain mass, and to propagate pressure changes. The requirement to entrain mass into the growing separation will reduce the thickness of the reattaching free shear layer, and it is proposed that this is the primary cause of the measured increases in reattachment peak heat transfer. Simple analytic models have been developed based on these individual mechanisms of adjustment.

3. ANALYTICAL MODELLING

3.1 Mass Entrainment

The principles of a mass transfer model by Ihrig & Korst (Ref. 1) for turbulent base separations are here applied to a moving flap in a steady freestream, generating fully laminar separated flow. The continuity equation for unsteady flow is applied to the complete separation. It is assumed that pressure equalisation throughout is instantaneous. For the separation region to grow it must entrain mass. This mass is entrained from the free shear layer in the recompression zone (Fig. 8), and at any instant this is,

$$\int_{y=o}^{y_r} \rho\, u\, dy = G \qquad (1)$$

This integral represents the mass flow rate, per unit width, between the separation streamline, and the reattaching streamline which satisfies the reattachment escape criterion. This integral is evaluated at the beginning of the recompression process, which for the wedge separation is assumed to occur at a position in the free shear layer in line with the hinge. The magnitude of this integrated mass flow rate determines the rate of separation response, and subsequently any lag in its growth. To evaluate this term, the method of Cooke (Ref. 10) has been applied to predict the free shear layer development. Assumptions in this prediction include a 'dead-air' region beneath the free-shear layer, and assumed velocity profiles. In modelling the dynamic behaviour of the separation it is

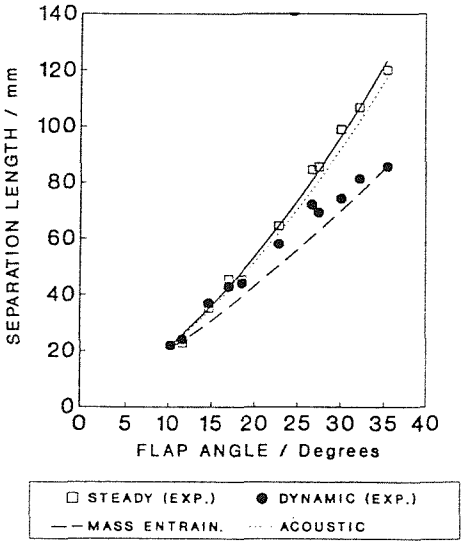

Fig. 7 Experimental measurement and theoretical prediction of separation lengths. No side plates. M_∞ = 6.85, Re_∞ = 2.6×10^6/m.

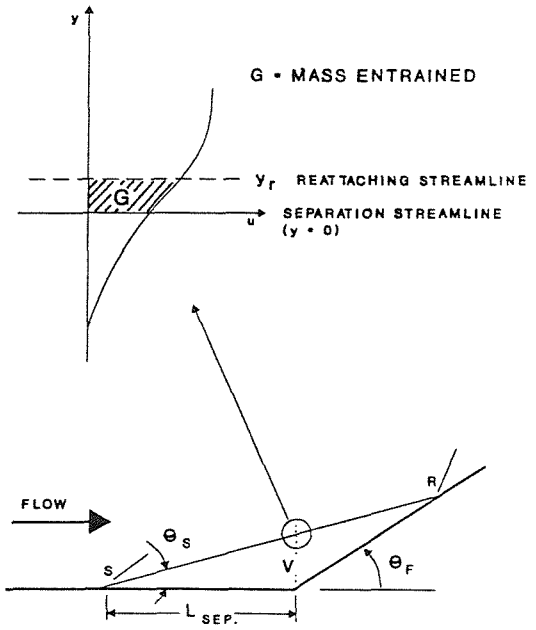

R - REATTACHMENT POINT, S - SEPARATION POINT

Fig. 8 Simplified separation geometry, and mass entrainment mechanism.

assumed that the free shear layer has a quasi-steady response to changes in the adjacent external freestream flow. At any flap angle an escape criterion must be applied to determine which streamline can reattach. To avoid the errors inherent in attempting to model the reattachment process to determine this, the steady separation lengths have been used. For these steady separations, it is the separation streamline which satisfies the escape criterion to form a single dividing streamline. By applying a prediction of the free shear layer development from the measured separation point, the velocity on this dividing streamline, in line with the hinge, can be determined for each steady separation point, and hence flap angle. This velocity in the free shear layer is the escape criterion for a particular flap angle. This is applied to the unsteady separation development. The perturbation pressure created by the moving flap is negligible compared to the shock compression pressure rise at reattachment.
The 'dead-air' is assumed to have a uniform temperature, equal to the isothermal wall temperature. For an isobaric mixing process, this temperature determines the density in this region. The separated flow is approximated as a triangular section (Fig. 8). To satisfy the equation for continuity during the unsteady separation development,

$$\frac{\partial m_d}{\partial t} = \frac{\partial(\rho_d V_d)}{\partial t} = G \qquad (2)$$

This expression can be rearranged to give a differential equation for the development of the separation length,

$$\frac{dL_{sep}}{dt} = f\left\{G_d, \frac{d\theta_f}{dt}, L_{sep}, \theta_s, \frac{d\theta_s}{dL_{sep}}, \frac{dRe_o}{dL_{sep}}, T_w, M_\infty, Re_o, \theta_s, \theta_f, P_\infty\right\} \qquad (3)$$

This equation is solved numerically to determine the separation growth. This model has been applied for a flap deflection from 10 to 35 degrees (Fig. 7). The flap velocity at each angle is that produced experimentally. The initial angle of 10 degrees produces a sufficiently large separation to be modelled, and there is a negligible 'lag' in the unsteady growth accumulated at angles below this.

3.2 Acoustic Propagation

The mechanism for a forward displacement of the separation point is the increase in pressure gradient in this region which is driven, ultimately, from the changing pressure rise at reattachment. These pressure disturbances are communicated through the separated flow at combined acoustic and local convective velocities. In this analytical model of the separation dynamic response it is assumed that this propagation time is the limiting factor in determining the rate of separation growth, and that mass entrainment times are negligible.
To estimate this adjustment time, the communication distance is taken to be the length between the separation and reattachment points, along the dividing streamline. Reverse flow velocities in the separation region are neglected, and the local speed of sound is taken to be that which exists at the isothermal wall temperature.
The correlation of steady separation length with flap angle gives,

$$L_s = f\{\theta_f\} \qquad (4)$$

For the dynamic flap, $\theta_f = \theta_f(t)$. If the acoustic 'lag' is defined as 'ϕ', then for the unsteady separation development,

$$L_s = f\{\theta_f(t-\phi)\} \qquad (5)$$

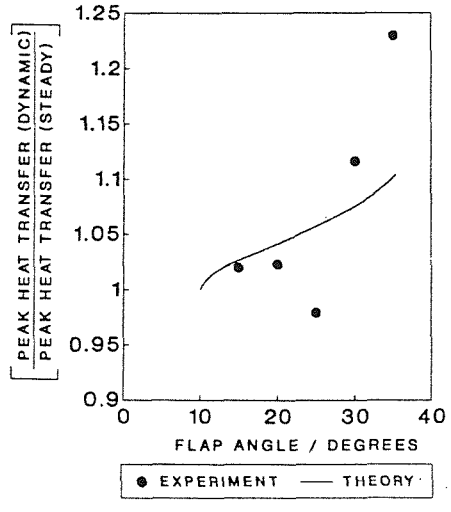

Fig. 9 Dynamic effect on peak reattachment heat transfer. No side plates. M_∞ = 6.85, Re_∞ = 2.6×10^6/m.

with

$$\phi = \frac{L_{ds}}{a}$$

This 'lag' in growth is integrated over the time of imposed flap deflection. This analytical model has been applied with the same boundary conditions used for the mass entrainment model (Fig. 7).

The results of these simple models indicate that mass entrainment has the dominant characteristic time for laminar separated flow adjustment. When these predictions are compared with the experimental measurements (Fig. 7), the mass entrainment model gives a good estimate of the 'lag' at larger flap angles, although it generally over-predicts the 'lag' in response. The pressure propagation model significantly underestimates the 'lag' for moderate to large flap deflections. The experiments are subject to the influence of transition. This will give a more energetic mass exchange mechanism in the free shear layer, which will produce a more rapid dynamic separation response compared to a fully laminar flow. This, together with the use of transitional experimental data in the theory to determine the reattachment condition, may account for over predictions of the 'lag' by the laminar mass entrainment theory. A comparison of this theory with the experimental data obtained with side plates has not been completed.

3.3 Reattachment Heat Transfer

The basic assumption in this model of the reattachment heat transfer is that, following reattachment, a laminar sub-boundary layer develops on the flap from the reattachment point, which is insensitive to the pressure gradient (Ref. 11). Zero mass entrainment in the free shear layer during the reattachment process is assumed. A velocity profile for the developing sub-boundary layer is assumed, of a form consistent with that used for the free shear layer model. With mass conservation, the distance from the reattachment point at which this developing sub-boundary layer has entrained all the reattaching free shear layer mass flow can be determined. This is taken as the location of peak heating. If this is applied to dynamic, and steady separations at each flap angle, assuming the same post reattachment freestream conditions, then

$$\frac{q_{peak,\,dynamic}}{q_{peak,\,steady}} = \left\{ \frac{Reatt.\ mass\ flow\ (dynamic)}{Reatt.\ mass\ flow\ (steady)} \right\}^{-1} \qquad (6)$$

The results of this are compared with the experimental measurements in Fig. 9. The theory predicts an increase in peak reattachment heat transfer for the dynamic flap of up to 10%. This is less than the measured increase at the highest flap angle. The peak heat transfer will be affected by the location of transition within the free shear layer. As this location is a function of the dynamic response without side plates, this complicates the comparison between steady, and dynamic conditions.

4. CONCLUSIONS

There is a measured 'lag' in the growth of the separation in response to the rapidly actuated flap. This dynamic behaviour increases the peak reattachment heat transfer at high flap angles, in excess of that for steady flow. There is a dynamic effect which delays transition in the unsteady separation when no side plates are used. This dynamic influence is reduced with side plates. Further investigation of this phenomenon is required. The results of simple analytic models indicate that mass entrainment has the dominant effect in determining the time of adjustment for fully laminar separated flow, and that this requirement is a mechanism for increasing the peak reattachment heat transfer.

5. REFERENCES

1. Ihrig Jr. H.K. & Korst, H.H. 1963, Quasi-steady aspects of the adjustment of separated flow regions to transient external flows, AIAA Journal, Vol. 1, No. 4, p934.

2. Wilkinson, P.R. 1966, Non-steady separation in laminar hypersonic flow, Ph.D. Thesis, University of Southampton.

3. Holden, M.S. 1971, Establishment time of laminar separated flows, AIAA Journal, Vol. 9, No. 11, p2296.

4. Roberts, T.P. 1989, Dynamic effects of hypersonic separated flows, Ph.D. Thesis, University of Southampton.

5. Kazakov, A.V. 1981, Unsteady viscous flow over a short flap, IZVESTIYA AKADEMII NAUK SSSR, MEKHANIKA ZHIDKOSTI I GAZA, No. 4, p111.

6. Oldfield, M.L.G. et. al. 1978, On-line computer for transient turbine cascade instrumentation, IEEE Trans. on Aerospace & Electronic Systems, Vol. AES-14, No. 5.

7. Johnson, C.B. 1970, Heat transfer measurements at Mach 8 on a flat plate with deflected trailing edge flap with effects of transition included, NASA TN D-5899.

8. Sterrett, J.P. & Holloway, D.F. 1964, On the effects of transition on parameters within a separation region at hypersonic speeds: with emphasis on heat transfer, Symp. on fully separated flows, ASME, New York.

9. Needham, D.A. & Stollery, J.L. 1966, Boundary layer separation in hypersonic flow, AIAA Paper, No. 66-455, AIAA 4th Aerospace Sciences Meeting, Los Angeles, Calif.

10. Cooke, J.C. 1963, Separated supersonic flow, RAE TN No. AERO 2879.

11. Holden, M.S. 1964, Heat transfer in separated flow, Ph.D. Thesis, Univ. of London.

References.

Adamson, T.C., and Messiter, A.F., 1980, "Analysis of Two-Dimensional Interactions between Shock Waves and Boundary Layers," *Annual Review of Fluid Mechanics*, Vol.12, pp.103-138.

Anderson, J.D., 1989, *Hypersonic and High Temperature Gas Dynamics*, Publ. McGraw-Hill.

Ball, K.O.W., 1969a, "Effects of Flap Length and Slot Suction on Separated Laminar Boundary Layers," AIAA Paper 69-36.

Ball, K.O.W., 1969b, "The Extent of Laminar, Two-Dimensional Boundary Layer Separation Due to a Compression Corner at Moderately Hypersonic Speeds," ARL Rept. 69-0013.

Ball, K.O.W., and Korkegi, R.H., 1968, "An Investigation of the Effect of Suction on Hypersonic Laminar Boundary-Layer Separation," *AIAA Journal*, Vol.6., No.2, pp.239-243.

Batham, J.P., 1972, "An Experimental Study of Turbulent Separations and Reattaching Flows at High Mach Number," *Journal of Fluid Mechanics*, Vol.52, Part 3, pp.425-435.

Battin, W.J., 1963, "Thermal Adjustment of Separated Flow to Transient External Flow Conditions in Short Duration Experiments," PhD Thesis, Dept. of Mech. Eng., Univ of Illinois.

Baxter, D.R.J., 1990, Private communication.

BDH Ltd., 1988, *LICRITHERM Thermochromic Liquid Crystals*, Product catalogue.

Bergland, G.D., 1969, "A Guided Tour of the Fast Fourier Transform," *IEEE Spectrum*, July, pp.41-52.

Berry, R.W., Hall, P.M., and Harris, M.T., 1968, *Thin Film Technology*, Publ. D. Van Nostrand Company Inc., New Jersey.

Bogdonoff, S.M., and Kepler, C.E., 1955, "Separation of a Supersonic Turbulent Boundary Layer," *Journal of the Aeronautical Sciences*, Vol.22, pp.414-424.

Bogdonoff, S.M., and Vas, I.E., 1962, "Some Experiments on Hypersonic Separated Flows," *ARS Journal*, Vol.32, pp.1564-1572.

Broch, J.T., 1981, *Principles of Analog and Digital Frequency Analysis*, Publ. Tapir.

Burd, H.J., and Doe, N.G., 1980, "The Computer Analysis, and Design of, an Electrical Analogue of the Heat Conduction Process, for Use in a Transient Cascade to Obtain Heat Transfer From Temperature Measurements," Third Year Hons. Degree Project Rept., Dept. of Engineering Science, Oxford Univ.

Bushnell, D.M., and Weinstein, L.M., 1968, "Correlation of Peak Heating for Reattachment of Separated Flows," *Journal of Spacecraft*, Vol.5, No.9, pp.1111-1112.

Carriére, P., and Sirieux, M., 1961, "Facteurs d'influence du recollement d'un écoulement supersonique. ONERA Memo. Tech. No.20.

Champeney, D.C., 1973, *Fourier Transforms and their Physical Applications*, Publ. Academic Press.

Chapman, D.R., 1950, "Laminar Mixing of a Compressible Fluid," NACA Rept. 958.

Chapman, D.R., Kuehn, D.M., and Larson, K.H., 1958, "Investigation of Separated Flows in Supersonic and Subsonic Streams with Emphasis on the Effects of Transition," NACA Rep.1356.

Charwat, A.F., 1970, "Supersonic Flows with Embedded Separated Regions," In: Advances in Heat Transfer, Vol.6, Ed. Hartnett, J.P., and Irvine, T.F.

Cheng, H.K., Hall, G.J., Golian, T.C., and Hertzberg, A., 1961, "Boundary-Layer Displacement and Leading Edge Bluntness Effects in High-Temperature Hypersonic Flow," *Journal of the Aeronautical Sciences*, Vol.28, No.5, pp.353-381.

Chilcott, R.E., 1967, "A Review of Separated and Reattaching Flows with Heat Transfer," *Int. Journal of Heat and Mass Transfer*, Vol.10, pp.783-797.

Childs, M.E., Paynter, G.C., and Redeker, E., 1966, "The Prediction of Separation and Reattachment Flow Characteristics for Two-Dimensional Supersonic and Hypersonic Turbulent Boundary Layers," AGARD Conf. Proc. No.4, Separated Flows, Part I.

Choudhury, P.N., 1970, "Unsteady Heat Transfer and Fluid Flow," PhD Thesis, Univ. of Southampton.

Chpoun, A., 1989, "Hypersonic Flow in a Compression Corner in 2D and 3D Configurations," AIAA Paper 89-1876.

Coleman, G.T., and Stollery, J.L., 1972, "Heat Transfer from Hypersonic Turbulent Flow at a Wedge Compression Corner," *Journal of Fluid Mechanics*, Vol.56, Part 4, pp.741-752.

Cooke, J.C., 1963, "Separated Supersonic Flow," RAE TN No. AERO 2879.

Cook, W.J., 1970, "Determination of Heat Transfer Rates from Transient Surface Temperature Measurements," *AIAA Journal*, Vol.8, No.7, pp.1366-1368.

Cook, W.J., and Felderman, E.J., 1966, "Reduction of Data from Thin Film Heat Transfer Gauges. A Concise Numerical Technique," *AIAA Journal*, Vol.3, No.4, p.561.

Cox, R.N., and Crabtree, L.F., 1965, *Elements of Hypersonic Aerodynamics*, Publ. The English Universities Press.

Crocco, L., and Lees, L., 1952, "A Mixing Theory for the Interaction Between Dissipative Flows and Nearly Isentropic Streams," *Journal of the Aeronautical Sciences*, Vol.19, No.10, pp.649-676.

Curle, N., 1961, "The Effects of Heat Transfer on Laminar Boundary Layer Separation in Supersonic Flow," *The Aero. Quarterly*, Vol.XII, pp.309-336.

Delery, J., and Marvin, J.G., 1986, "Shock Wave Boundary Layer Interactions," AGARDograph AG-280.

den Ouden, C., and Hoogendoorn, C.J., 1974, "Local Convective Heat Transfer Coefficients for Jets Impinging on a Plate: Experiments Using a Liquid Crystal Technique," In: Proc. of the Fifth International Heat Transfer Conf., Vol.V, AIChE, New York, pp.293-297.

Disimile, P.J., and Scaggs, N.E., 1989, "High Reynolds Number Wedge Induced Separation Lengths at Mach 6," *AIAA Journal*, Vol.27, No.12, pp.1827-1828.

Doorly, J.E., and Oldfield, M.L.G., 1987, "The Theory of Advanced Multi-Layered Thin Film Heat Transfer Gauges," *Int. Journal of Heat and Mass Transfer*, Vol.30, No.6, pp.1159-1168.

East, R.A., 1992, Private communication.

East, R.A., and Qasrawi, A.M.S., 1978, "A Long Stroke Isentropic Free Piston Hypersonic Wind Tunnel," Aeronautical Research Council, Reports and Memoranda No.3844.

East, R.A., and Smith, A.J.D., 1990, "Unsteadiness in Separated Hypersonic Flows," Contract Rept., European Space Agency.

East, R.A., and Smith, A.J.D., 1991, "Unsteadiness in Separated Hypersonic Flows," Interim Contract Rept., European Space Agency.

East, R.A., and Smith, A.J.D., 1993, "Unsteadiness in Separated Hypersonic Flows," Final Contract Rept., European Space Agency.

Eckert, E.R.G., 1955, "Engineering Relations for Skin Friction and Heat Transfer to Surfaces in High Velocity Flows," *Journal of the Aeronautical Sciences*, Vol.22, No.8, pp.585-587.

Elfstrom, G.M., 1972, "Turbulent Hypersonic Flow at a Wedge-Compression Corner," *Journal of Fluid Mechanics*, Vol.53, pp.113-127.

Erdos, J, and Pallone, A, 1962, "Shock-Boundary Layer Interaction and Flow Separation," In: Proc. of the 1962 Heat Transfer and Fluid Mechs. Inst., Stanford Univ. Press, Stanford, Calif.

Giles, H.L., and Thomas, J.W., 1966, "Analysis of Hypersonic Pressure and Heat Transfer Tests on a Flat Plate with a Flap and a Delta Wing with Body, Elevons, Fins, and Rudders," NASA CR-536.

Ginoux, J.J., 1969a, "High Speed Flows over Wedges and Flares with a Method of Detecting Transition," In: Proc. of the 1969 Symposium on Viscous Interaction Phenomena in Supersonic and Hypersonic Flow, Hypersonic Research Laboratory, Aerospace Research Laboratories, 7-8 May.

Ginoux, J.J., 1969b, "On some Properties of Reattaching Laminar and Transitional High Speed Flows," Von Karman Inst. for Fluid Dynamics, Tech. Note 53.

Görtler, H., "On the Three-Dimensional Instability of Laminar Boundary Layers on Concave Walls," NACA TM 1375.
Gray, J.D., 1964, "A Correlation of Axisymmetric Laminar Flow Separation Characteristics," AIAA Paper 64-475.

Green, J.E., 1970, "Interactions between Shock Waves and Turbulent Boundary Layers," *Prog. in Aerospace Sciences*, Publ. Pergamon Press, Vol.11, pp.235-340.

Hakkinen, R.J., Greber, I., Trilling, L., and Abarbanel, S.S., 1959, "The Interaction of an Oblique Shock Wave with a Laminar Boundary Layer," NASA Memo. 2-18-59 W.

Hammitt, A.G., and Hight, S., 1959, "Scale Effects in Turbulent Boundary Layer Interactions," USA AFOSR TN 60-82, Procs. 6th Midwestern Conf. on Fluid Mech., Sept.

Hankey, W.L., and Holden, M.S., 1975, "Two-Dimensional Shock Wave - Boundary Layer Interactions in High Speed Flows," AGARDograph No.203.

Haq, Z.U., Roberts, G.T., and East, R.A., 1989, "Interference Heating in Corner Regions at Hypersonic Speeds," In: Proc. of the Royal Aeronautical Society Int. Conf. on Hypersonic Aerodynamics, Univ. of Manchester.

Haq, Z.U., Roberts, G.T., and East, R.A., 1991, "Interference Heating Near Fin / Body Junctions on Hypersonic Vehicles," In: Aerothermodynamics for Space Vehicles, Proc. of the First European Symp., ESTEC, Noordwijk, The Netherlands, May 28-30.

Hartunian, R.A., and Varwig, R.L., 1962, "On Thin-Film Heat Transfer Measurements in Shock Tubes and Shock Tunnels," *The Physics of Fluids*, Vol.5, No.2, pp.169-174.

Harvey, W.D., 1968, "Experimental Investigation of Laminar Flow Separation on a Flat Plate Induced by Deflected Trailing Edge Flap at Mach 19," NASA TN D-4671.

Hayes, W.D., and Probstein, R.F., 1959, *Hypersonic Flow Theory*, Publ. Academic Press, New York.

Hill, W.G., 1967, "Analysis of Experiments on Hypersonic Flow Separation Ahead of Flaps using a Simple Flow Model," Grumman Research Dept., Memo RM-383.

Hoelmer, W., 1967, "Laminar Boundary-Layer Separation in Hypersonic Flow," *AIAA Journal*, Vol.5, No.2., pp.360-362.

Holden, M.S., 1964, "Heat Transfer in Separated Flow," PhD Thesis, Univ. of London.

Holden, M.S., 1966a, "Experimental Studies of Separated Flows at Hypersonic Speeds. PartII: 2-D Wedge Separated Flow Studies," *AIAA Journal*, Vol.4, No.5, pp.790-799.

Holden, M.S., 1966b, "Theoretical and Experimental Studies of Separated Flows Induced by Shock-Wave-Boundary-Layer Interaction," AGARG Conf. Proc., No.4, Separated Flows, Part I.

Holden, M.S., 1967, "Theoretical and Experimental Studies of Laminar Flow Separation on Flat Plate - Wedge Compression Surfaces in the Hypersonic Interaction Regime," Rept. AF-1894-A-2, Cornell Aeronautical Lab. Inc., Buffalo, New York.

Holden, M.S., 1971a, "Boundary Layer Displacement and Leading Edge Bluntness Effects on Attached and Separated Laminar Boundary Layers in a Compression Corner. PartII: Experimental Study," *AIAA Journal*, Vol.9, No.1, pp.84-93.

Holden, M.S., 1971b, "Establishment Time of Laminar Separated Flow," *AIAA Journal*, Vol.9, No.11, pp.2296-2298.

Holden, M.S., 1972, "Shock Wave - Turbulent Boundary Layer Interaction in Hypersonic Flow," AIAA Paper 72-74.

Holden, M.S., 1977 "Shock Wave - Turbulent Boundary Layer Interaction in Hypersonic Flow," AIAA Paper 77-45.

Holden, M.S., 1978, "A Study of Flow Separation in Regions of Shock Wave - Boundary Layer Interaction in Hypersonic Flow," AIAA Paper 78-1169.

Holden, M.S., 1986, "A Review of Aerothermal Problems Associated with Hypersonic Flight," AIAA Paper 86-0267.

Holden, M.S., and Moselle, J.R., 1970, "Theoretical and Experimental Studies of the Shock Wave - Boundary Layer Interaction on Compression Surfaces in Hypersonic Flow," ARL 70-0002, Aerospace Research Labs., Wright-Patterson AFB.

Hung, C.M., and MacCormack, R.W., 1976, "Numerical Solutions of Supersonic and Hypersonic Laminar Compression Corner Flows," *AIAA Journal*, Vol.14, No.4, pp.475-481.

Hung, F.T., 1973, "Interference Heating due to Shock Wave Impingement on Laminar Boundary Layers," AIAA Paper 73-678.

Hung, F.T., and Barnett, D.O., 1973, "Shock Wave - Boundary Layer Interference Heating Analysis," AIAA Paper 73-237.

Hung, F.T., and Greenschlag, S.N., 1976, "Interference Heating due to Shock Wave Impingement on Laminar and Turbulent Boundary Layers," AIAA Paper 76-355.

Ihrig, H.K., and Korst, H.H., 1963, "Quasi-Steady Aspects of the Adjustment of Separated Flow Regions to Transient External Flows," *AIAA Journal*, Vol.1, No.4, pp.934-937.

Ireland, P.T., and Jones, T.V., 1986, "Detailed Measurements of Heat Transfer On and Around a Pedestal in Fully Developed Passage Flow," Proc. of the 8th Int. Heat Transfer Conf., Vol.3, pp.975-980.

Ireland, P.T., and Jones, T.V., 1987, "The Response Time of a Surface Thermometer Employing Encapsulated Thermochromic Liquid Crystals," *Journ. Phys.E: Sci. Instrum.*, Vol.20, pp.1195-1199.

Johnson, C.B., 1970, "Heat Transfer Measurements at Mach 8 on a Flat Plate with Deflected Trailing-Edge Flap with Effects of Transition Included," NASA TN D-5899.

Jones, T.V., Schultz, D.L., and Hendley, A.D., 1973, "On the Flow in an Isentropic Light Piston Tunnel," Aeronautical Research Council, Repts. and Memos. No.3731.

Kaufman, L.G., Meckler, L., and Hartofilis, S.A., 1966, "An Investigation of Flow Separation and Aerodynamic Controls at Hypersonic Speeds," *Journal of Aircraft*, Vol.3, No.6, pp.555-561.

Kazakov, A.V., 1981, "Unsteady Viscous Supersonic Flow over a Short Flap," *IZVESTIYA AKADEMII NAUK SSSR, MEKHANIKA ZHIDKOSTI I GAZA*, No.4, pp.111-118.

Kipp, H.W., and Helms, V.T., 1985, "Some Observations on the Occurrence of Striation Heating," AIAA Paper 85-0324.

Kirk, F.N., 1959, "An Approximate Theory of Base Pressure in Two-Dimensional Flow at Supersonic Speeds," RAE TN No. AERO 2377.

Klein, E.J., 1968, "Application of Liquid Crystals to Boundary Layer Flow Visualisation," AIAA Paper 68-376.

Klein, E.J., and Margozzi, A.P., 1969, "Exploratory Investigation on the Measurement of Skin Friction by Means of Liquid Crystals," NASA TM X-1774.

Korkegi, R.H., 1971, "Survey of Viscous Interactions Associated with High Mach Number flight," *AIAA Journal*, Vol.9, No.5, pp.771-784.

Koromilas, C.A., and Telionis, D.P., 1980, "Unsteady Laminar Separation: An Experimental Study," *Journal of Fluid Mechanics*, Vol.97, pp.347-384.

Korst, H.H., 1956, "A Theory for Base Pressures in Transonic and Supersonic Flow," *Journal Appl. Mech.*, Vol.23, pp.593-600.

Kuehn, D.M., 1959, "Experimental Investigation of the Pressure Rise Required for the Incipient Separation of Turbulent Boundary Layers in Two-Dimensional Supersonic Flow," NASA Memo. 1-21-59A.

Lee, J.Y., and Lewis, M.J., 1993, "Numerical Study of the Flow Establishment Time in Hypersonic Shock Tunnels," *Journal of Spacecraft and Rockets*, Vol.30, No.2, pp.152-163.

Lees, L., and Probstein, R.F., 1952, "Hypersonic Viscous Flow Over a Flat Plate," Rept. No.195, Dept. of Aero. Eng., Princeton Univ., Princeton, N.J.

Lees, L., and Reeves, B.L., 1964, "Supersonic Separated and Reattaching Laminar Flows: I. General Theory and Application to Adiabatic Boundary-Layer / Shock-Wave Interactions," *AIAA Journal*, Vol.2, No.11, pp.1907-1920.

Lewis, J.E., Kubota, T., and Lees, L., 1968, "Experimental Investigation of Supersonic Laminar, Two-Dimensional Separation in a Compression Corner with and without Cooling," *AIAA Journal*, Vol.6, No.1, pp.7-14.

Liepmann, H.W., and Roshko, A., 1957, *Elements of Gasdynamics*, Publ. John Wiley & Sons Inc.

Lock, R.C., 1951, "The Velocity Distribution in the Laminar Boundary Layer Between Parallel Streams," *Quart. Jour. Mech. and App. Math.*," Vol.4.

Mattews, R.D., and Ginoux, J.J., 1974, "Correlation of Peak Heating in the Reattachment Region of Separated Flows," *AIAA Journal*, Vol.12, pp.397-399.

McElderry, E.D., 1970, "Boundary Layer Transition at Supersonic Speeds Measured by Liquid Crystals," Air Force Flight Dynamics Lab., FDMG Tm 70-3.

Merritt, G.E., 1964, "Hypersonic Laminar Flow Over Cavities and Steps," PhD Thesis, Univ. of Southampton.

Meyer, R.F., 1960, "A Heat Flux Meter for Use with Thin Film Surface Thermometers," NRC Canada, Aero. Rept. LR-279.

Miller, C.G., 1981, "Comparison of Thin-Film Resistance Heat Transfer Gages with Thin-Skin Transient Calorimeter Gages in Conventional Hypersonic Wind Tunnels," NASA TM 83197.

Miller, C.G., 1985, "Refinement of an Alternate Method for Measuring Heating Rates in Hypersonic Wind Tunnels," *AIAA Journal*, Vol.23, No.5, pp.810-812.

Miller, D.S., Hijman, R., and Childs, M.E., 1964, "Mach 8 to 22 Studies of Flow Separation Due to Deflected Control Surfaces," *AIAA Journal*, Vol.2, No.2, pp.312-321.

Monaghan, R.J., 1953, "An Approximate Solution of the Compressible Laminar Boundary Layer on a Flat Plate, " British ARC R&M 2760.

Moore, F.K., 1951 "Unsteady Laminar Boundary Layer Flow," NACA Tech. Note 2471.

Murphy, J.D., 1969, "A Critical Evaluation of Analytic Methods for Predicting Laminar Boundary Layer Shock Wave Interaction," NASA SP-228, pp.515-539.

Naysmith, A., 1962, "Measurements of Heat Transfer in Bubbles of Separated Flow in Supersonic Air Streams," Air Streams Int. Heat Transfer Conf., ASME Publ. (Part2. Sect. A and B).

Needham, D.A., 1965a, "Laminar Separation in Hypersonic Flow," PhD Thesis, Univ. of London.

Needham, D.A., 1965b, "A Heat Transfer Criterion for the Detection of Incipient Separation in Hypersonic Flow," *AIAA Journal*, Vol.3, No.4, pp.781-783.

Needham, D.A., and Stollery, J.L., 1966a, "Hypersonic Studies of Incipient Separation and Separated Flows," AGARD Conf. Proc. No.4, Separated Flows, Part I.

Needham, D.A., and Stollery, J.L., 1966b, "Boundary Layer Separation in Hypersonic Flow," AIAA Paper 66-455.

Newmann, R.D., 1987, "Defining the Aerothermodynamic Methodology," In: *Hypersonics, Vol.I. Defining the Hypersonic Environment.* Ed. Bertin, J.J., et al, Publ. Birkhäuser.

Newmann, R.D., 1988, "Aerothermodynamic Instrumentation," In: AGARD Rept. No.761.

Oldfield, M.L.G., Jones, T.V., and Schultz, D.L., 1973, "A Ludweig Tube with Light Piston Compression Heating," Aeronautical Research Council, Rept. 34 255.

Parker, R., 1971, "Transient Surface Temperature Response of Liquid Crystal Films," Lawrence Livermore Lab., Rept. UCLR-73583.

Popinski, Z., and Ehlrich, C.F., 1966, "Development Design Methods for Predicting Hypersonic Control Characteristics," USAF Tech. Rept., AFFDL-TR-66-85.

Potter, J.L., and Whitfield, J.D., 1960, "Effects of Unit Reynolds Number, Nose Bluntness, and Roughness on Boundary Layer Transition," AEDC-TR-60-5.

Probstein, R.F., and Lees, L., 1953, "On the Recovery Factor for Hypersonic Flow with a Self-Induced Pressure Gradient," *Journal of the Aeronautical Sciences*, Vol.20, pp.291-292.

Putnam, L.E., 1965, "Investigation of Effects of Ramp Span and Deflection Angle on Laminar Boundary Layer Separation at M = 10.03," NASA TN D-2833.

Qasrawi, A.M.S., 1977, "Measurements of Hypersonic Dynamic Stability of Pitching Blunt-Nosed Bodies in a Short Duration Facility," PhD Thesis, Univ. of Southampton.

Reece, J.W., 1966, "Non-Linear Effects Due to High Heat Flux in Thin Film Thermometry and Means for their Compensation," In: Proc. 2nd Int. Congress on Instrumentation in Aerospace Simulation Facilities, IEEE/6-AES, 10-1.

Rhudy, R.W., 1970, "Investigation of Laminar Boundary-Layer Separation on a Flat-Plate-Ramp Combination with and without Mass Removal at Mach Numbers 6, 8, and 10," Arnold Eng. Development Center, TR-69-199.

Richards, B.E., 1977, In: *Measurement of Unsteady Fluid Dynamic Phenomena*, Von Karman Inst. book, ed. B.E. Richards, Publ. Hemisphere.

Roberts, M., 1970, "Transitional Flow Separation Upstream of a Compression Corner," AIAA Paper 70-764.

Roberts, T.P., 1989, "Dynamic Effects of Hypersonic Separated Flow," PhD Thesis, Univ. of Southampton.

Roshko, A., and Thomke, G.J., 1969, "Supersonic Turbulent Boundary Layer Interaction with a Compression Corner at Very High Reynolds Number," In: Proc. of the 1969 Symposium on Viscous Interaction Phenomena in Supersonic and Hypersonic Flow, Hypersonic Research Lab., Aerospace Research Labs., May 7-8.

Rudy, D.H., Thomas, J.L., Kumar, A., and Gnoffo, P.A., 1991, "Computation of Laminar Hypersonic Compression Corner Flows," *AIAA Journal*, Vol.29, No.7, pp.1108-1113.

Sartell, R.J., and Lorenz, G.C., 1964, "A New Technique for Measurement of Aerodynamic Heating Distributions on Models of Hypersonic Vehicles," In: Proc. 1964 Heat Transfer and Fluid Mech. Inst., Stanford Univ. Press, p.130.

Scholer, H., and Banerji, A., 1984, "Visualisation of Boundary Layer Transition on a Cone with Liquid Crystals," DFVLR Internal Rept.

Schultz, D.L., and Jones, T.V., 1973, "Heat Transfer Measurements in Short Duration Hypersonic Facilities," AGARDograph No.165.

Simeonides, G., and Wendt, J.F., 1991, "Fundamental Experiments of Control Effectiveness and Heating at Hypersonic Mach Numbers," In: Aerothermodynamics for Space Vehicles, Proc. of the First European Symposium , ESTEC, Noordwijk, The Netherlands, May 28-30.

Smith, A.J.D., 1987, "The Response Time of the Liquid Crystal Flow Visualisation Technique and its Application to Heat Transfer Analysis," BSc Project Rept., Dept. of Aero. & Astro., Univ. of Southampton.

Smith, A.J.D., and Baxter, D.R.J., 1989, "Liquid Crystal Thermography for Aerodynamic Heating Measurements in Short Duration Hypersonic Facilities," In: Proc. of the Int. Congress on Instrumentation in Aerospace Simulation Facilities, Sept., pp.104-112.

Smith, A.J.D., and East, R.A., 1991, "The Dynamic Response of Separated Hypersonic Flows," In: Aerothermodynamics for Space Vehicles, Proc. of the First European Symp., ESTEC, Noordwijk, The Netherlands, May 28-30.

Spaid, F.W., and Cassel, L.A., 1973, "Aerodynamic Interference Induced by Reaction Controls," AGARDograph, No.173.

Spaid, F.W., and Frishnett, J.C., 1972, "Incipient Separation of a Supersonic Turbulent Boundary Layer Including the Effects of Heat Transfer," AIAA Paper 72-114.

Sterrett, J.R., and Emery, J.C., 1960, "Extension of Boundary Layer Separation Criteria to a Mach Number of 6.5 by Utilising Flat Plates with Forward Facing Steps," NASA TN D-618.

Sterrett, J.R., and Holloway, D.F., 1964, "On the Effects of Transition on Parameters within a Separation Region at Hypersonic Speeds: With Emphasis on Heat Transfer," Symp. on Fully Separated Flows, ASME, New York.

Thompson, W.P., 1981, "Heat Transfer Gages," *Methods of Experimental Physics: Fluid Dynamics*, Vol.18, pp.663-685.

Todisco, A., and Reeves, B.L., 1969, "Turbulent Boundary Layer Separation and Reattachment at Supersonic and Hypersonic Speeds," In: Proc. of the 1969 Symposium on Viscous Interaction Phenomena in Supersonic and Hypersonic flow, Hypersonic Research Lab., Aerospace Research Labs., May 7-8.

Vidal, R.J., 1956, "Model Instrumentation Techniques for Heat Transfer and Force Measurements in a Hypersonic Shock Tunnel," C.A.L. Rept. AD-917-A-1.

Vidal, R.J., Golian, T.C., and Bartz, J.A., 1963, "An Experimental Study of Hypersonic Low Density Viscous Effects on a Sharp Flat Plate," AIAA Paper 63-435.

Westby, M.F., 1988, "A Study of the Hypersonic Aerodynamics of a Hotol Like Re-Entry Vehicle," BSc Project Rept., Dept. of Aero. & Astro., Univ. of Southampton.

Wilkinson, P.R., 1966, "Non-Steady Separation in Laminar Hypersonic Flow," PhD Thesis, Univ. of Southampton.

Williams, C.S., 1986, *Designing Digital Filters*, Publ. Prentice Hall.

Winding, C.C., Topper, L., and Baus, B.V., 1955, "Metal-Film Resistance Thermometers for Measuring Surface Temperatures," *Industrial and Engineering Chemistry*, Vol.47, No.3, pp.386-392.

Zakkay, V., and Paolo, N., 1975, "Two-Dimensional Turbulent Boundary-Layer Separation and Reattachment on a Flat Plate with Ramp at M = 3.7 and 6.3 in Supersonic and Hypersonic Flow," In: Proc. of the Israel Annual Conf. on Aviation and Astronautics, 17th, Tel Aviv and Haifa, May 21-22.

Zhang, Z.C., Roberts, G.T., and Pratt, N.H., 1989, "An Experimental Evaluation of Thermochromic Liquid Crystals for Temperature and Heat Flux Measurements in Shock Tube Flows," In: Proc. of the 17th Int. Symp. on Shock Tubes and Waves, Pennsylvania.

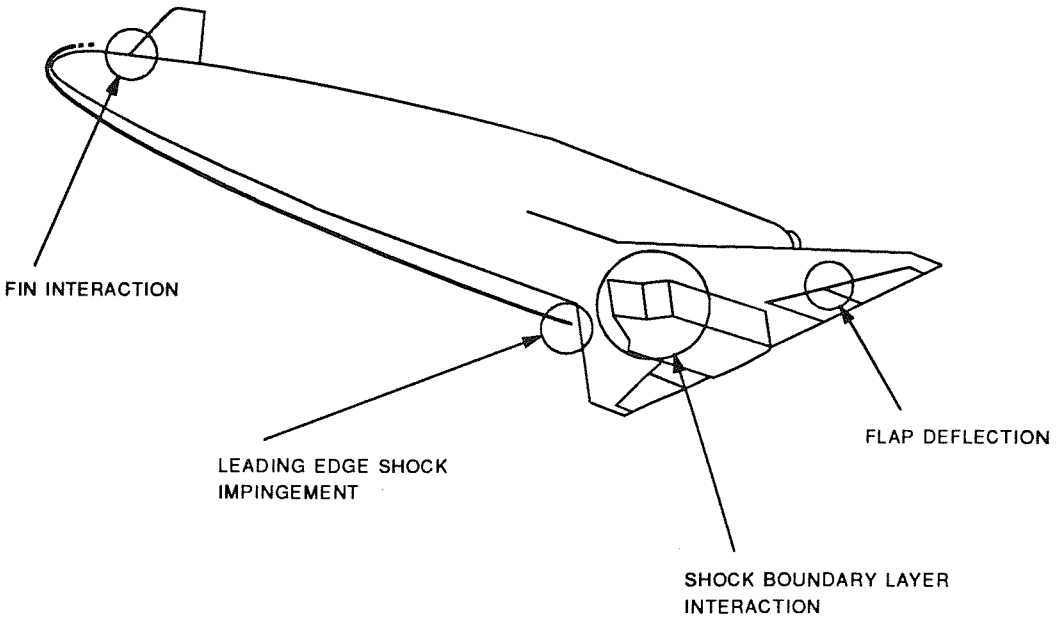

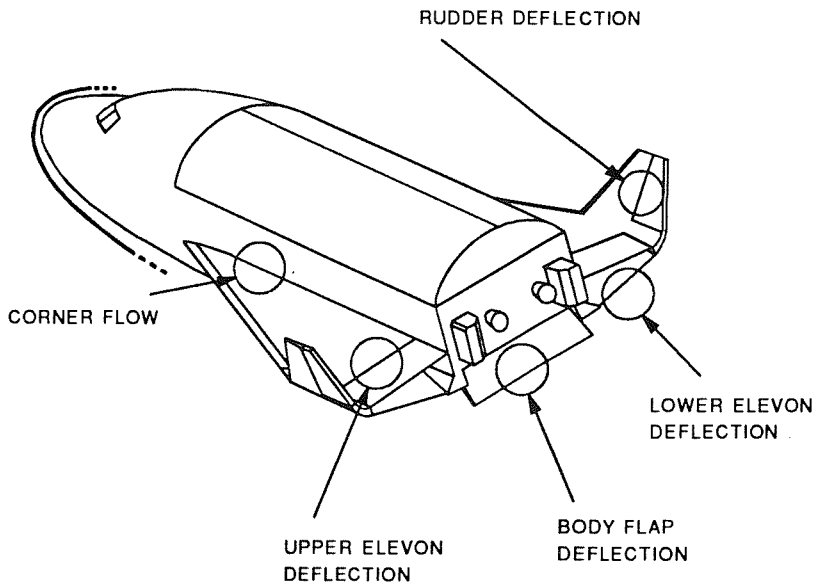

Fig.1. Examples of strong viscous interaction regions occurring on hypersonic vehicles.

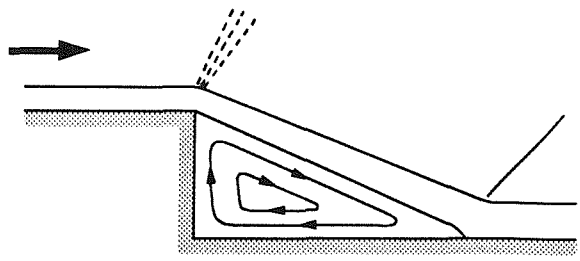

(i) Backward facing step.

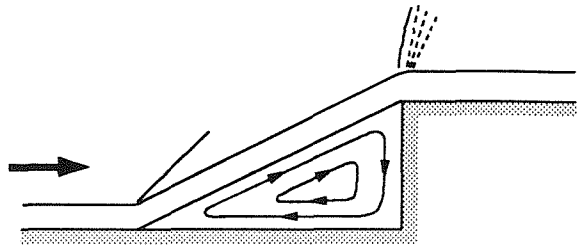

(ii) Forward facing step.

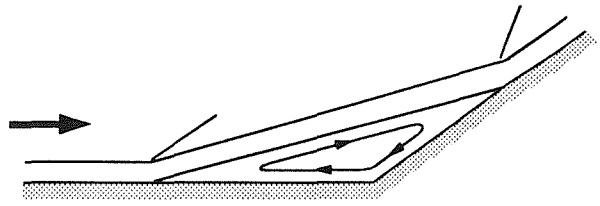

(iii) Compression corner flow.

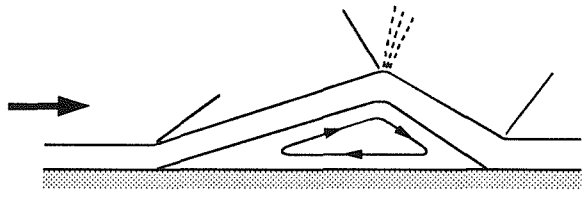

(iv) Incident shock.

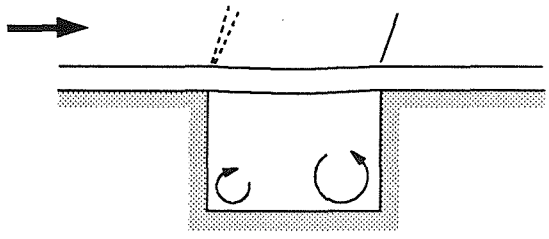

(v) Cavity.

Fig.2. Basic types of two-dimensional shock wave - boundary layer interaction.

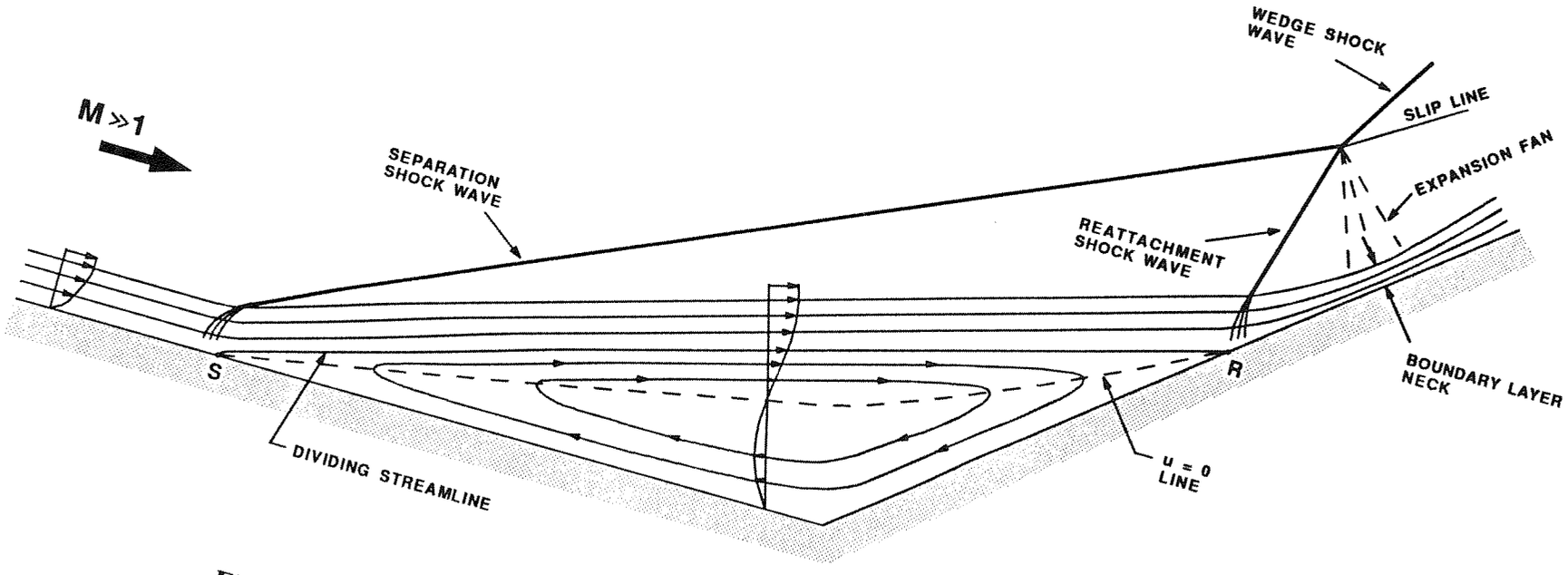

Fig.3. Schematic of the compression corner separated flow (not to scale).

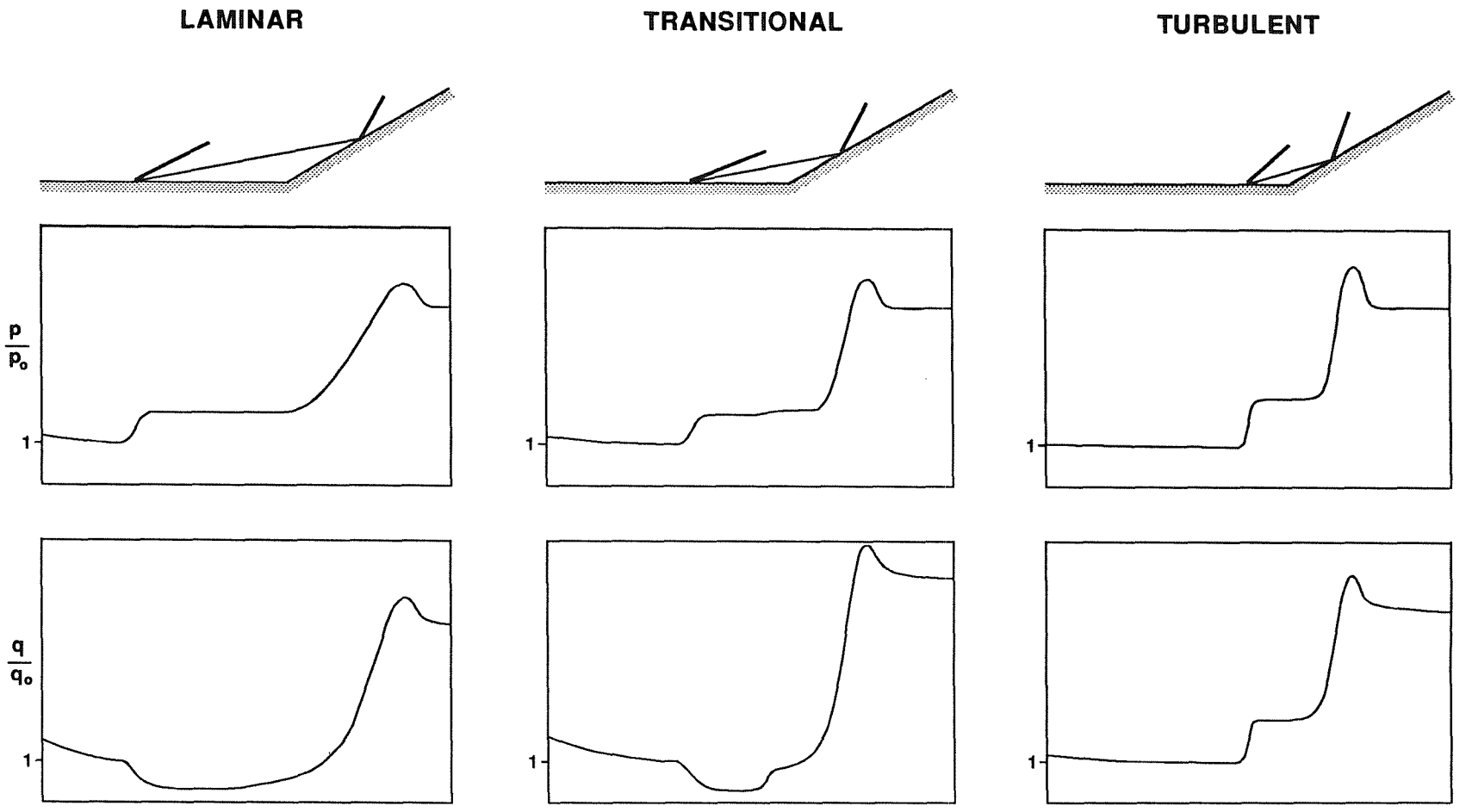

Fig.4. Typical form of surface pressure, and heat transfer, distributions in compression corner separated hypersonic flows (not scaled).

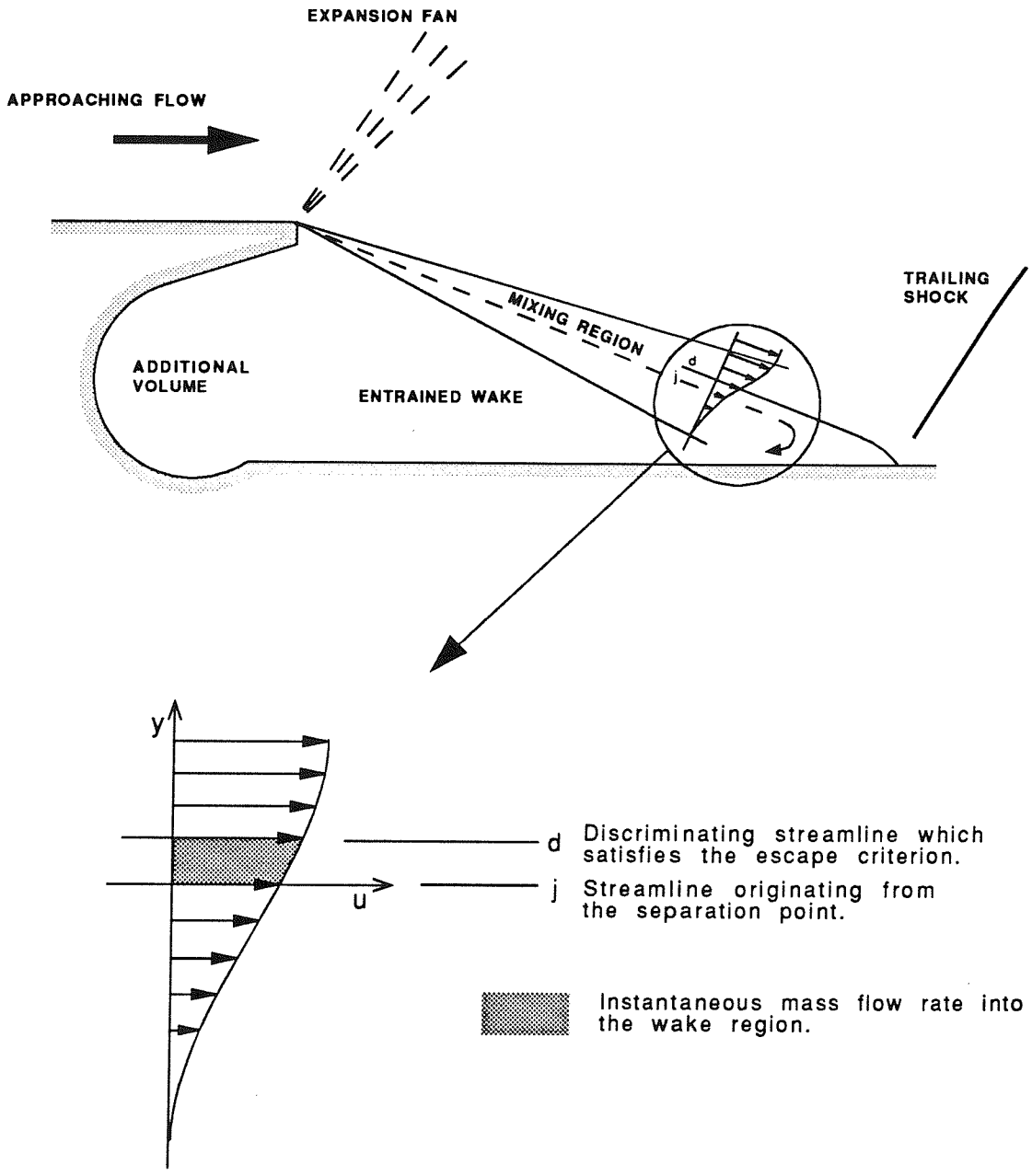

Fig.5. Mass transfer mechanism to an unsteady base separated flow (Ihrig & Korst 1963).

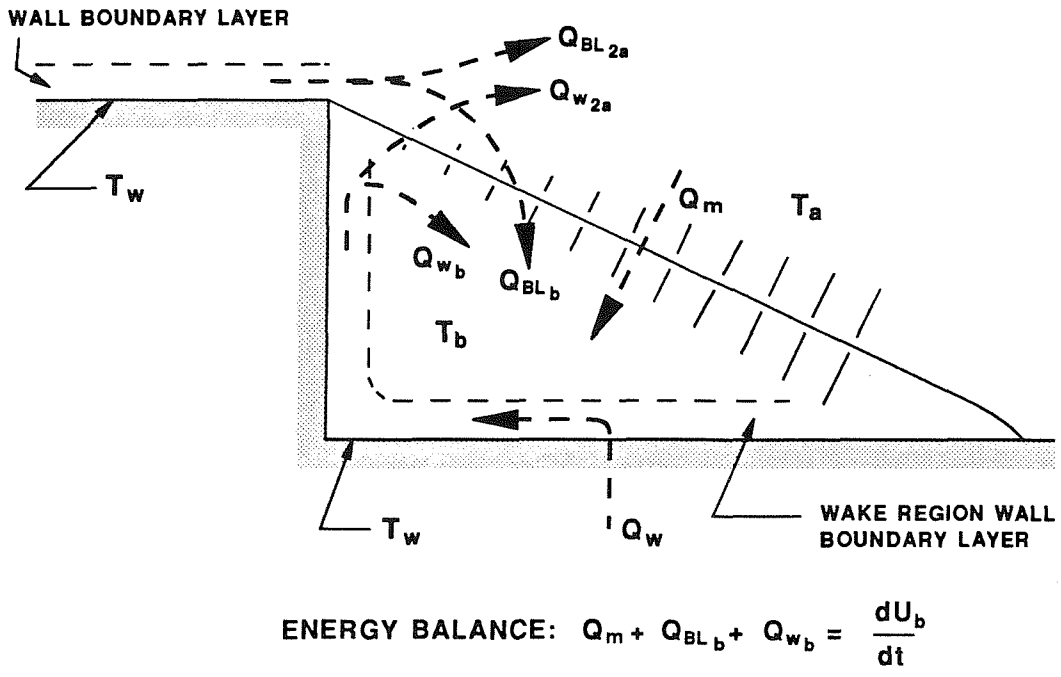

Fig.6. Wake transient energy system proposed by Battin (1963).

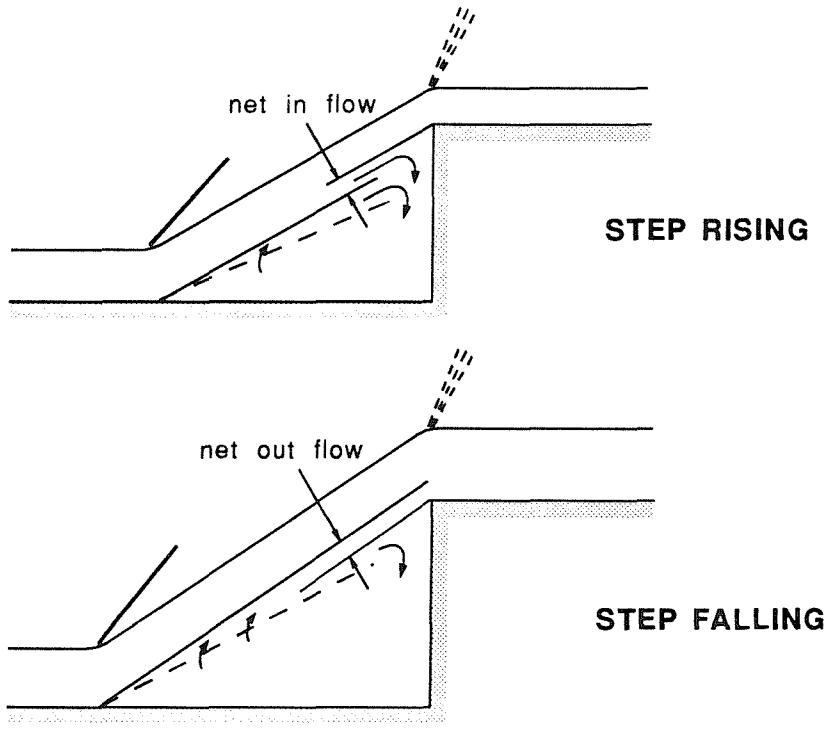

Fig.7. Wilkinson's (1966) model of mass transfer adjustment in an unsteady separated flow.

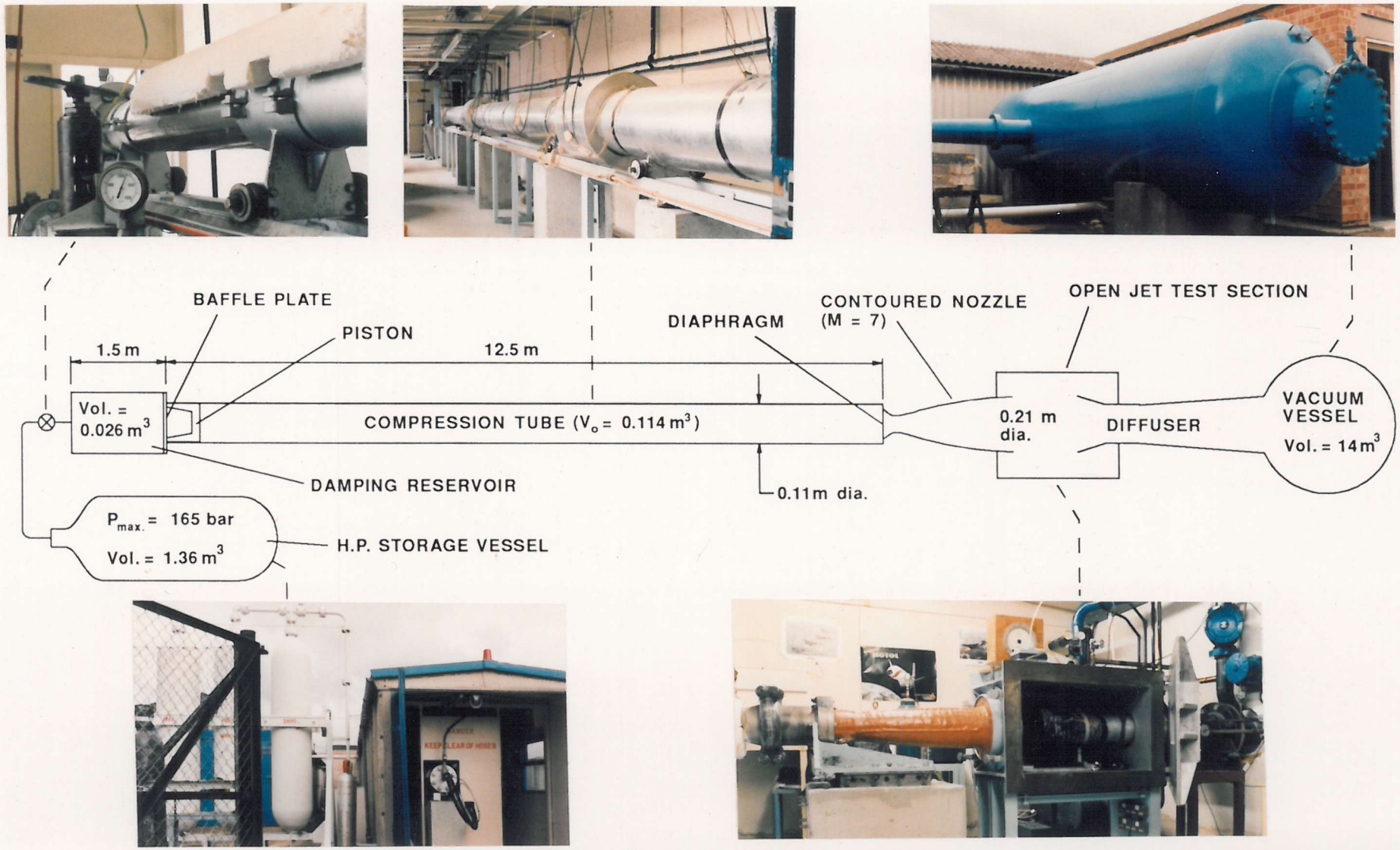

Fig.8. The University of Southampton ILPT hypersonic wind tunnel.

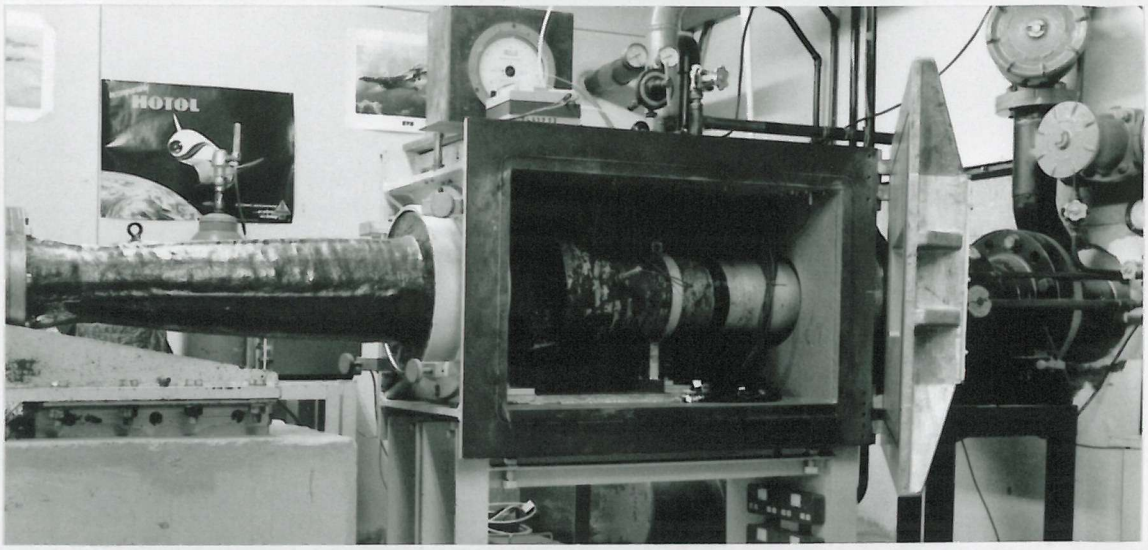

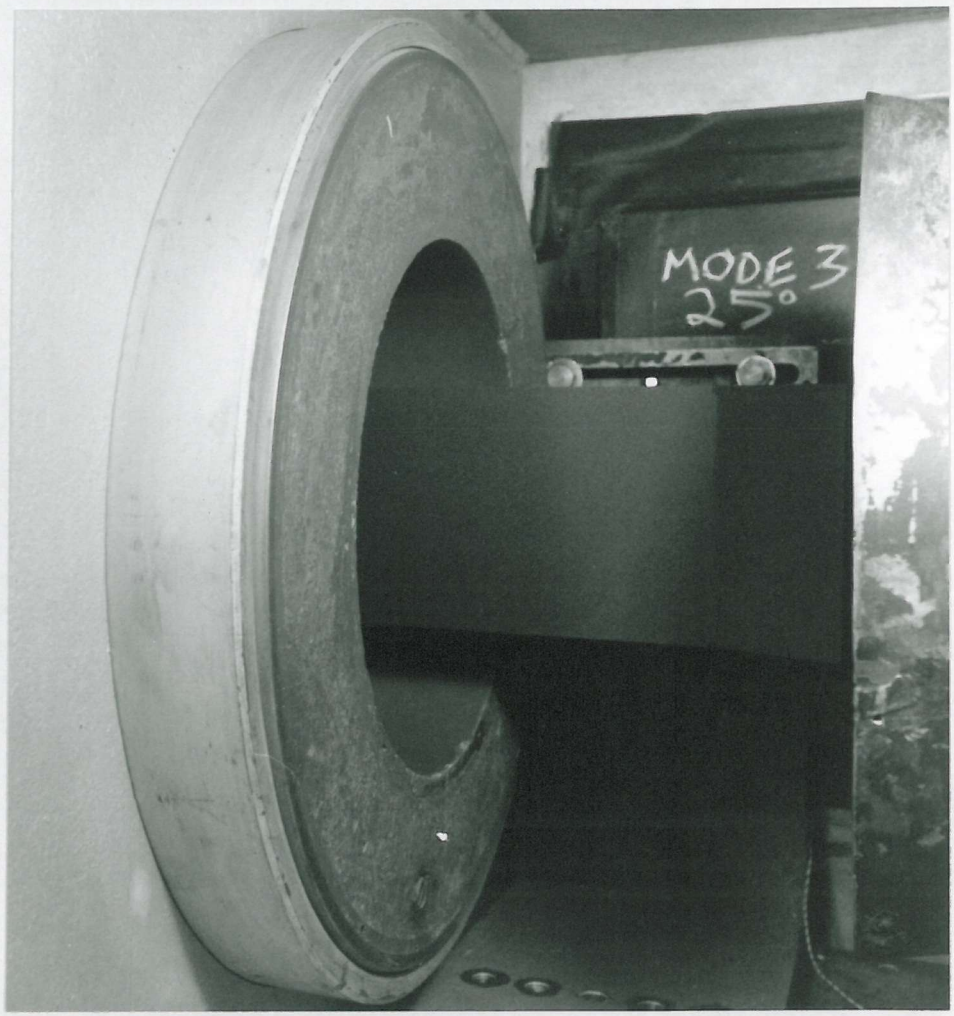

Fig.9. The ILPT open jet test section.

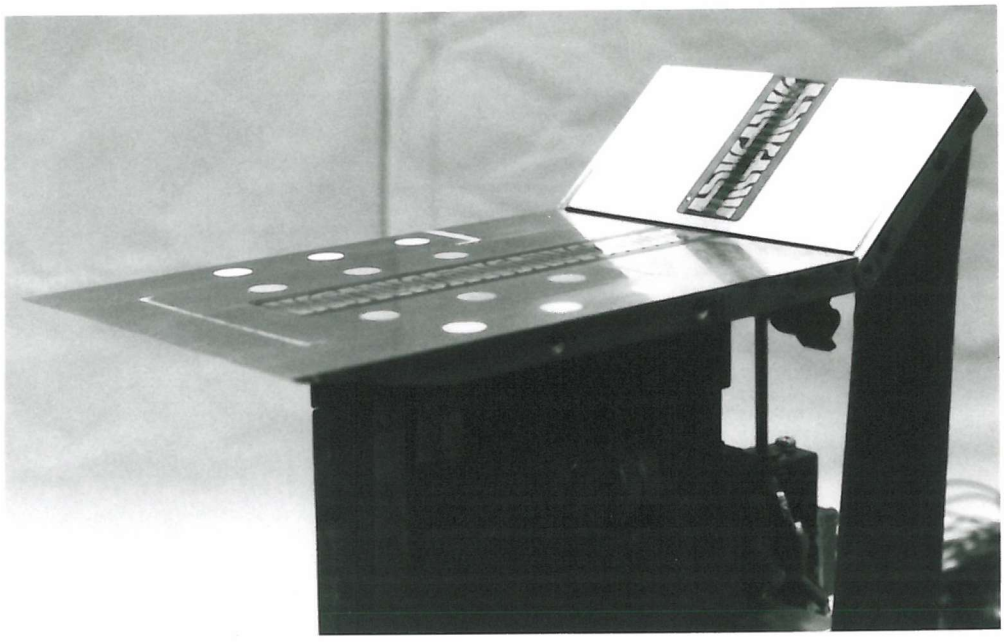

Fig.10. The fixed / dynamic flap test model.

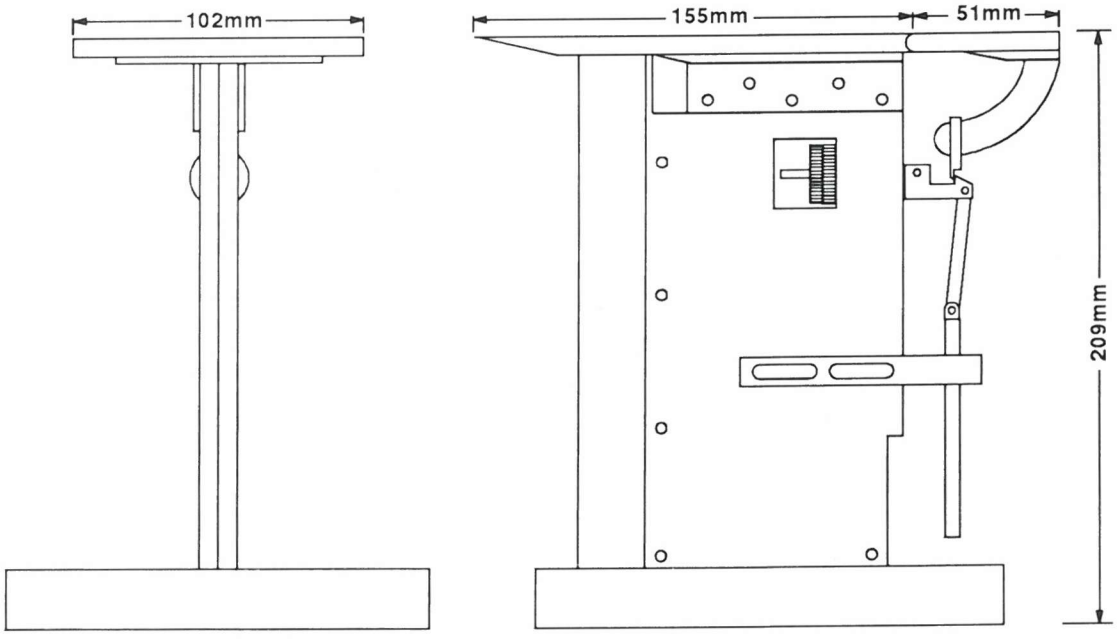

Fig.11. Test model dimensions.

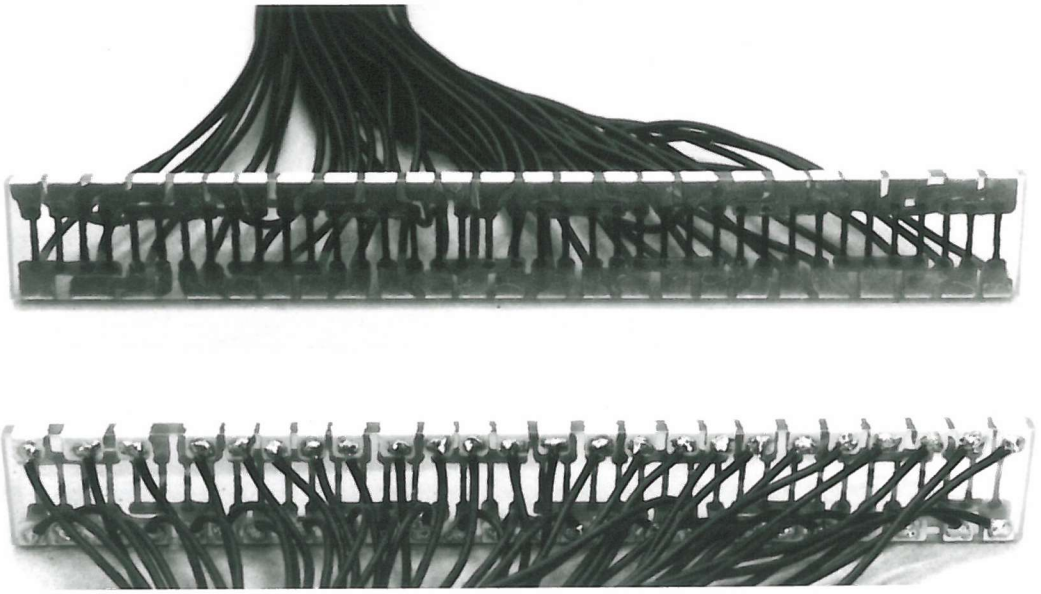

Fig.12. Example of a thin film gauge insert.

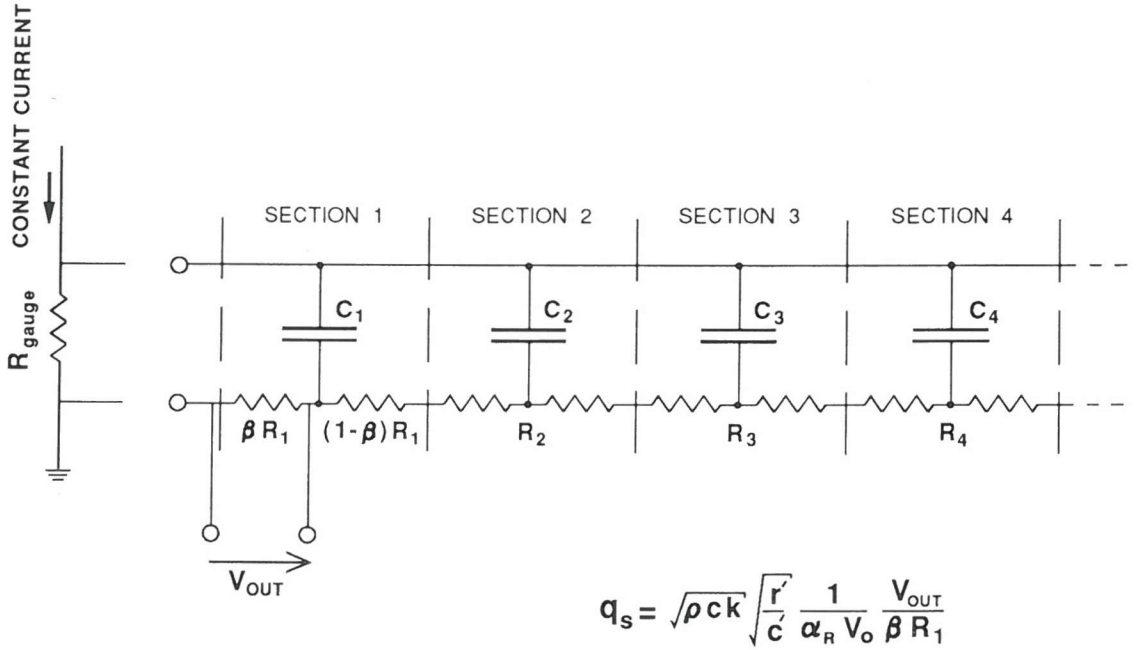

Fig.13. Conventional RC analogue arrangement with the thin film resistance gauge temperature signal.

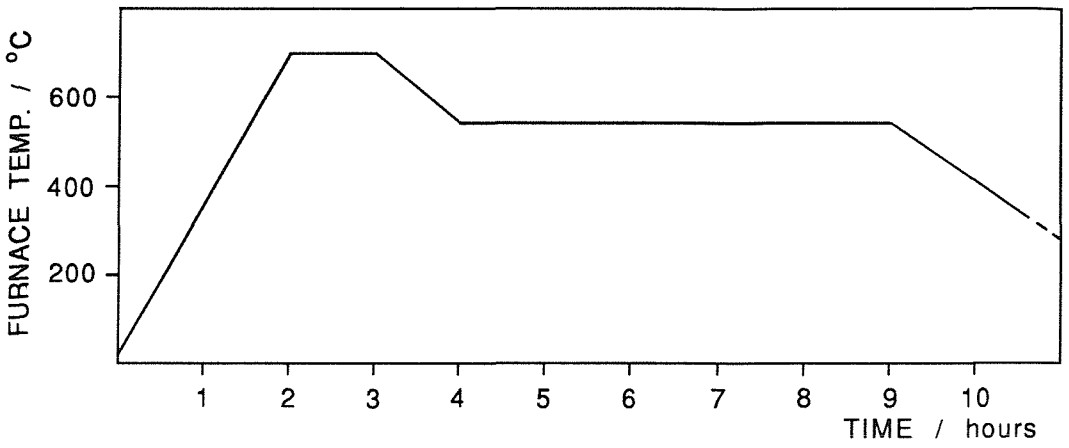

Fig.14. Firing cycle for the manufacture of painted thin film resistance gauges.

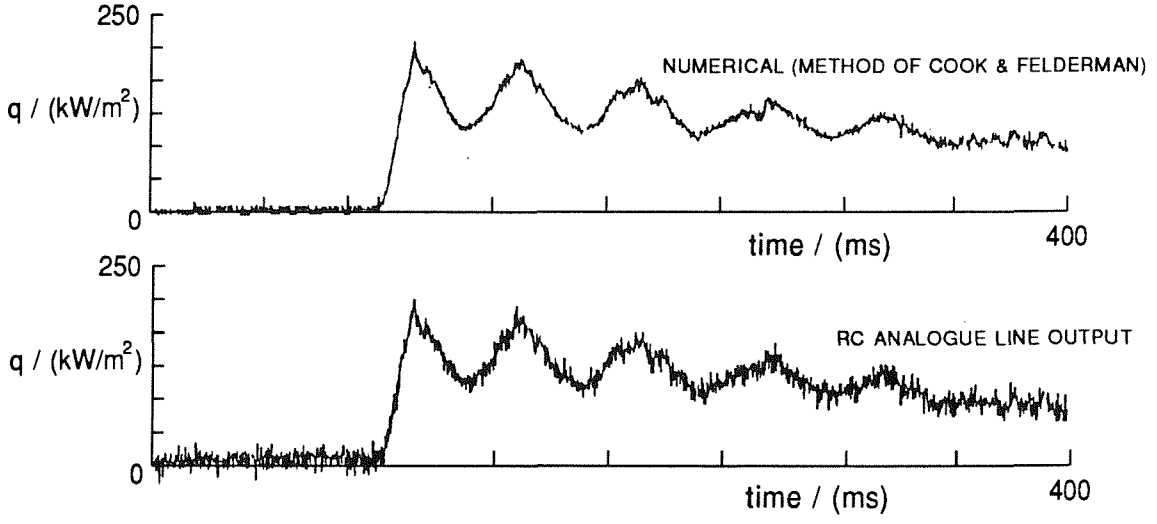

Fig.15. Comparison of an RC analogue, and numerical, conversion of temperature to heat transfer.

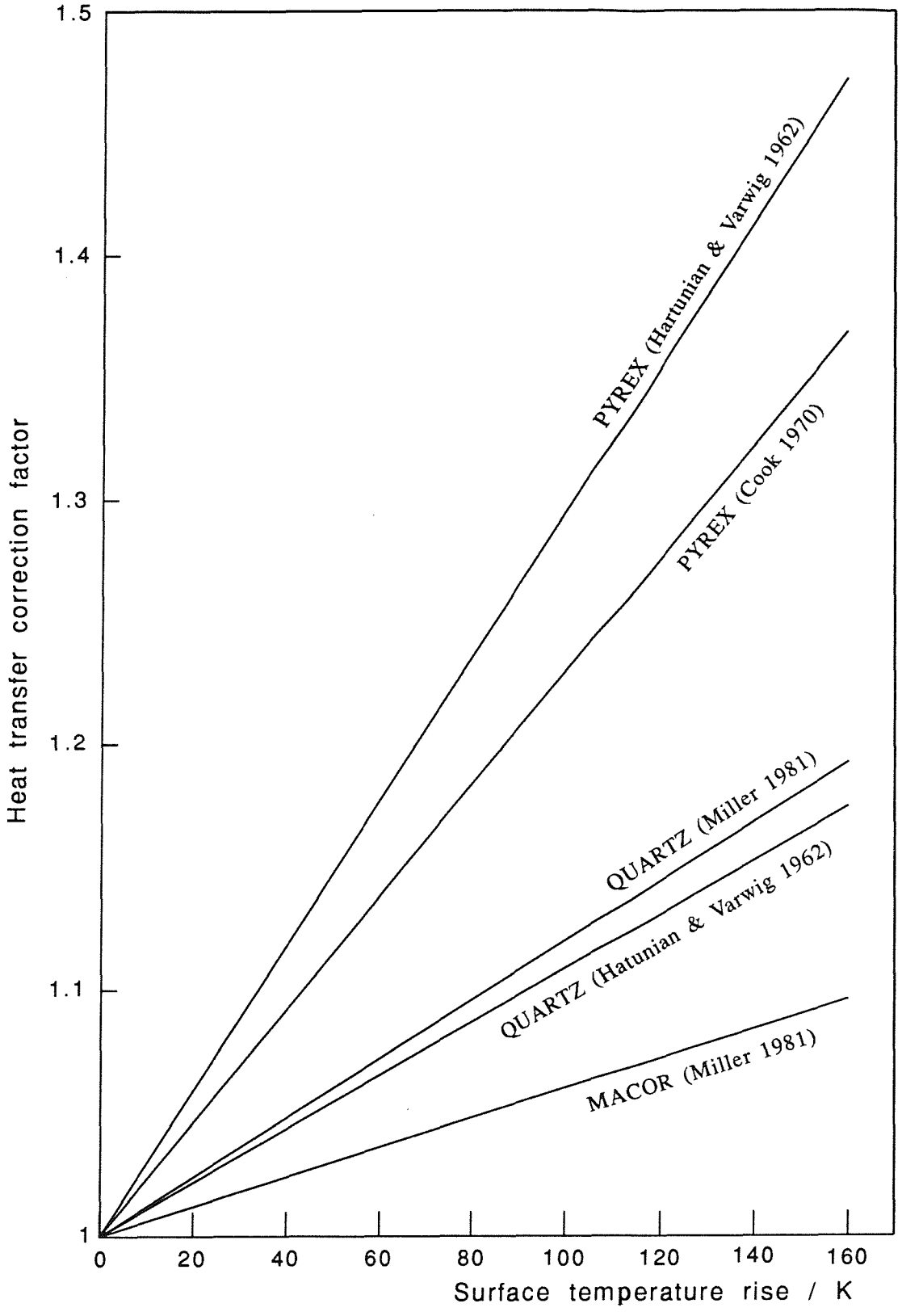

Fig.16. Correction factor for the measured heat transfer to account for the temperature effects on the substrate ρck.

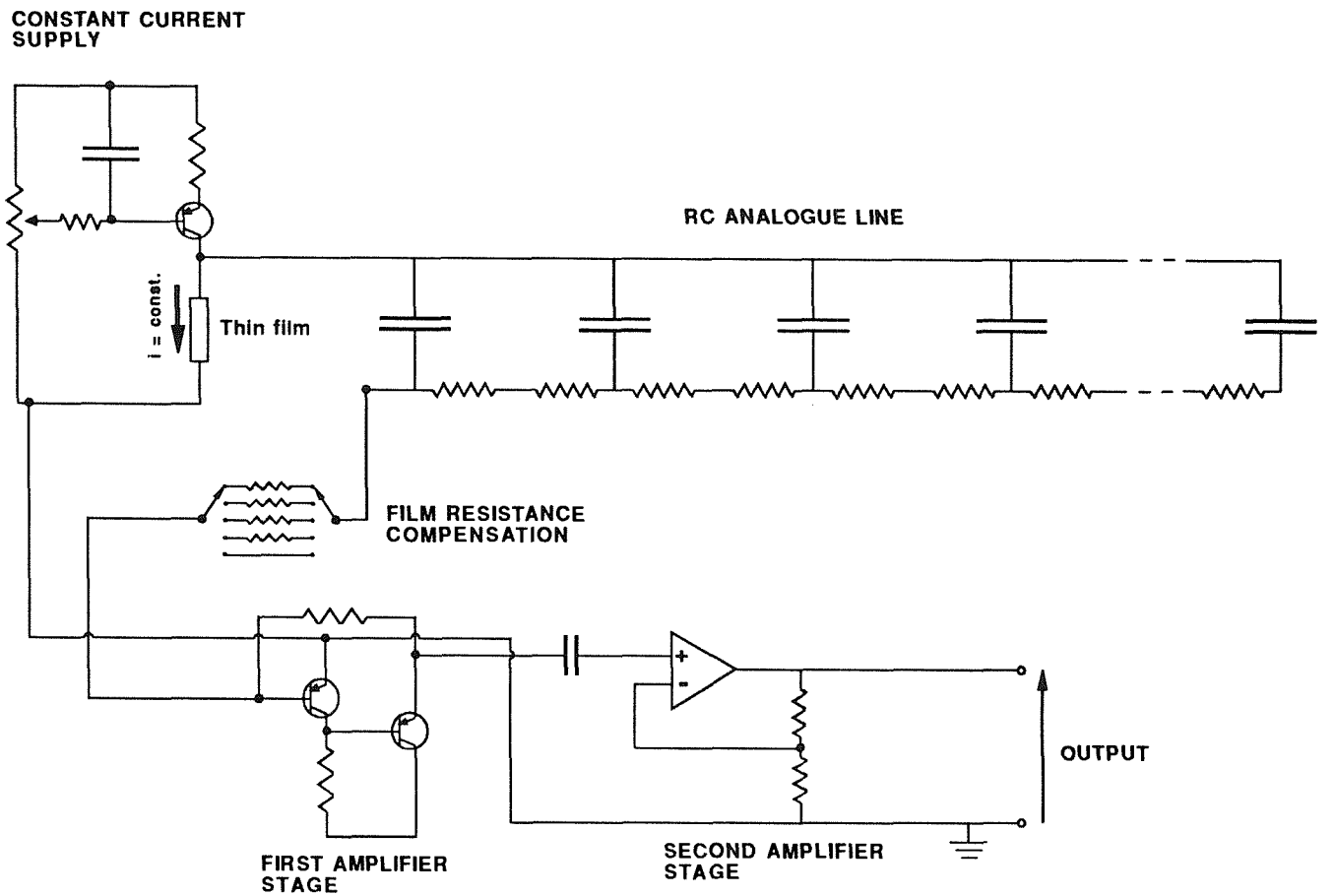

Fig.17. Low noise circuit arrangement for the measurement of heat transfer with thin film resistance gauges.

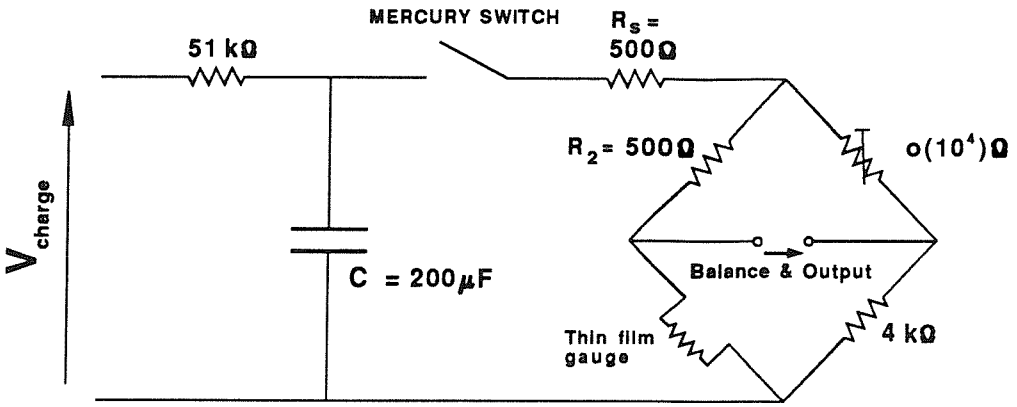

Fig.18. Calibration circuit for the gauge substrate thermal product.

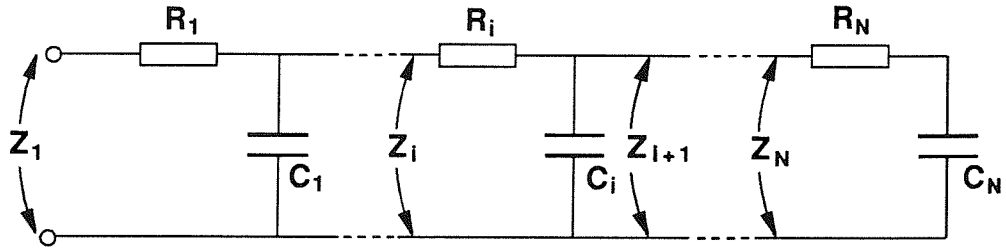

$$Z_i = R_i + \frac{Z_{i+1}}{1 + j\omega C_i Z_{i+1}} \qquad Z_N = R_N + \frac{1}{j\omega C_N}$$

Fig.19. Numerical evaluation of an RC analogue input impedance v's frequency.

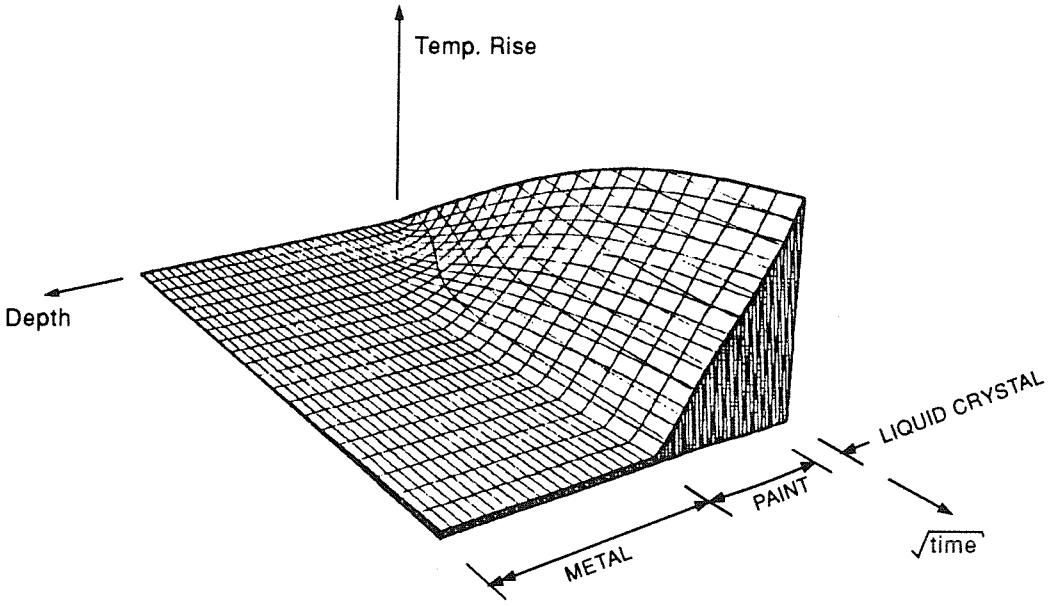

Fig.20. Temperature distribution through the three substrate model of liquid crystal, paint, and semi-infinite metal base.

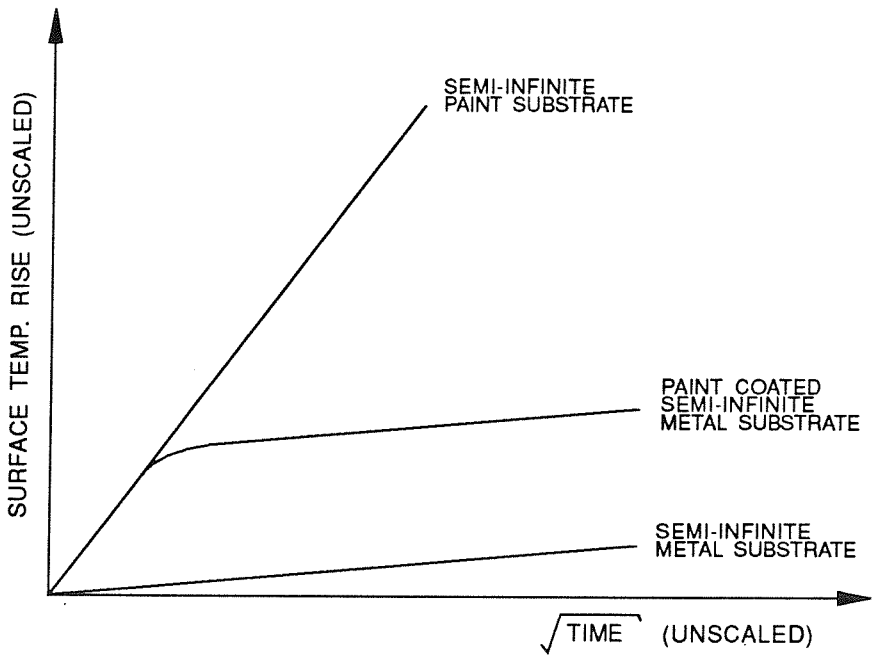

Fig.21. Surface temperature rise for different types of semi-infinite model substrate construction.

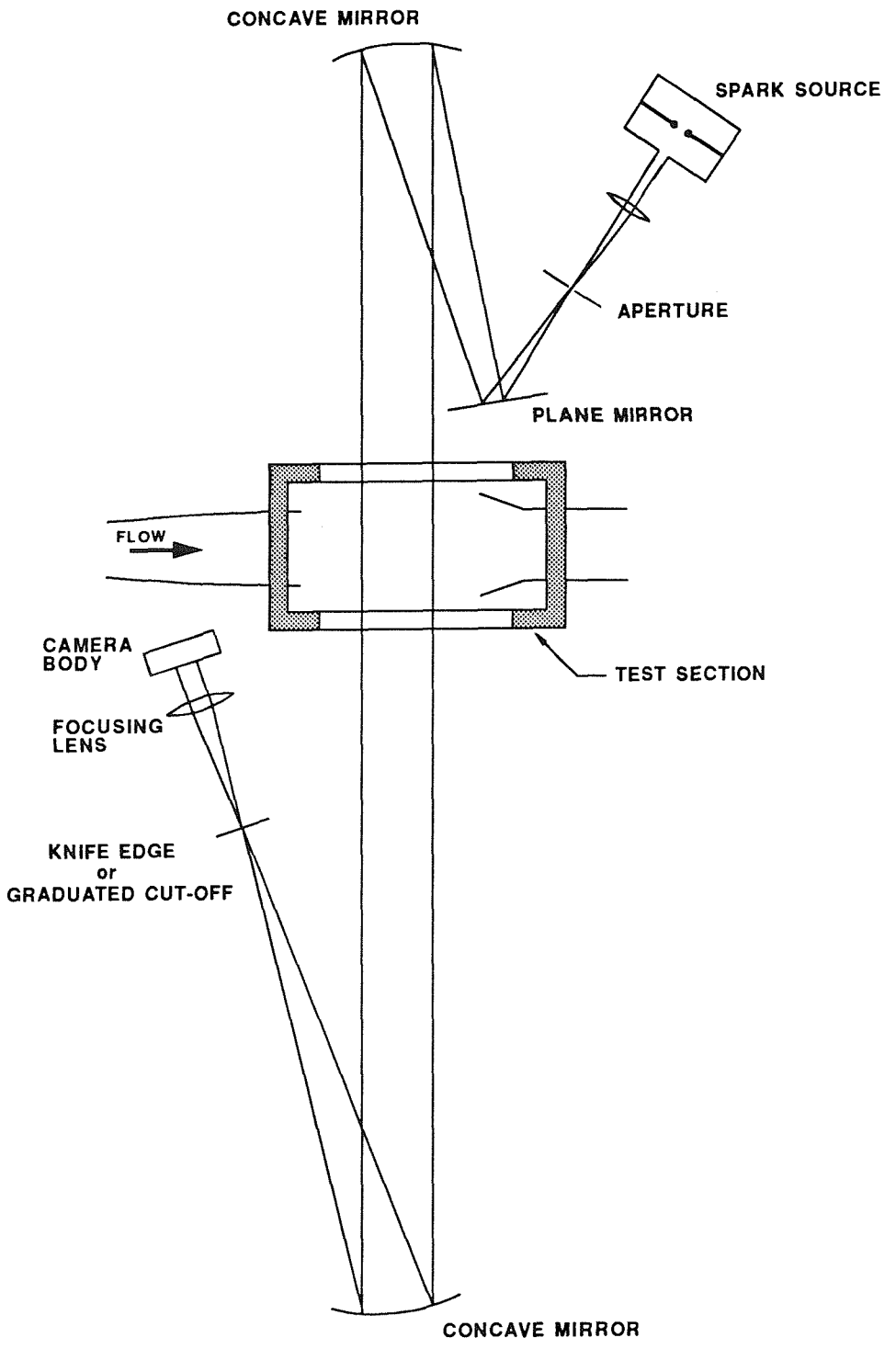

Fig.22. Layout of the conventional single pass schlieren system.

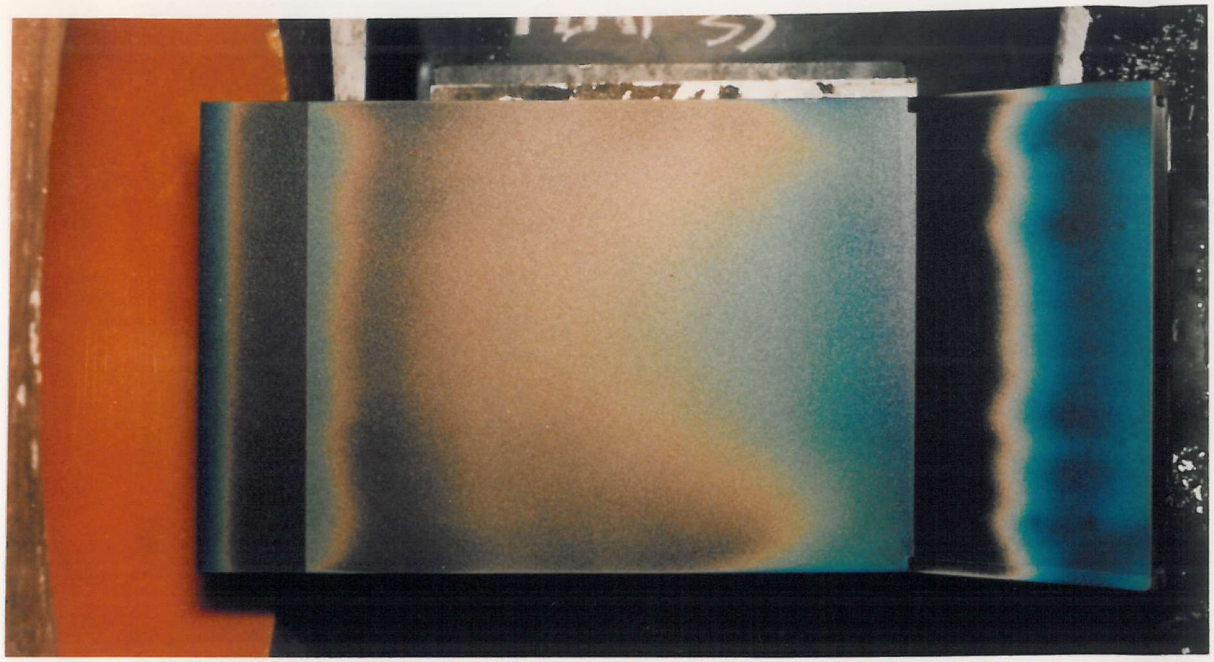

a. Model position downstream of the nozzle exit plane.
Flap angle = 35 degrees. No side plates.

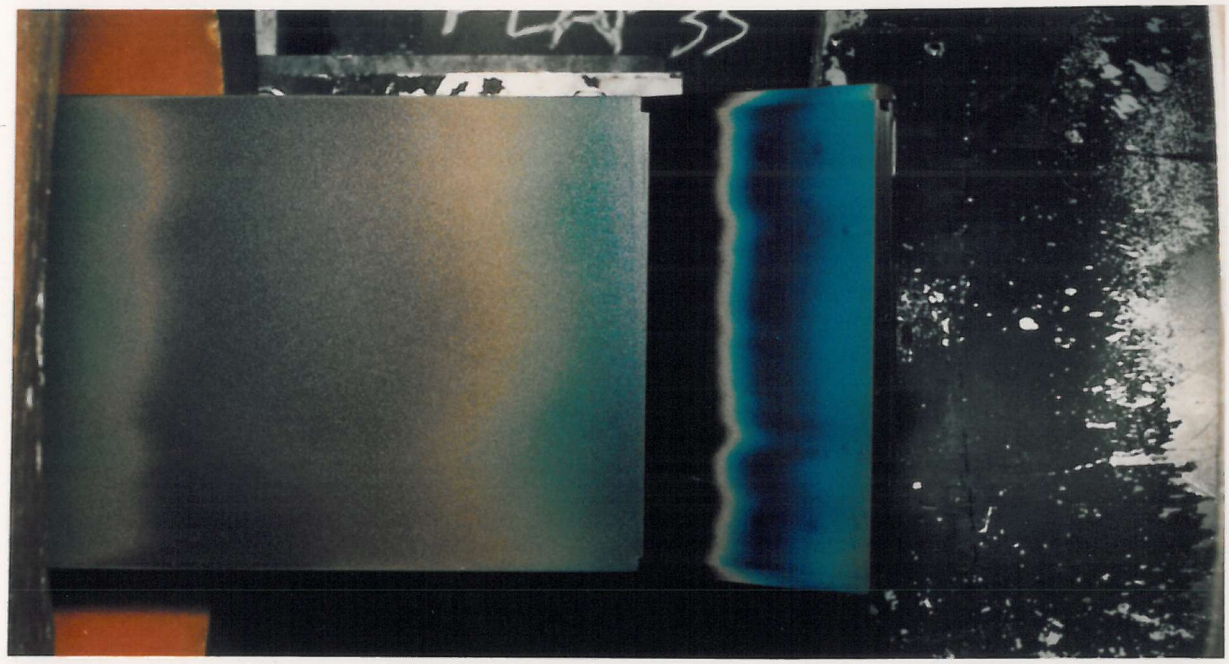

b. Model in its forward position.
Flap angle = 35 degrees. No side plates.

Fig.23. Liquid crystal surface thermographs. Effects of the model position, flap angle, and side plates. M_∞ = 6.85, Re_∞ = 2.45x10^6/m.

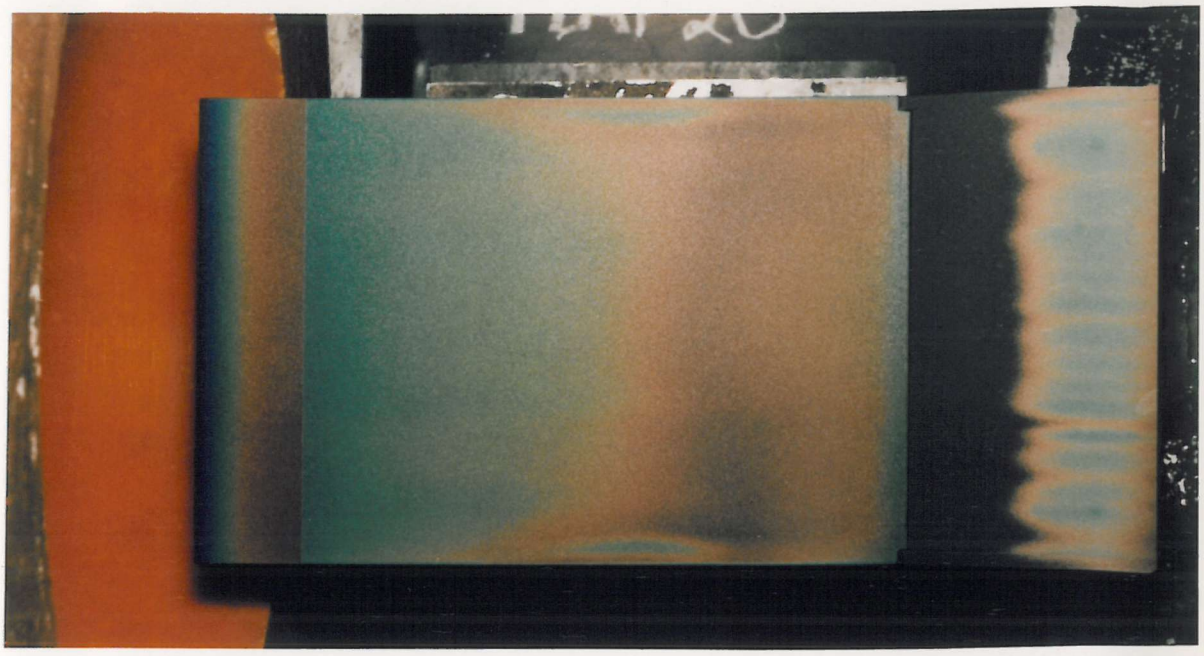

c. Model position downstream of the nozzle exit plane.
Flap angle = 20 degrees. No side plates.

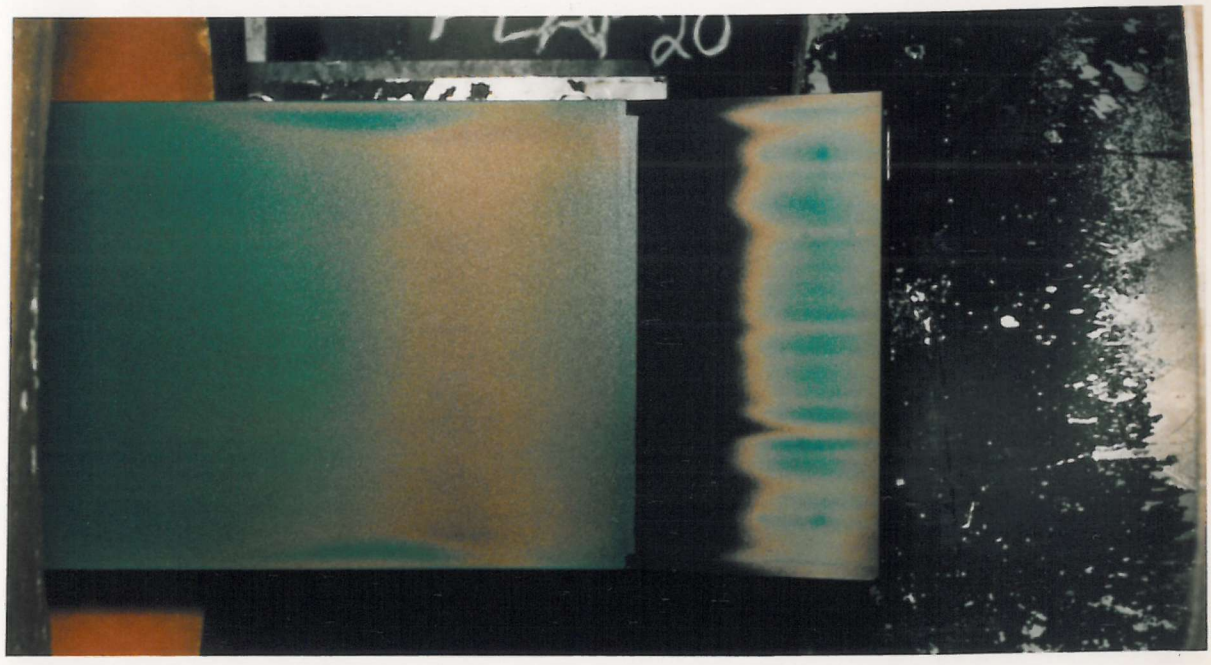

d. Model in its forward position.
Flap angle = 20 degrees. No side plates.

Fig.23. continued.

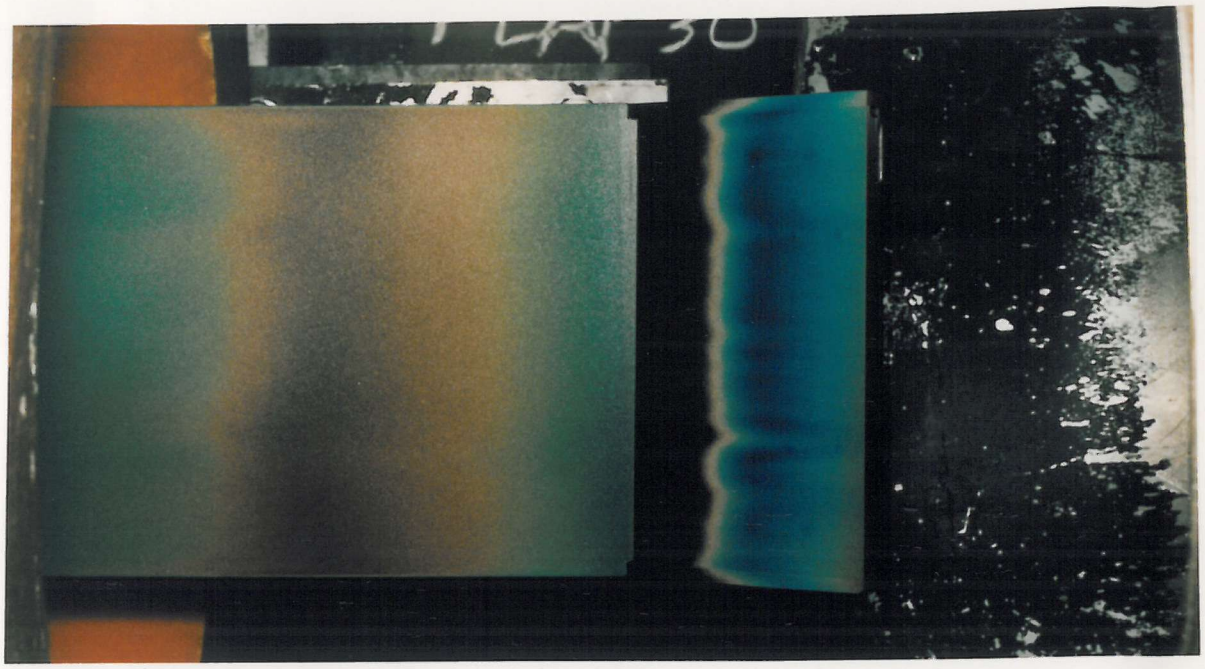

e. Flap angle = 30 degrees. No side plates.

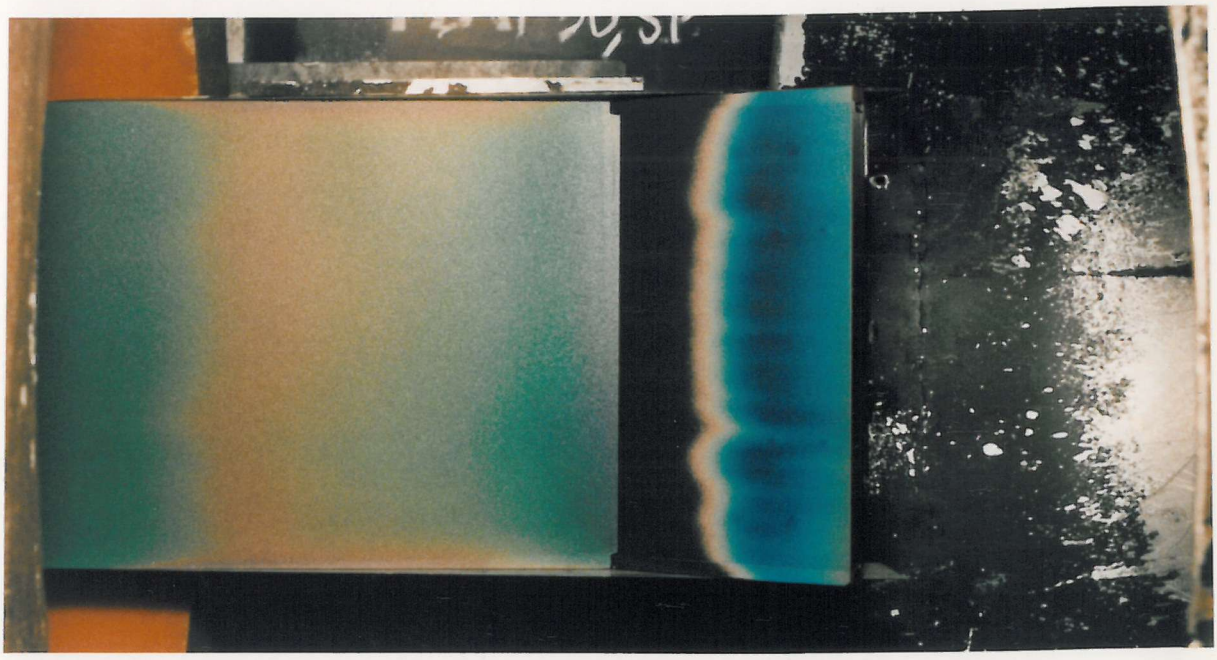

f. Flap angle = 30 degrees. Side plates fitted.

Fig.23. continued.

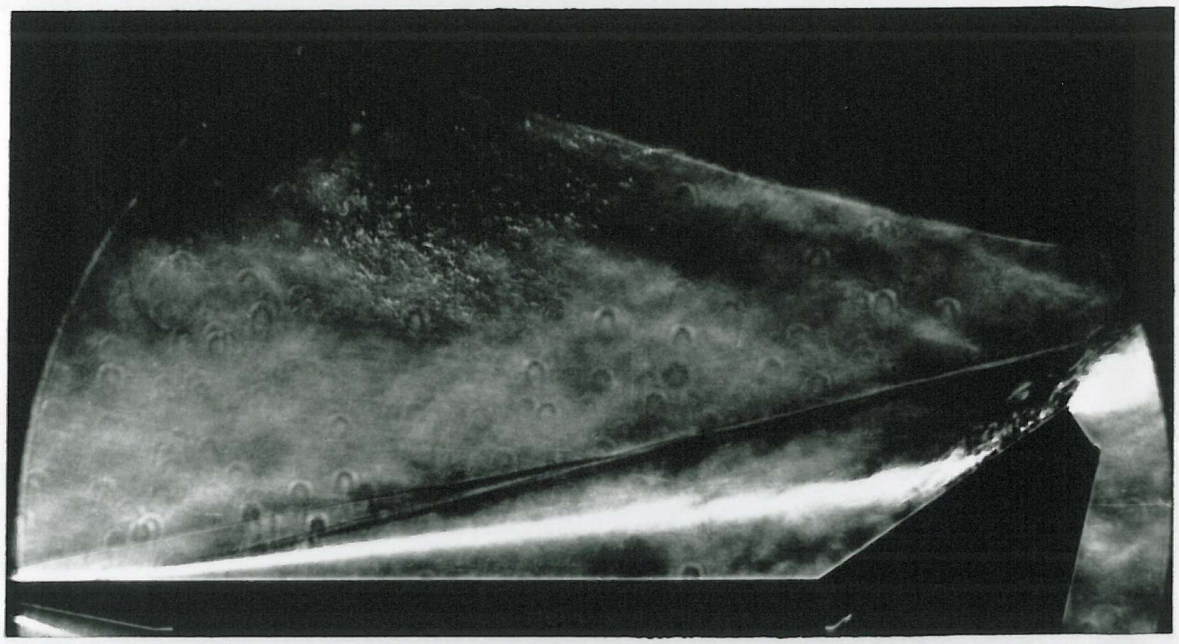

a. Model position downstream of the nozzle exit plane.

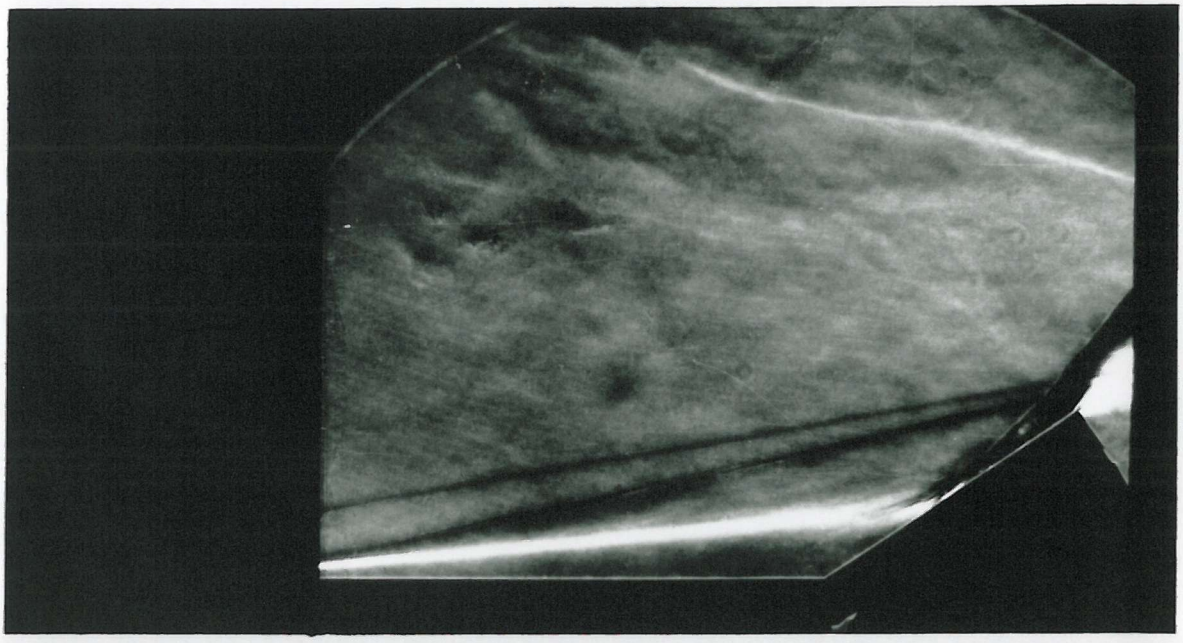

b. Model in its forward position.

Fig.24. Schlieren flow visualisation. Effect of the model position. Flap angle = 35 degrees. M_∞ = 6.85, Re_∞ = 2.45x10^6/m.

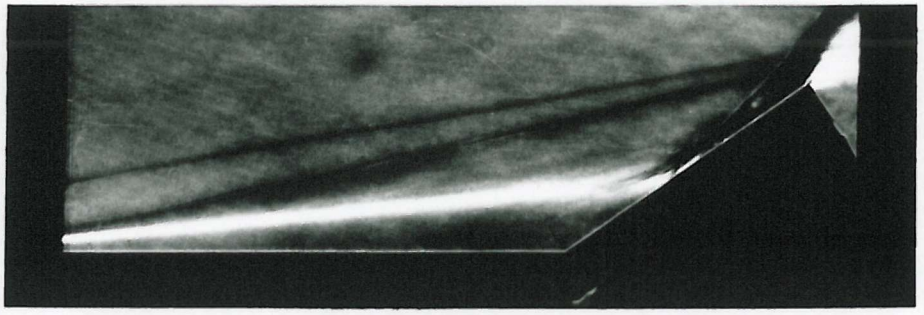

a. $Re_\infty = 2.45 \times 10^6$/m.

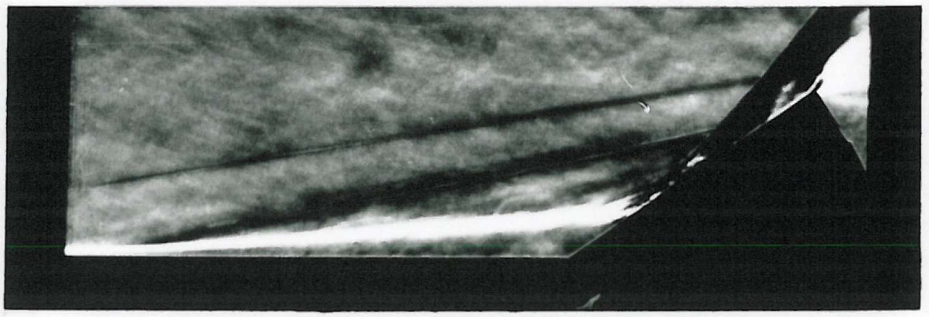

b. $Re_\infty = 6.45 \times 10^6$/m.

c. $Re_\infty = 9.72 \times 10^6$/m.

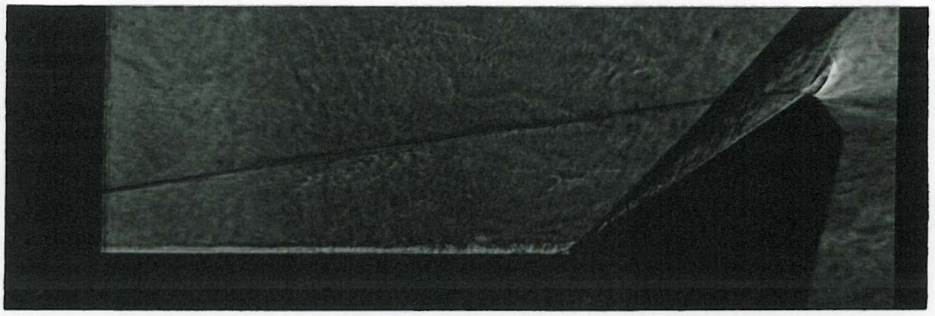

d. $Re_\infty = 3.30 \times 10^7$/m.

Fig.25. Schlieren flow visualisation. Effect of freestream Reynolds number. Flap angle = 35 degrees. $M_\infty = 6.85$.

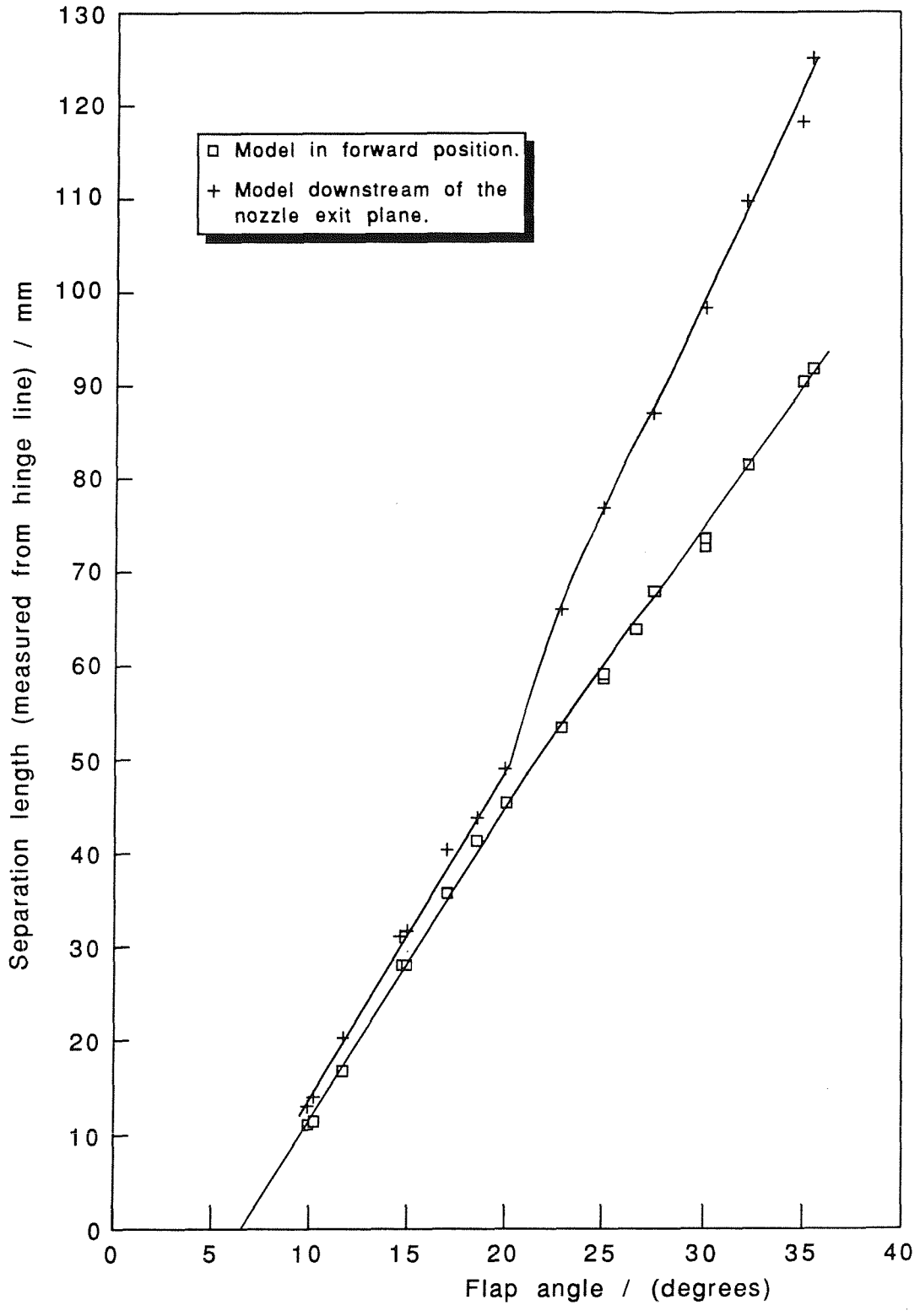

Fig.26. Fixed flap separation lengths (measured from the schlieren photographs). Effect of the model position. M_∞= 6.85, Re_∞= 2.45x10^6/m.

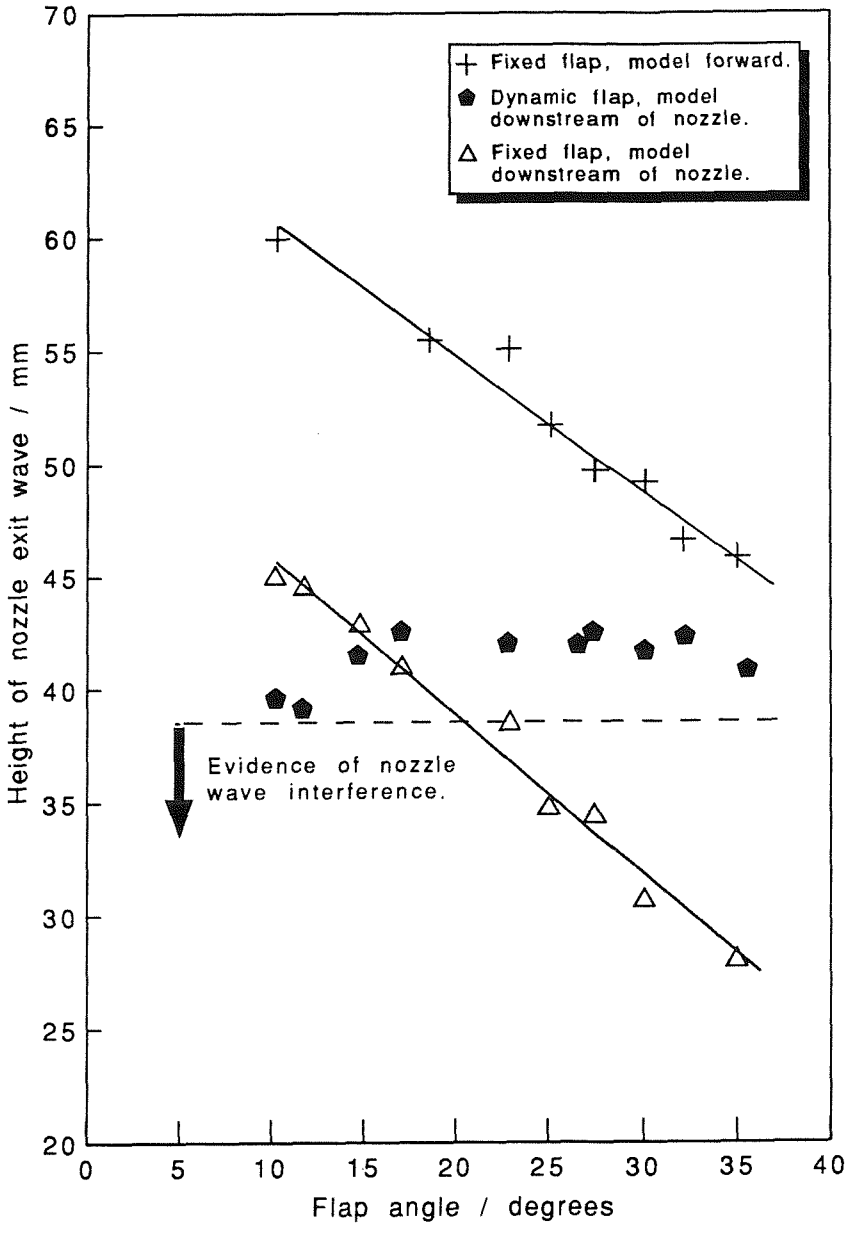

Fig.27. Nozzle wave heights above the flow centre line (at the flap trailing edge location). M_∞= 6.85, Re_∞= 2.45x10^6/m.

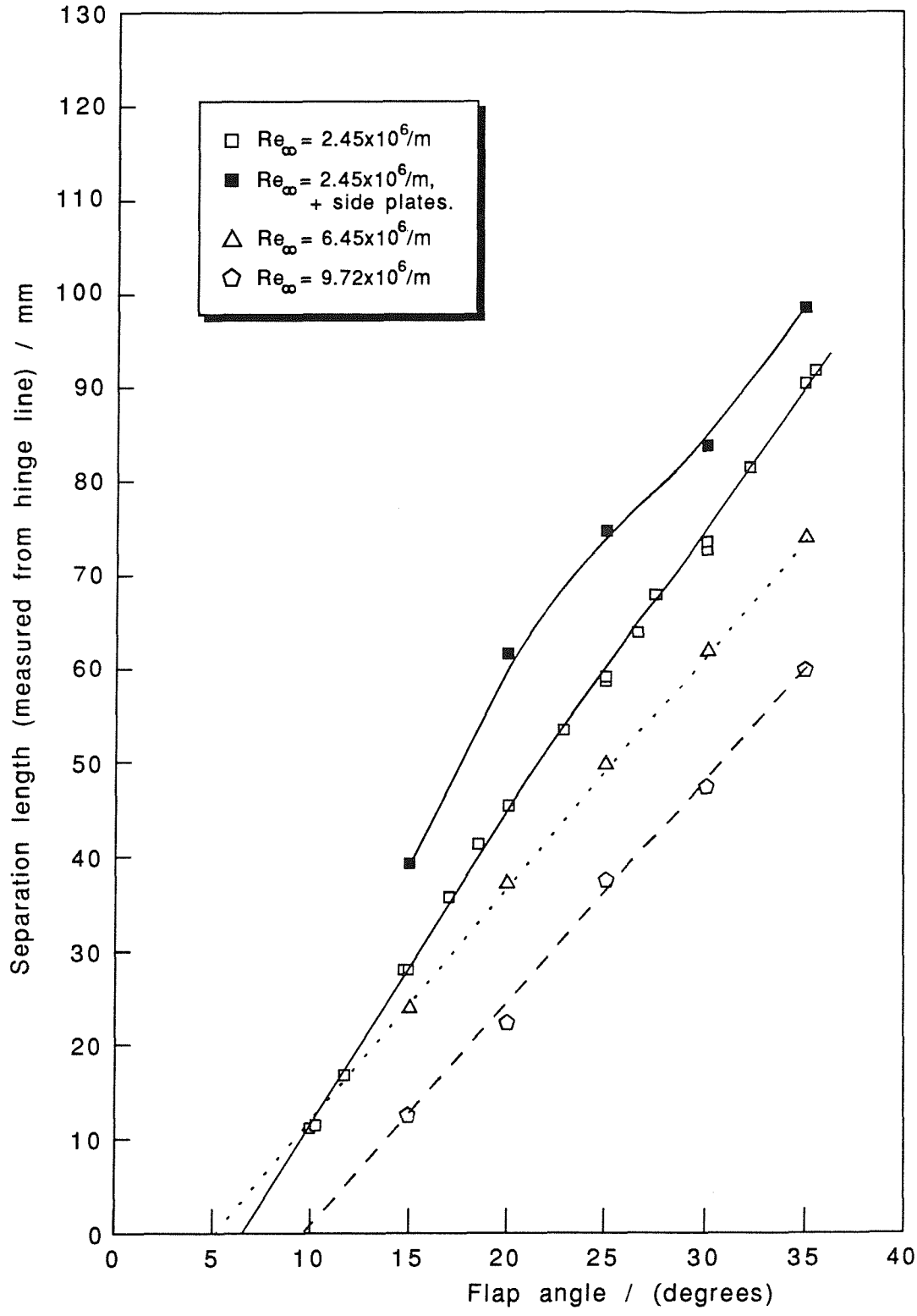

Fig.28. Fixed flap separation lengths with the model moved forward (measured from the schlieren photographs). Effect of the freestream Reynolds number. M_∞= 6.85.

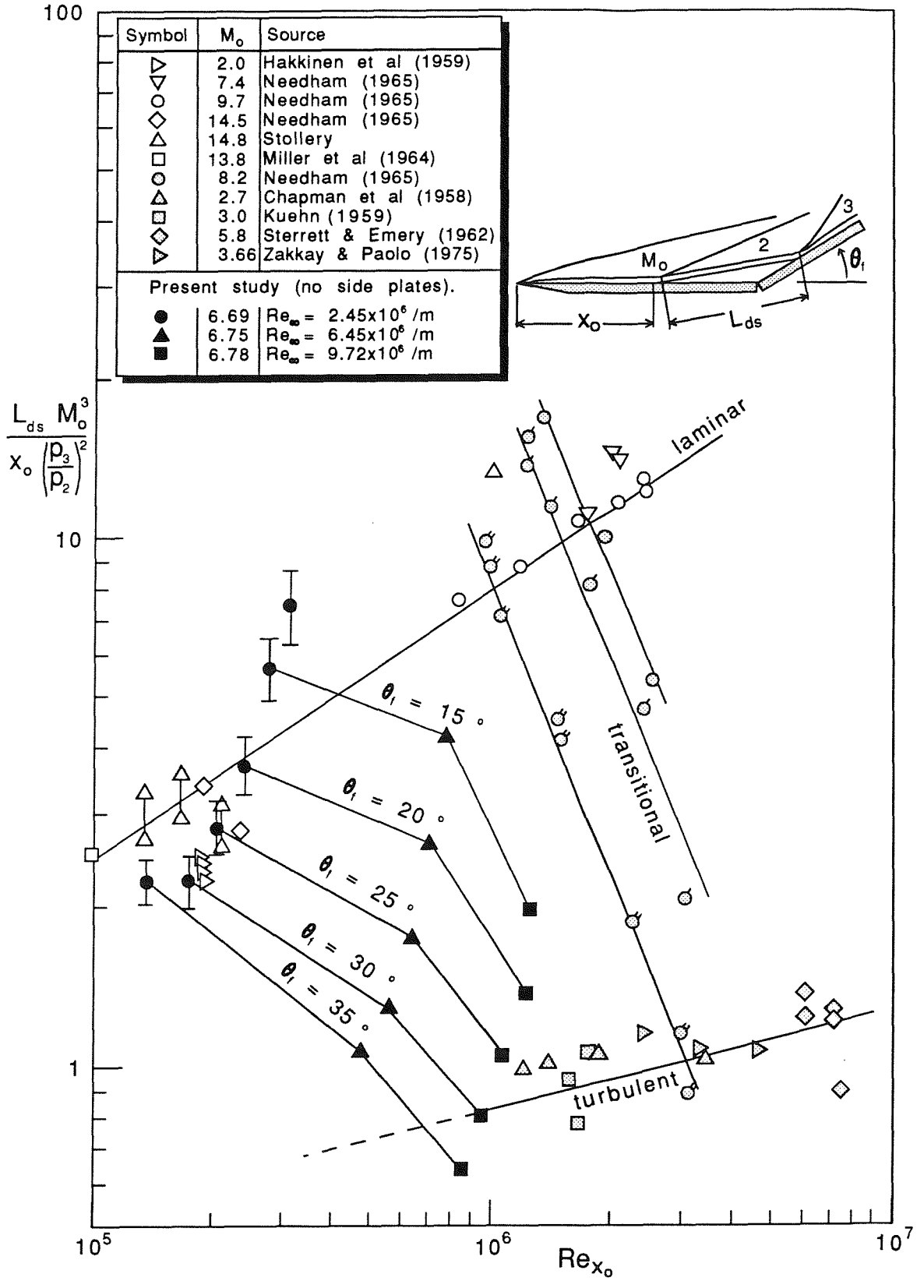

a. Needham & Stollery (1966b) parameters.

Fig.29. Correlation of the separation lengths.

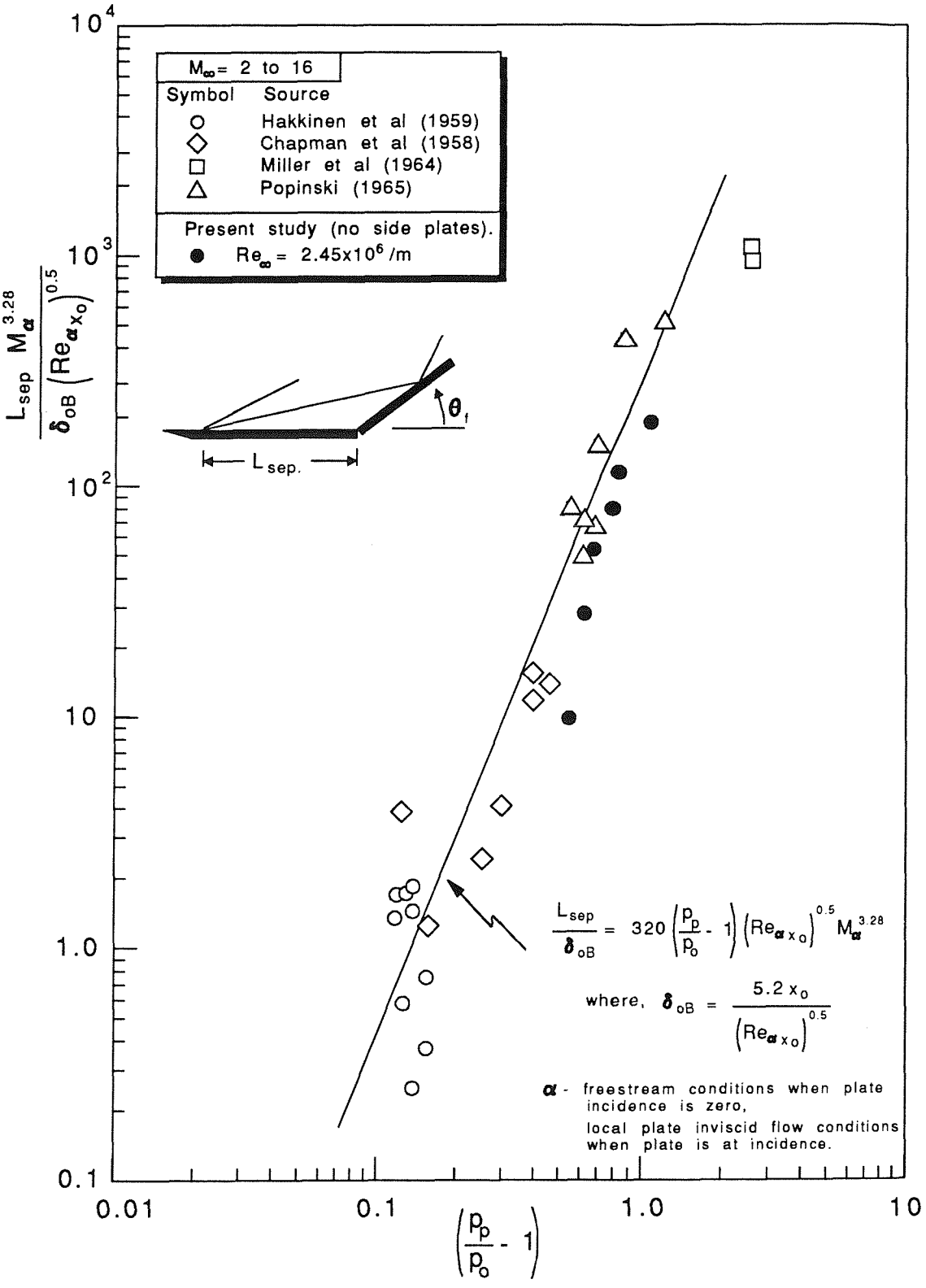

b. Popinski & Ehlrich (1966) parameters for fully laminar separations.

Fig.29. continued.

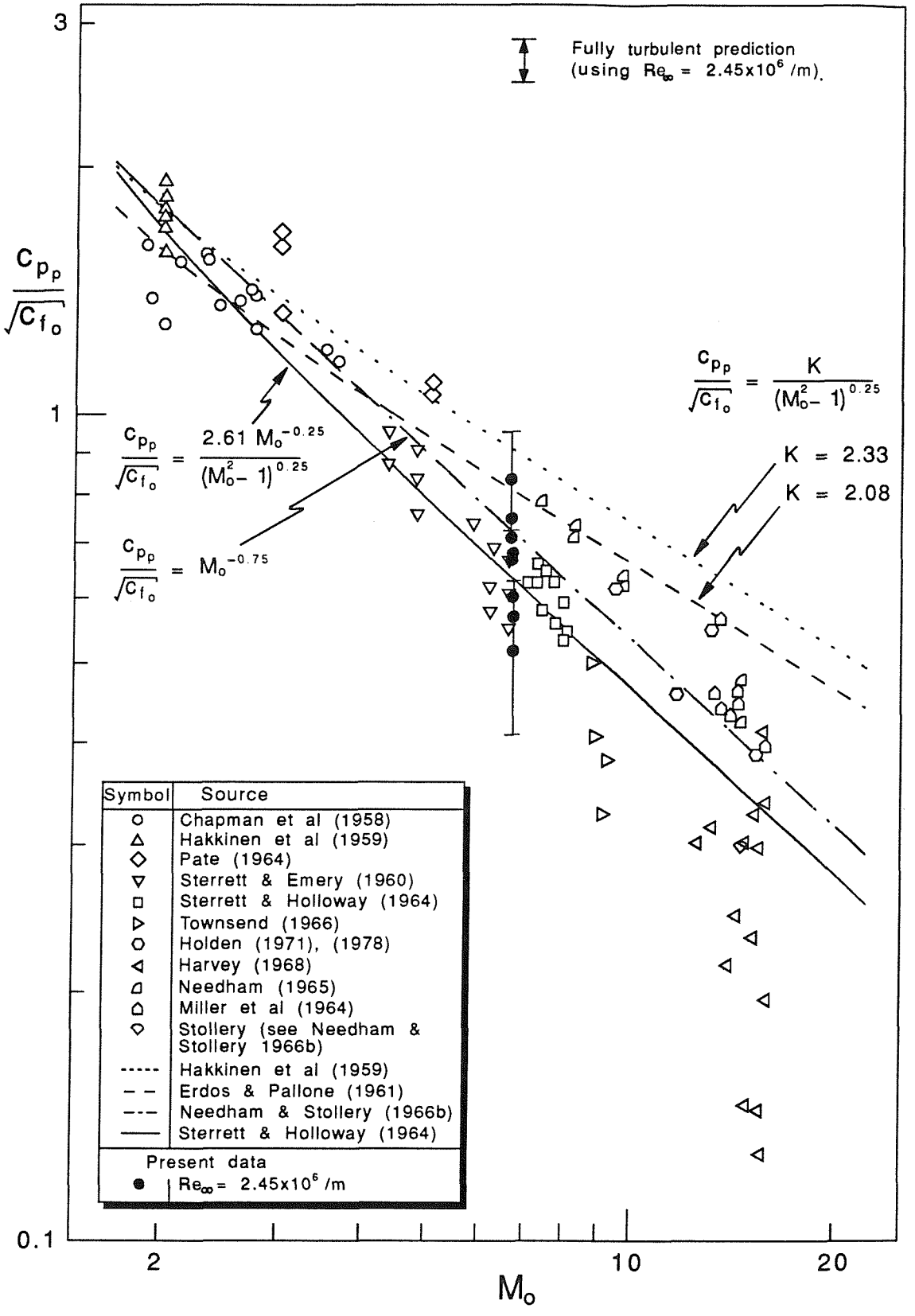

Fig.30. Correlation of laminar plateau pressures using Chapman's (1958) free-interaction parameters.

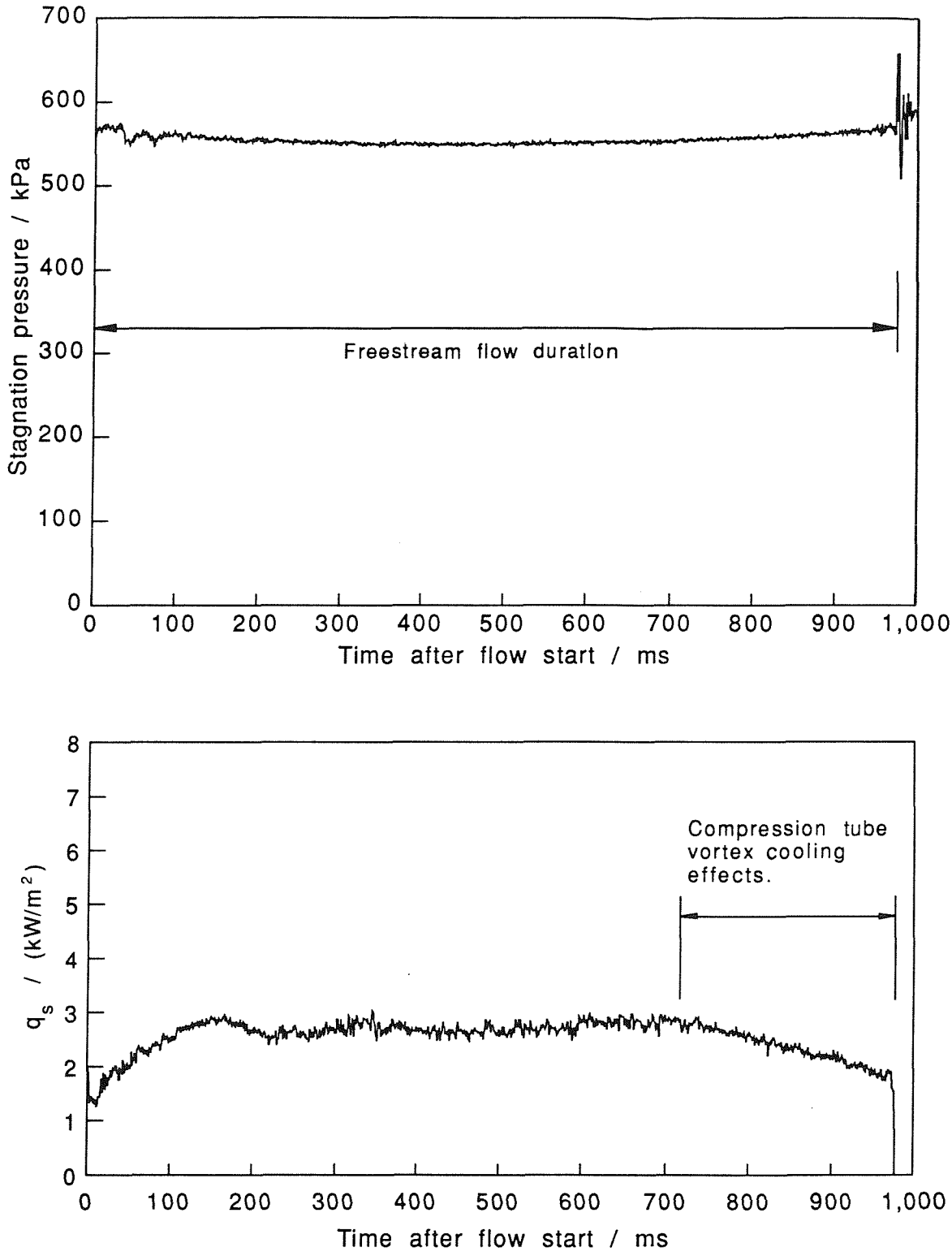

Fig.31. Comparison of the absolute stagnation pressure, and heat transfer signal from the first plate thin film resistance gauge (ahead of the separation interaction). M_∞= 6.85, Re_∞= 2.45x10^6/m.

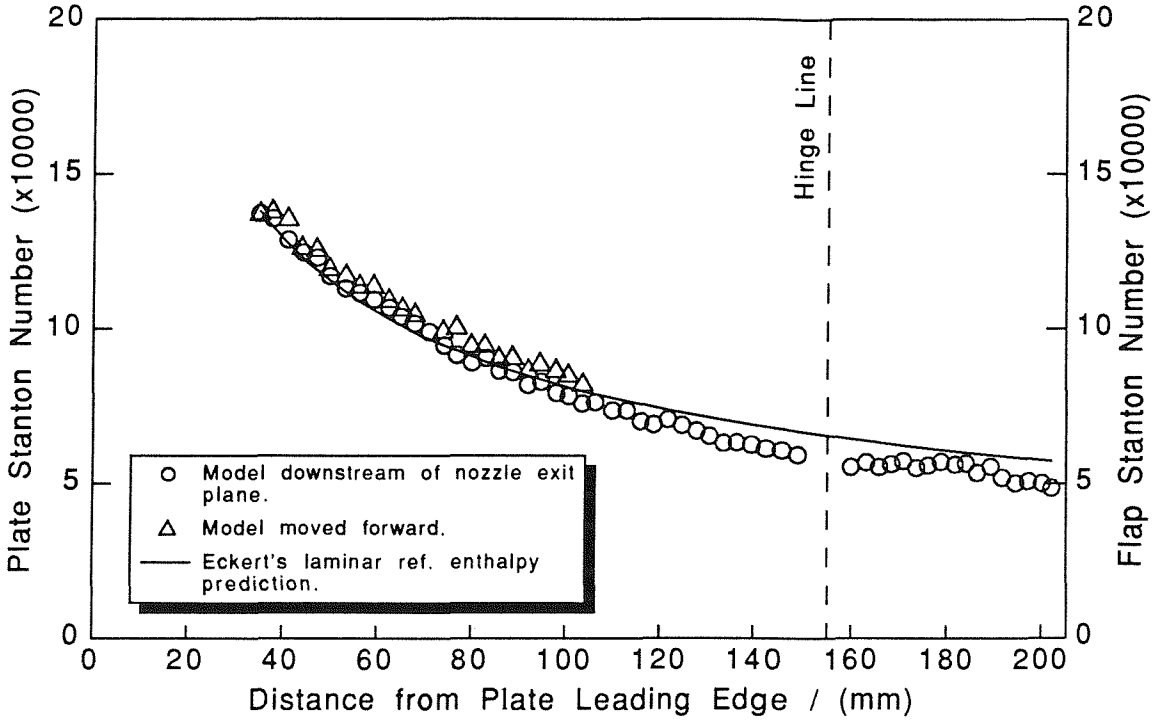

Fig.32. Flat plate heat transfer distribution. $M_\infty = 6.85$, $Re_\infty = 2.45 \times 10^6/m$.

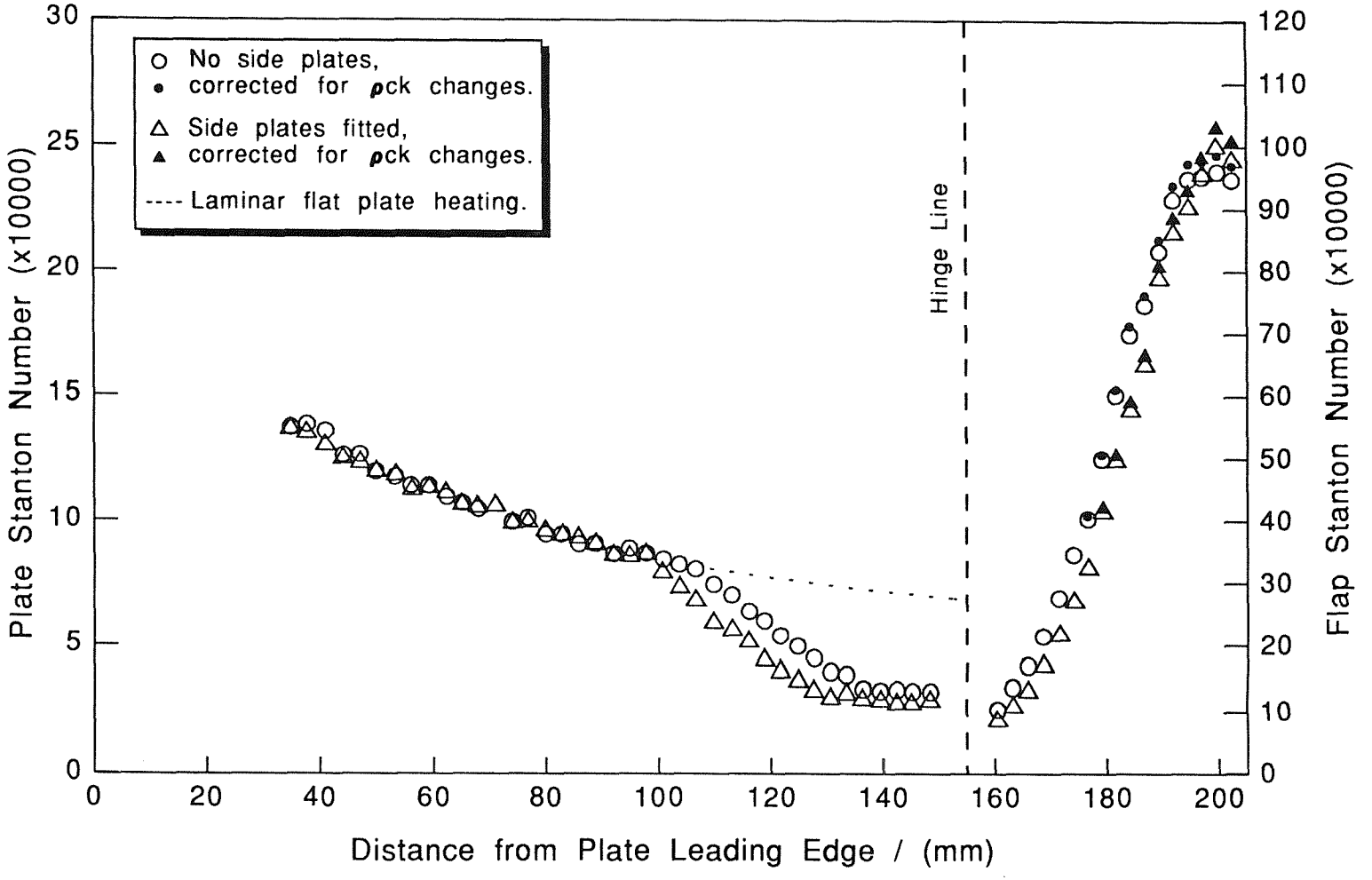

a. Flap angle = 15 degrees.

Fig.33. Heat transfer distributions at fixed flap angles, with, and without side plates. $M_\infty = 6.85$, $Re_\infty = 2.45 \times 10^6$/m. (Laminar recovery temperature used throughout in the reduction to Stanton numbers)

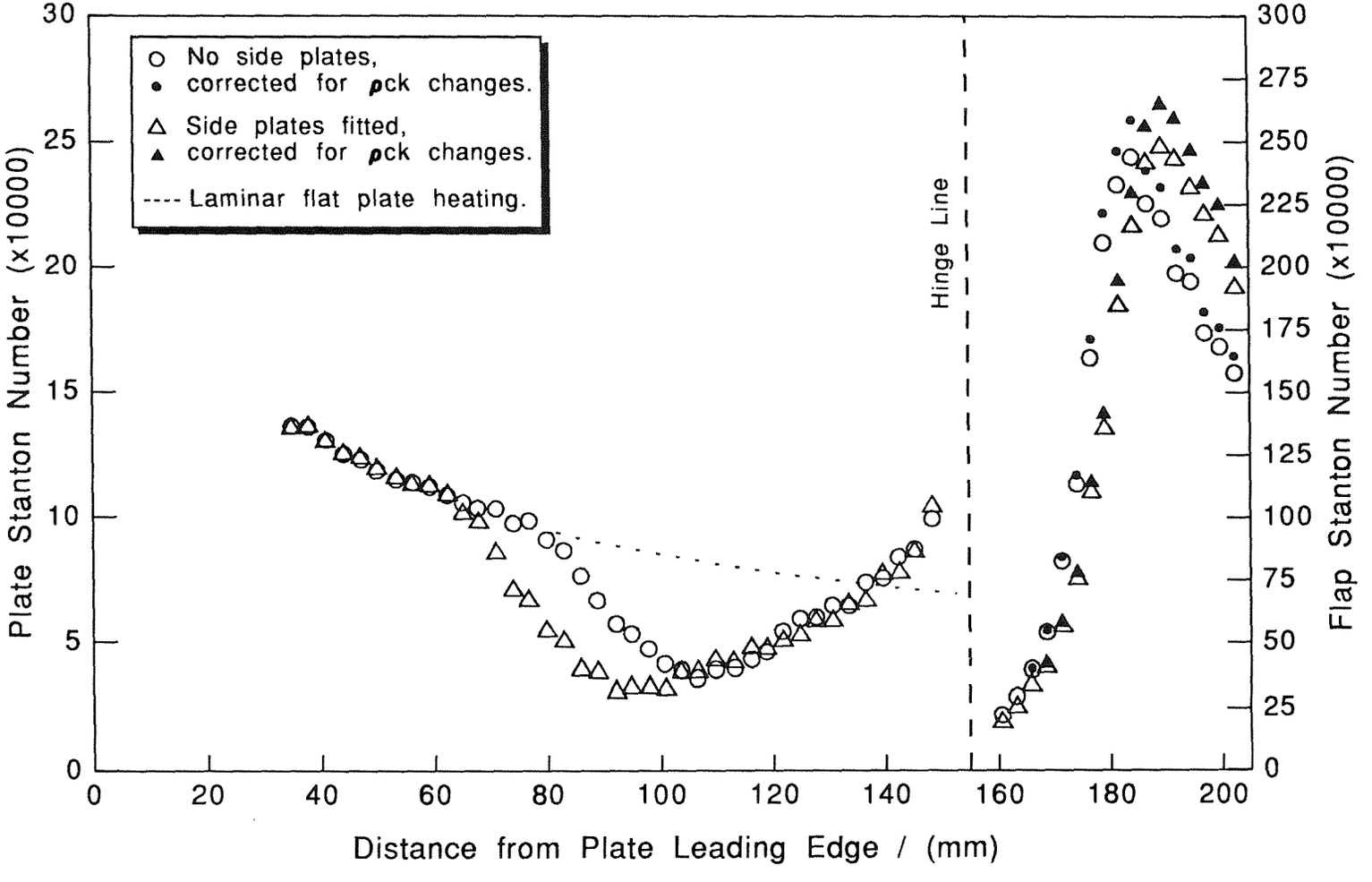

b. Flap angle = 25 degrees.

Fig.33. continued.

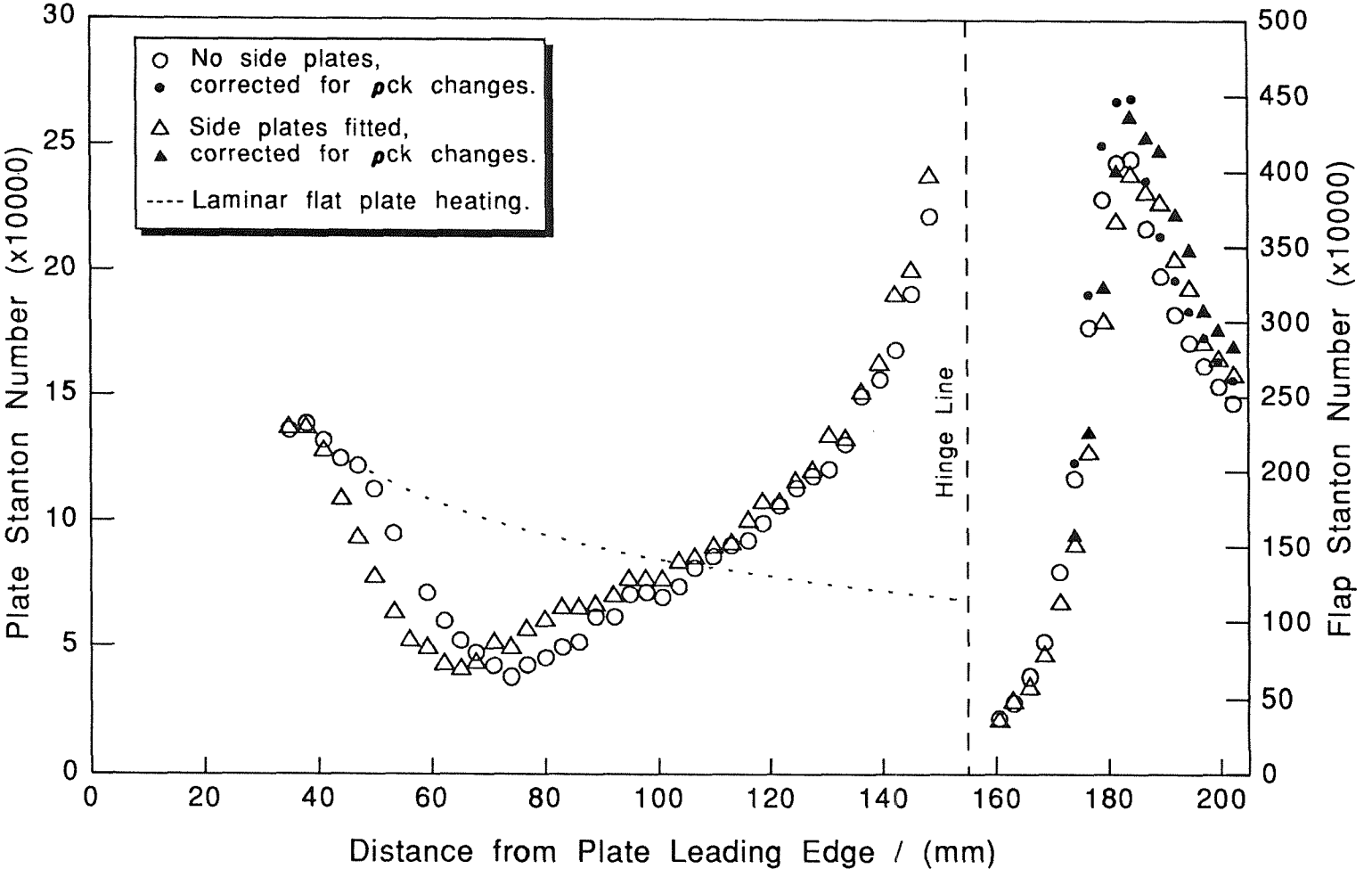

c. Flap angle = 35 degrees.

Fig.33. continued.

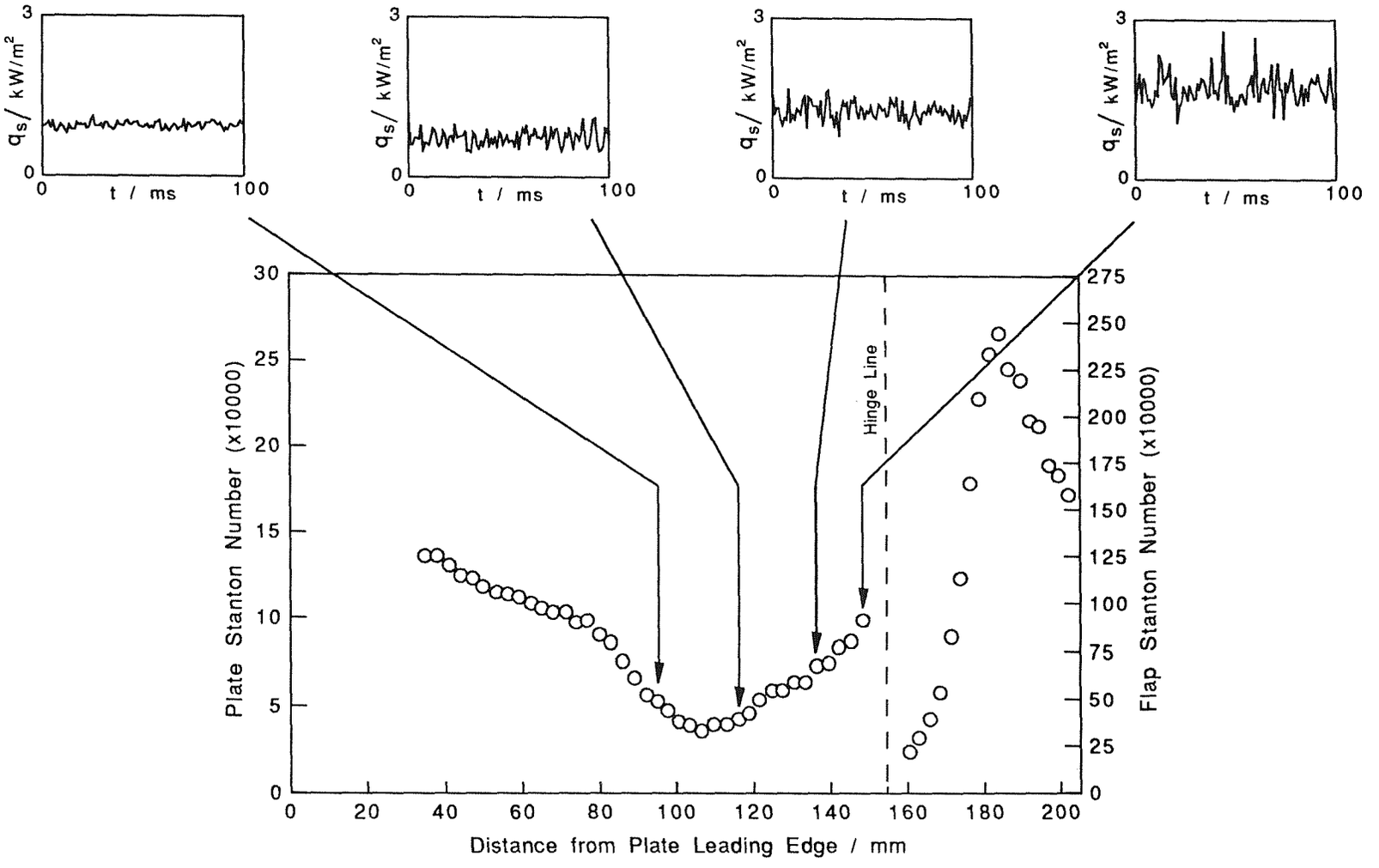

Fig.34. Effects of transition on the separated flow heat transfer distribution, and the signal noise content. Flap angle = 25 degrees. M_∞= 6.85, Re_∞= 2.45x10^6/m.

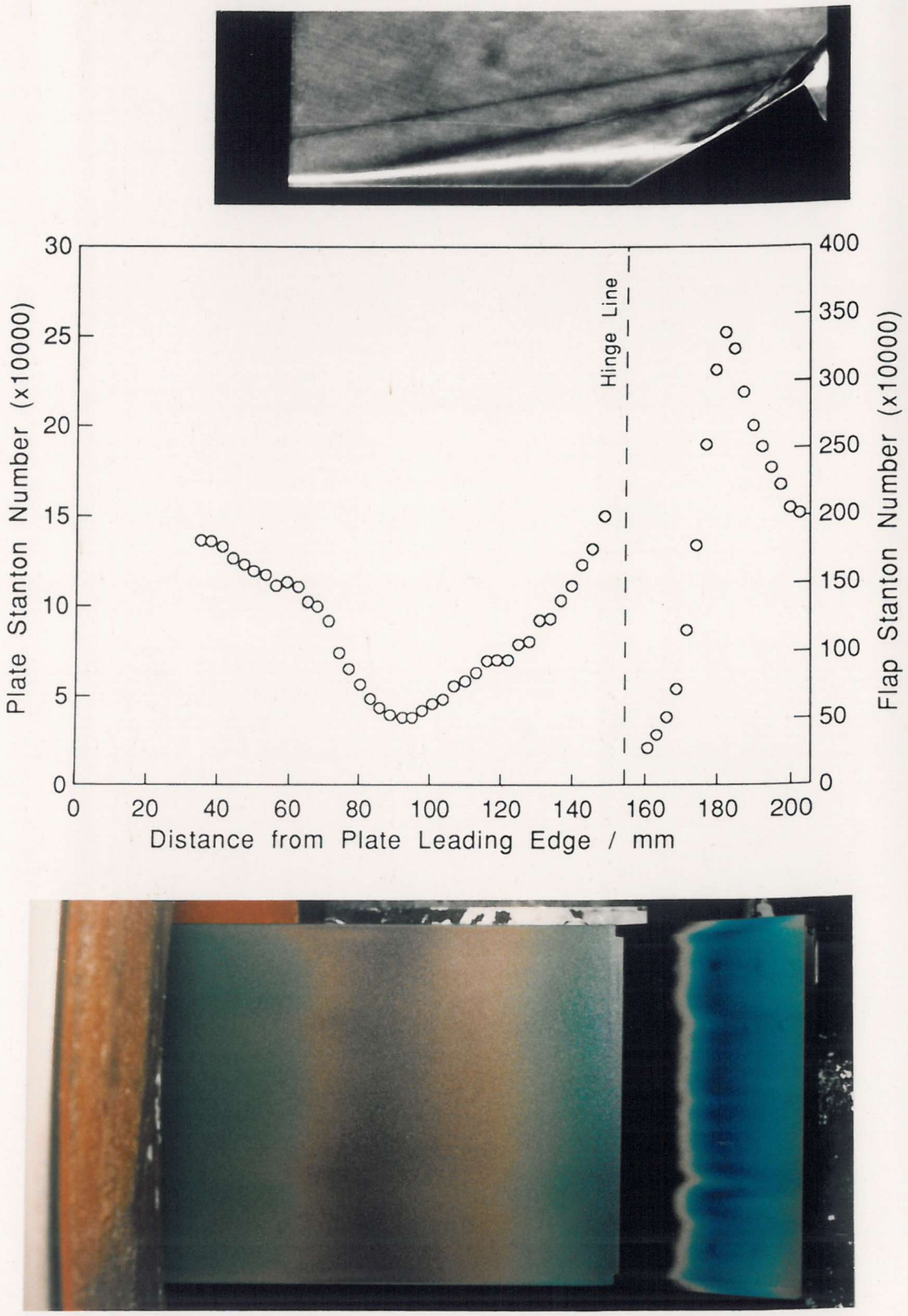

Fig.35. Comparison of schlieren flow visualisation, thin film gauge measurements, and liquid crystal thermography.
Flap angle = 30 degrees. $M_\infty = 6.85$, $Re_\infty = 2.45 \times 10^6/m$.

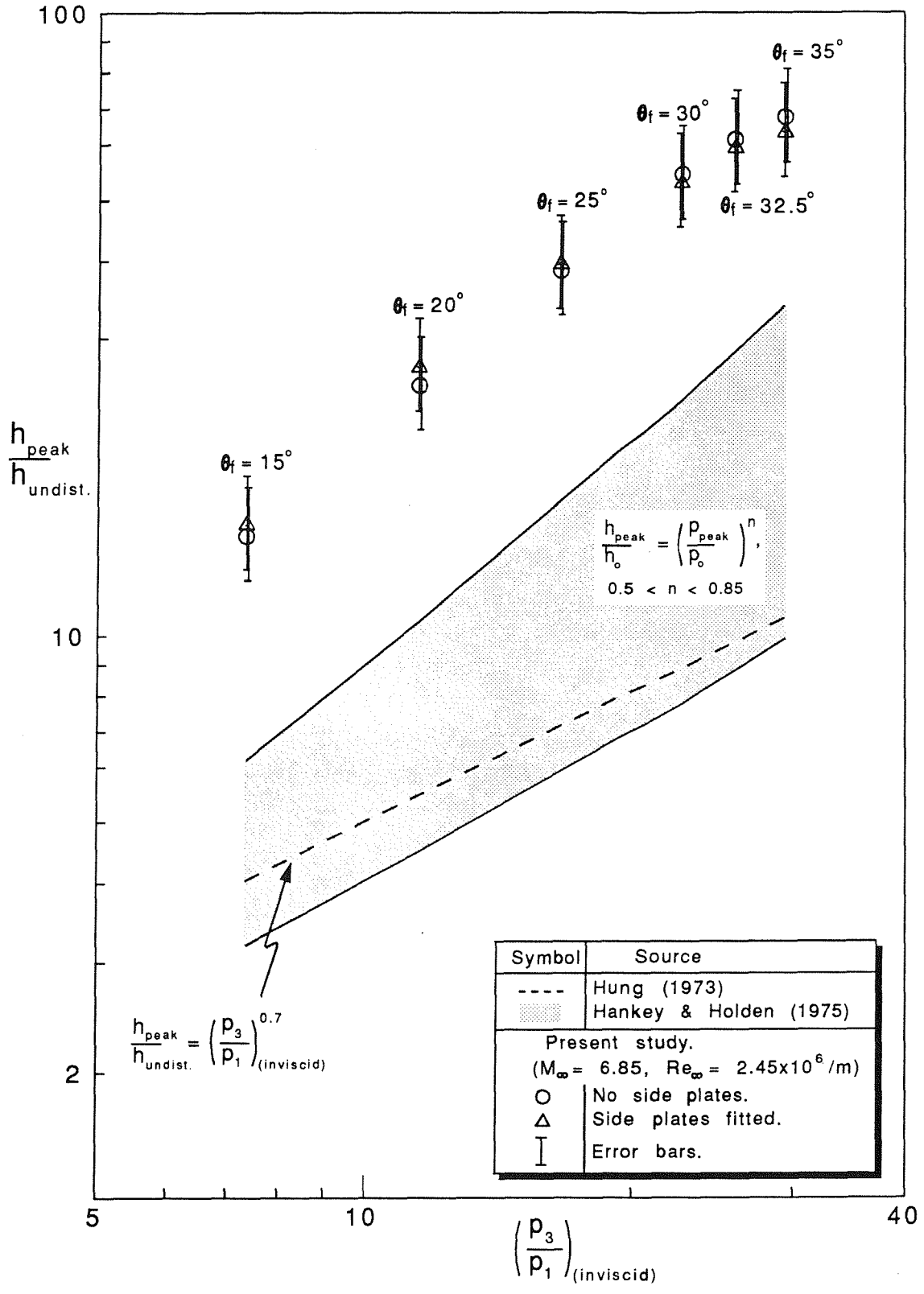

Fig.36. Comparison of the peak reattachment heat transfer values with laminar interference heating correlations.

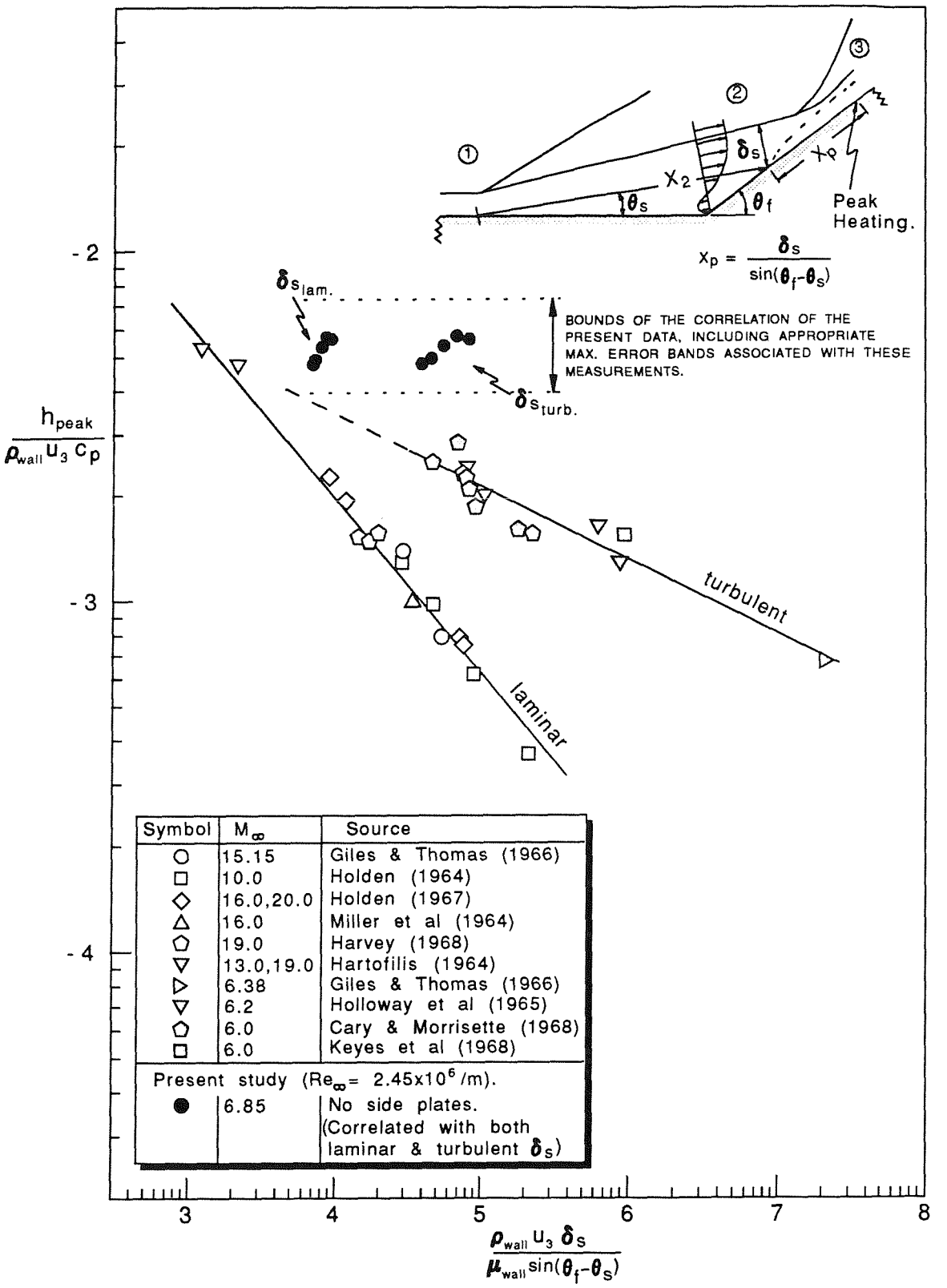

Fig.37. Bushnell & Weinstein (1968) correlation of peak reattachment heating for laminar, and turbulent, wedge separated flows.

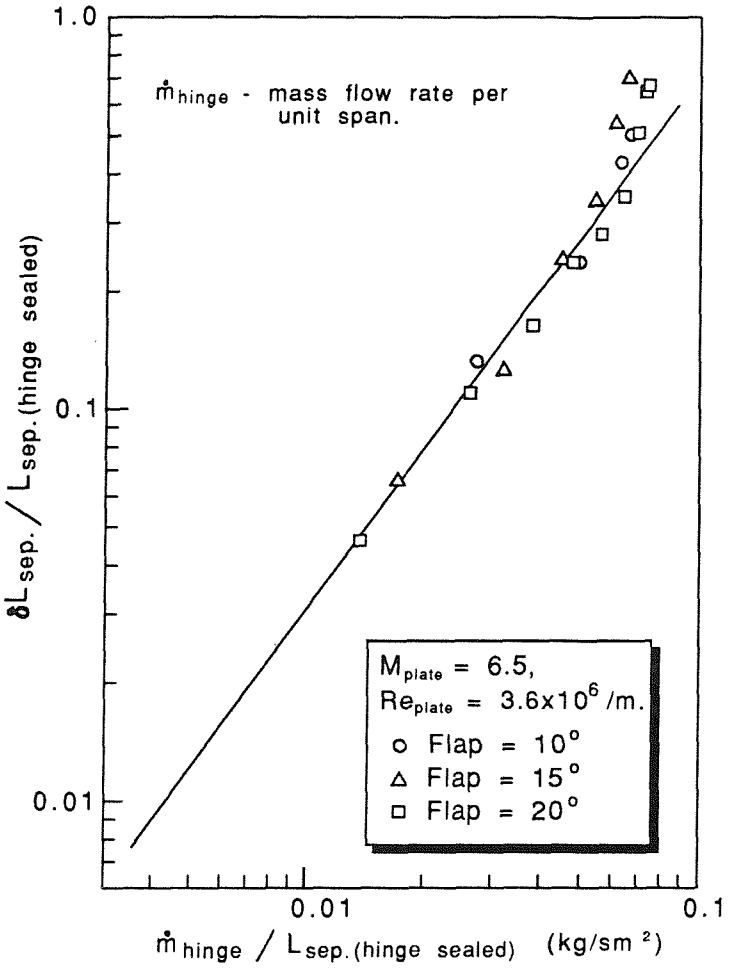

Fig.38a. A correlation of the hinge line bleed data of Ball & Korkegi (1968).

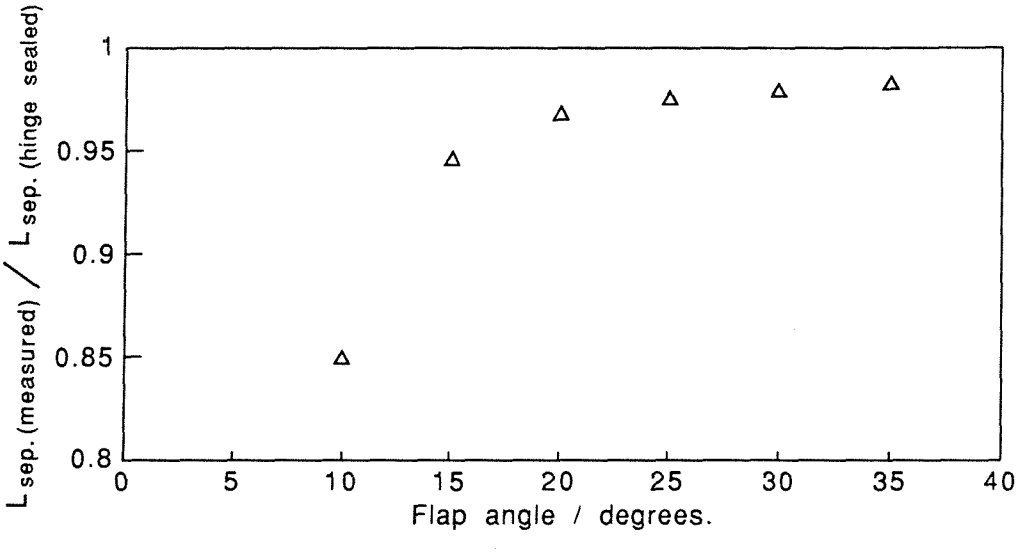

Fig.38b. Application of the correlation in fig.38a to the present data. M_∞ = 6.85, Re_∞ = 2.45x10^6/m.

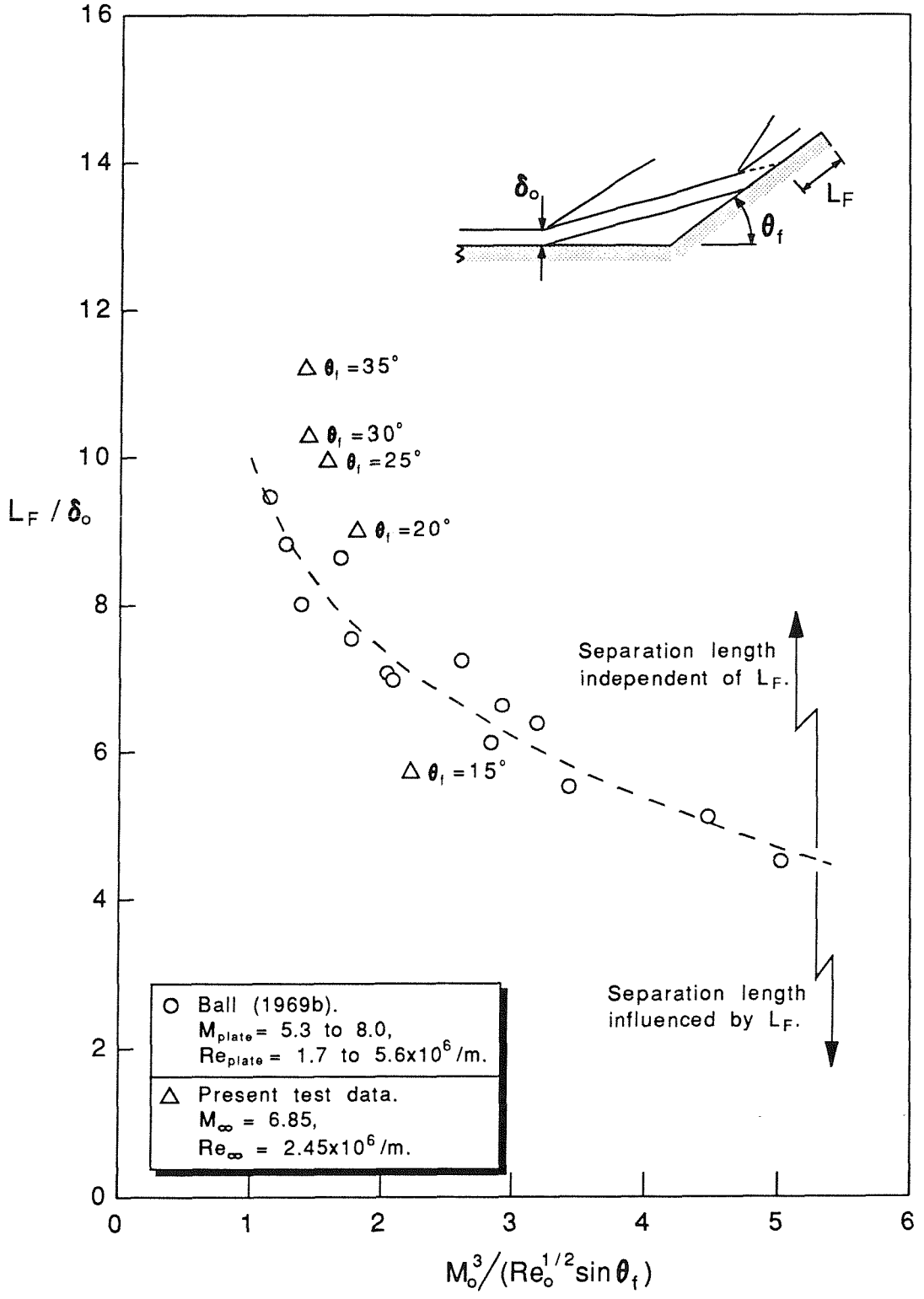

Fig.39. Correlation of finite flap length effects on the scale of wedge separated flows (Ball 1969b).

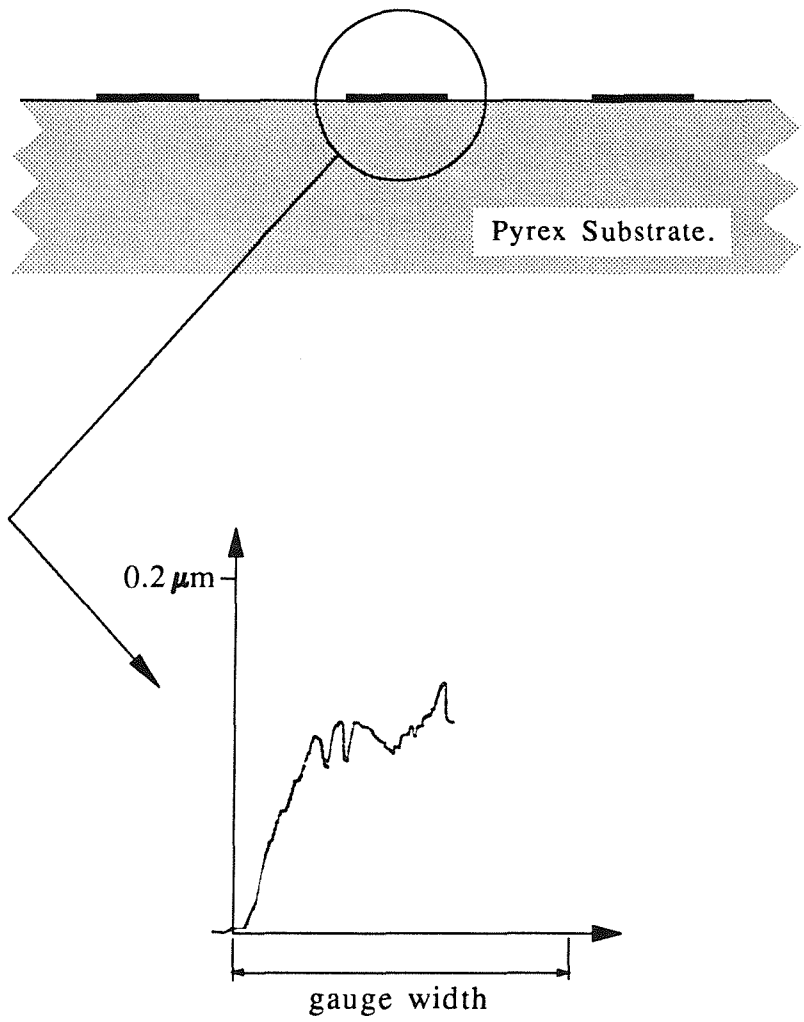

Fig.40. Profile measurement of a surface deposited thin film resistance gauge.

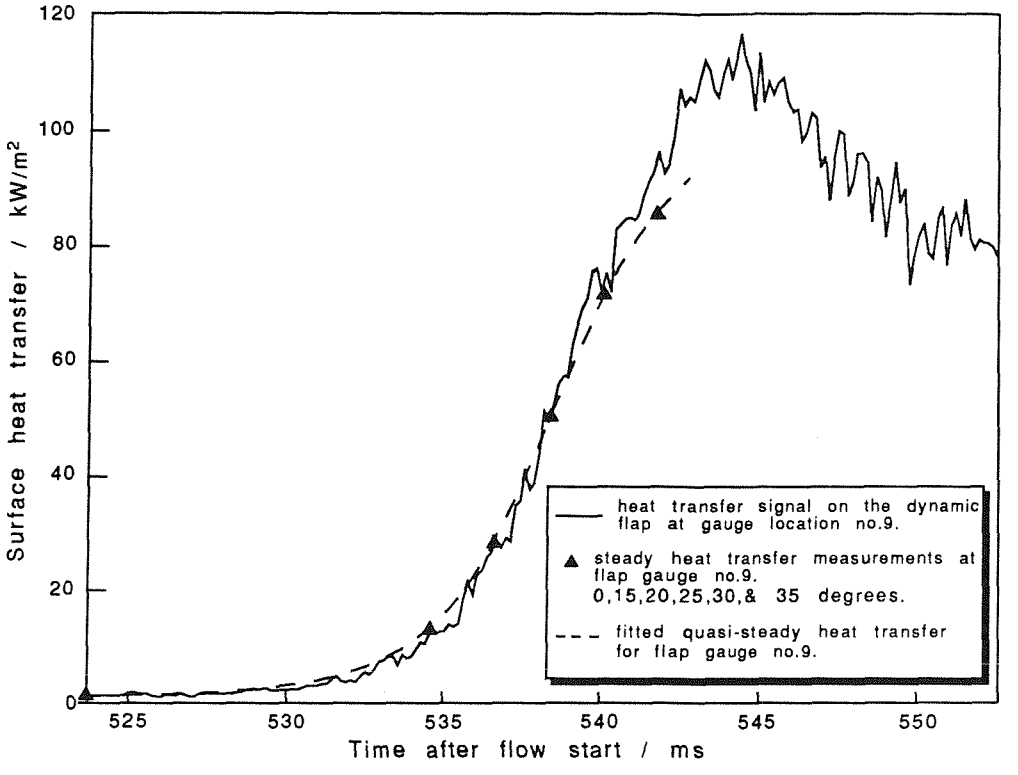

Fig.41. Comparison of the quasi-steady, and measured dynamic, heat transfer signals at the flap gauge no. 9. $M_\infty = 6.85$, $Re_\infty = 2.45 \times 10^6$/m.

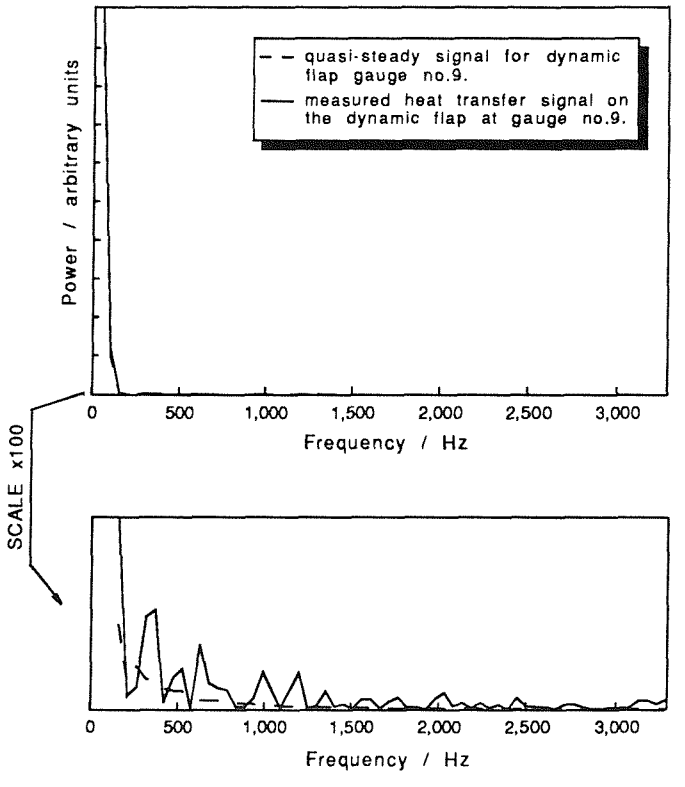

Fig.42. Power spectrums of the constructed quasi-steady, and dynamic heat transfer signals, in fig.41.

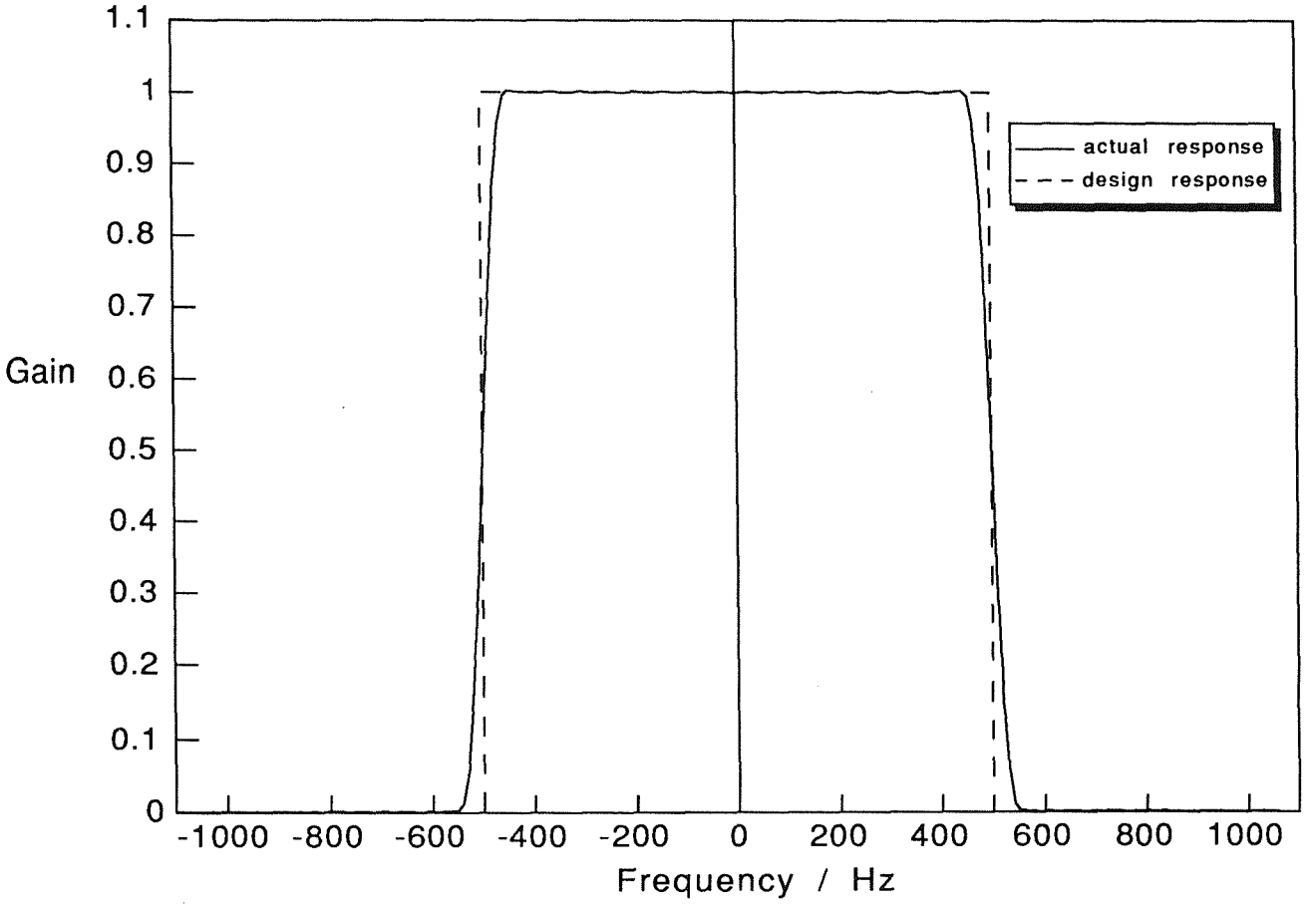

Fig.43. Numerical filter frequency response.

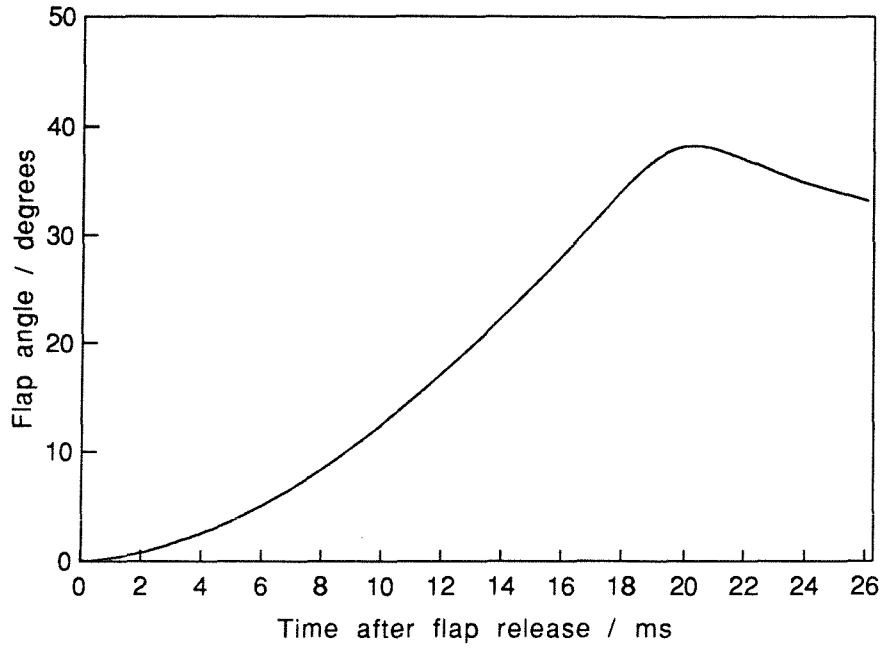

Fig.44. Dynamic flap motion.

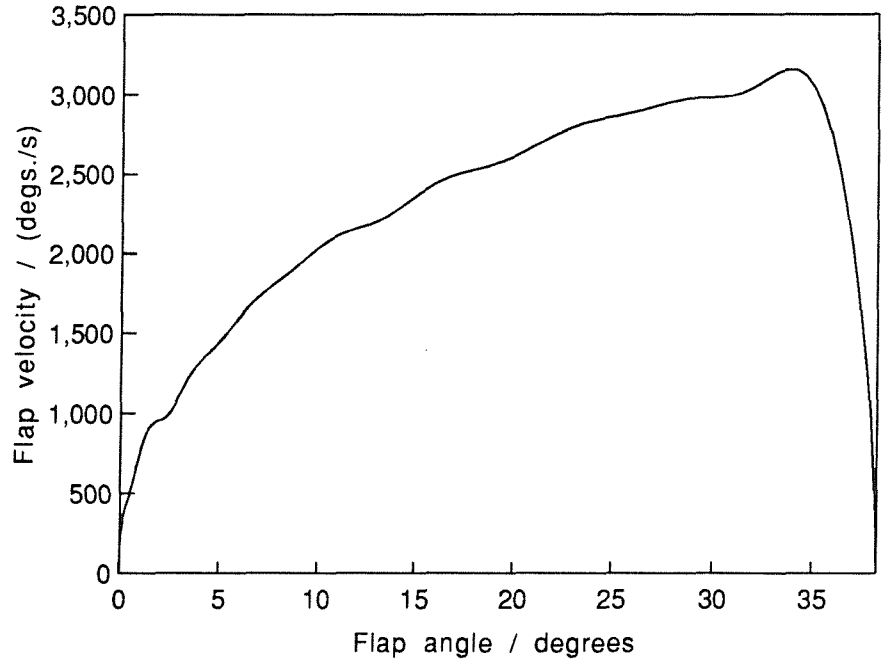

Fig.45. Dynamic flap velocity as a function of the angle of deflection.

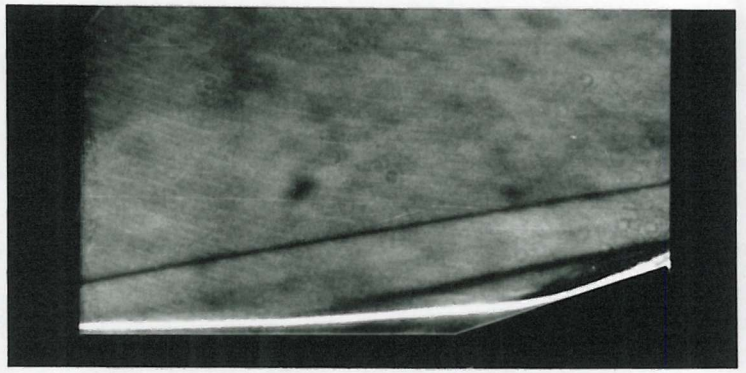

Fixed flap.

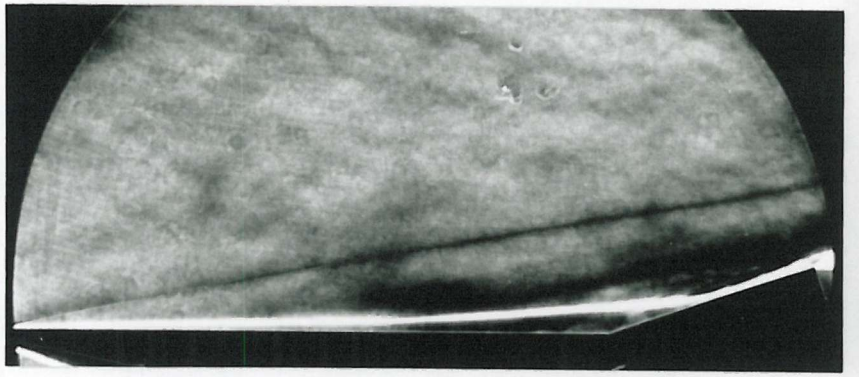

Flap velocity = 2545 degs./s

a. Flap angle = 18.6 degrees.

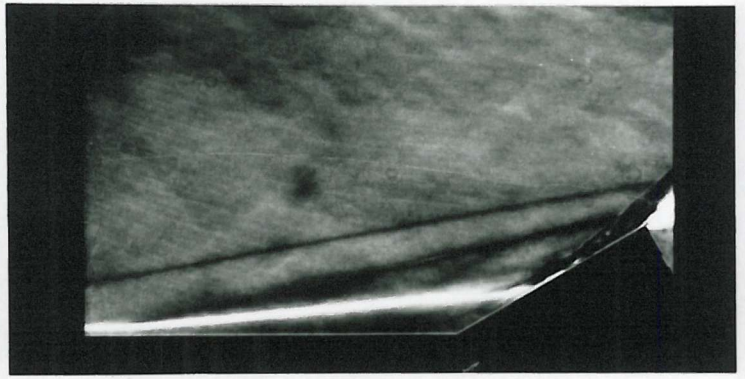

Fixed flap.

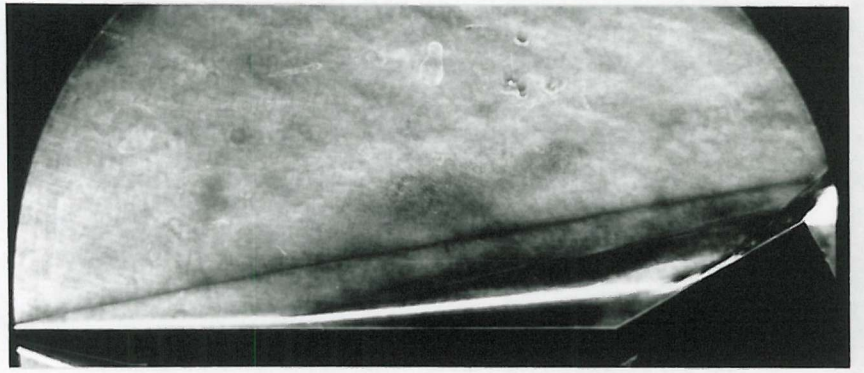

Flap velocity = 2980 degs./s

b. Flap angle = 30.0 degrees.

Fig.46. Schlieren flow visualisation of the dynamic, and equivalent fixed flap, induced separated flows. $M_\infty = 6.85$, $Re_\infty = 2.45 \times 10^6/m$.

Fixed flap.

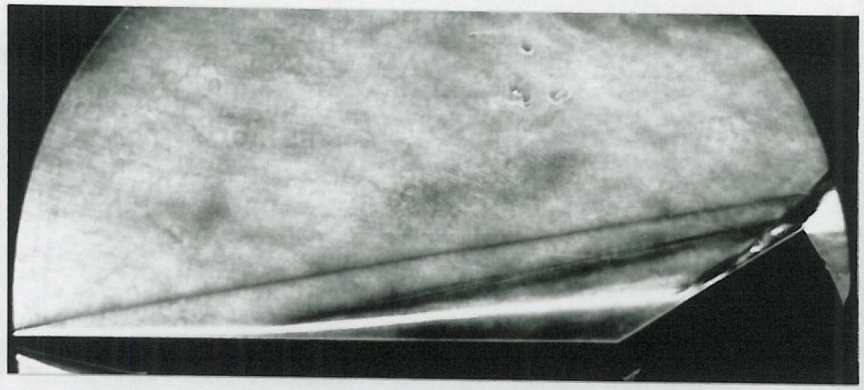

Flap velocity = 3053 degs./s

c. Flap angle = 32.2 degrees.

Fixed flap.

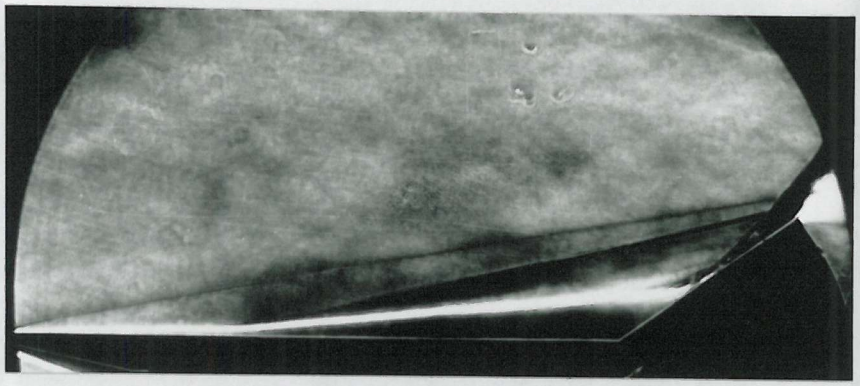

Flap velocity = 2927 degs./s

d. Flap angle = 35.5 degrees.

Fig.46. continued.

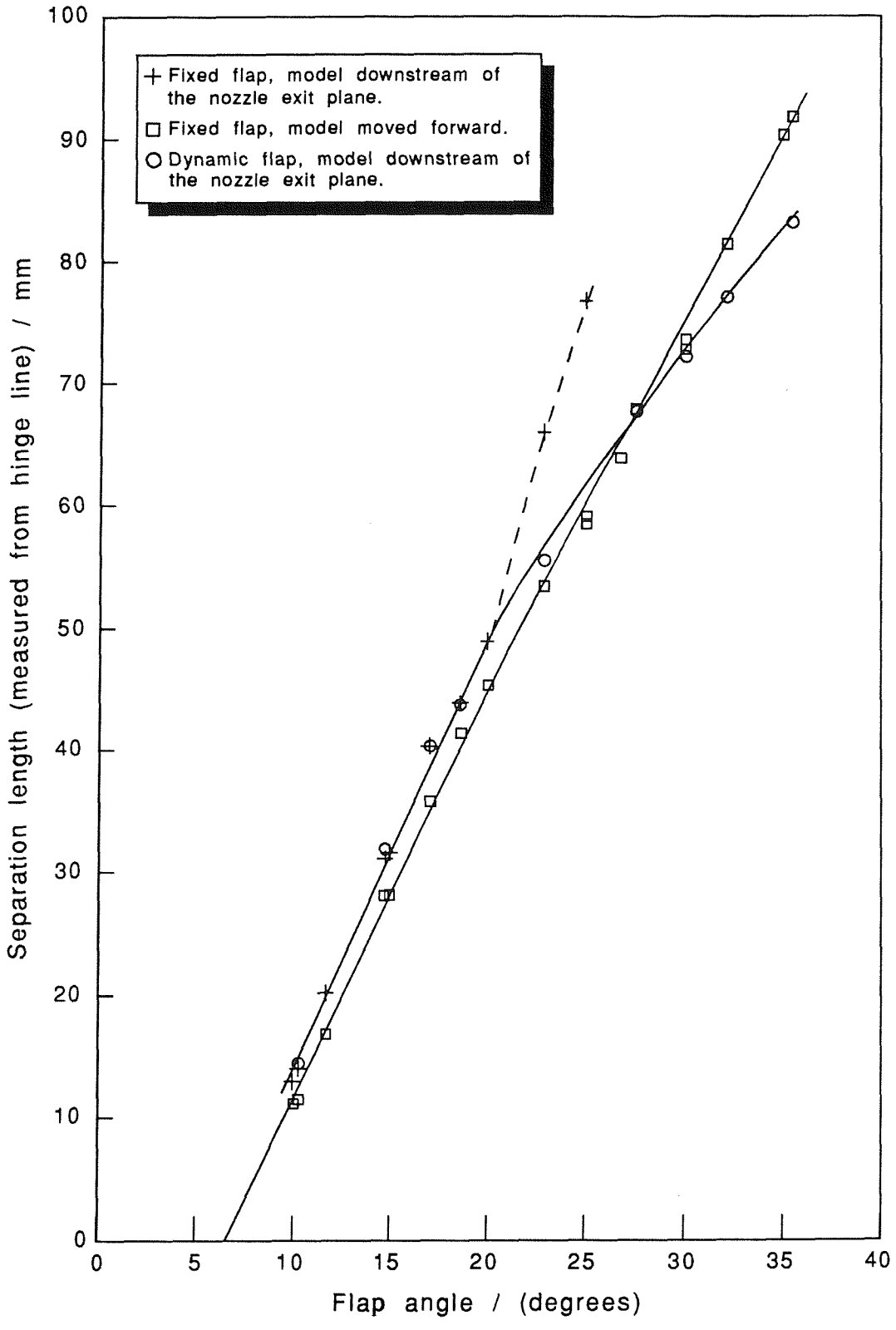

Fig.47. Unsteady, and steady, separation lengths measured from the schlieren flow visualisation. $M_\infty = 6.85$, $Re_\infty = 2.45 \times 10^6$/m.

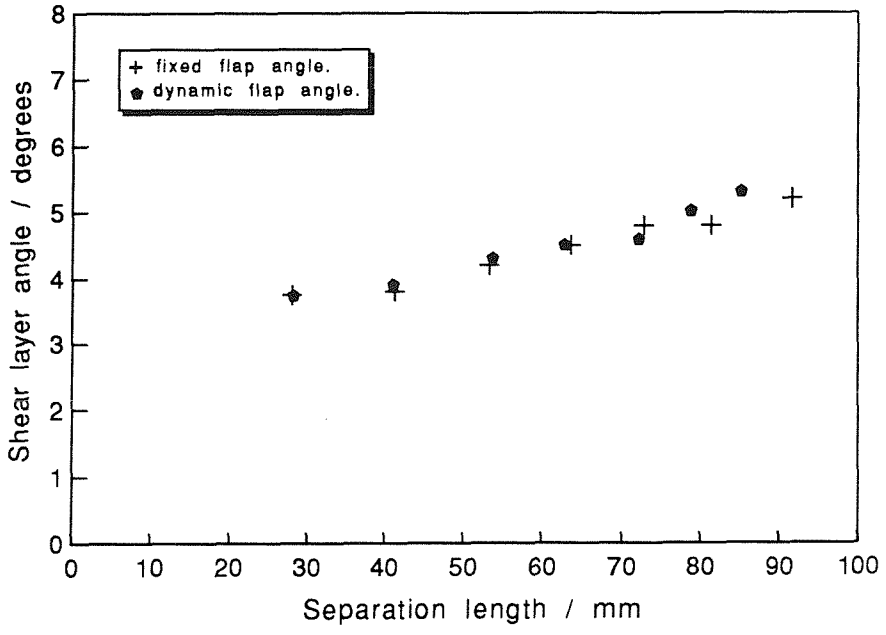

Fig.48. Shear layer deflection angles measured from the schlieren photographs. M_∞= 6.85, Re_∞= 2.45x10^6/m.

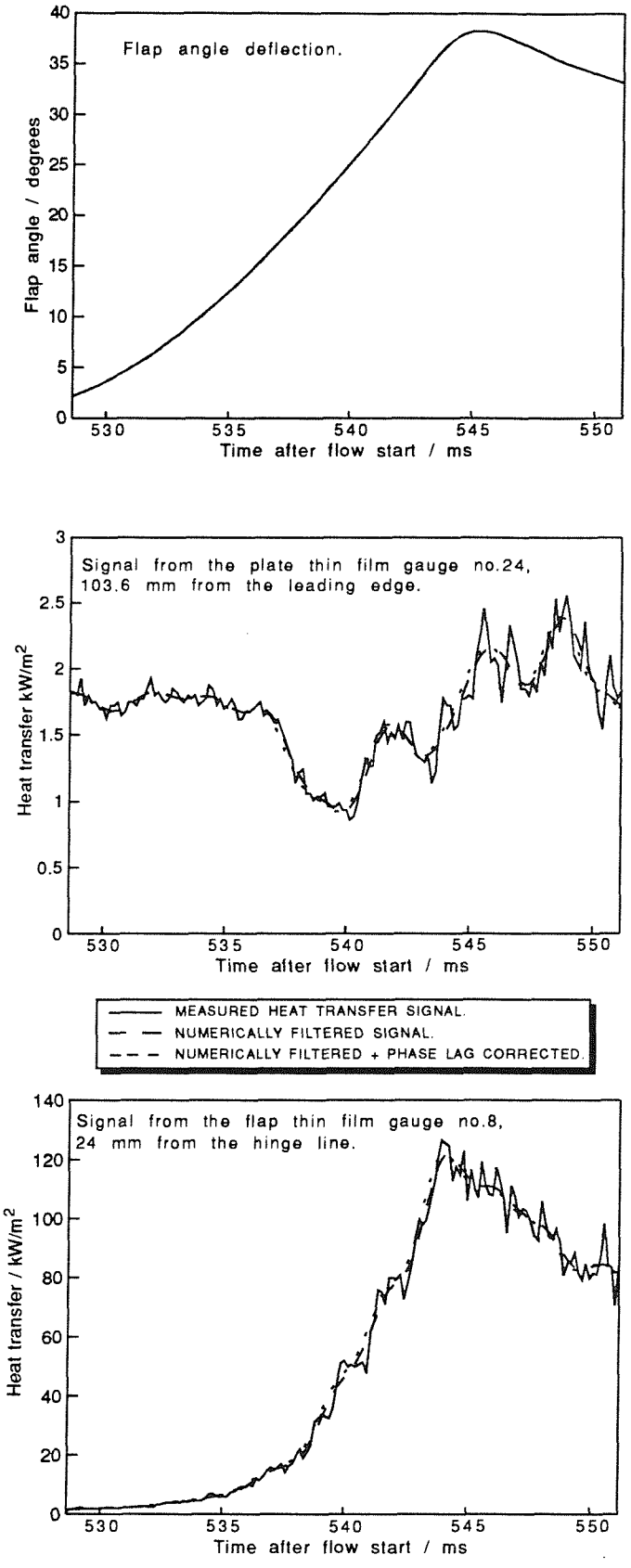

Fig.49. Examples of the unsteady heat transfer signals (no side plates), compared with the flap deflection. $M_\infty = 6.85$, $Re_\infty = 2.45 \times 10^6$/m.

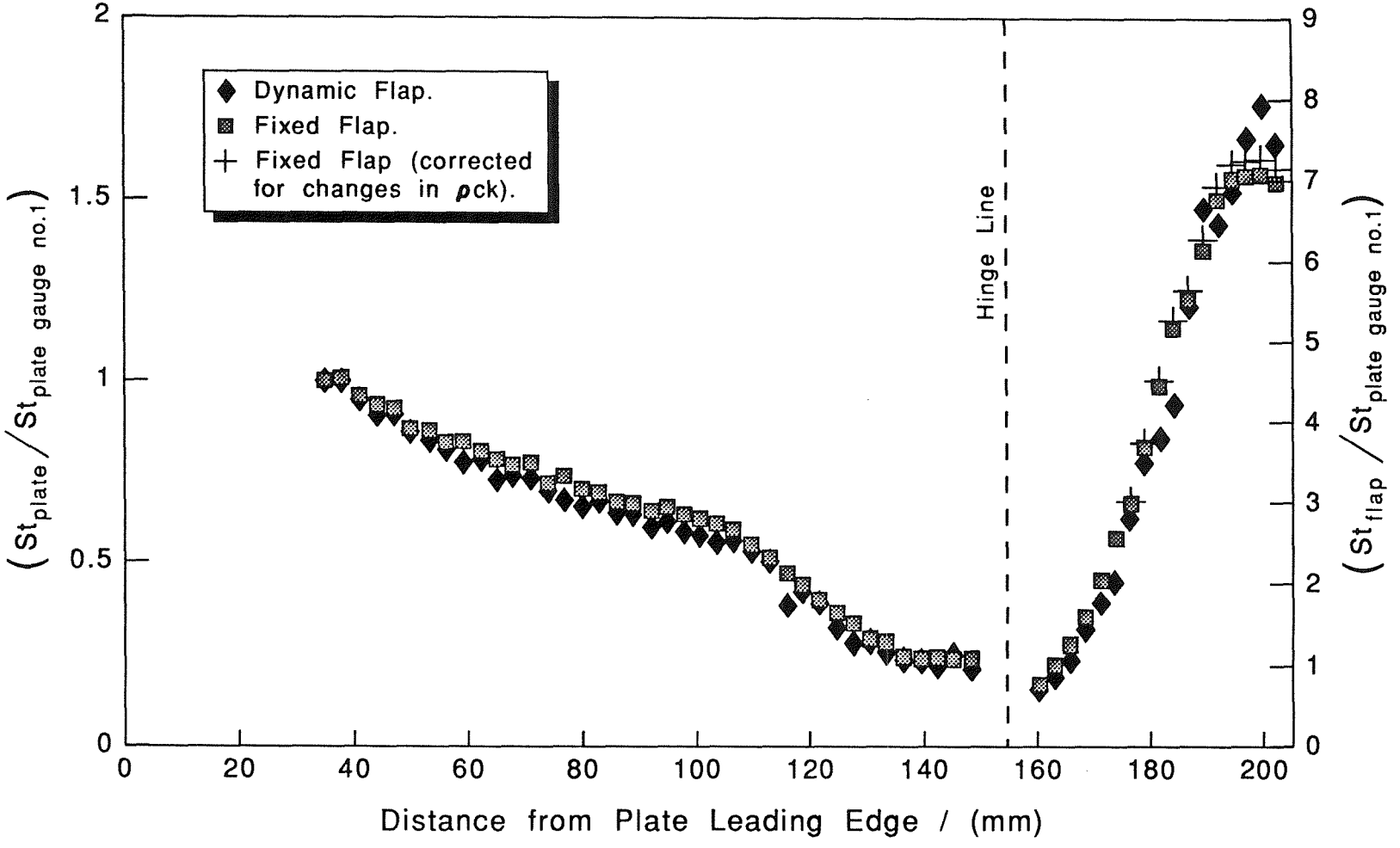

a. Flap angle = 15 degrees.

Fig.50. Comparison of the dynamic, and fixed flap heat transfer distributions. No side plates. M_∞= 6.85, Re_∞= 2.45x10^6/m. (Laminar recovery temperature assumed throughout)

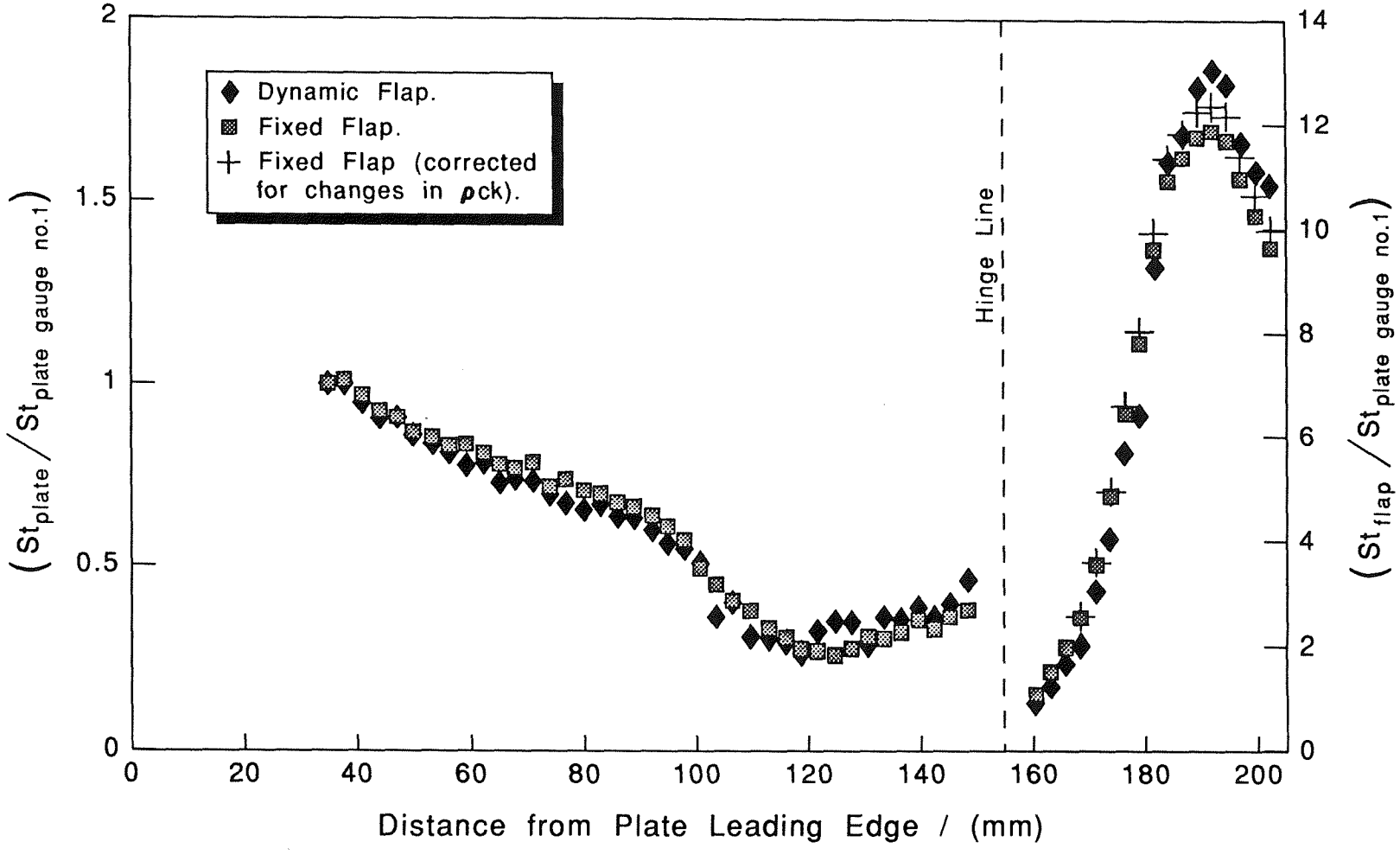

b. Flap angle = 20 degrees.

Fig.50. continued.

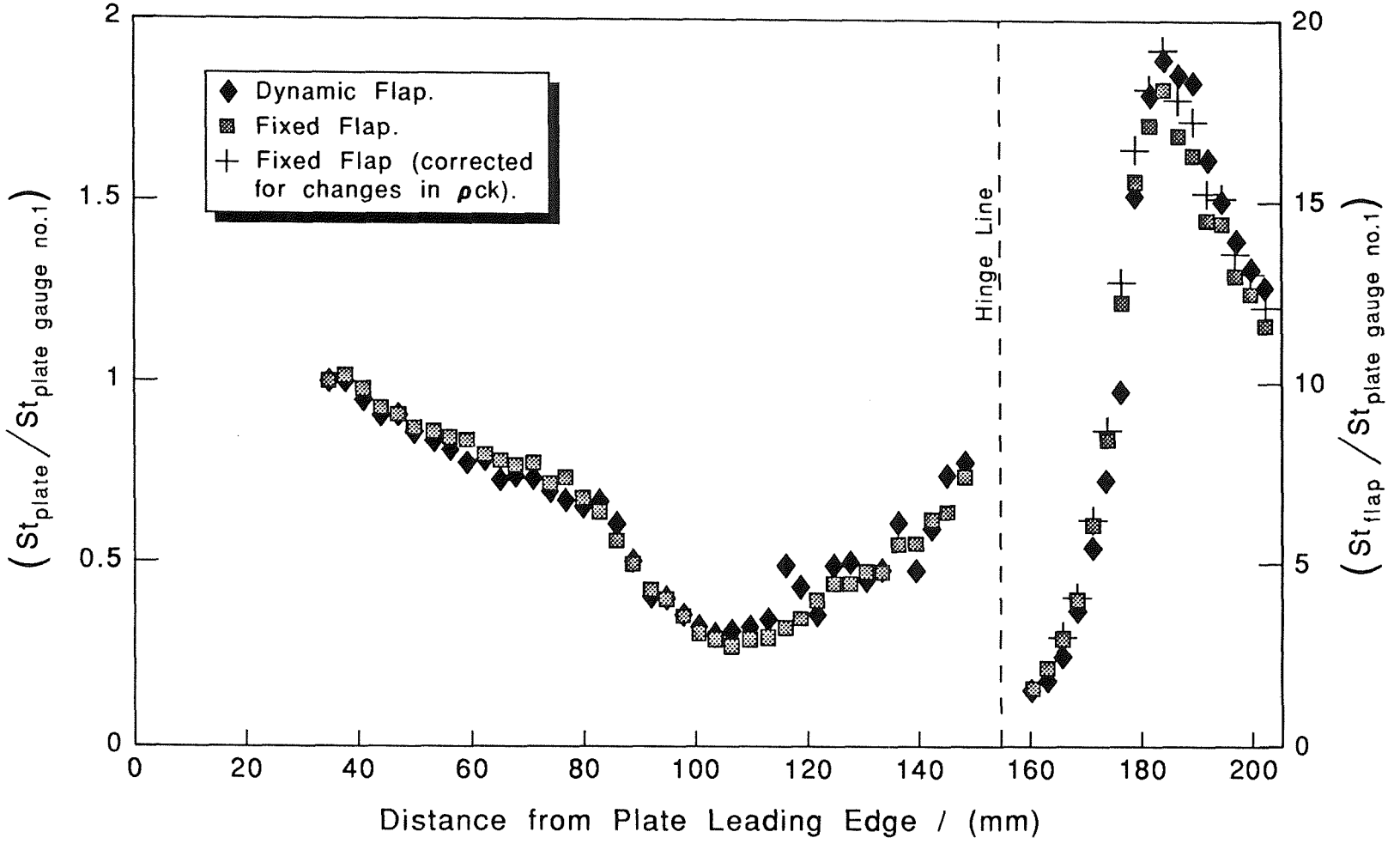

c. Flap angle = 25 degrees.

Fig.50. continued.

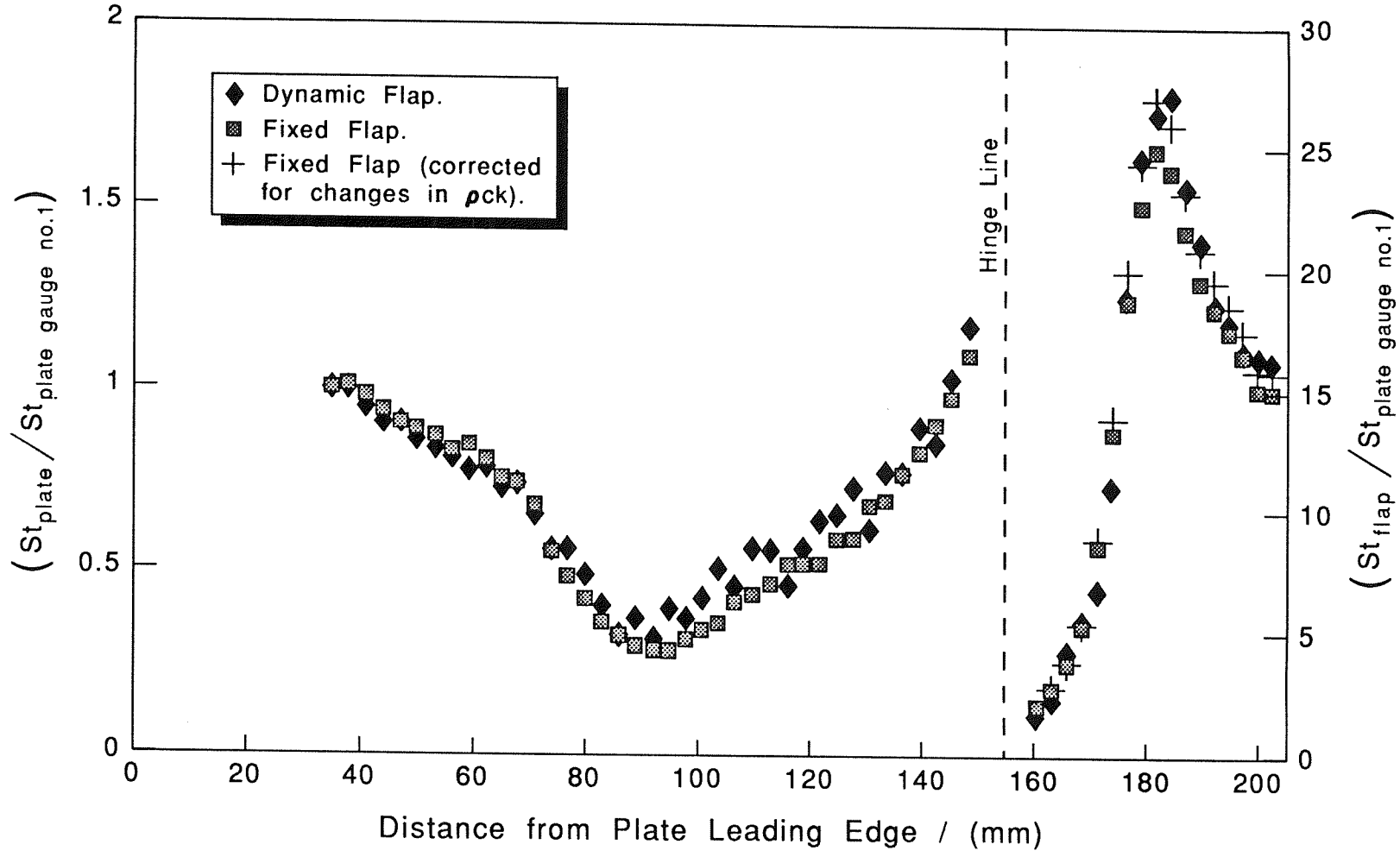

d. Flap angle = 30 degrees.

Fig.50. continued.

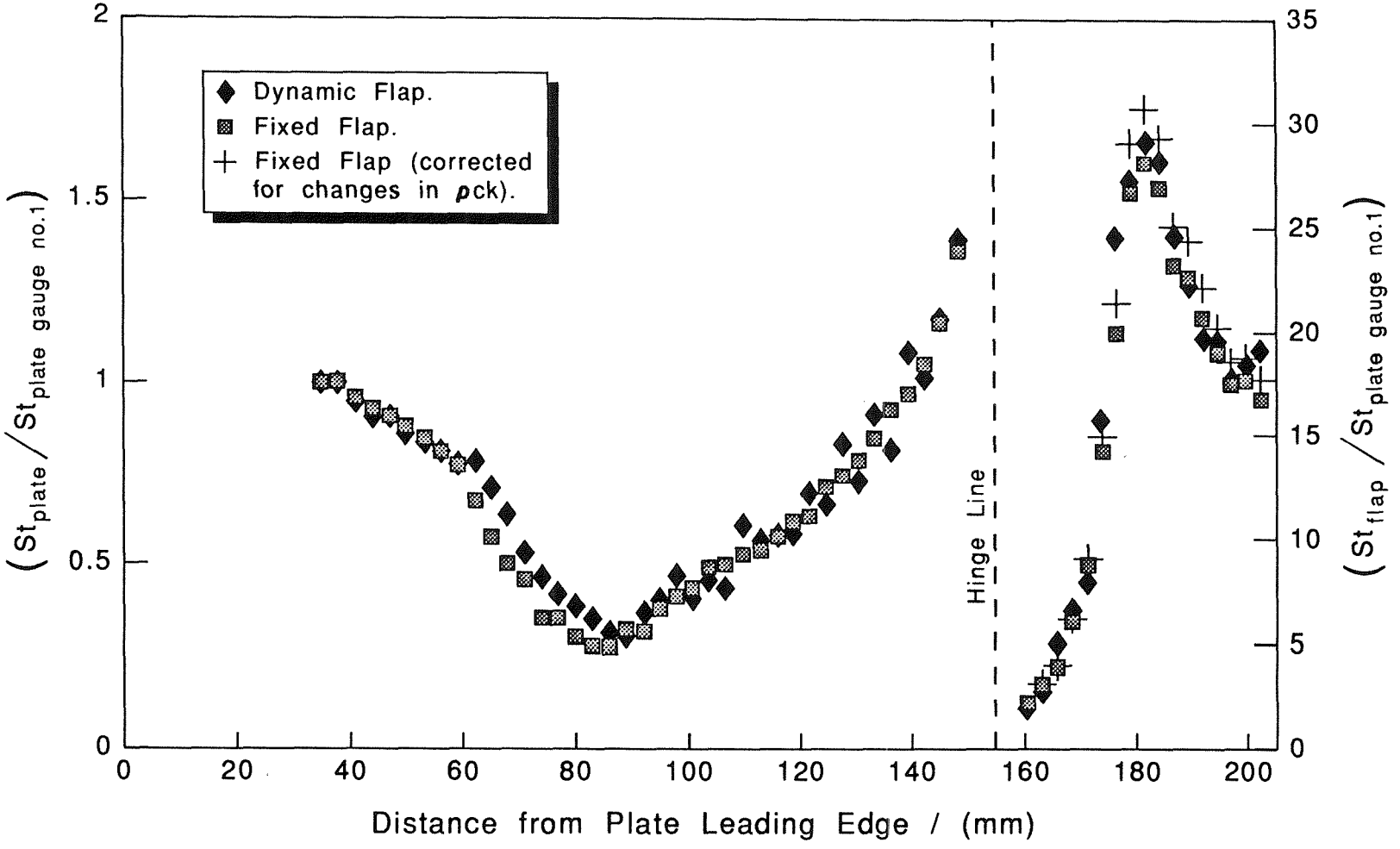

e. Flap angle = 32.5 degrees.

Fig.50. continued.

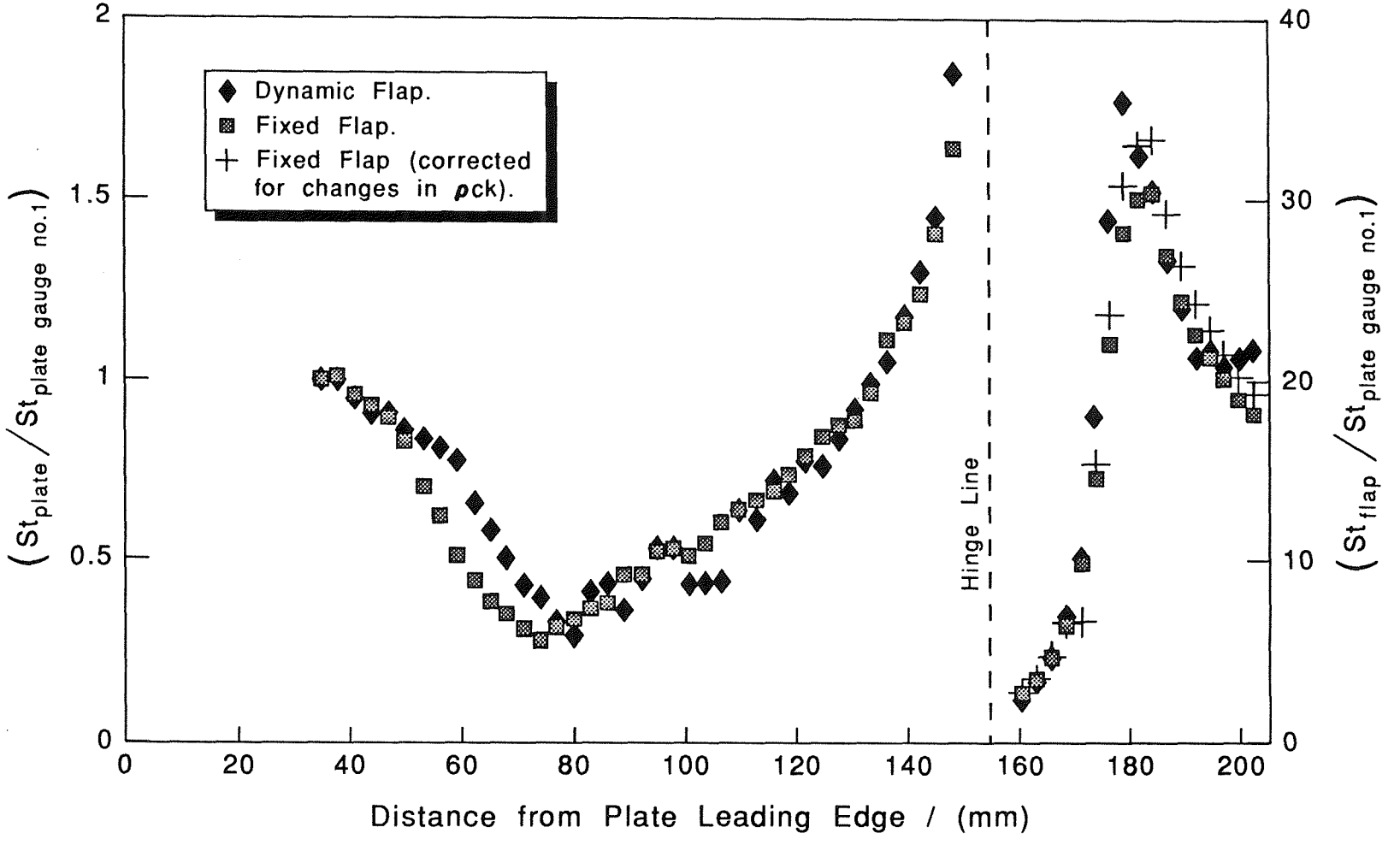

f. Flap angle = 35 degrees.

Fig.50. continued.

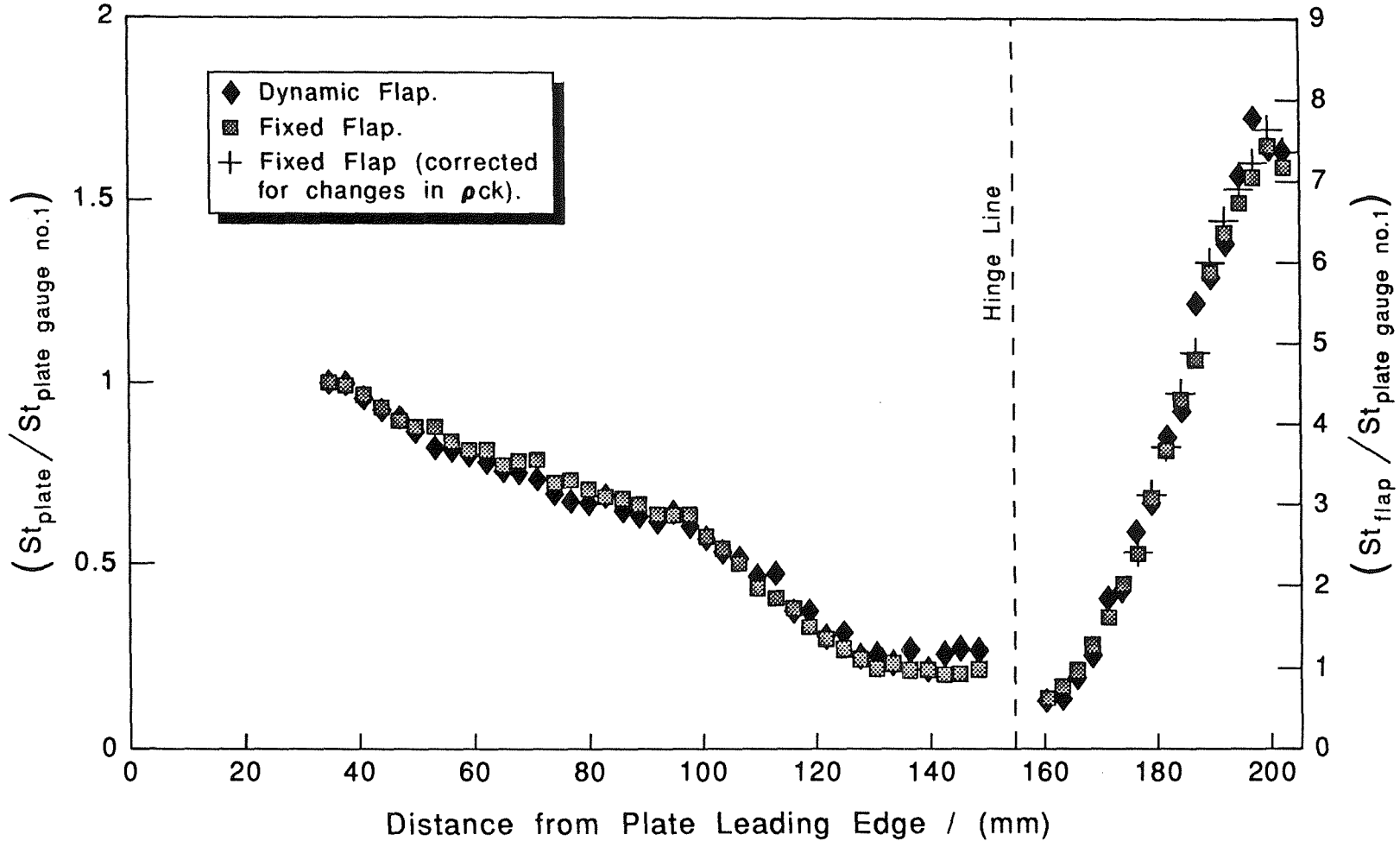

a. Flap angle = 15 degrees.

Fig.51. Comparison of the dynamic, and fixed flap heat transfer distributions. Side plates attached. M_∞= 6.85, Re_∞= 2.45x10^6/m. (Laminar recovery temperature assumed throughout)

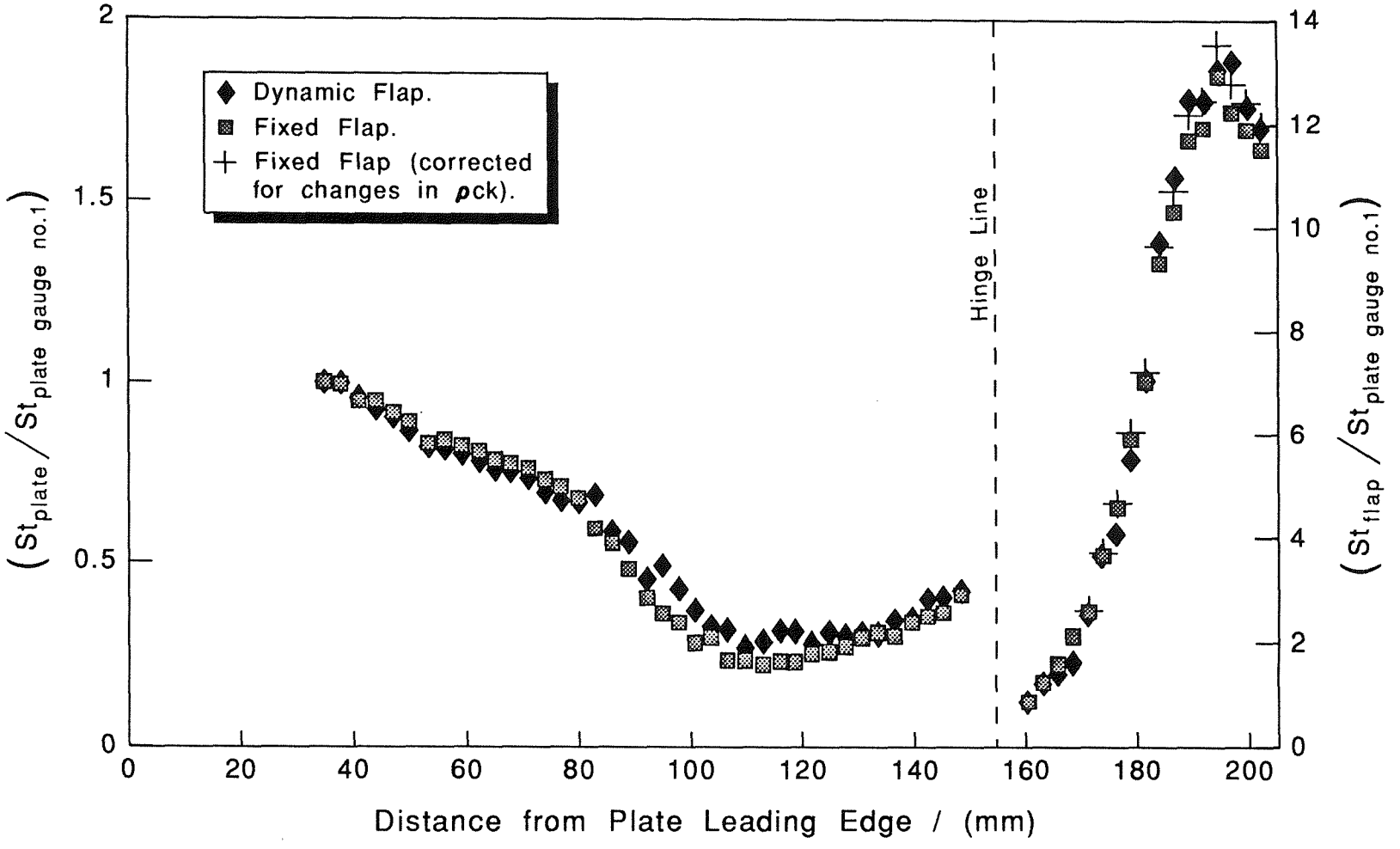

b. Flap angle = 20 degrees.

Fig.51. continued.

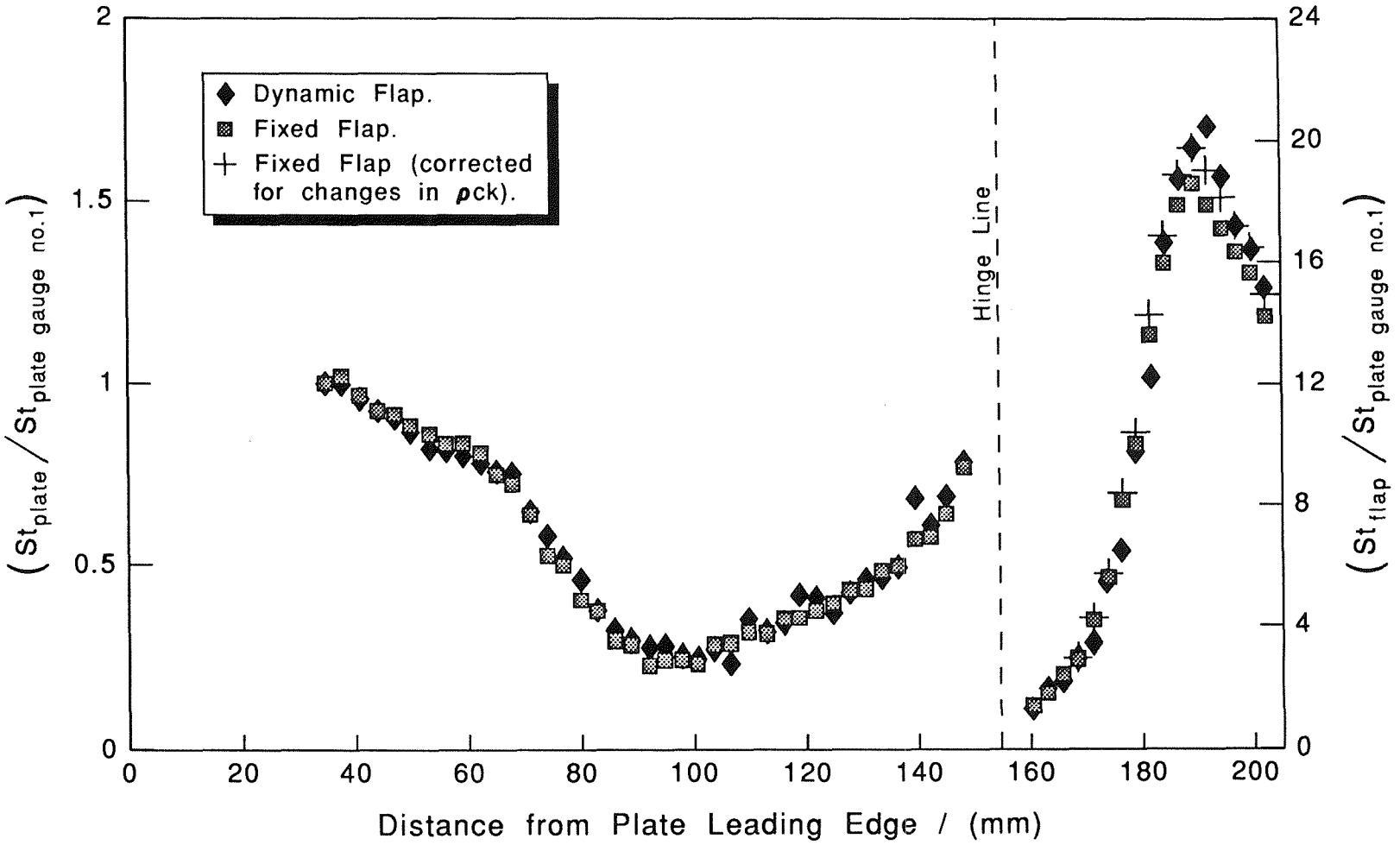

c. Flap angle = 25 degrees.

Fig.51. continued.

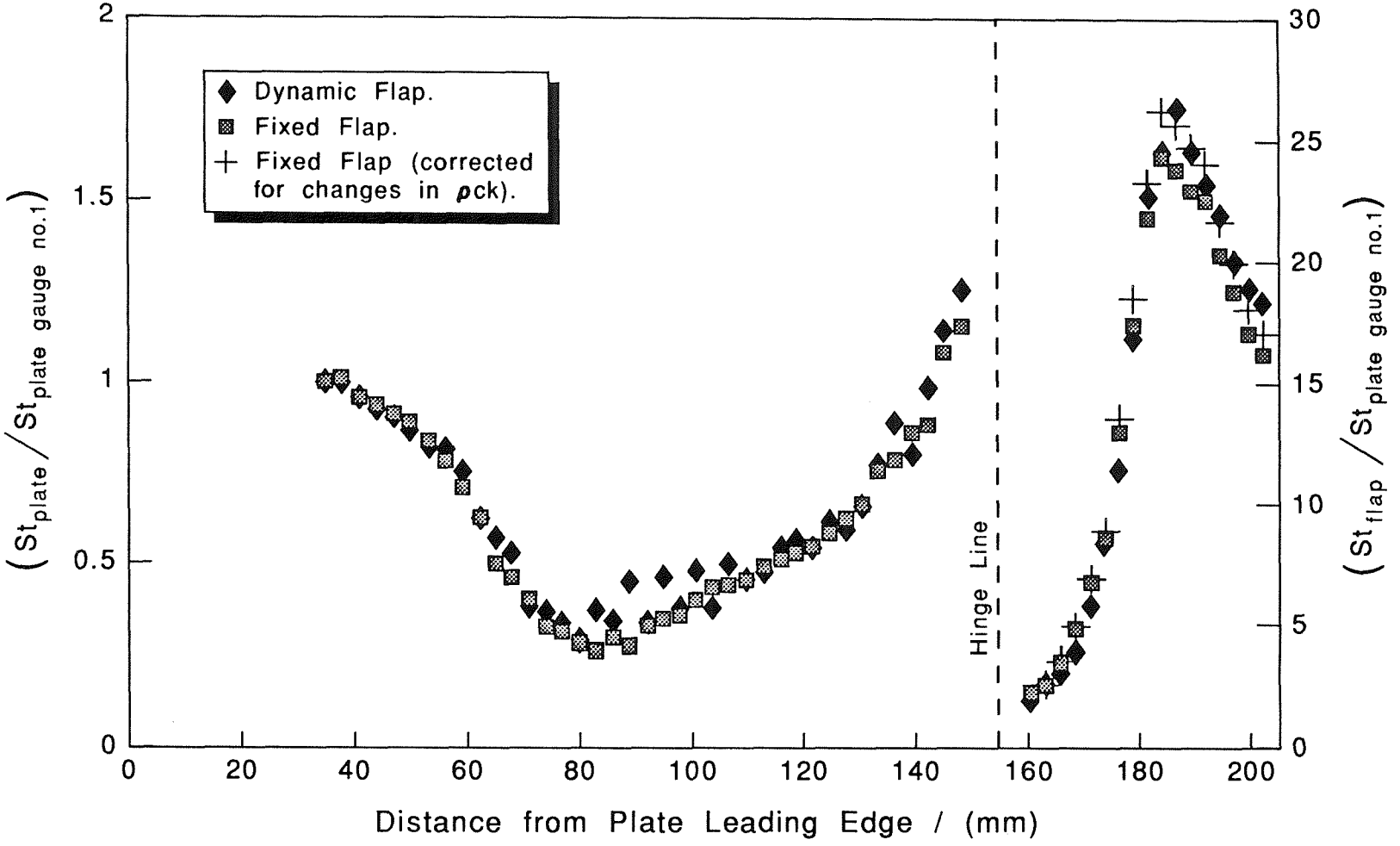

d. Flap angle = 30 degrees.

Fig.51. continued.

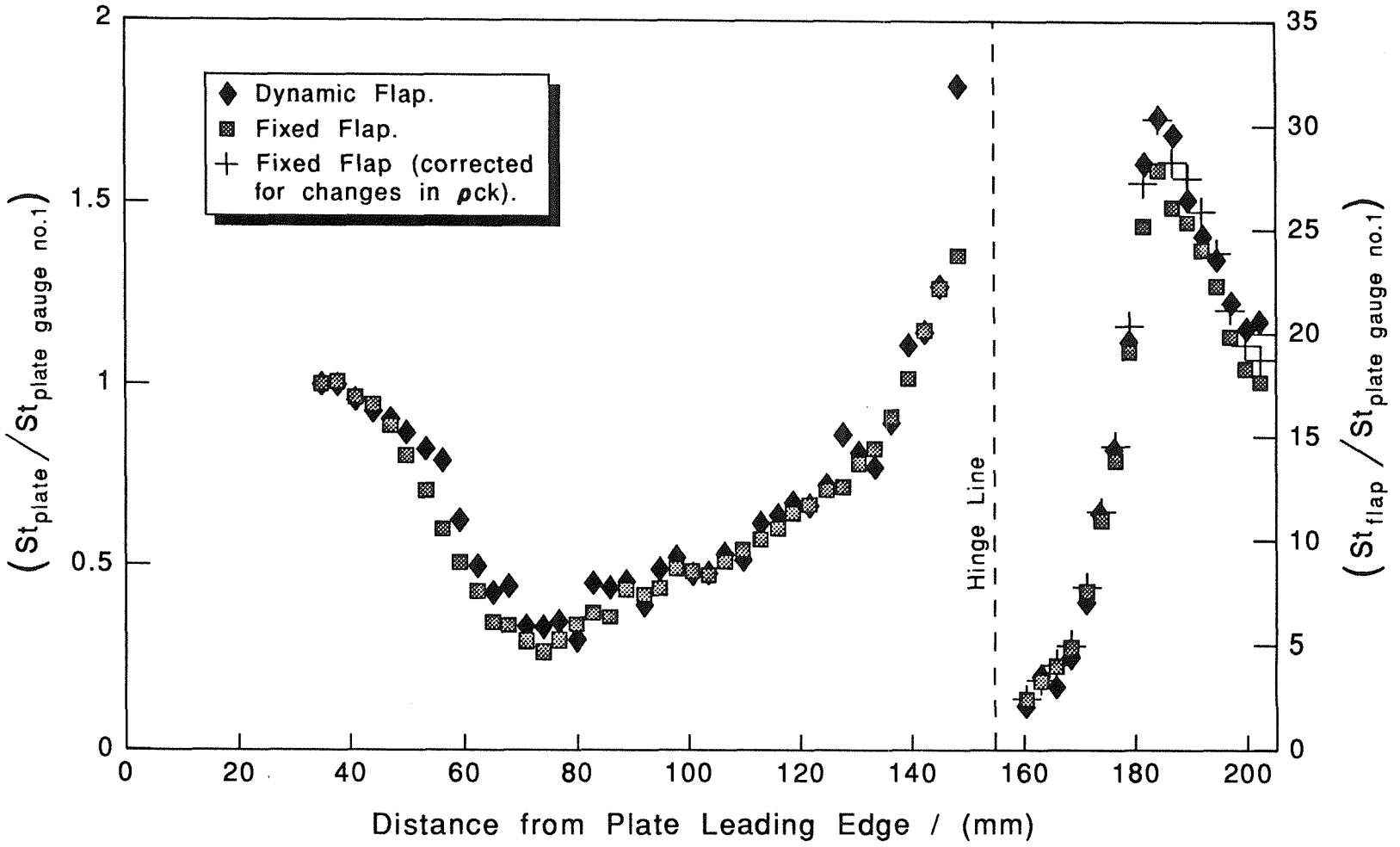

e. Flap angle = 32.5 degrees.

Fig.51. continued.

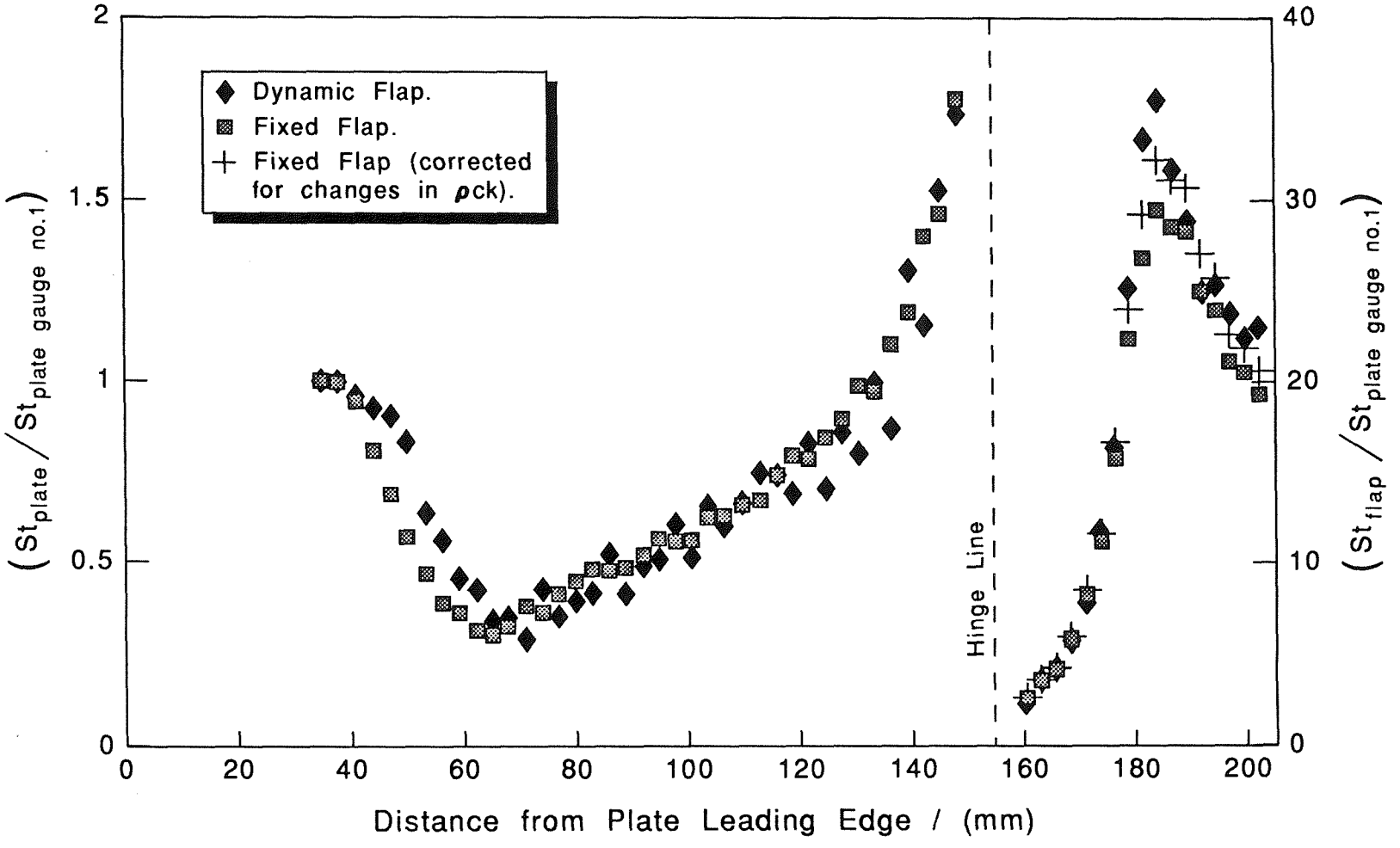

f. Flap angle = 35 degrees.

Fig.51. continued.

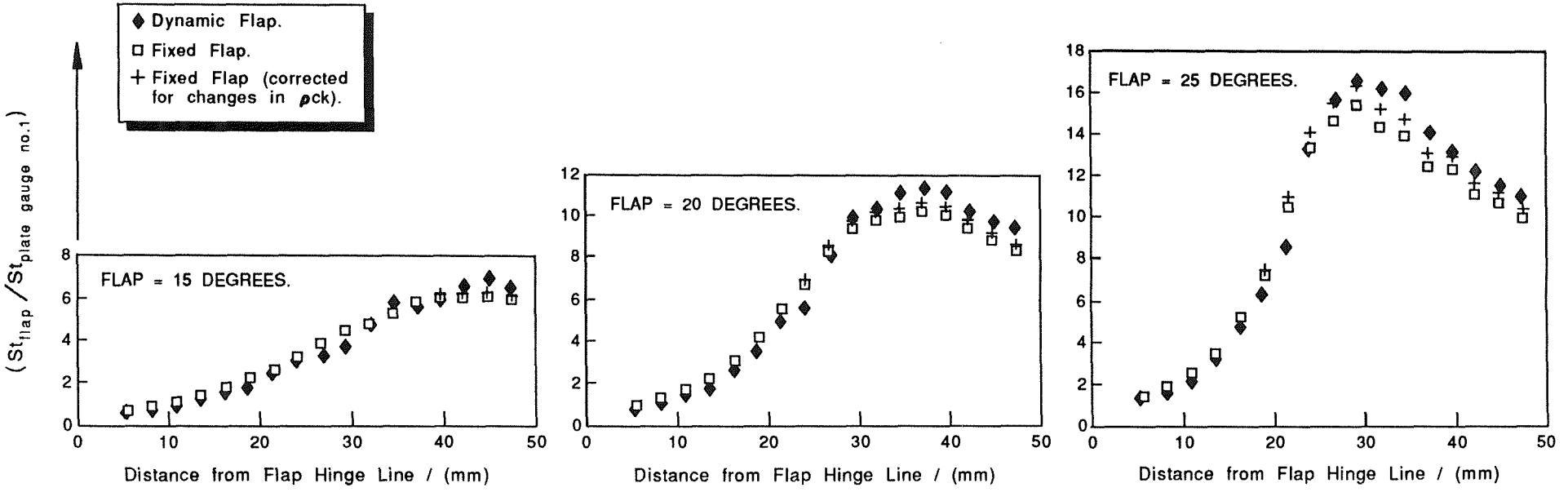

Fig.52. Heat transfer distributions on the flap, reduced using a turbulent recovery factor. No side plates. $M_\infty = 6.85$, $Re_\infty = 2.45 \times 10^6$/m.

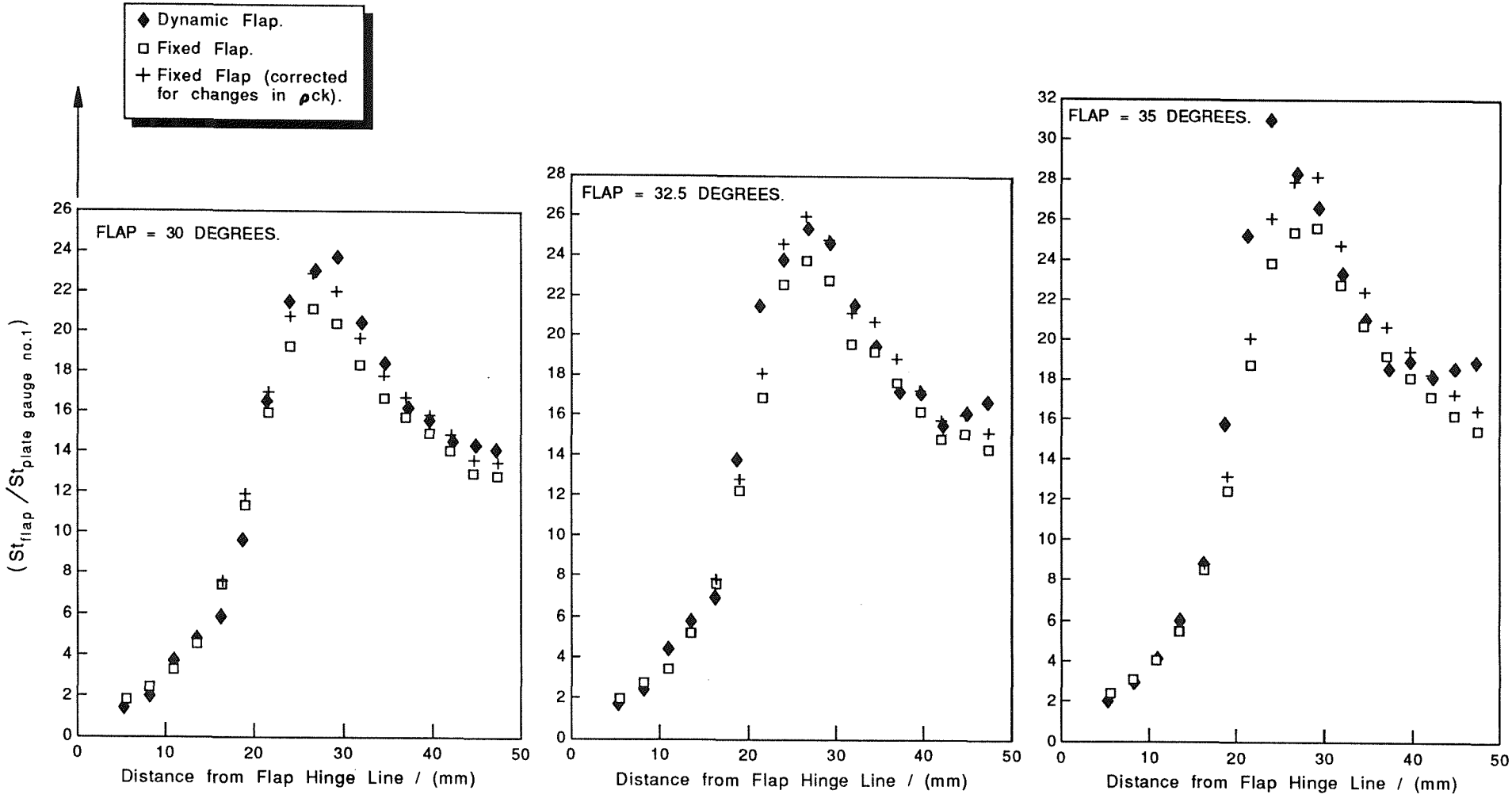

Fig.52. continued.

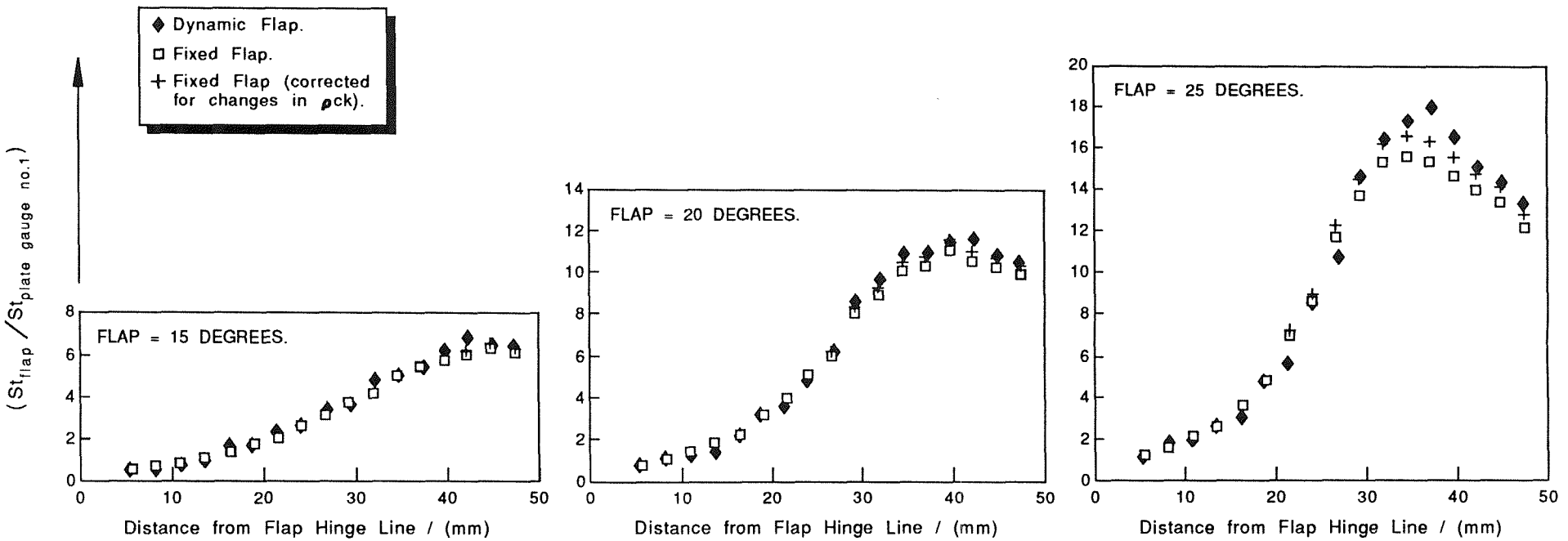

Fig.53. Heat transfer distributions on the flap, reduced using a turbulent recovery factor. + side plates. $M_\infty = 6.85$, $Re_\infty = 2.45 \times 10^6/m$.

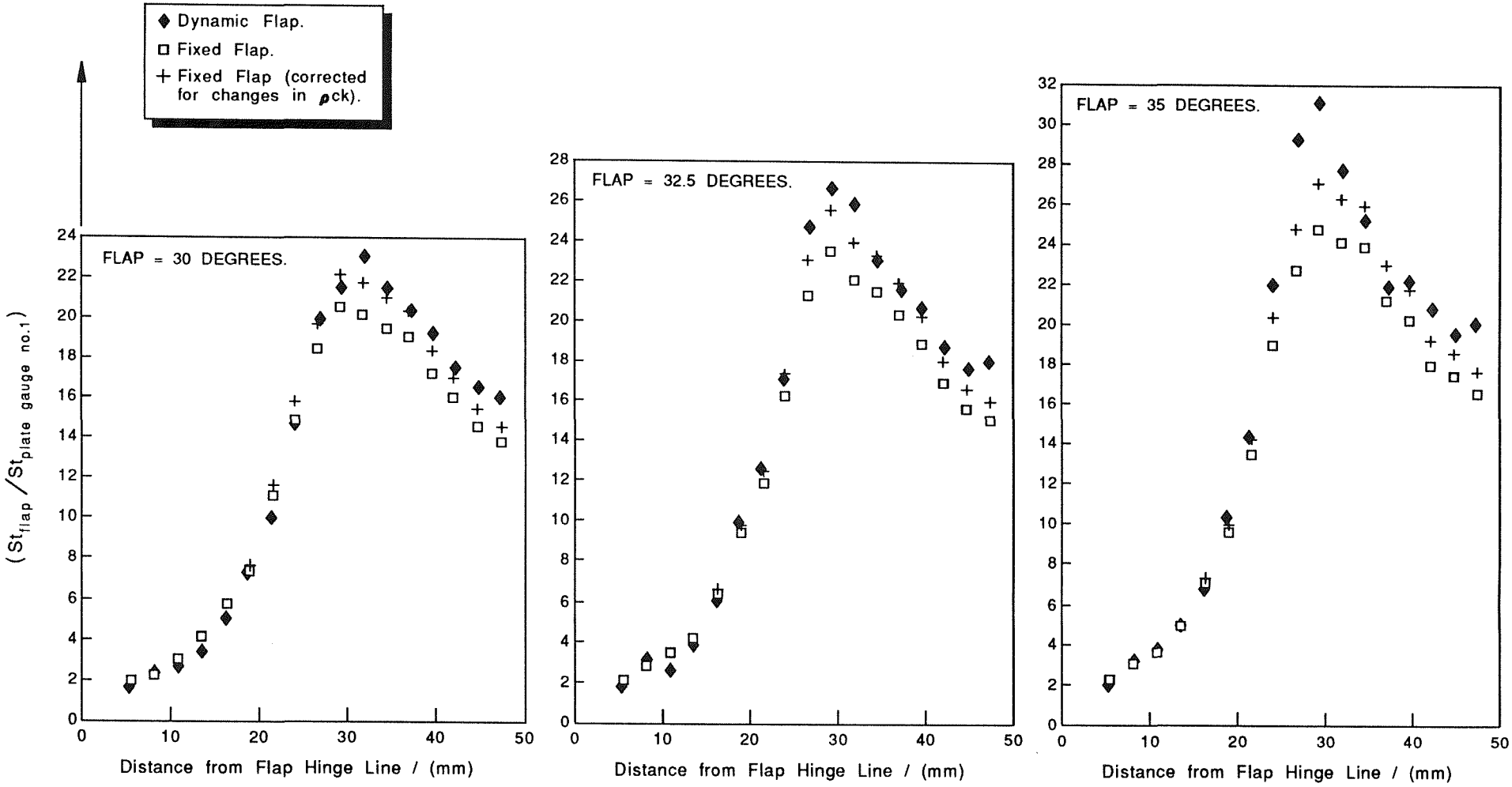

Fig.53. continued.

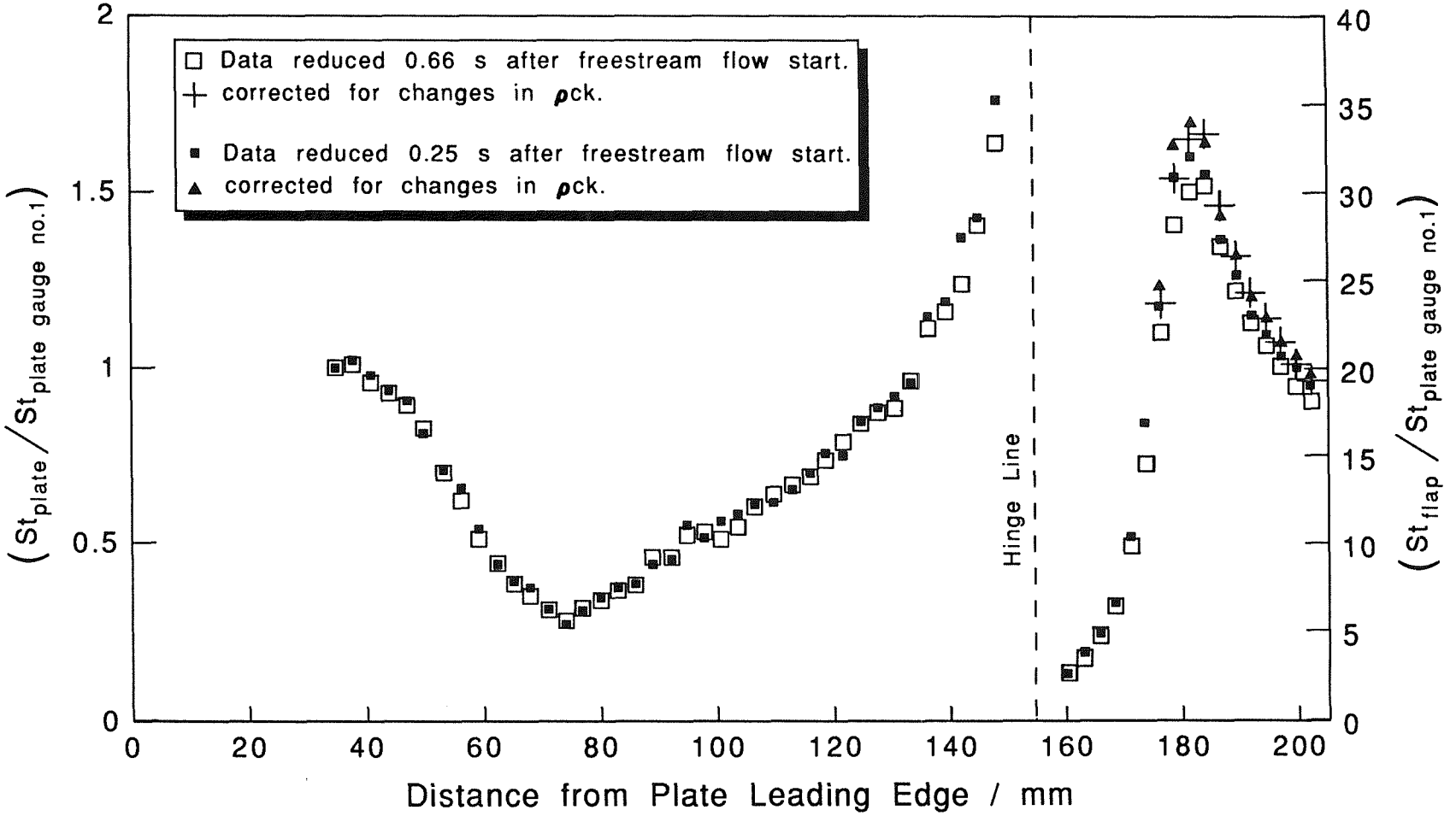

Fig.54. Effect of the flap wall temperature on the separated flow. Flap angle = 35 degrees, no side plates. M_∞= 6.85, Re_∞= 2.45x10^6/m.

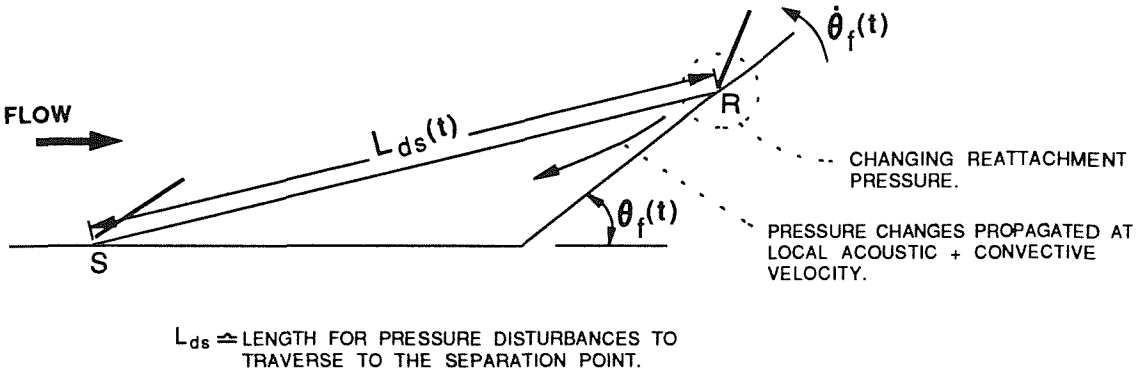

Fig.55. Characteristic length for pressure wave communication in the unsteady separation.

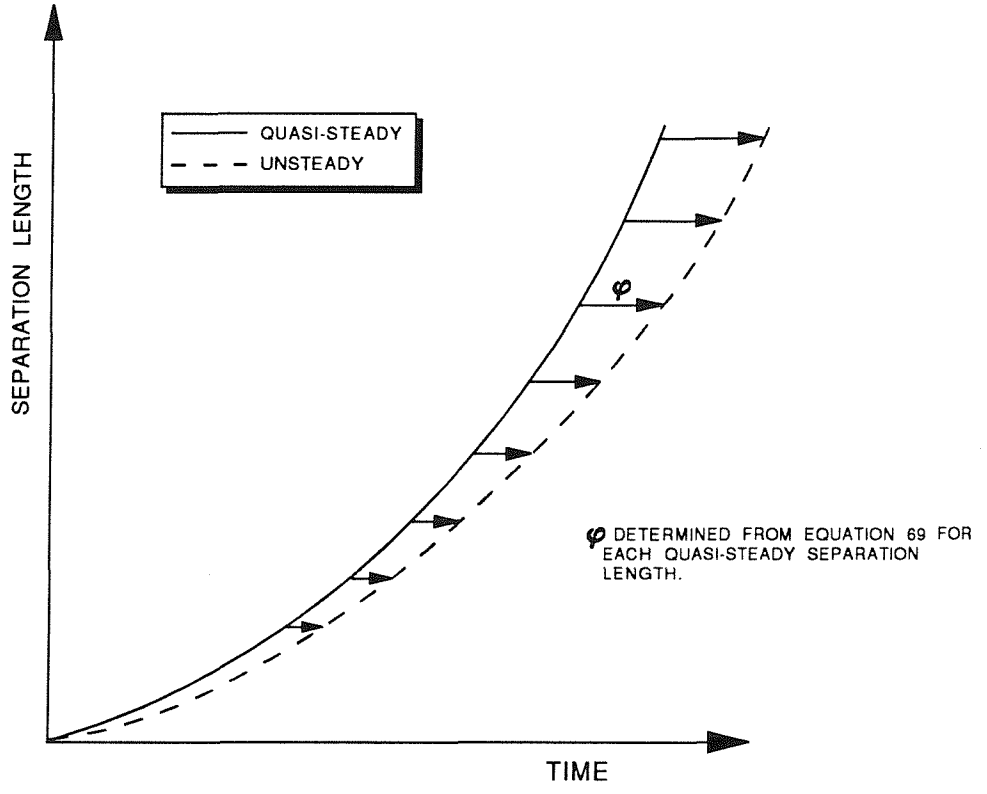

Fig.56. Method of determining the unsteady separation growth with respect to pressure wave adjustment.

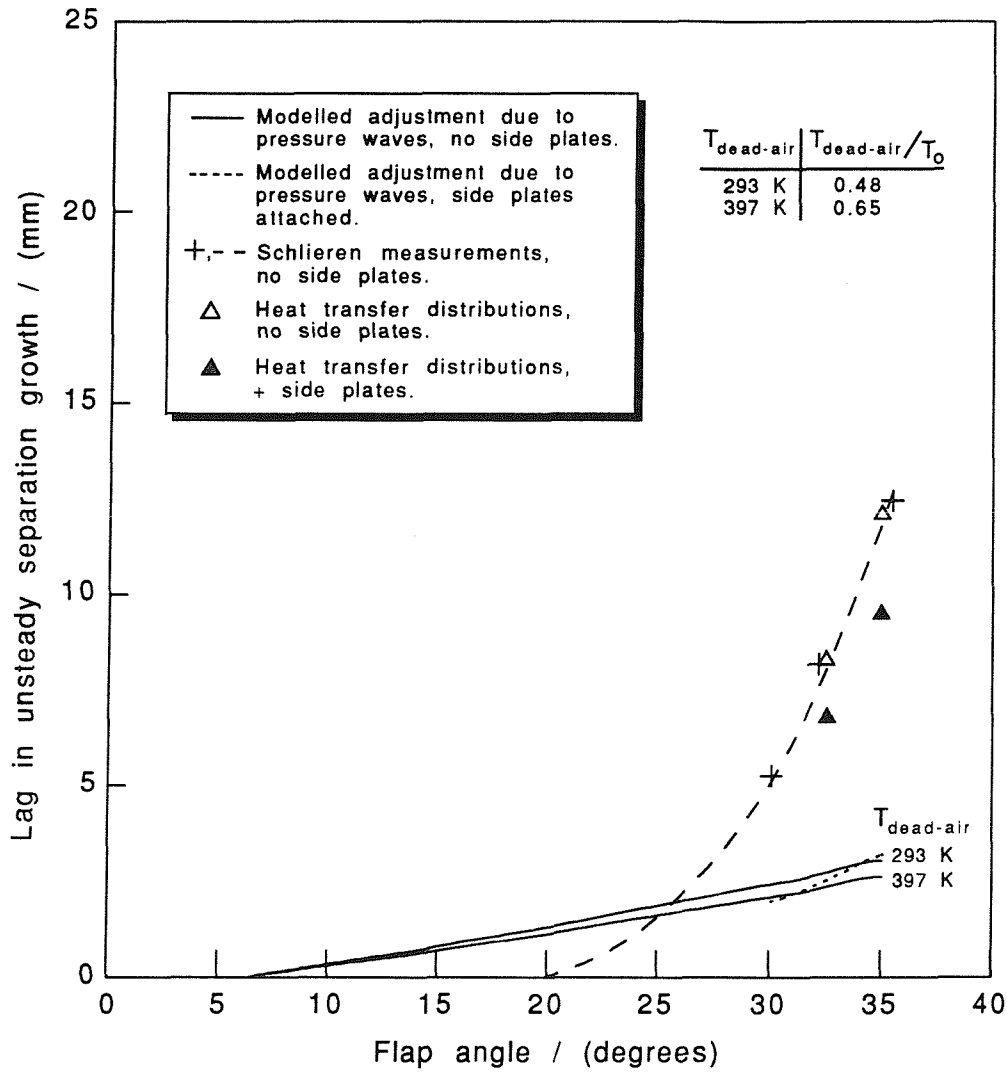

Fig.57. Comparison of the predicted lags in unsteady separation growth, based on pressure wave adjustment, and the experimental measurements (corrected for model position effects).

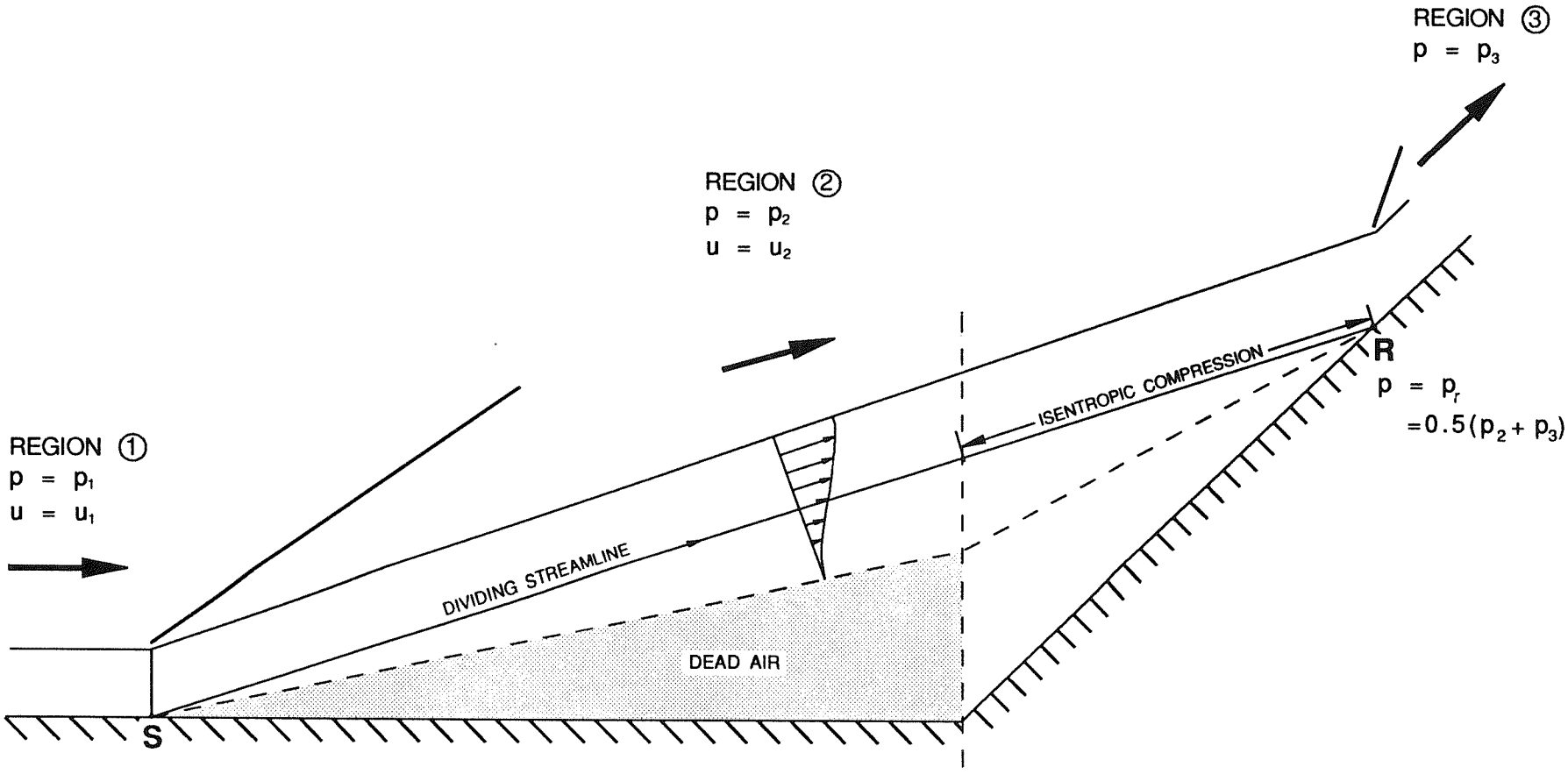

Fig.58. Cooke's (1963) simplified flowfield for the modelling of a supersonic wedge separation.

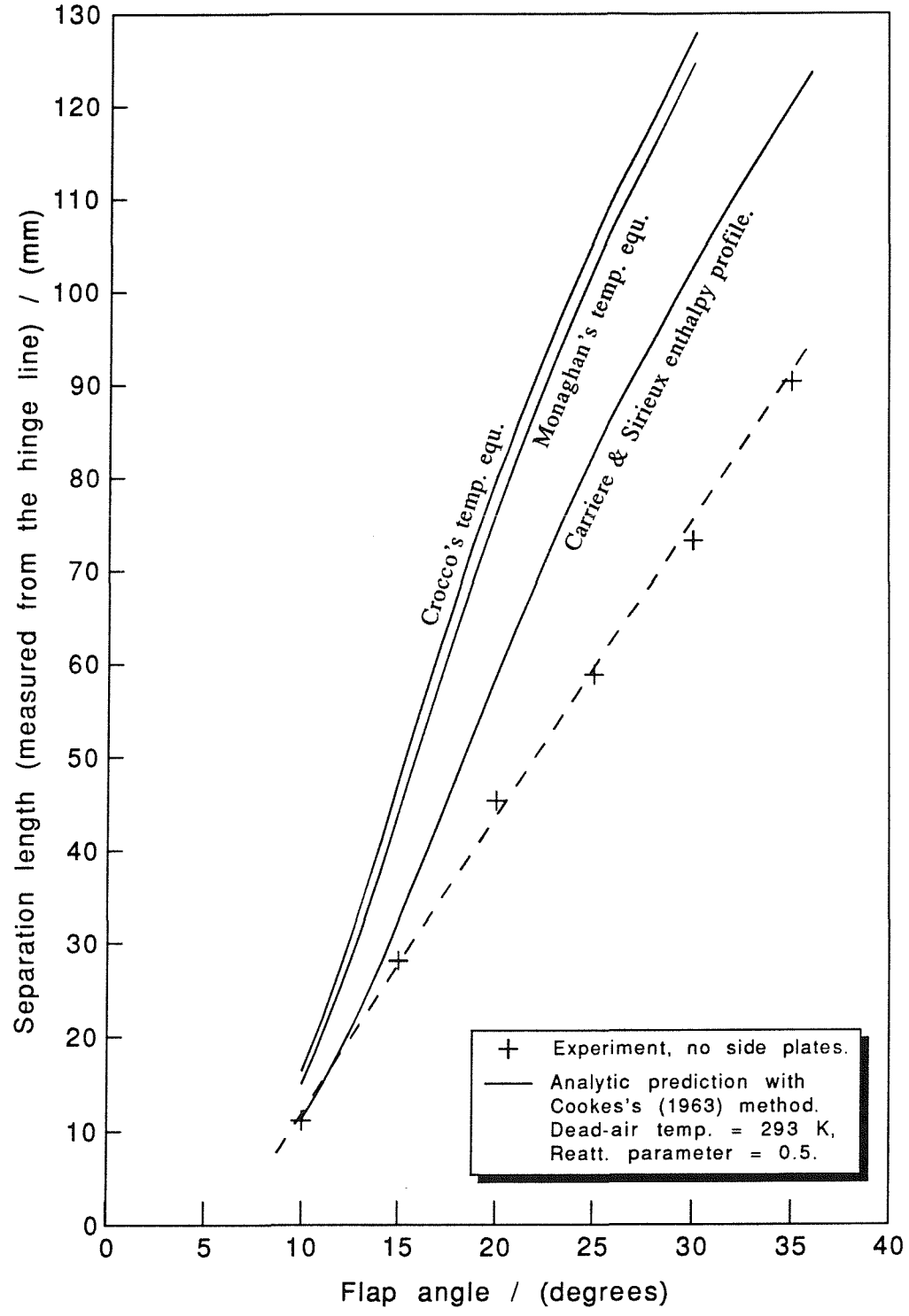

Fig.59. Steady wedge separation lengths predicted with Cooke's (1963) analytic model.

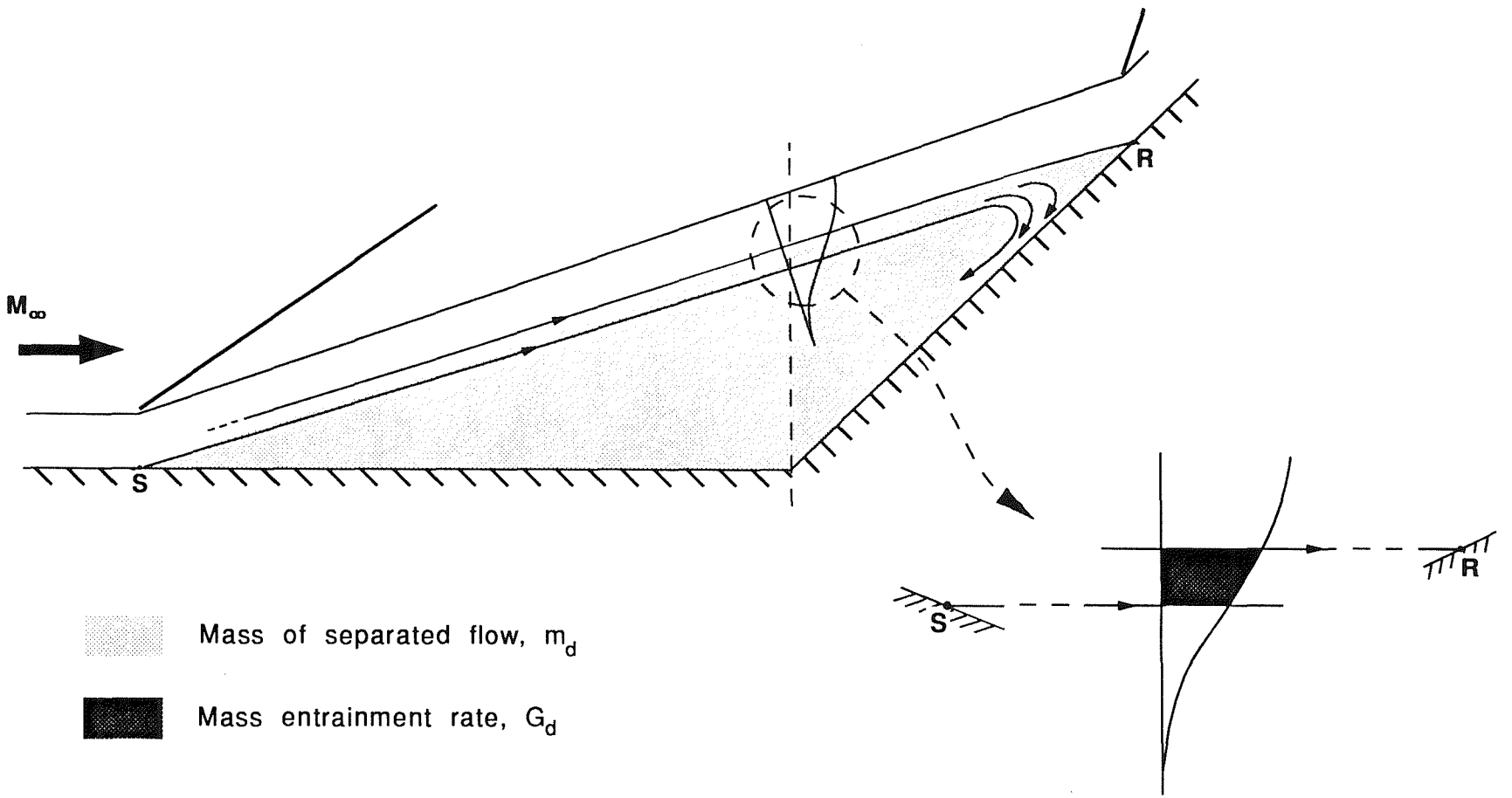

Fig.60. Mass transfer mechanism in the growth of an unsteady wedge separated flow.

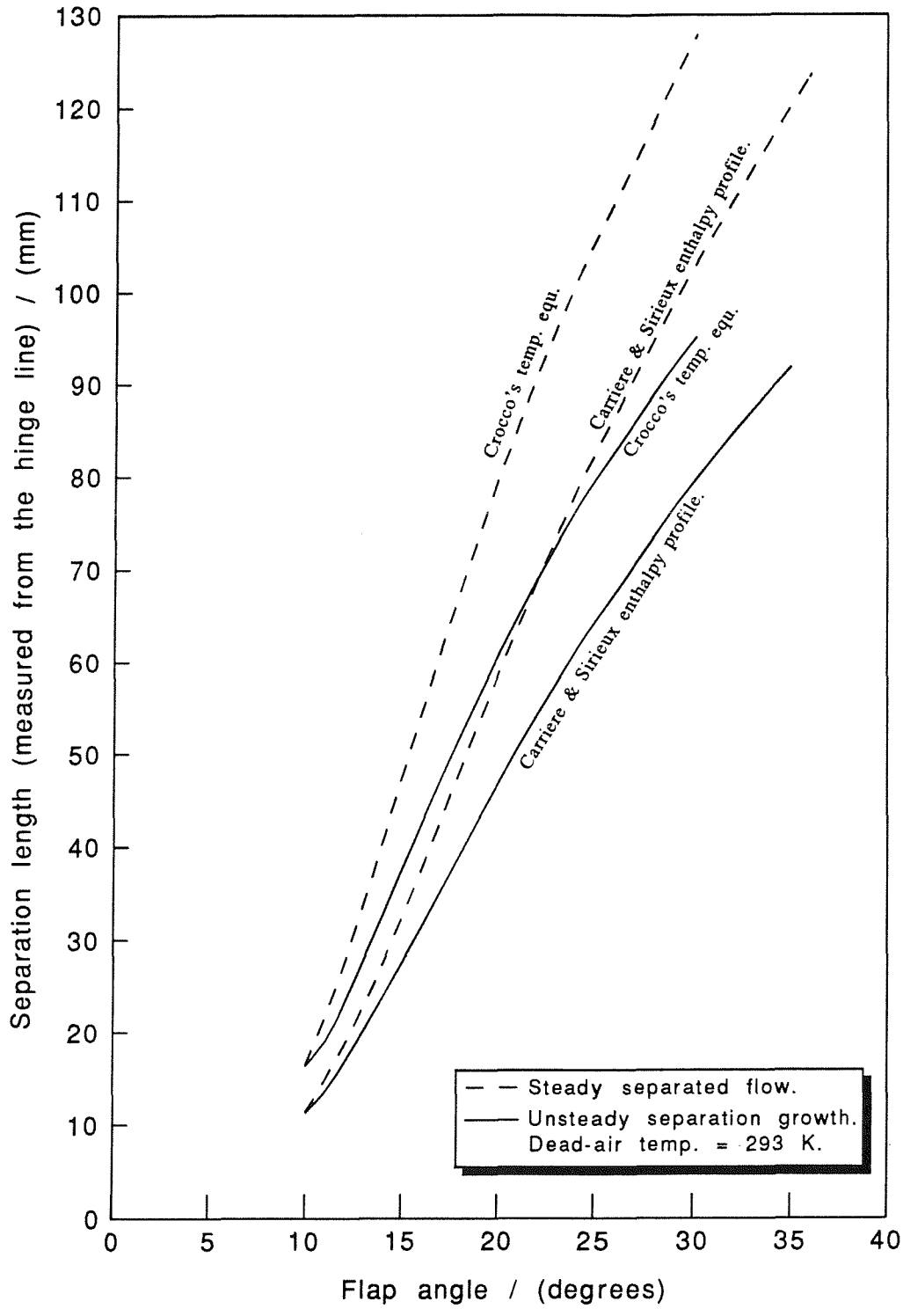

Fig.61. Modelled unsteady separation growth based on mass exchange, assuming an isentropic reattachment process, with N = 0.5.

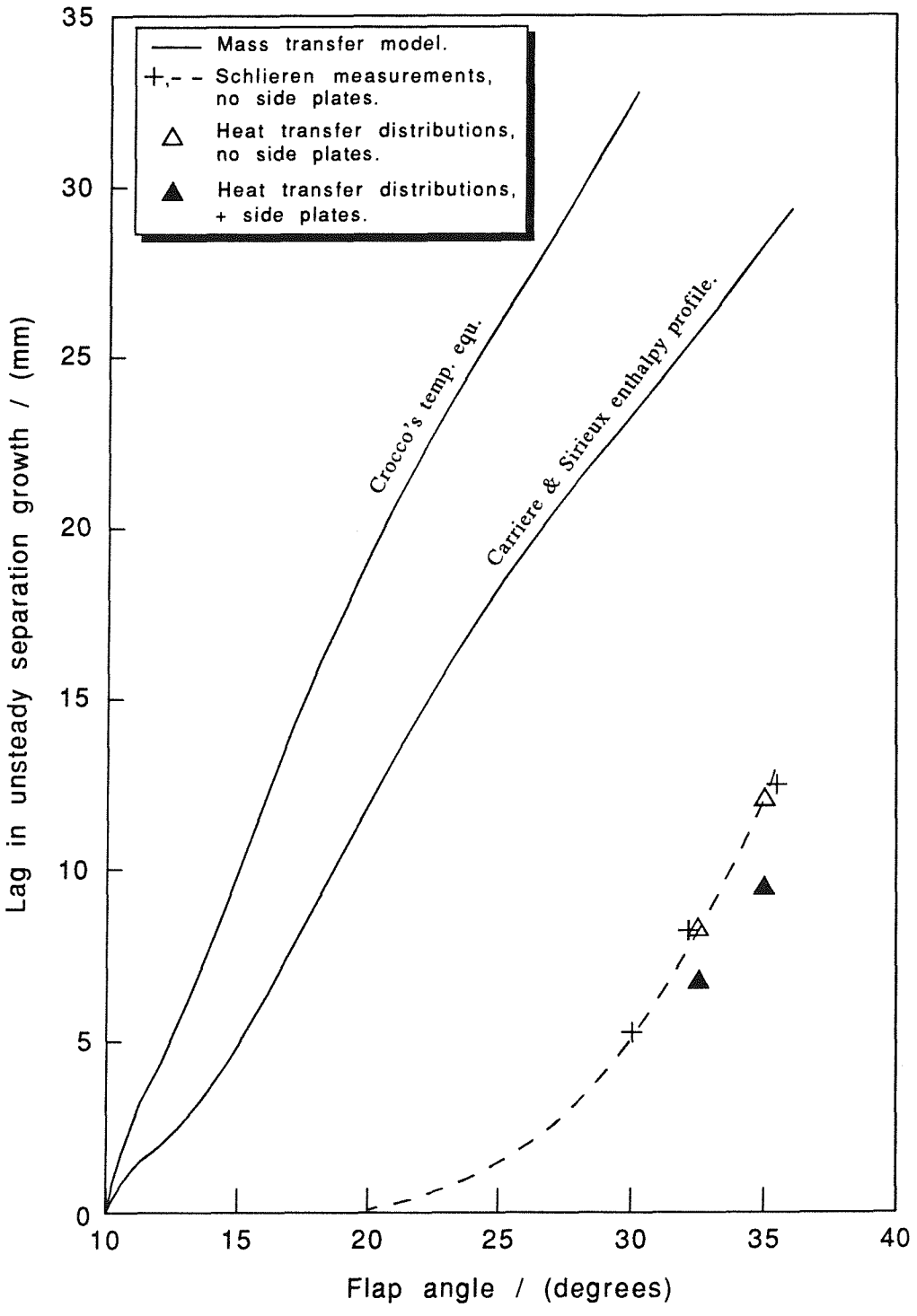

Fig.62. Comparison of the predicted lags in unsteady separation growth (isentropic reattachment, N = 0.5) with the experimental measurements (corrected for model position effects).

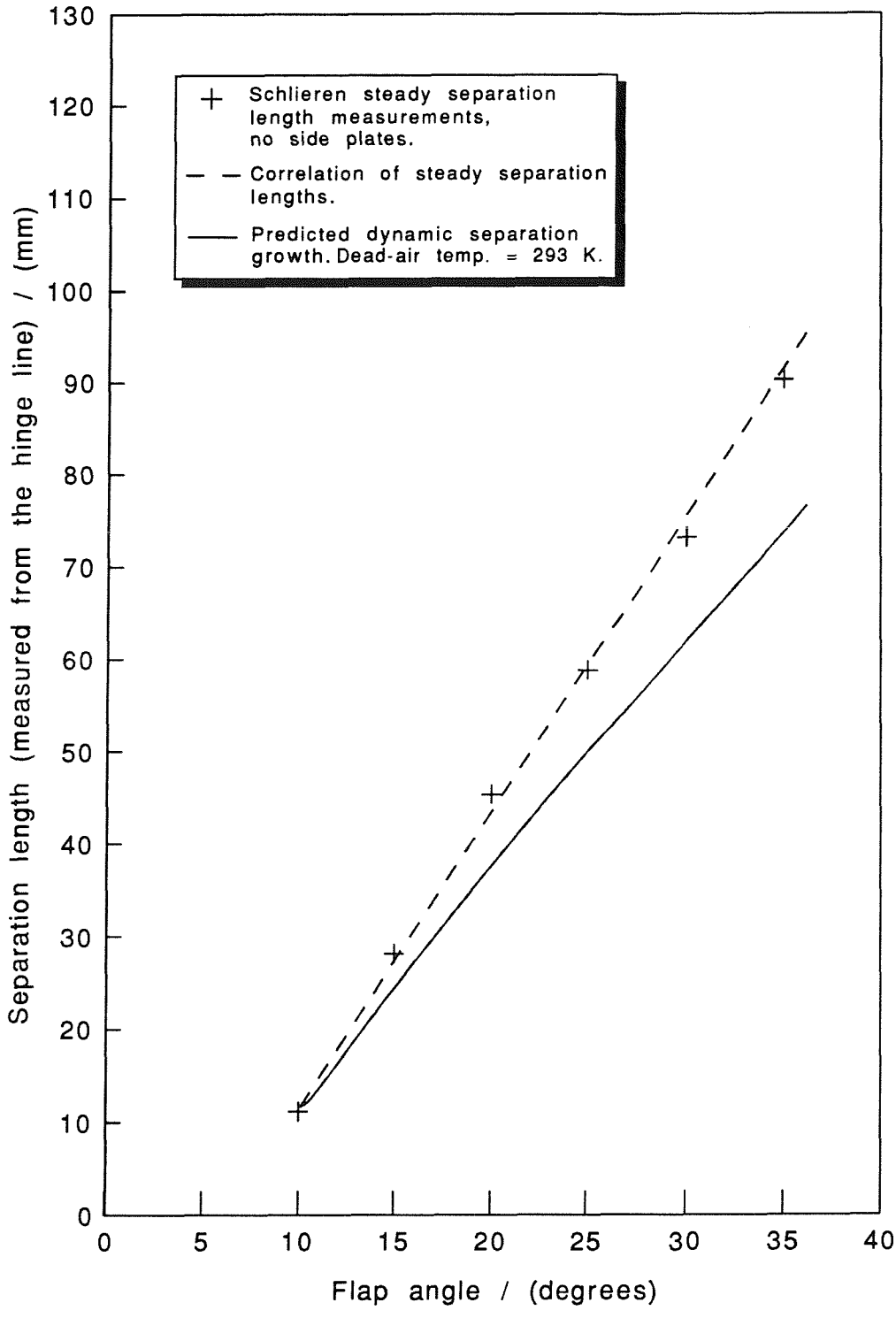

Fig.63. Modelled unsteady separation growth based on mass exchange, with the measured, and modelled, steady separation lengths matched (no side plates).

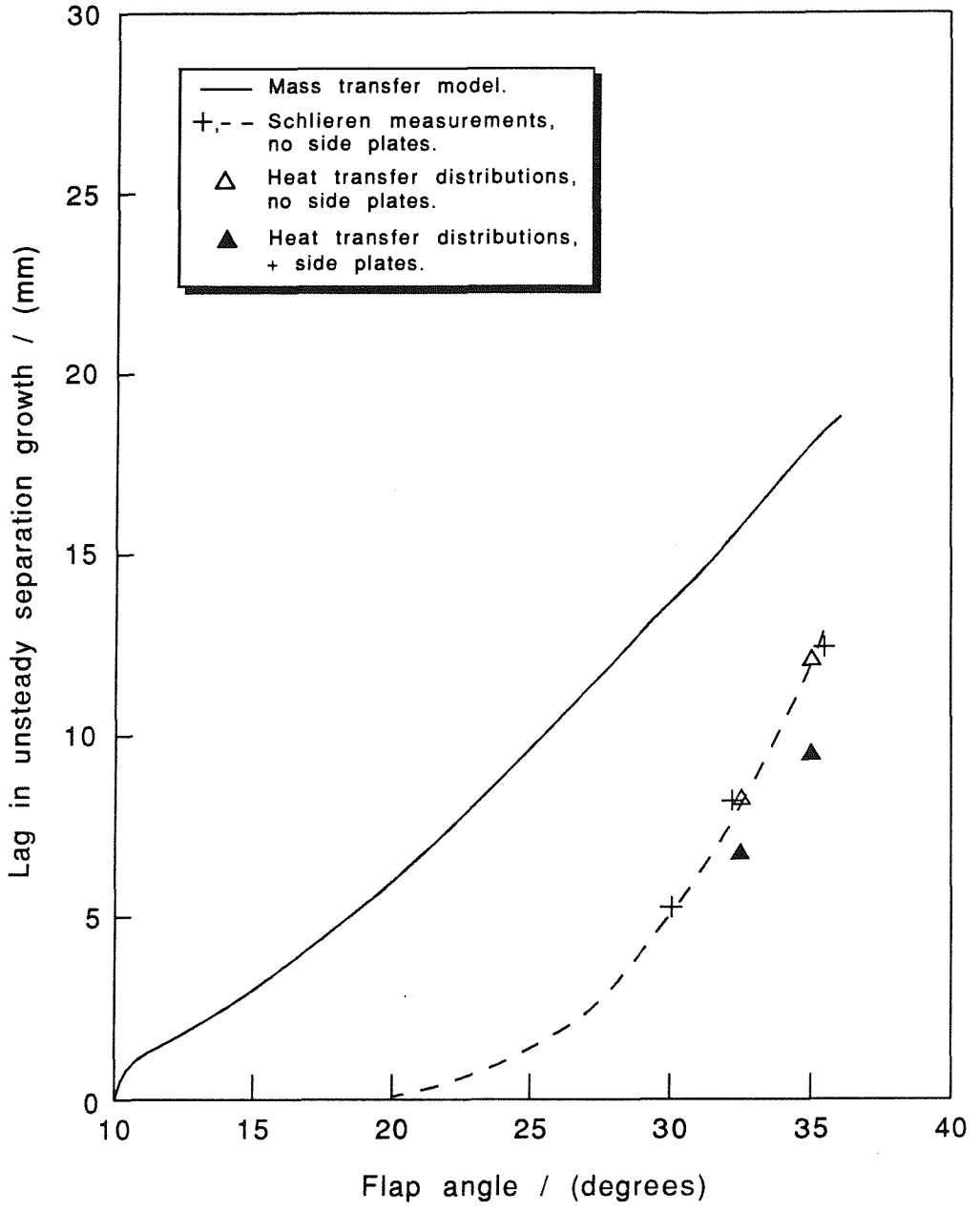

Fig.64. Comparison of the predicted lags in unsteady separation growth with the experimental measurements. Measured, and modelled, steady separation lengths matched (no side plates).

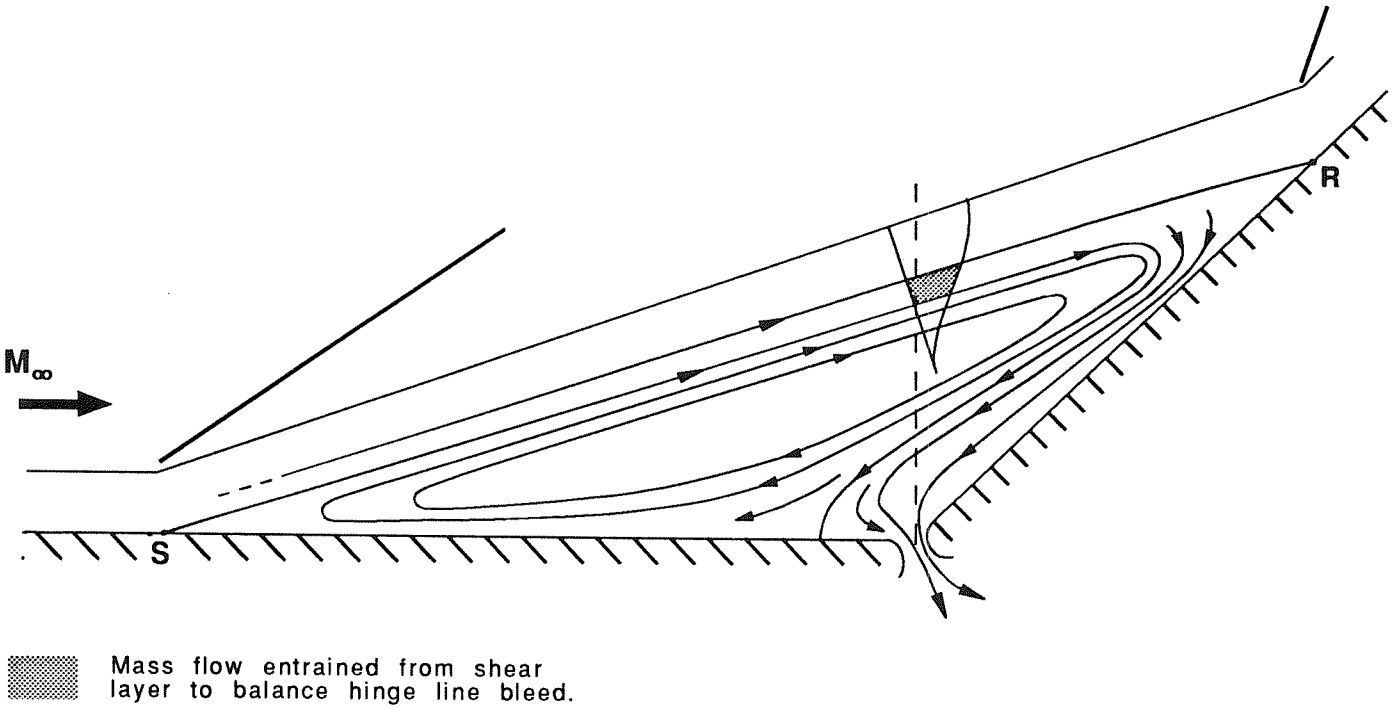

Fig.65. Mass balance in a steady wedge separated flow with hinge line bleed.

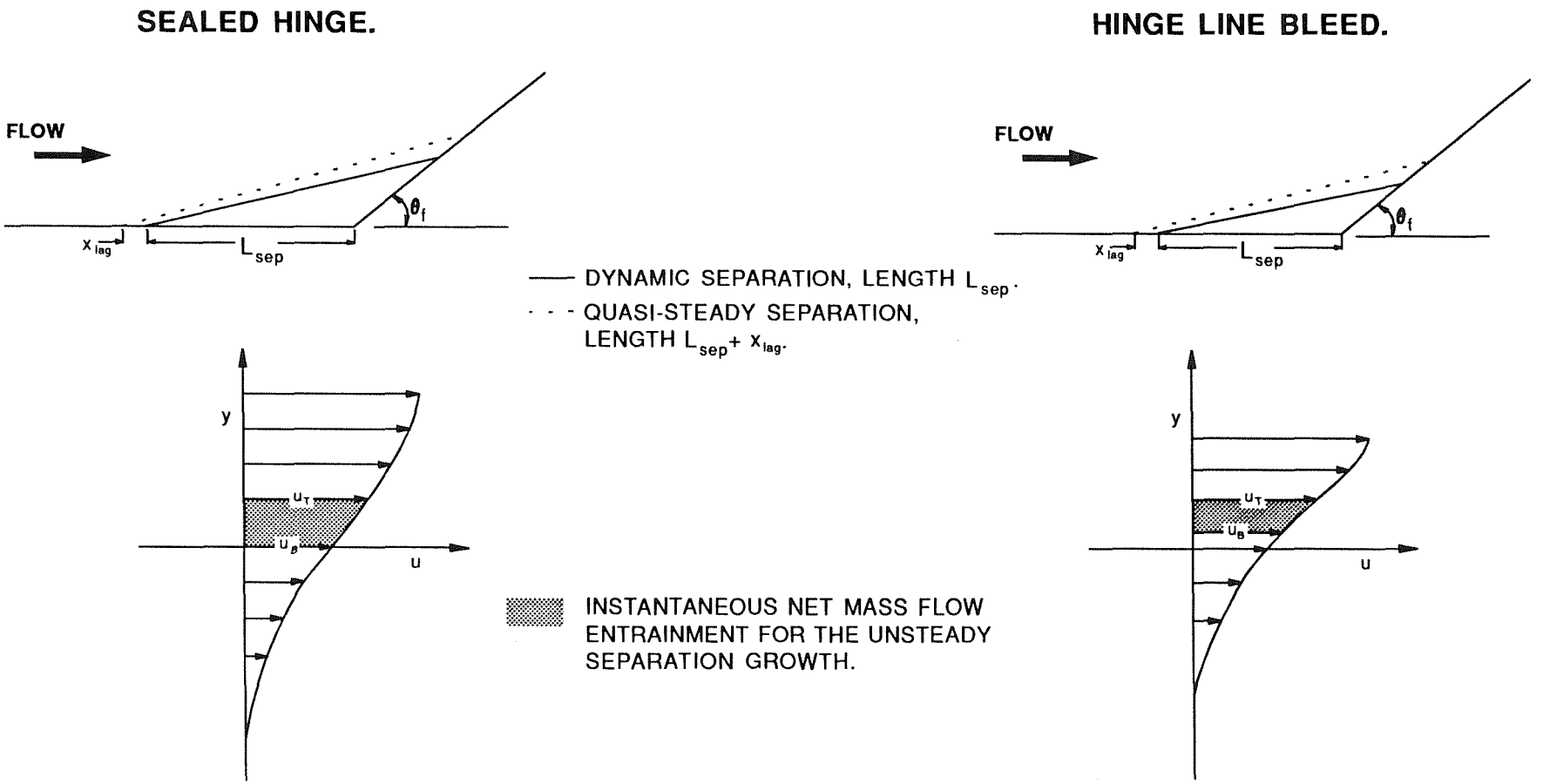

Fig.66. Effect of hinge line bleed on the mass flow entrainment for an unsteady separation growth.

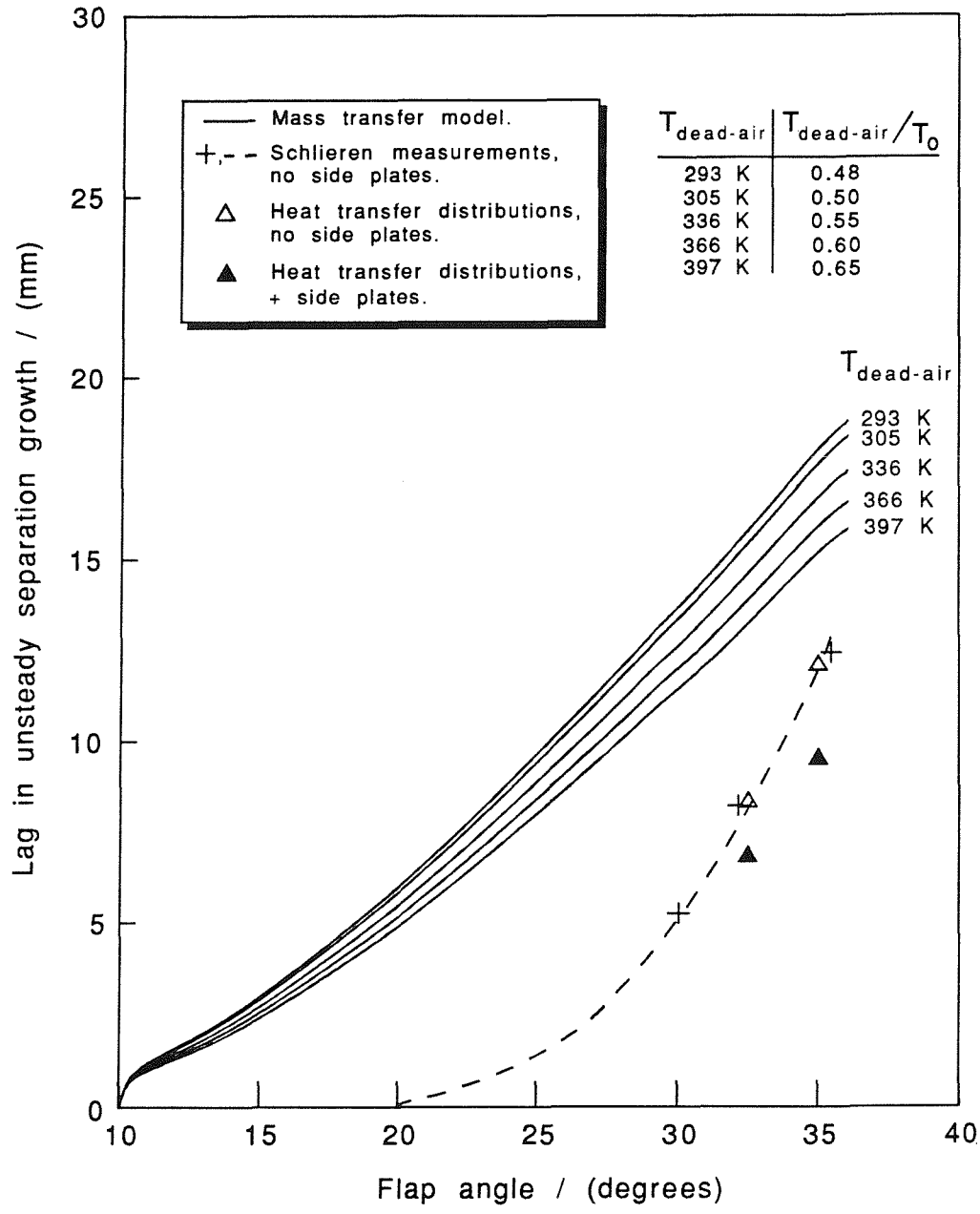

Fig.67. Effect of the assumed dead-air temperature on the predicted lags in unsteady separation growth. Measured, and modelled, steady separation lengths matched (no side plates).

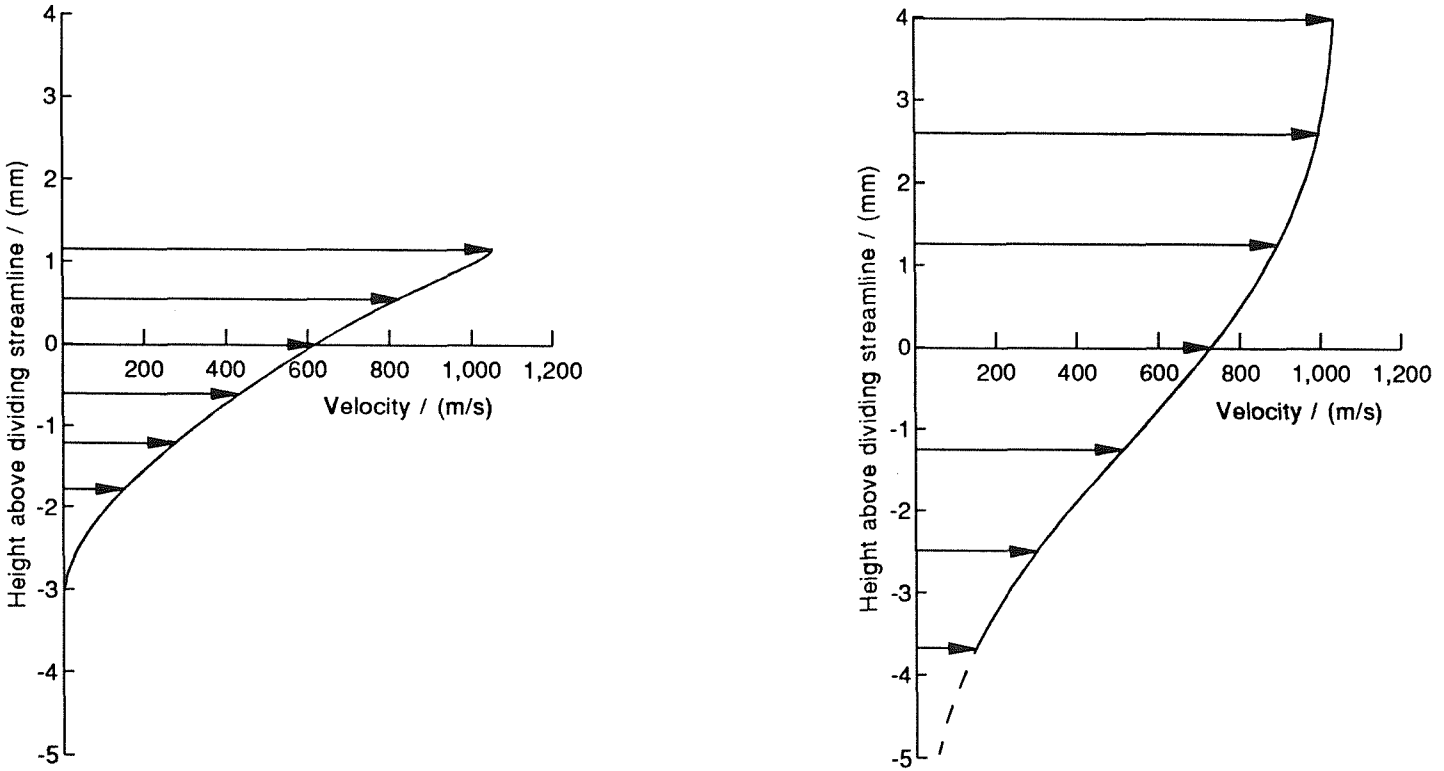

Fig.68. Comparison of fully laminar, and fully turbulent, asymptotic shear layer velocity profiles. Local freestream flow conditions matched to those that occur adjacent to the shear layer with the fixed flap angle of 35 degrees, no side plates.

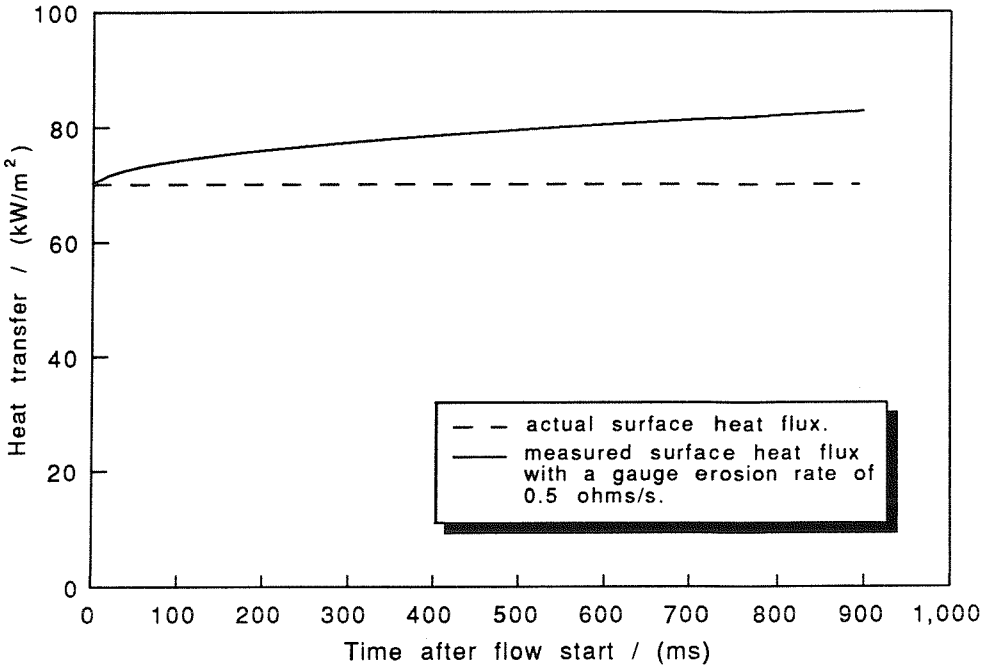

Fig.A4.1. Simulated effect of gauge erosion on the measured surface heat transfer rate.

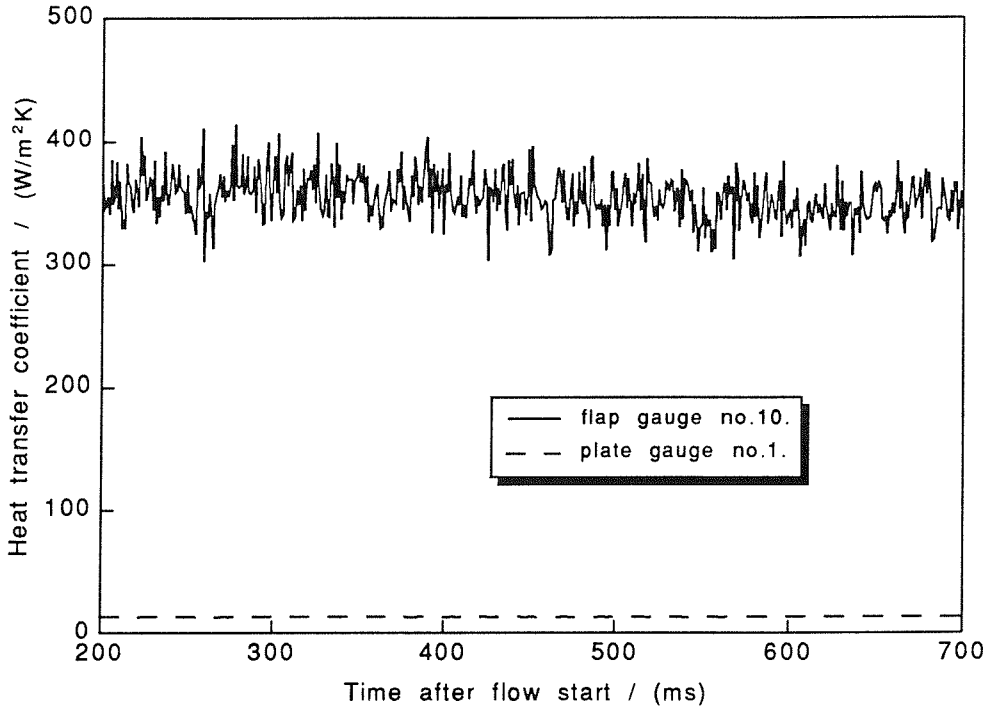

Fig.A4.2. Variation of measured heat transfer coefficients during the test period, with a fixed flap angle of 35 degrees.

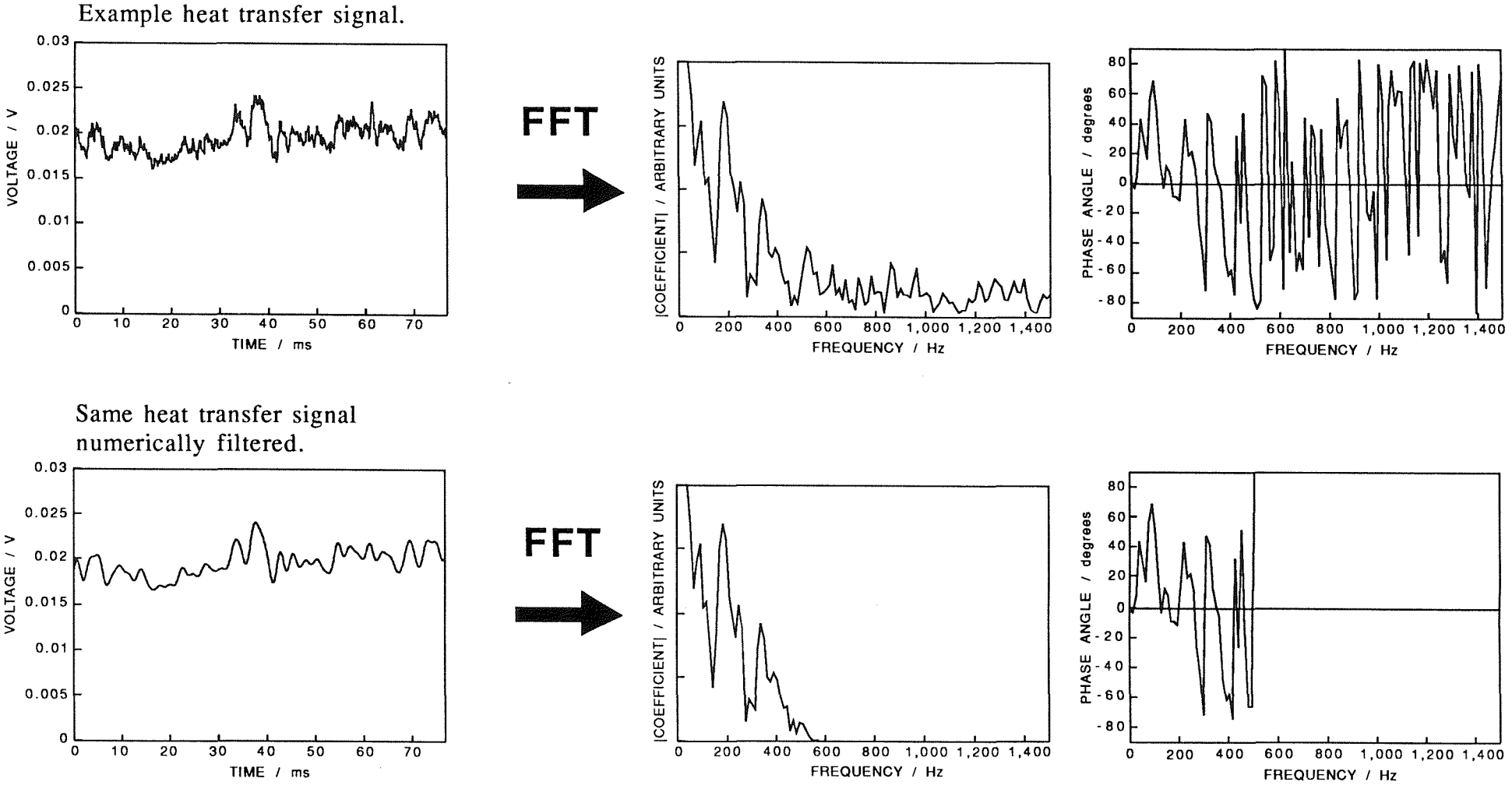

Fig.A8.1. Example application, and verification, of the numerical filter.